Université de Montréal

Survival of the Fittest: Understanding the Role of eIF4E in Cancer Invasion and Treatment Evasion

par

Hiba Ahmad Zahreddine

Département de Pathologie et Biologie Cellulaire

Faculté de Médicine

Thése présentée à la Faculté de

Médicine

en vue de l'obtention du grade de Philosophiae Doctorat (Ph.D.)

en Biologie Moléculaire

Option Biologie des Systémes

Mai 2017

Université de Montréal

Faculté des études supérieures

Cette thèse intitulée

Survival of the Fittest: Understanding the Role of eIF4E in Cancer Invasion and Treatment Evasion

Présentée par

Hiba Ahmad Zahreddine

à été évaluée par un jury compose des personnes suivantes:

Dr. Lea Harrington
Président-rapporteur

Dr. Katherine LB Borden
Directeur de thèse

Dr. Daniel Zenklusen
Membre du Jury

Dr. Aaron Schimmer
Examinatuer Externe
Université de Toronto

Dr. Richard Bertrand
Représentant du doyen la FES

Thése accepté le: May 10th, 2017

Déclaration

Direction des bibliothèques

AVIS

Declaration

The thesis presented is the work of the author except when clearly stated otherwise by reference and/or acknowledgement. Any work performed in collaboration or conducted by others is explicitly acknowledged. The work has not been submitted for any other degree or professional qualification.

Hiba Ahmad Zahreddine	**May 10th, 2017**
	DD/MM/YYYY

RESUME EN FRANÇAIS ET MOTS CLES FRANÇAIS

La métastase et la chimiorésistance sont les principales causes de mortalité chez les patients atteints d'un cancer. La compréhension des mécanismes moléculaires régissant ces deux processus devient donc un domaine de recherche important pour la conception de nouvelles stratégies thérapeutiques. Dans ma thèse, je me concentre sur la compréhension du rôle du facteur d'initiation de la traduction chez les eucaryotes 4E (eIF4E) dans l'invasion du cancer, et je décris un nouveau mécanisme de résistance que nous avons découvert en étudiant le développement de la résistance à un inhibiteur connu d'eIF4E, la ribavirine.

eIF4E est un puissant oncogène qui est connu pour être élevé dans une multitude de cancers comprenant entre autres les sous-types M4 / M5 de la leucémie myéloïde aiguë (AML). Il fonctionne dans la traduction et l'exportation nucléocytoplasmique d'ARNm en se liant à la coiffe m^7G des ARNm possédant des codes USER spécifiques dans leur région UTR 5' et/ou 3'. En reconnaissant ces codes USER, le complexe dans lequel se trouve eIF4E régule de manière coordonnée l'expression de gènes essentiels à la croissance, à la prolifération et à la survie, et ainsi, eIF4E a été placée en tant que nœud central d'un régulon d'ARN régissant la prolifération. En analysant les voies dans lesquelles l'export est régulé de façon coordonnée par eIF4E et les effets physiologiques qui en découlent, j'ai trouvé un enrichissement de la voie biosynthétique de l'acide hyaluronique (HA) et de son principal récepteur CD44 qui sont des médiateurs clés connus des métastases cancéreuses. J'ai également démontré que l'élévation d'eIF4E modifie la surface des cellules cancéreuses en les recouvrant de protrusions riches en HA de type microvillus et enrichies d'armes de destruction métastatique. Heureusement, en dégradant le manteau HA ou en utilisant des inhibiteurs de CD44 en combinaison avec la ribavirine, nous pouvons alors nous défendre.

Compte tenu de l'avantage prolifératif que confère la surexpression d'eIF4E, il est devenu un talon d'Achille attrayant pour le traitement de cancers ayant un niveau élevé d'eIF4E. En effet, lors d'un essai clinique de phase II parmi des patients atteints de leucémie myéloïde aiguë M4 / M5 réfractaire et récidivante, la ribavirine a conduit au ciblage d'eIF4E et a donné lieu à des réponses cliniques significatives, incluant des réponses complètes ou partielles. Cependant, tel qu'attendu lors d'un traitement monothérapique, les patients ayant répondu finissent par développer une résistance au médicament. Mon analyse a révélé que cette résistance est due à

un mécanisme nouveau caractérisé par l'élévation du facteur de transcription Sonic Hedgehog GLI1 qui conduit à la glucuronidation du médicament et donc à la perte de l'interaction entre la drogue et sa cible. Heureusement, ce mécanisme peut être inversé en utilisant des inhibiteurs de la voie Hedgehog.

En conclusion, ces découvertes fournissent de nouvelles cibles thérapeutiques pour le traitement des cellules cancéreuses agressives et résistantes.

Mots clés : eIF4E, Cancer, Résistance multi-drogue, Invasion, GLI1, UGT1A, Acide Hyaluronique, CD44

RESUME EN ANGLAIS ET MOTS CLES ANGLAIS

Metastasis and chemoresistance are the leading cause of mortality among cancer patients. The discovery of molecular mechanisms governing these two processes is becoming an important area of research for the design of novel therapeutic strategies. In my thesis, I focus on understanding the role of the eukaryotic translation initiation factor 4E (eIF4E) in cancer invasion and describe a novel mechanism of resistance that we discovered while studying the development of resistance to a known eIF4E inhibitor, ribavirin.

eIF4E is a potent oncogene that is known to be elevated in a multitude of cancers including M4/M5 subtypes of acute myeloid leukemia (AML). It functions in mRNA translation and nucleocytoplasmic export by binding to the m^7G cap of mRNAs possessing specific USER codes in their 5' and/or 3' UTRs. By recognizing these USER codes, eIF4E complex coordinately regulates the expression of genes essential for growth, proliferation and survival and as such has been placed as a central node of an RNA regulon governing proliferation. When analyzing which pathways have their export coordinately regulated by eIF4E and what physiological effects arise from it, I found an enrichment in the hyaluronic acid (HA) biosynthetic pathway as well as its major receptor CD44 which are known key mediators of cancer metastasis. I demonstrate that eIF4E elevation changes the surface of cancer cells sugar-coating them with HA-rich microvillus-like protrusions that are enriched with weapons of metastatic destruction. Luckily, through degrading the HA-coat or using inhibitors of CD44 in combination with ribavirin we can strike back.

Given the proliferative advantage that eIF4E overexpression conveys, this rendered it as an attractive Achilles heel for the treatment of cancers where eIF4E levels are high. Indeed, in a phase II clinical trial in refractory and relapsed poor prognosis M4/M5 AML patients, ribavirin led to eIF4E targeting and resulted in significant clinical responses including complete and partial remissions. However, as it is expected for monotherapy treatment, all responding patients eventually developed resistance to the drug. My analysis revealed that resistance is due to a novel mechanism characterized by elevation of the Sonic Hedgehog transcription factor GLI1 which leads to drug glucuronidation and the subsequent loss of drug-to-target interaction. Fortunately, this mechanism can be reversed using Hedgehog pathway inhibitors.

Taken together, these findings provide novel therapeutic venues for the treatment of aggressive and resistant cancer cells.

Keywords: eIF4E, Cancer, Multidrug Resistance, Invasion, GLI1, UGT1A, Hyaluronic acid, CD44

List of Publications

This thesis is based on the following:

A-Main Research Papers:

1-*The sonic hedgehog factor GLI1 imparts drug resistance through inducible glucuronidation.*

Zahreddine HA, Culjkovic-Kraljacic B, Assouline S, Gendron P, Romeo AA, Morris SJ, Cormack G, Jaquith JB, Cerchietti L, Cocolakis E, Amri A, Bergeron J, Leber B, Becker MW, Pei S, Jordan CT, Miller WH, Borden KL.

Nature. 2014 Jul 3;511(7507):90-3. doi: 10.1038/nature13283.

2-*A phase I trial of ribavirin and low-dose cytarabine for the treatment of relapsed and refractory acute myeloid leukemia with elevated eIF4E.*

Assouline S, Culjkovic-Kraljacic B, Bergeron J, Caplan S, Cocolakis E, Lambert C, Lau CJ, **Zahreddine HA**, Miller WH Jr, Borden KL.

Haematologica. 2015 Jan;100(1):e7-9. doi: 10.3324/haematol.2014.111245.

3-*The eukaryotic translation initiation factor eIF4E harnesses hyaluronan production to drive its malignant activity*

Hiba Ahmad Zahreddine[1], Biljana Culjkovic-Kraljacic[1], Lucy Skrabanek[2], Ronald Midura[3], Mark Lauer[3], Sonia Del Rincon[4], Audrey Emond[4], Valbona Cali[3], Leandro Cerchietti[5], Wilson H Miller[4], Vincent Hascall[3], Katherine LB Borden[1]

Nature. 2017 (Submitted)

B-Extra Research Papers:

4-*Conformational changes induced in the eukaryotic translation initiation factor eIF4E by a clinically relevant inhibitor, ribavirin triphosphate.*

Volpon L, Osborne MJ, **Zahreddine H**, Romeo AA, Borden KL.

Biochem Biophys Res Commun. 2013 May 10;434(3):614-9. doi: 10.1016/j.bbrc.2013.03.125.

5-*Combinatorial targeting of nuclear export and translation of RNA inhibits aggressive B-cell lymphomas.*

Culjkovic-Kraljacic B, Fernando TM, Marullo R, Calvo-Vidal N, Verma A, Yang S, Tabbò F, Gaudiano M, **Zahreddine H**, Goldstein RL, Patel J, Taldone T, Chiosis G, Ladetto M, Ghione P, Machiorlatti R, Elemento O, Inghirami G, Melnick A, Borden KL, Cerchietti L.

Blood. 2016 Feb 18;127(7):858-68. doi: 10.1182/blood-2015-05-645069.

C-Reviews:

1-*Mechanisms and insights into drug resistance in cancer*.

Zahreddine H, Borden KL.

Front Pharmacol. 2013 Mar 14;4:28. doi: 10.3389/fphar.2013.00028.

2-*Inducible drug modification: a new form of resistance.*

Culjkovic-Kraljacic B, **Zahreddine HA**, Borden KL.

Cell Cycle. 2014;13(16):2485-6. doi: 10.4161/15384101.2014.946372.

3-*Sonic Hedgehog factor Gli1: As good as resistant.*

Zahreddine HA, Culjkovic-Kraljacic B, Borden KL.

Mol Cell Oncol. 2015 Feb 24;2(1):e961827. doi: 10.4161/23723548.2014.961827.

4-*Molecular Pathways: GLI1-Induced Drug Glucuronidation in Resistant Cancer Cells.*

***Zahreddine HA**, Borden KL.*

Clin Cancer Res. 2015 May 15;21(10):2207-10. doi: 10.1158/1078-0432.CCR-14-1370.

Table of Contents

List of Tables

List of Figures

-Chapter 1:

-Chapter 2:

-Chapter 3:

Abbreviations

4E-BP	eIF4E Binding Protein
4E-SE	eIF4E-Sensitivty Element
4GI	4E/4G Inhibitor
ADK	Adenosine Kinase
AhR	Aryl Hydrocarbon Receptor
AKT	Serine/Threonine-Specific Protein Kinase
AMAC	2-Aminoacridone
AML	Acute Myeloid Leukemia
AraC	Cytarabine
ARE	AU Rich Element
AUF1	ARE Binding Factor
AZA	Azacitidine
BC-CML	Blast Crisis Chronic Myelogenous Leukemia
BCL2	B-Cell Lymphoma 2
BM	Bone Marrow
BSA	Bovine Serum Albumin
β–TrCP	F-box/WD Repeat-Containing Protein 1A (FBXW1A)
C-MET	Receptor Tyrosine Kinase
CAR	Constitutive Androstane Receptor
CD34	Hematopoietic Progenitor Cell Antigen
CD44	Indian blood group
CML	Chronic Myelogenous Leukemia
CO_2	Carbon Dioxide
CRM1	Chromosome Region Maintenance 1
CUL	Cullin
DEPC	Diethyl Pyrocarbonate
DilC$_{12}$(3)	1,1'-Didodecyl-3,3,3',3'-Tetramethylindocarbocyanine Perchlorate

DTT	Dithiothreitol
DDX	DEAD-box Helicases
DMEM	Dulbecco's Modified Eagle Medium
DNA	Deoxyribonucleic Acid
ECM	Extracellular Matrix
EDTA	Ethylenediaminetetraacetic Acid
eIF3	Eukaryotic Initiation Factor 3
eIF4A	Eukaryotic Translation Initiation Factor 4A
eIF4E	Eukaryotic Translation Initiation Factor 4E
eIF4G	Eukaryotic Translation Initiation Factor 4G
EGF	Epidermal Growth Factor
EGFR	Epidermal Growth Factor Receptor
EMT	Epithelial-Mesenchymal Transition
ENT	Equilibrative Nucleoside Transporter
ER	Endoplasmic Reticulum
ERBB4	erb-b2 Receptor Tyrosine Kinase 4
ERM	Ankyrin and Ezrin, Radixin and Moesin proteins
EWS-FLI1	Ewing's Sarcoma - Friend Leukemia Integration 1 Transcription Factor Fusion protein
FBS	Fetal Bovine Serum
FDA	Food and Drug Administration
FITC	Fluorescein Isothiocyanate
FKBPL	FK506 binding protein like
GA	Glucuronic Acid
GAG	Glycosaminoglycan
GAPDH	Glyeraldehyde 3-Phosphate Dehydrogenase
GATA	Erythroid Transcription Factor
GEM	Glycolipid-Enriched Microdomains

GLI	Glioblastoma Associated Protein
GRB2	Growth Factor Receptor-Bound Protein 2
GTP	Guanosine Triphosphate
HA	Hyaluronan
H&E	Hematoxylin and eosin
HAS	Hyaluronan Synthase
HEPES	(4-(2-Hydroxyethyl)-1-piperazineethanesulfonic Acid)
HEX	Hematopoietically Expressed Homeobox
HH	Hedgehog Protein
HNF	Hepatic Nuclear Factor
hnRNPA1	Heteronuclear Ribonuclear Protein A
HOXA9	Homeodomain Box Protein A9
HPG	L-Homopropargylglycine
HuR	Human Antigen R
IGF	Insulin Growth Factor
ITCH	E3 Ubiquitin-Protein Ligase Itchy Homolog
LRP/PRC	Leucine-Rich Pentatricopeptide Repeat Containing
m^7G	Methyl-7-Guanosine
M-MLV	Moloney murine leukemia virus
MCL1	Myeloid Cell Leukemia Protein 1
MDM2	Mouse Double Minute 2 Homolog
MDR	Multidrug Resistance
MDS	Myelodysplastic Syndrome
MMP	Matrix Metalloproteinase
mRNA	Messenger Ribonucleic Acid
mRNP	Messenger Ribonucleoprotein
MYC	Myelocytomatosis Protein
$MgCl_2$	Magnesium Chloride

NaCl	Sodium Chloride
NB	Nuclear Body
NBS1	Nibrin
NFAT	Nuclear Factor of Activated T-cells
NF-κB	Nuclear Factor Kappa-light-chain-enhancer of activated B-cells
NMR	Nuclear Magnetic Resonance
NP-40	Nonyl Phenoxypolyethoxylethanol
NPC	Nuclear Pore Complex
NUMB	Endocytic Adaptor Protein
NUP	Nucleoporin
ODC	Ornithine Decarboxylase
P53	Tumour Protein p53
PAX	Paired Box Protein
PBS	Phosphate-buffered saline
Pen/Strep	Penicillin Streptomycin
PET	Polyethylene Terephthalate
PFA	Paraformaldehyde
PIM-1	Proto-Oncogene, Serine/Threonine Kinase
PML	Promyelocytic Leukemia
PPAR	Peroxisome Proliferation-Activated Receptor
PRH	Proline-Rich Protein HaeIII Subfamily
PTCH	PATCHED
PTEN	Phosphatase and Tensin Homolog
PU.1	Purine Rich (PU) box Binding Protein
RANBP	Ran-Binding Protein
RPMI	Roswell Park Memorial Institute medium
RBV	Ribavirin
RING	Really Interesting New Gene Protein

RIP	RNA Immunoprecipitation
RNA	Ribonucleic Acid
RTP	Ribavirin- 5'-Triphosphate
SDF-1	Stromal Cell-Derived Factor 1
SMO	SMOOTHENED
SNAIL	Zinc Finger Protein SNAI1
SP1	Specificity Protein 1
SPOP	Speckle Type BTB/POZ Protein
STAT	Signal Transducer and Activator of Transcription
SUFU	Suppressor of Fused
TAP/NXF1	Nuclear RNA Export Factor 1
TBS	Tris-Buffered Saline
TGFβ	Transforming Growth Factor β
TK	Thymidine Kinase
UAP56	ATP-dependent RNA helicase
UDPGA	Uridine 5'-diphosphoglucuronic acid
UGT	UDP-Glucuronosyltransferases
USER	Untranslated Sequence Elements for Regulation
UTR	Untranslated Regions
VEGF	Vascular Endothelial Growth Factor
VpG	Viral Protein Genome-linked
WHO	World Health Organization
Z-PROTEIN	Arenavirus Protein Z

Dedicated to my father, Ahmad Zahreddine

My mother, Mariam Dib

And all my family and friends,

Acknowledgements

The research resulting in this thesis was conducted at the Institute for Research in Immunology and Cancer (IRIC), Faculty of Medicine, University of Montreal, CANADA, from September 2011 to January 2017.

I am sincerely indebted to all the people who encouraged and supported me through out my Ph.D. It is my pleasure to pay tribute to them.

Foremost, I would like to extend my sincere gratitude to Dr. Katherine LB Borden for being the best supervisor I could have asked for. Thank you for your patience, guidance, encouragement and positive spirit over the course of this research. Without your time, energy and enthusiasm this work would not have been accomplished. My sincerest thank you for all your effort to help me grow as an independent researcher.

I genuinely acknowledge all the funding agencies that had supported my research: The Cole Foundation, and the National Council for Scientific Research _Lebanon (CNRS).

Thank you to the members of my thesis committee for their scientific knowledge and input. Dr. Lea Harrington (IRIC-UdeM), Dr. Koren Mann (LDI-McGill University), Dr. Aron Schimmer (University of Toronto), Dr. Daniel Zenklusen (UdeM), Dr. Claude Perreault (IRIC-UdeM) as well as Dr. Trang Hoang (IRIC-UdeM). I am forever grateful for the excellent advice.

Dr, Biljana Culjkovic-Kraljacic, our research associate; What would I have done without you? Thank you for your intellectual input, collaborative efforts and guidance. You are the principal source of motivation that has kept me focused and moving forward. Your endless support has

allowed me to work tirelessly. The time I have spent on this thesis was filled with joy and happiness because of your companionship.

I would also like to acknowledge my past and present lab mates (Laurent Volpon, Mike Osborne, Lotfi Amri Abdellatif, Maggie Davis, Luciana Coutinho de Oliveira, Jadwiga Gasiorek, Daria Krutauz, Mildred Delaleau and Sahil Mann) for their help, support and suggestions throughout my Ph.D. Furthermore, I would like to thank all the staff at the histology, genomics and imagery platforms at IRIC. A special tribute to Dr. Sylvie Mader's lab members for always being there and for the fun times we have spent together. Mohammad El Ezzy, your friendship and conversations have gone long ways to preserve my sanity!

My parents Ahmad and Mariam who have given me a lifetime of love and support. Thank you for being so patient throughout this period of my life. You have sacrificed so much in order for me to have amazing life opportunities. Special thanks to my Aunt Fatima Muldowney, without you I would not have accomplished anything. You have shaped me in to a better person with your life advice and knowledge.

Last but not least, I want to thank my siblings (Lama, Zainab, Marwa, Mohammad and Issa) and friends (Mano Jbai, Houssam Ismail, Samir Jlassi, Ahmad Raza, Ahmad Koleilat, Alex Pilon, and Caroline Cote!) for their endless friendship and encouragement. You guys have helped me to remain clear-headed and confident. I love you guys!

Hiba Zahreddine

May 10th 2017

CHAPTER 1

INTRODUCTION

It was probably 2,500 years BC when the first evidence of cancer had been documented in The Papyrus of Edwin Smith, "*a bulging tumour in the breast… like touching a ball of wrappings*". Discussing treatment, the ancient scribe noted: "*There is none*" [(1)]. From the fire drill and natural remedies recommended by ancient Egyptian medicine to our era's most recent concepts of "magic bullet" and "molecular-targeted therapies" [(2)], the cancer matrix remains unlocked. Even though targeted therapy has achieved encouraging results in the treatment of specific types of neoplasms, primary or acquired resistance to chemotherapeutics as well as metastasis of cancer cells remain as two of the main causes of failure in the treatment of patients. It might be that our failure to eradicate most tumours is as fundamental as our lack of understanding to their origin. Had it been the consequence of multicellularity and longer lifespans, then how come not all whales have cancer- given that the more cells we have and the longer we live the higher the risk of developing tumours- a question raised by Peto R. and his colleagues back in 1975 [(3)]. Peto's Paradox depicts that no correlation exists between body size and age with increased cancer risk; rather it is the mere fact that age equals duration of exposure to carcinogenic stimuli. Since then, resolving Peto's Paradox has become the focus for many researchers, as it might hold the key to curing or even preventing cancer. Perhaps evolution of these large organisms had selected for intrinsic cancer suppression mechanisms, such as decreased rates of somatic mutations, redundancy of tumour suppressor genes, shorter telomeres, the presence of hypertumours that grow on and destroy their parent tumour, more efficient immune system and suppression of inflammation, higher resistance to oncogenic viruses, …etc. [(4-6)]. Which of these mechanisms, if any, is/are likely to contribute to the observed suppression remains elusive [(3)]. What is clear is that resolving this paradox might direct towards a better understanding of the molecular mechanisms governing cancer drug resistance and metastasis.

The new era of targeted therapy has proven that the complexity of human cancers can be broken down by targeting a single hijacked oncogene, a phenomenon referred to as "oncogene addiction". This phenomenon allowed initial steps towards a breakthrough in the treatment of tumour cells without affecting their normal counterparts. In my thesis, I aim at understanding the oncogenic dependency of cancer cells on the roles of a protein known as the eukaryotic translation initiation factor 4E (eIF4E) for their survival and metastasis. I demonstrate how eIF4E changes the surface of tumour cells arming them with microvillus-like protrusions that

are enriched with molecules required for invasion, including Hyaluronic acid (HA), CD44, and matrix metalloproteinases, among others. Results from this study provide first evidence of an oncogene that post-transcriptionally regulates the biosynthesis of HA to harness its oncogenic potential. It also suggests that direct targeting of HA-positive tumour cells with available FDA-approved Hyaluronidases could be a valuable addition to treatment regimens for high-eIF4E, and potentially other cancers. In another chapter, I discuss the serendipitous discovery of a novel multidrug resistance mechanism while investigating the molecular underpinnings of the development of resistance to a given eIF4E inhibitor, Ribavirin. I show that elevation of the Sonic Hedgehog transcription factor GLI1 correlates with increased drug glucuronidation which in turn disrupts drug-to-target interaction. Fortunately, I further demonstrate that this mechanism can be reversed using FDA approved Sonic Hedgehog signalling pathway inhibitors.

1.1 The eukaryotic translation initiation factor 4E: a multifaceted protein

In response to environmental signals, cells regulate gene expression and protein synthesis in a coordinated fashion. Compared to corn and fruit fly, the human genome encodes approximately the same or nearly twice the number of genes, respectively. In addition, it has become increasingly clear that the majority of eukaryotic proteins function in different cellular processes. This multitasking phenomenon suggests that, as the number of genes does not proportionally increase with size and complexity of organisms, the eukaryotic regulatory mechanisms therefore act to diversify the proteome by shuffling the limited number of genes to use them in multiple combinations. Indeed, many eukaryotic proteins have been shown to multitask as components of different cellular complexes, the roles of which might differ with subcellular localization. This multitasking phenomenon holds true for the eukaryotic translation initiation factor 4E (eIF4E), which is traditionally known for its function in translation initiation of 5'-capped mRNA in the cytoplasm [7-9]. Recent studies have highlighted a novel role of eIF4E in the nucleus where it regulates mRNA export (**Figure 1**). Accordingly, eIF4E provides an example of a factor that differentially regulates coordinated gene expression patterns.

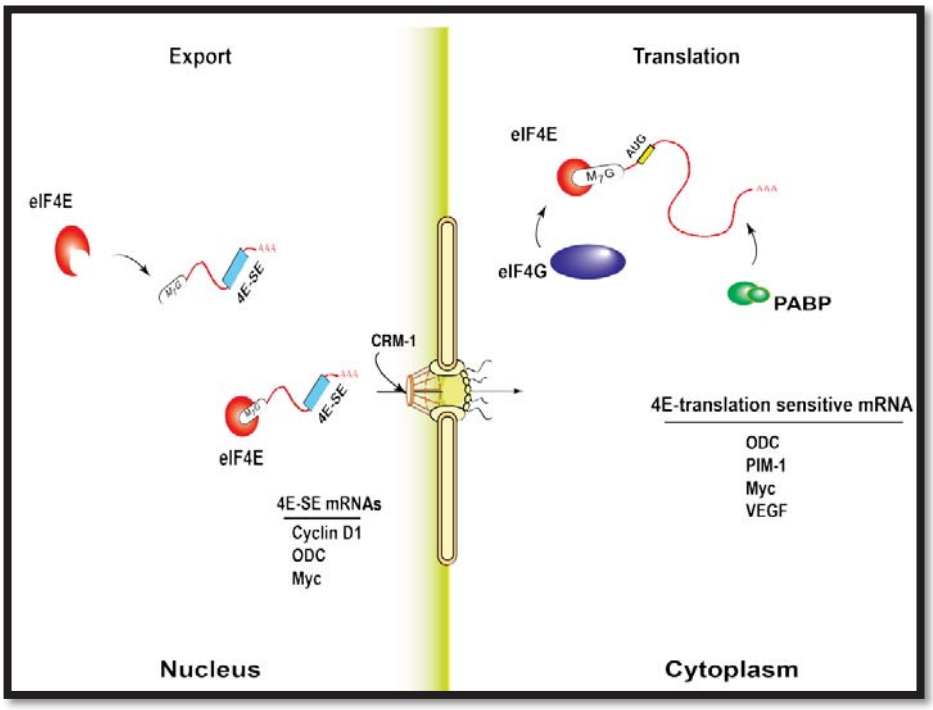

Figure 1: eIF4E regulates mRNA translation and mRNA export. Cytoplasmic eIF4E regulates the translation of mRNAs possessing highly structured GC rich 5'UTRs such as *ODC*, *PIM-1*, *c-Myc*, and *VEGF*. Nuclear eIF4E mediates the export of mRNA molecules containing a unique ~ 50 nucleotides sequence element known as eIF4E-senstivity element (4E-SE), including *Cyclin D1*, *ODC* and *c-Myc*.

1.1.1 Cytoplasmic eIF4E: Initiates mRNA translation

In 1976, *Witold Filipowicz* discovered eIF4E as a cap binding protein involved in cytoplasmic mRNA translation [10, 11]. Here, eIF4E binds the 7-methyl guanosine dinucleotide cap structure m^7GpppN (where N is any nucleotide) located on the 5' end of mRNA [10, 12-14]. Consequently, protein synthesis commences. Sensitivity of given mRNAs to eIF4E's translational activity does not only rely on the binding of eIF4E to the m^7G cap [8, 10, 13, 15]. Overexpression studies have shown that eIF4E does not lead to global increase in protein expression [12, 16]. Analyses indicated that only a given subset of mRNAs possessing highly structured GC rich 5'UTRs have their translation regulated by eIF4E [8, 10, 13, 15]. These mRNAs usually encode for growth and survival factors. Thus when overexpressed, eIF4E disproportionally and dramatically induces the translation of mRNAs encoding for cancer-related proteins that control cell proliferation [8, 13].

1.1.2 Cap-Dependent Eukaryotic Translation Initiation

mRNA translation is the process in which mRNA molecules are decoded to produce specific sequences of amino acids, or proteins [17-19]. It proceeds in three stages: initiation, elongation and termination; with initiation being the rate-limiting step and as such is subject to tight control [20-23]. Translation initiation consists of the recruitment of ribosomes to target mRNA. At least two different mechanisms of ribosome binding have been identified in eukaryotic cells: the cap-dependent and the cap-independent scanning [21, 24, 25]. In this thesis, I focus on the eukaryotic translation initiation factor 4E which is an inherent component of the cap-dependent translation initiation. eIF4E mediates binding of the 40S ribosomal subunit to the 5'end of capped mRNAs in the cytoplasm [18, 20, 21, 23]. Together with eIF4A (an RNA-dependent ATPase/ATP-dependent RNA helicase) and eIF4G (a high molecular weight scaffold protein that binds eIF4E and eIF4A) it forms the eukaryotic translation initiation factor 4F (eIF4F) [18, 20, 21, 23]. Through interaction of eIF4G with the 40S ribosomal binding factor eIF3 and the poly(A)-binding protein, the eIF4F complex forms a critical link between mRNAs and ribosomes [18, 20, 21, 23].

Given that expression of the various eIF4F factors in most cells is readily different, with eIF4E being the least abundant, formation of the aforementioned link therefore relies on the availability of latter [19, 26, 27]. A family of small translation repressor molecules known as eIF4E-binding

proteins (4E-BPs) have been shown to interact with eIF4E and modulate the assembly of eIF4F [28-30]. Binding of 4E-BPs to eIF4E is modulated by phosphorylation [17, 31, 32]. In the presence of hormonal or nutritional stimuli, 4E-BPs are hyperphosphorylated and do not interact with eIF4E allowing for protein synthesis to occur. On the contrary, environmental or nutritional stress elicit hypophosphorylation of 4E-BPs which can now bind strongly to eIF4E thus rendering it unavailable for initiation of mRNA translation. In addition to regulation by signalling pathways via 4E-BPs, eIF4E expression and activity is controlled by transcriptional and posttranscriptional mechanisms, which will be discussed in this chapter.

1.1.3 Nuclear eIF4E: mediates mRNA export

Discovery of the role of eIF4E in catalyzing nucleocytoplasmic export of mRNA has been a major advance. Up to 68% of eIF4E is found in the nucleus of most eukaryotic cell types either in distinct mulitprotein structures known as eIF4E nuclear bodies (NBs) or distributed throughout the nucleoplasm [33, 34]. Electron microscopy studies in Saccharomyces cerevisiae, and later on in Drosophila melanogaster S2 cells and *Xenopus laevis* embryos, also showed nuclear eIF4E localization [35-37]; suggesting that nuclear eIF4E is conserved across eukaryotes.

eIF4E-dependent mRNA export was first reported by *Rousseau et al.* where eIF4E overexpression increased nucleocytoplasmic export but not translation of cyclin D1 [38]. Later studies showed that treatment of eIF4E nuclear bodies with cap but not RNases results in complete release of eIF4E and dispersal of these bodies [39]. As such, similar to its cytoplasmic counterpart, nuclear eIF4E also binds the m^7G cap and that the cap, but not the mRNA per se, is essential for nuclear localization and function of eIF4E [35]. However, cap binding is not the sole determinant of mRNA export mediated through eIF4E; as indicated by the increased export of cyclin D1 but not the housekeeping mRNAs (such as GAPDH) following eIF4E overexpression [38, 40, 41]. Mapping of the 3' and 5'-UTRs identified that the basis for this discriminatory interaction is an approximately 50-nucleotide sequence in the 3'-UTR, which is referred to as eIF4E sensitivity element (4E-SE) [40]. Further, differential display analysis of nuclear eIF4E-associated mRNAs following immunoprecipitation of endogenous eIF4E from nuclear lysates, revealed that among the hundreds of mRNAs many of the identified genes are involved in cell cycle progression and survival, including c-Myc, cyclin E1, Mdm2 and NBS1

[41]. Accordingly, in addition to its role in regulating translation initiation, eIF4E-mediated nuclear export of a specific subset of mRNA also contributes to oncogenesiss.

The functions of eIF4E in mRNA export and translation appear to be decoupled as they rely on different USER codes, i.e. mRNAs require both the 3' 4E-SE and the 5' USER code to be modulated by eIF4E at both levels [12, 41]. For instance, some mRNAs are said to be export targets only (such as cyclinD1), others are translational targets (such as VEGF), and in some cases, mRNAs could possess both USER codes and thus have their export and translation regulated by eIF4E (such as ODC, c-Myc and Pim-1) [12, 41]. According to the RNA regulon model, gene expression is combinatorial, i.e. related to the different USER codes found in a given mRNA [42, 43]. Therefore, through promotion of mRNA export and translation, the eIF4E regulon provides a coordinated and combinatorial way for the cell to more finely tune gene expression. It is one of the earliest examples of an RNA regulon which through coordinately modulating proliferation and survival signal gene expression networks is positioned to directly impact human diseases, including oncogenic transformation; necessitating tight control over its expression and activity.

1.1.4 eIF4E dependent mRNA export goes through a pathway distinct from bulk mRNA export

The molecular basis for the mRNA nuclear export function of eIF4E is less well understood than its role in translation. eIF4E only associates with its target mRNAs post-splicing and the eIF4E-4E-SE RNA complexes are found in the soluble export competent fraction within the nucleus. While the majority of messenger ribonucleoproteins (mRNPs) exit the nucleus using bulk mRNA export pathway, catalyzed by TAP/NXF1 factors, eIF4E mRNPs do not [41, 44]. Treatment of cells with leptomycin B, a specific inhibitor of the nuclear pore receptor chromosome region maintenance 1 (CRM1), inhibited the export of these mRNAs; indicating, that eIF4E-dependent mRNA export is CRM1 dependent (**Figure 2**) [41, 44]. Recently, our lab identified the leucine-rich pentatricopeptide repeat protein C (LRPPPC) as platform for the assembly of eIF4E, 4E-SE mRNA, and CRM1 [44]. Following release of mRNA cargo in the cytoplasm, cap-free eIF4E and 4E-SE-free LRPPRC are recycled back in to the nucleus via Importin 8, a member of the karyopherin family of transporters (unpulished data). Interestingly,

the fact that both LRPPRC and eIF4E use Importin 8 to re-enter the nucleus suggests that their import could be coordinated in a way to increase the efficiency of future export cycles. The molecular mechanisms underlying eIF4E-mediated mRNA export and the specific composition of the eIF4E mRNA export complex are becoming increasingly clear. As such, LRPPRC could be one of several assembly platform proteins involved in the selective export of mRNA subgroups whose expression could be context/cell type specific. Further, a better understanding of the physiological role of the eIF4E-4E-SE RNA complexes is an important area of future work.

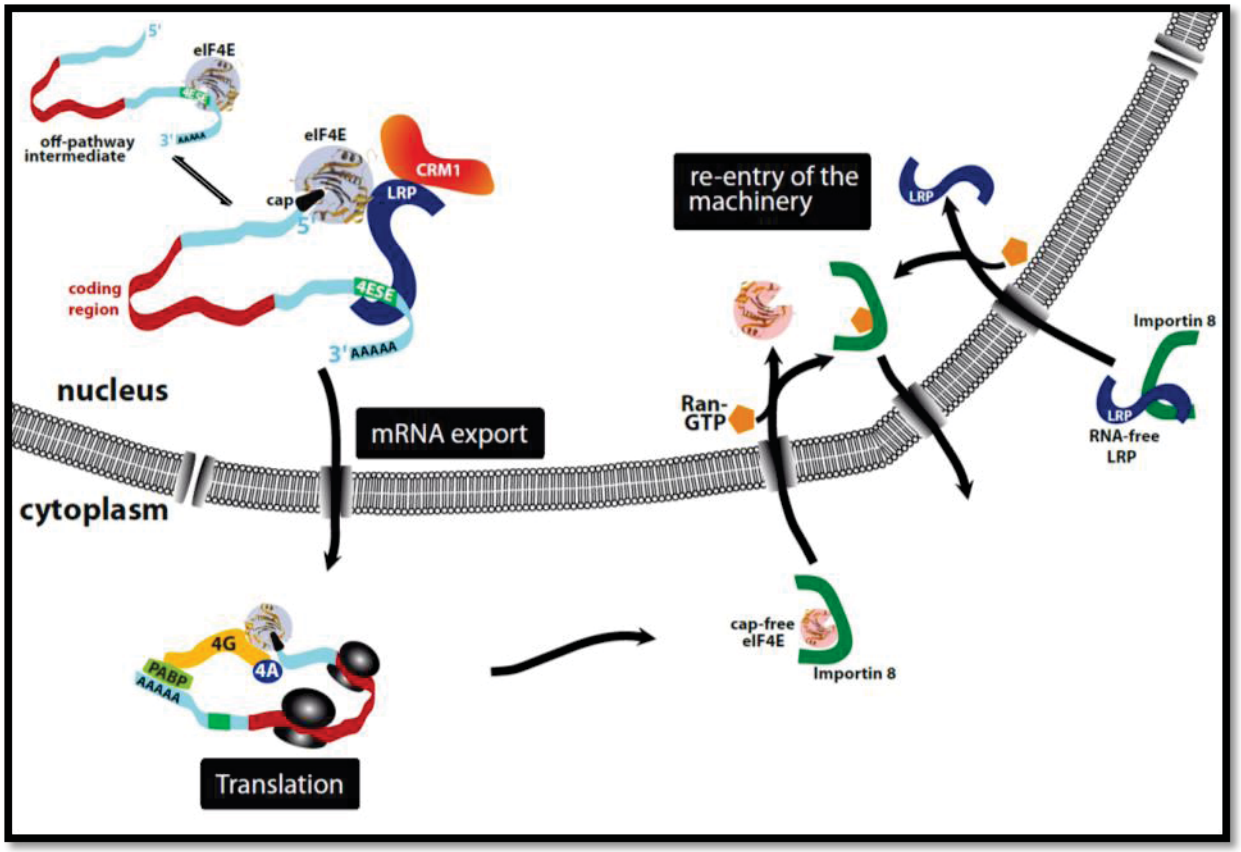

Figure 2: Model for the eIF4E-dependent mRNA export and re-entry of the machinery via importin 8. LRPPRC binds to both eIF4E and 4ESE RNA using distinct N- and C-terminal motifs, and binds CRM1 supporting transit though the nuclear pore complex (NPC). Once the complex arrives at the cytoplasmic side and after the dissociation of 4ESE RNA cargoes, eIF4E and LRPPRC return to the nucleus via Importin 8. Here, Importin 8 only binds cap-free

eIF4Eand RNA-free LRPPRC thereby reducing futile export cycles. (*Taken from Volpon L. et al. RNA 2016*)

1.1.5 eIF4E mRNP traversing the nuclear pore complex

In addition to LRPPRC, eIF4E export mRNPs contain some factors shared with the bulk export pathway, including UAP56, hnRNPA1, and DDX3 [44-46]. Also, in the nucleus CRM1 binds its cargo in the presence of the GTP-bound form of Ran. Accordingly, as the CRM1-Ran GTP-eIF4E mRNP complexes are formed, these are targeted to traverse the nuclear pore complex (NPC) by virtue of the transport receptor interaction with specific NPC-proteins lining the central transport channel, namely Nucleoporins (Nups) [45, 47]. Reaching the cytoplasmic face of NPCs, loading and release of the CRM1-cargo complexes occurs by either one of two mechanisms; (1) docking of the CRM1-cargo complex on cytoplasmic fibrils mainly composed of Nup358 proteins anchored to the NPC via two nucleoproteins Nup88 and Nup214; thus sequestering the CRM1-cargo complex; or (2) binding of CRM1-cargo complexes to a soluble form of nucleoporins known as RanBP1 which provides a fast release mechanism [13, 45]. Either way, association is then followed by the recruitment of Ran GTPase-activating protein (RanGAP) enabling GTP hydrolysis by Ran [13, 45]. Once this step is completed, CRM1-cargo complexes dissociate, permitting the RNA to enter the cytoplasm and the export factors to be recycled back to the nucleus [13, 45, 47]. Note that, in nuclear import, RanGTP acts as a dissociation factor since import factors cannot bind both cargo and RanGTP simultaneously [13, 45, 47]. Hence, RanGTP gradient across the nuclear envelope results in the activation several proteins including the cytoplasmic GTPase-activating protein RanGAP, and is considered the major driving force for nuclear transport in both directions [47, 48]. Importantly, endogenous 4E-SE mRNAs could be targets of both bulk and eIF4E-dependent processes, where 3'-UTRs can be 1000s of nucleotides in length and contain many USER codes [41]. Thus, eIF4E competes with bulk mRNA export pathway to enhance preferentially the export of specific subset of transcripts [13, 45, 46].

1.1.6 eIF4E remodels the nuclear pore

The loading and release options that CRM1 has at the cytoplasmic face of the NPC question whether the link between eIF4E's transforming ability and its mRNA export activity is due to the favoring of RanBP1-mediated fast release over the rate limiting RanBP2-mediated process; and whether eIF4E could be driving this preference. Consequently, would eIF4E upregulation alter the expression and/or localization of NPC components.

Indeed, work presented by *Culjkovic B. et al.* revealed that eIF4E overexpression correlates with changes in the composition of the cytoplasmic face of the NPC [13, 47]. The authors identified RanBP1 but not RanBP2 as a direct export target of eIF4E. As such, the expression of these two proteins is inversely correlated following eIF4E overexpression. While RanBP1 levels are upregulated, eIF4E overexpression indirectly decreases RanBP2 proteins; with the remaining RanBP2 being more dispersed throughout the nucleoplasm. Further, the RanBP2 partner, Nup214, is not a direct eIF4E target but its localization is also altered from rim-concentrated to a more dispersed form throughout the nucleoplasm. Accordingly, these results indicate that eIF4E overexpression does favor a RanBP1 release pathway which enables enhanced mRNA export by promoting release and/or recycling of export complexes. This is consistent with data showing that RanBP2 hypomorph mice, which have genetically lower RanBP2 levels, do not have bulk mRNA export defects but have increased export of specific mRNAs.

Interestingly, eIF4E overexpression may not only change the CRM1-mediated export of 4E-SE mRNAs, but it can also alter the export of a subset of mRNAs using bulk export pathway (mediated by TAP/NXF1) [13, 47]. This occurs via upregulating the expression of DDX19 and its cofactor Gle1 which catalyze the loading and release step of the TAP/NXF1 pathway. These data indicate the presence of a cross talk between RNA export pathways or that the helicase activity of DDX19 is required for remodeling 4E-SE export RNPs. On the other hand, both DDX19 and Gle1 have been shown to play independent roles in the initiation and termination steps of translation of certain mRNAs, indicating that eIF4E can impact on translation in an indirect way, in addition to its direct effects [13, 47]. Thus, eIF4E not only is exported by CRM1 via its interactions with LPRPRC, but also modulates proteins acting in the CRM1 pathway to likely maximize its mRNA export potential.

In conclusion, these observations indicate that eIF4E has the capacity to alter the composition of NPC in favor of increasing its mRNA export and oncogenic activities.

1.2 eIF4E is regulated at multiple levels

Clearly, eukaryotic cells evolved means to regulate different nodes in RNA regulons in order to alter gene expression and prevent deleterious outcomes. Studies aiming to identify regulators of eIF4E expression and activity are still ongoing and regulation can be divided into four levels: transcriptional regulation and regulation through mRNA stability, protein interactions and post-translational modifications (**Figure 3**).

1.2.1 Regulation of eIF4E transcription (Myc, NF-kB)

Dysregulation of eIF4E in cancer is correlated with increased RNA and protein levels (~ 3-to 10-fold in M4/M5 AML specimens relative to normal samples). While c-Myc has long been thought as the sole transcriptional regulator of eIF4E [49-51], recent studies are unveiling novel mediators. Analysis of eIF4E promoter demonstrates enrichment with binding sites for various transcription factors including NF-κB, PU.1, NFAT, GATA, STAT, PAX and SP1 [52-54]. For instance, NF-κB has four putative binding sites (termed κB 1 to 4) in eIF4E promoter [52]. These sites are occupied by a heterodimer comprising two members of the NF- κB family, namely cRel and p65. Binding results in the recruitment of p300 and phosphorylated RNA polymerase II to the κB sites and the coding region, respectively, thus marking transcription activation [52]. This is consistent with the presence of more NF-κB complexes on eIF4E promoter in primary M4/M5 myeloid samples as compared to normal primary hematopoietic cells and other myeloid subtypes [52]. As such, genetic and pharmacological inhibition of NF-κB in this population abrogates eIF4E transcription resulting in downregulation of eIF4E targets [52]. Interestingly, there is a significant overlap between eIF4E target genes and those of NF-κB (such as c-Myc and cyclin D1) which suggests that these two pathways cooperate forming a nexus between transcriptional and posttranscriptional gene expression networks to drive proliferation (Hariri, F unpublished data). Consequently, targeting both nodes, i.e. eIF4E and NF-κB, could have significant clinical utility in cancer patients where both proteins are elevated.

1.2.2 Regulation of eIF4E mRNA stability

Independent of the transcript levels, eIF4E expression is also regulated post-transcriptionally. The 3'UTR of eIF4E mRNA contains three AU rich elements (AREs) that dictate binding of competing proteins, HuR and p42 AUF1, to enhance or reduce eIF4E transcript stability, respectively [44]. As such, HuR is found to be elevated in cancers with high eIF4E levels and its knockdown is associated with downregulation of eIF4E [44].

1.2.3 Regulation of eIF4E activity by protein interactions

eIF4E is subject to additional level of regulation where its activity is tightly controlled via inhibitory or activating binding partners. So far, four classes of direct binding partners have been identified:

i. *Proteins containing conserved eIF4E binding site, such as 4E-BPs, eIF4G, HOXA9 and PRH/Hex* [14, 35]. These proteins share a short conserved amino acid motif YXXXXLϕ, where X is any residue and ϕ is a hydrophobic amino acid. As a result, their binding to eIF4E is said to be competitive to inhibit or enhance its mRNA export and/or translation activity. More than 200 homeodomain proteins containing this consensus binding motif have been identified; suggesting a redundancy in eIF4E regulators as 4E-BP knockout mice, for instance, were not more prone to developing cancers than their normal counterparts.
ii. *RING domain containing proteins including PML, Z-protein, and HHAR1* [55]. This class of binding partners lacks the eIF4E binding motif but possess a RING domain instead. Direct binding of these proteins via the RING domain to eIF4E reduces its affinity to the m^7G cap (~ 100 fold by PML and Z-protein).
iii. *Amphipathic helix strategy used by VpG proteins* [56, 57]. Binding of VpG to eIF4E also reduces its affinity to the m^7G cap but the mechanism by which it does that is still not known.
iv. *Importin 8 binding to eIF4E at its cap-binding site* [48]. This binding selects only RNA-free eIF4E for nuclear entry and represents a new class of interacting partners.

In addition to the aforementioned regulatory modes, novel structural and biochemical functions of an eIF4E family member, eIF4E3, implicating it as a repressor of eIF4E activity via an mRNA

competition mechanism has been identified [58-60]. Here, eIF4E3 competes for the same mRNA pools through a novel cap binding activity which inhibits expression of both mRNA export and translation targets of eIF4E.

1.2.4 Regulation of eIF4E activity by post-translational modifications

Lastly, regulation of eIF4E activity also occurs via post-translational modifications, including phosphorylation, sumolyation and ubiquitination [61-65]. While phosphorylation has been implicated in enhanced eIF4E-mediated mRNA export and increased cell transformation capacity, the role of ubiquitination and sumolyation on eIF4E activity is still ambiguous.

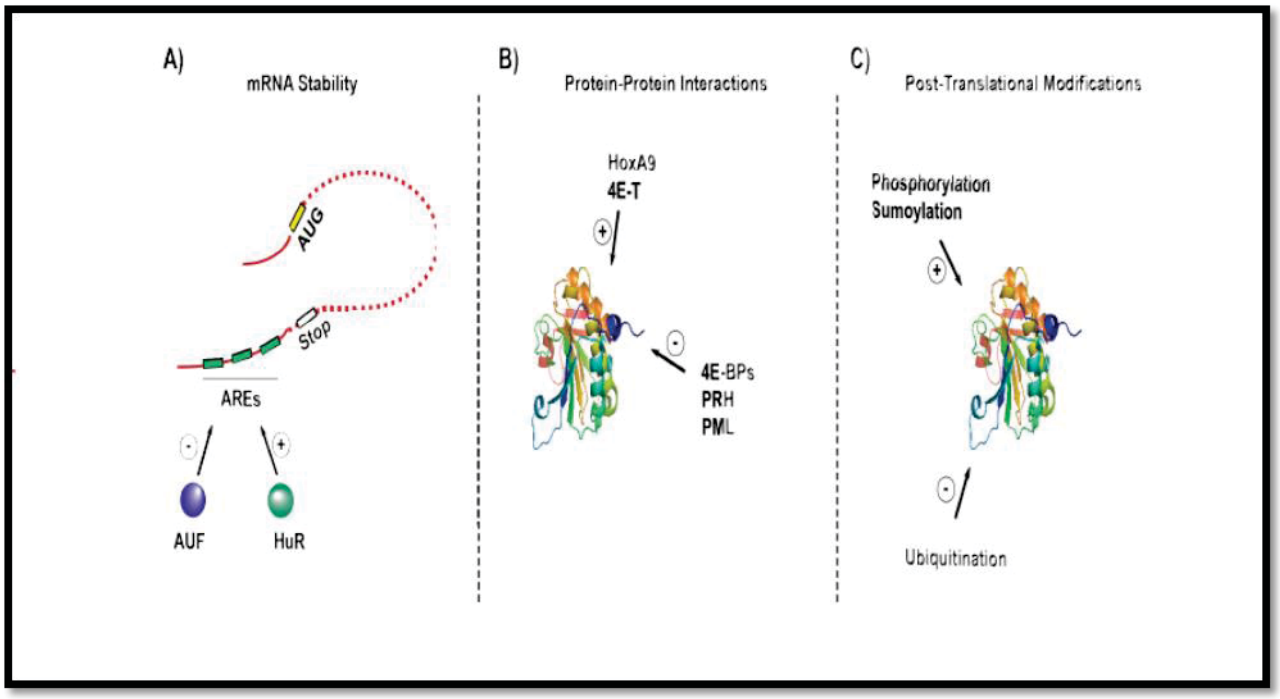

Figure 3: eIF4E is regulated at multiple levels. (A) Regulation of mRNA stability via HuR and AUF proteins which bind to AU rich elements (AREs) in the 3'UTR of the eIF4E transcript **(B)** Regulation of eIF4E activity through protein-protein interactions. For instance, HOXA9 promotes the export and translation functions of eIF4E, while PML and PRH negatively regulate eIF4E-mediated mRNA export **(C)** Regulation by post-translational modifications including phosphorylation, sumolyation and ubiquitination.

1.3 Dysregulation of eIF4E levels in Cancer

Aberrant regulation of eIF4E expression and/or activity has been linked to malignancies as well as cell transformation. The pro-survival properties of eIF4E have been underscored by various evidence. For instance, its overexpression blocks apoptosis upon serum starvation, inhibits c-Myc-driven apoptosis, promotes DNA synthesis, decreases cell cycle transit time and represses differentiation [41, 66-68]. Of which, downregulation of eIF4E reverts these phenotypes. Further, moderate overexpression of eIF4E results in increased production of growth factors that are essential for malignant transformation [10, 69]. And high eIF4E levels have been correlated with oncogenic transformation in cell lines, cancers in animal models and poor prognosis in several human cancers [10, 69]. Approximately 30% of human cancers including: breast, prostate, lung, colon, squamous head and neck carcinoma, Hodgkin and non-Hodgkin lymphomas, as well as M4 and M5 subtypes of acute myeloid leukaemia (AML), have high eIF4E expression [10, 69, 70].

1.3.1 Acute Myeloid Leukemia (AML)

Acute myeloid leukemia is a hematologic malignancy characterized by aberrant proliferation of immature cells (myeloblasts) of the myeloid lineage. It is a particularly challenging malignancy since the majority of patients diagnosed are older than 60 years of age and often cannot receive intensive chemotherapy [70, 71]. The overall survival of such patients has been estimated to be around 4 months, with a five-year survival rate of less than 10%, highlighting the need for new treatments and increasing the interest in developing them [71-73].

1.3.2 The French-American-British classification of AML

According the French-American-British (FAB) system, AML is subdivided into 9 distinct types based on the cell of origin and its level of maturity [74, 75]. It includes: M0 (undifferentiated acute myeloblastic leukemia), M1 (Acute myeloblastic leukemia with minimal maturation), M2 (Acute myeloblastic leukemia with maturation), M3 (Acute promyelocytic leukemia (APL)), M4 (Acute myelomonocytic leukemia), M4eos (Acute myelomonocytic leukemia with eosinophilia) M5a (Acute monoblastic leukemia), M5b (Acute monocytic leukemia), M6 (Acute erythroid leukemia) and M7 (Acute megakaryoblastic leukemia).

1.3.3 The World Health Organization (WHO) classification of AML

A new classification for hematopoietic and lymphoid malignancies has been published recently by the World Health Organization (WHO) [76, 77]. This new system classifies AML into three clinical prognosis groups based on not only morphologic findings but also on available clinical features, and genetic, biologic and immunophenotypic data. These subgroups include: (1) AML with recurrent genetic abnormalities, (2) AML with multilineage dysplasia, and (3) AML and MDS (myelodysplastic syndrome), therapy related.

1.3.4 AML: Aberrant eIF4E expression and activity

eIF4E levels are upregulated in various genetically distinct leukemias [10, 69]. Strikingly, eIF4E overexpression is observed in M4/M5 poor prognosis AML but not in most M1/M2 specimens examined [78]. Inline with this observation, inhibition of eIF4E using low concentrations (10 times less than physiological levels) of the m^7G cap physical mimic, Ribavirin, leads to growth inhibition in M4/M5 but not normal or M1/M2 AML specimens which are inhibited at much higher levels [78, 79]. Interestingly, not only the levels of eIF4E are upregulated in M4/M5 AML cells but also its nuclear localization is predominantly augmented [47, 48, 71, 73]. This correlates with increased eIF4E-dependent mRNA export [40, 69, 79]. Accordingly, both the mRNA export and translation initiation activities are required for eIF4E-mediated malignant transformation. And these findings suggest that AML cells have developed an oncogenic dependency to eIF4E for their proliferation and survival.

1.4 Targeting eIF4E with Ribavirin in Cancer

Collectively, targeting eIF4E should have a major impact on tumorigenesis and cancer progression and as such has derived interest in identifying therapeutic agents that could directly or indirectly target its aberrant activation. Indeed, several preclinical and clinical methods have been defined including (i) anti-sense oligos targeting eIF4E in xenograft models [80-82], (ii) synthetic peptides inhibiting the interaction of eIF4E with proteins involved in translation, such as eIF4G using 4EGI-1 to block formation of the eIF4F complex in T-cell leukemia and non-small-cell lung cancer cells [83], (iii) suicide gene therapy characterized by fusing a complex 5'UTR upstream of the toxic thymidine kinase (TK) gene as a way to promote its expression in

eIF4E overexpressing cells in mouse xenograft models [84], and (iv) using a cap mimetic, known as Ribavirin [71, 73, 79, 85, 86].

1.4.1 Ribavirin suppresses eIF4E mediated transformation by physical mimicry of m7G cap

Ribavirin (RBV) is an FDA approved antiviral drug used for the treatment of patients with hepatitis C virus [71, 73, 79]. It belongs to a family of nucleoside drugs and has a structure that is closely related to guanosine. RBV is imported into cells using the equilibrative nucleoside transporter 1 (ENT1) which mediates facilitated bidirectional diffusion of nucleosides across cell membranes. In order to stay in the cell, ribavirin is phosphorylated in a three-steps reaction to its major intracellular metabolite, ribavirin- 5'-triphosphate (RTP); where the rate-limiting enzyme is adenosine kinase (ADK) catalyzing step one [87]. *In vitro* biophysical assays identified RTP as a physical mimic of m^7G cap and ultimately as a direct inhibitor of eIF4E [79, 86].

Direct binding of RTP to eIF4E has been shown by fluorescence, circular dichroism, mass spectrometry, nuclear magnetic resonance (NMR) and cap chromatography with affinities for eIF4E similar to that of cap [79, 86]. 1H-15N chemical shift mapping studies at low eIF4E and RTP concentrations are consistent with the high affinity binding previously reported. Chemical shift perturbations indicate that binding is located around the m^7G cap binding site, which is consistent with the model that RTP competes for m^7G cap binding. Further evidence for this is supported by the W56A cap-binding mutant which reduces RTP affinity for eIF4E by ~ 15-fold similar to the effects for cap; additionally, amide chemical shifts for W56A eIF4E mutant are not perturbed upon addition of RTP, indicating loss of interaction. Similar to m^7G cap, RTP binding perturbs peaks at the dorsal surface: although different residues are perturbed. Whether RTP binding can affect proteins binding at the dorsal surface different to m^7G cap has to be determined but these data suggest this is possible. Finally, although NMR data indicate binding is close to the m^7G cap binding site: it is likely not identical. Other binding sites in the eIF4E cap binding site have recently been exploited by structure based drug design efforts. These indicate that there are sites deeper in the cap binding pocket available for binding. Unfortunately, efforts to solve the eIF4E-RTP structure are hindered by the concentration dependence in this interaction. Both X-ray and NMR techniques require high eIF4E/RTP concentrations, yet NMR data indicate that only at lower concentrations the high affinity complex can be observed.

In living cells, immunoprecipitation studies show that ^{3}H-ribaivirin directly binds eIF4E in treated cells versus IgG controls [69, 87]. Note that low micromolar levels of RTP are readily achievable intracellularly which is within the range for its dissociation constant for eIF4E and achievable clinically. Further, treatment is associated with reduced association of endogenous eIF4E with its mRNA export targets in nuclear lysates [79]. These experiments strongly suggest that ribavirin directly binds eIF4E, in or near the cap-binding site, successfully competing for cap binding *in vitro* and in living cells. Effects of ribavirin treatment are similar to those observed by genetic knockdown of eIF4E. Phenotypically, it impedes growth of eIF4E dependent xenografts, impairs growth of eIF4E mediated foci formation and eIF4E mediated apoptotic rescue of serum-deprived fibroblasts and leads to cell cycle arrest, rather than apoptosis, at least in the contexts examined thus far [71, 73, 79, 85, 88]. At the molecular level, inhibition of eIF4E with ribavirin correlates with reduced expression of eIF4E target genes, re-localization of nuclear eIF4E to the cytoplasm and inhibition of the nuclear functions of eIF4E [35, 71, 79]. Biochemically, ribavirin reduces the translation efficiency of transcripts that are enhanced by eIF4E such as VEGF and ODC and inhibits eIF4E dependent nuclear mRNA export [71, 79, 87, 88].

Treatment of M4/M5 AML specimens with 1-10 μM ribavirin leads to significant impairment of colony growth in methylcellulose [79, 85]. Importantly, ribavirin, at this concentration range, does not substantially affect the growth of normal CD34+ cells or blasts isolated from M1/M2 AML patients which had normal eIF4E levels as verified by western and/or RNA analysis. Ribavirin affects growth of these latter groups only in the 100+ micromolar range [79]. These studies strongly suggest that M4/M5 AML specimens have developed an oncogene addiction to, or dependency on, eIF4E. This is consistent with findings that prostate cancer cells with elevated eIF4E were more sensitive to knockdown of eIF4E than normal cells [81].

1.4.2 Ribavirin treatment targets eIF4E and leads to clinical benefit in poor prognosis AML patients

Ribavirin treatment beneficially impacted M4/M5 AML patients in clinical trials. A phase II clinical trial was carried out to monitor the response to ribavirin monotherapy in refractory and relapsed patients as well as patients unable to undergo traditional chemotherapy regimens [71].

In this trial, ribavirin achieved significant clinical responses including one complete remission, two partial remissions, two blast responses and four stable diseases out of 11 evaluable patients. No therapy related toxicities were observed for any patients in the trial, even after 9 months of treatment [71]. Molecularly, beside dramatic re-localization of eIF4E to the cytoplasm in specimens from patients that responded, striking reduction in eIF4E mRNA and protein levels after 28 days are observed. Both reduction of eIF4E and its re-localization led to a phenotype nearly indistinguishable from normal cells (in terms of eIF4E) [71]. Continuous culturing of FaDu or THP-1 cell lines in ribavirin for over 200 days does not lead to any reduction in eIF4E levels [87] nor was this observed in shorter treatment times in cell lines tested. Thus, the reduction of eIF4E is surprising but likely yields unexpected clinical benefit. Further, substantial reduction in cyclin D1 and NBS1 proteins levels, reduced phospho-Akt levels, as well as inhibition of NBS1 and cyclin D1 mRNA export in specimens from responding patients is observed, which is consistent with inhibition of eIF4E activity and reduction in its levels. In summary, ribavirin targets eIF4E within the first 28 days of treatment and this correlates with clinical response.

1.4.3 Ribavirin combination therapy for AML treatment

Although substantial clinical benefit to ribavirin monotherapy is observed in patients; it is important to increase the frequency and duration of clinical responses. Accordingly, combination of ribavirin with known chemotherapy regimens is examined. Results of this trial are presented in **chapter four** of this thesis. *In vitro* studies of combination therapies suggest that ribavirin will cooperate with a wide variety of commonly used agents [85]. Thus, ribavirin may become a commonly added adjuvant to many treatment regimens.

1.5 Ribavirin resistance and non-responding patients

Unfortunately, despite the significant clinical responses that ribavirin has achieved in poor prognosis M4/M5 AML patients, loss of clinical response around 4 months of treatment was observed for most of the patients (with the exception of one patient which continued to respond for 9 months). As such, one of the aims of my thesis was to investigate the molecular mechanism(s) underlying ribavirin resistance. This work is presented in details in **chapter three**. Briefly, we have identified a novel mechanism of resistance whereby upregulation of the Sonic Hedgehog transcription factor GLI1 results in increased glucuronidation of ribavirin

which consequently can no longer bind eIF4E. We provide evidence that this mechanism of resistance can be reversed using the FDA approved inhibitor of the Sonic Hedgehog pathway, GDC-0449 (also know as Vismodegib). Ribavirin and GDC-0449 combination is currently being tested in a phase I clinical trial in M4/M5 AML patients.

More insights about the mechanisms of cancer drug resistance are provided in **chapter two**.

1.5.1 The Hedgehog Signalling Pathway in Cancer Treatment Resistance

The Hedgehog (HH) signalling pathway is evolutionary conserved from insects to vertebrates [89]. It is considered as a key regulator of embryonic development and is required for cell proliferation, differentiation, tissue patterning, maintenance of stem cells, and tissue repair and regeneration [90, 91]. However, it has a second-much darker side. It promotes growth and proliferation of tumour cells. Aberrant HH activity is reported in various types of human cancers including, brain, breast, lung, colon, prostate, pancreas, skin, melanoma, lymphoma and leukemia [90, 92].

1.5.1.1 Molecular Mechanism:

Canonical HH signalling is a complex pathway involving a multitude of factors. However, the key core players are few, including Hedgehog secretory glycoproteins (HH), PATCHED (PTCH) a 12-transmembrane receptor protein, SMOOTHENED (SMO) a serpentine transmembrane signal transducer, and the glioma-associated GLI family of transcription factors [90, 91, 93-95]. Vertebrates express three HH homologues, Desert Hh (Dhh), Sonic Hh (Shh) and Indian Hh (Ihh) [89, 90]. All three of which activate the same signalling pathway yet their expression is tissue-specific, with Shh being more broadly expressed than Ihh and Dhh [89, 90]. In the absence of secreted Hh glycoproteins, PTCH binds to and inhibit the activity of SMO thus repressing signal transduction. Upon binding of Hh ligand to its PTCH receptor, SMO repression is alleviated triggering the release of cytoplasmic GLI transcription factors from the repressive grip of the negative regulator Suppressor of Fused (SUFU) and their activation through sequential phosphorylation by various kinases. As a result, activated GLI proteins translocate into the nucleus where they induce or repress transcription of target genes. At least three GLI proteins exist in vertebrates [93, 95]. While GLI-1 and GLI-2 act primarily as activators

(with GLI-1 being a stronger activator than GLI-2 which in turn enhances the transcriptional activity of GLI-1), GLI-3 can undergo proteolysis to function as a transcriptional repressor. As such, the ratio of GLI activator to repressor is critical for the final transcription process [91, 92, 94, 96]. Further, Hh signalling undergoes both positive and negative autoregulatory feedback loops through controlling the expression of its core components, GLI and PTCH, respectively. Termination of HH signalling follows the proteasome-mediated degradation of activated GLI-proteins. Several studies showed that degradation could be achieved by three independent ubiquitin pathways: cullin 1 (CUL1) mediated β–TrCP E3 ubiquitin ligase, CUL3/SPOP and Numb/Itch mediated ubiquitination [97]. Canonical GLI target genes include, cyclin D1 (involved in cell cycle), vascular endothelial growth factor (VEGF) (involved in angiogenesis), *SNAIL* (involved in epithelial-mesenchymal transition (EMT) in cancer invasion) and Bcl2 (anti-apoptosis pathway) [90, 93, 96].

Further, non-canonical or oncogene-driven HH signalling pathway have been described. These pathways bypass the requirement of HH proteins and rely on major human oncogenes (e.g. EGF, AKT, and RAS), tumour suppressors (e.g. p53 and PTEN) or chromosomal translocation gene fusion products (e.g. EWS-FLI1) to regulate GLI activity [98].

1.5.1.2 HH signalling in cancer

HH signalling is central to various types of human cancers. In addition, increasing evidence indicates the importance of HH signalling in regulating cancer treatment resistance [99, 100]. For instance, GLI-1 overexpression is correlated with glioma recurrence after chemotherapy with Vincristine, VP16, ACNU and CDDP [100]. In addition, GLI-1 overexpression disrupts the activation of genotoxin-driven ATR-Chk1 checkpoint signal transduction pathway which regulate apoptosis, cell cycle progression and DNA repair [101]. Further, constitutive activation of the HH pathway in AML, and other cancers, stimulates the expression of multidrug resistant transporter system (MDR) which results in enhanced drug efflux from cancer cells [99, 100, 102]. The reason underlying the importance of HH signalling in cancer is not trivial but could explained by the basic role of this pathway in controlling stemness and multipotency or as a consequence of the GLI code integrating HH and non-HH signals [90, 103, 104]. Four basic models have been proposed for the activation of HH signalling pathway in cancer [90, 103, 104].

-Type I-Ligand independent constitutive activation of HH signalling*:* includes

(i) Loss-of-function mutation of negative regulators of HH signalling, such as loss f function and/or loss of heterozygosity of PTCH, loss of function mutation of SUFU and mis-sense mutation of GLI3.

(ii) Gain-of-mutation or amplification of activators, such as amplification of GLI-1 and GLI-2, and activating mutation of SMO.

-Type II-Ligand dependent autocrine activation of HH signalling*:* characterized by increased expression of HH proteins triggering auto-activation of HH pathway.

-Type III-Ligand dependent paracrine activation of HH signalling*:* characterized by increased secretion of HH proteins by tumour cells to induce signalling in neighboring stromal cells which in turn secrete factors essential for tumour growth including VEGF, Insulin-growth factor 2 (IGF2) and Wnt. Type III can also be reversed paracrine whereby stromal cells Hh ligands to activate tumours cells.

-Type IV-Cancer stem model*:* characterized by elevated HH signalling in a subpopulation of tumour cells known as cancer stem cells possessing a self-renewal ability.

Recent clinical studies indicate that targeting HH signalling pathway with small molecule inhibitors can have far-reaching implications in HH-dependent tumours. To date, inhibitors of HH (e.g. Robotnikinin), SMO (e.g. GDC-0449) and GLI proteins (e.g. GANT-61) have been the major focus of chemotherapies that target HH pathway-dependent cancers. For instance, phase I clinical studies of GDC-0449 in patients with basal cell carcinoma and medulloblastoma have highlighted significant response. And given its specificity for the HH pathway and its low toxicity, GDC-0449 is currently being evaluated in a phase II clinical trial for the treatment of solid tumours and may also be used in combination treatment with conventional chemotherapy or with inhibitors of activated oncogenes driving GLI activity.

1.5.2 Glucuronidation mediated by UGT enzymes

Glucuronidation is a major phase II detoxification reaction responsible for the inactivation of endogenous molecules and xenobiotics including therapeutic drugs [105, 106]. It was originally discovered in hepatic cells but evidence demonstrate that most human tissues express the enzymes catalyzing this process, known as UDP-glucuronosyltransferases (UGTs) [107, 108]. Namely, UGTs mediate transfer of glucuronic acid (GA) from the cofactor uridine 5'-diphosphoglucuronic acid (UDPGA) to the nucleophilic part of the drug (including amine, carbonyl, carboxyl, sulfuryl and hydroxyl groups) thus rendering it more hydrophilic. The most common glucuronidation reactions consist of *N*- and *O*-linked glucuronidation through conjugation of phenols, carboxylic acid, aliphatic alcohols, thiols and amines. Consequently, the resulting metabolites are excreted via anion transporters [105, 106]. However, efflux is not the only fate of glucuronides. For instance, glucuronidation has been shown to alter targeting [105, 109].

Eukaryotes have evolved to express four subfamilies of UGT enzymes, UGT1A, UGT2, UGT3 and UGT8. While UGT2 subfamily primarily conjugates endogenous compounds, UGT1A mainly metabolizes exogenous ones. Glucuronidation by UGT3 and UGT8 does not appear to contribute to drug inactivation [110, 111]. Accordingly, the major focus of this thesis is the UGT1A subfamily. We have identified that GLI-1-mediated glucuronidation of Ribavirin, among others, is namely catalyzed by UGT1A enzymes.

UGT1A subfamily includes nine functional isoforms (UGT1A1 and UGT1A3-10) encoded by a single gene locus comprising 5 exons; with exon 1 encoding the variable N-terminal substrate binding domain and exons 2-5 coding for the common C-terminal UDPGA binding domain [106, 110, 111]. Recently, a novel UGT1A isoform known as UGT1A_i2 has been identified as an alternative splice product of exon 5 [112, 113]. The resulting protein is truncated and inactive but is demonstrated to interact with and inhibit the activity of UGTs. Given the highly divergent N-terminal domain, substrate specificity varies among the different isoforms; with some accepting a wide variety of structurally unrelated substrates, while others having strict specificity [112, 113]. Predominantly, UGTs are localized to the ER membrane, with few reports demonstrating its localization to the nuclear envelope [114]. Synthesized as pre-proteins possessing endoplasmic

reticulum (ER) signal peptide sequence, UGT enzymes are embedded in the ER membrane via a single transmembrane spanning domain located near the C-terminus which in turn protrudes into the cytosol while the N-terminal domain extends in the lumen of the ER. It has been postulated that UGTs function as homo/hetero- dimers/tetramers in the ER [115, 116]. But in the absence of pure full length active proteins, and the lack of structural information regarding the amino-terminal domain and the binding of UDPGA to the C-terminus, validation of the oligomerization phenomenon is hindered. Expression of UGTs is controlled by several transcription factors (e.g. hepatic nuclear factors, HNF1α and HNF4α) and ligand-activated nuclear receptors in response to endo- and xenobiotics (e.g. aryl hydrocarbon receptor, AhR, the constitutive androstane receptor, CAR, and the peroxisome proliferation-activated receptor, PPARγ) ([106, 110, 111].

1.5.2.1 UGTs in Carcinogenesis

The role of UGT enzymes in cancer is discussed in details in **chapter five**.

1.6 eIF4E in cancer invasion and metastasis

eIF4E overexpression and activity promotes metastasis and increased tumour invasion [85, 117, 118]. For instance, high eIF4E levels are observed in vascularized malignant ductules of invasive breast carcinomas and are predictive of increased recurrence in head and neck squamous cell tumours [85, 117-120]. Further, eIF4E levels are correlated with increased number of tumours, invasion and metastases in xenograft mouse models. Consequently, knockdown of eIF4E or its pharmacological inhibition with ribavirin is shown to reduce breast cancer cell migration and metastasis [118].

The role of eIF4E in tumour metastasis has so far been linked with increased expression and activity of the extracellular matrix (ECM) degrading enzymes, matrix metalloproteinases (MMP)-3 and MMP-9, and the angiogenesis promoting factor, vascular endothelial growth factor (VEGF) [118, 119]. However, reduction in MMPs and VEGF expression and activity following treatment with ribavirin is only partly responsible for the observed decrease in the invasiveness of high eIF4E cancer cells; suggesting that modulation of additional factors is

required. In an attempt to identify proteins associated with the metastatic phenotype of such tumours, I (or we) identified that eIF4E coordinately modulates the expression of several enzymes involved in the synthesis of Hyaluronic Acid (HA) and its major receptor CD44. Increased HA and CD44 levels are associated with malignant phenotype and poor prognosis in several types of cancers. Results of this part of my thesis are discussed in details in **Chapter eight**.

1.6.1 The metastatic cascade:

Escape of malignant cells from primary tumour sites and lodgement at distant secondary organs is a complex multistep process involving: (i) angiogenesis of the tumour (ii) detachment of neoplastic cells from primary tumour (iii) local invasion of the ECM (iv) intravasation into lymphatic or blood vessels (v) survival of cells in circulation (vi) extravasation from vasculature into secondary organ tissue (vii) invasion of ECM and finally (viii) colonization and growth of secondary tumour [121, 122]. During this process only a few cells have the potential to become motile and of those that do only a small number (less than 0.1%) can give rise to secondary tumours. These cells often show resistance to adverse conditions (surveillance by the immune system, nutrient shortage, tumour hypoxia as well as chemo- and radio-therapies) and must have the ability to self-renew and differentiate in order to produce secondary tumours [121, 122].

Successful metastasis relies on the formation of a series of interactions between the cancer cell and its surroundings necessary for motility. Accordingly, cancer cells must undergo a process known as epithelial-to-mesenchymal transition (EMT) whereby the activation of multiple interconnected transcription factor networks (including Wnt, Notch, Sonic Hedgehog and NF-κB) leads to altered expression of proteins that are part of the ECM, secreted in the ECM or cell surface receptors required for invasion [121, 122].

1.6.2 Hyaluronic Acid is required for EMT of cancer cells

The glycosaminoglycan (GAG) hyaluronic acid, also known as hyaluronan, is a major constituent of the pericellular and extracellular matrix in most mammalian tissues [123, 124]. It regulates various cellular processes including embryonic development, tissue homeostasis, wound healing and inflammation and promotes tumour growth, invasion and EMT [123, 124]. In

cancer, increased HA levels are correlated with formation of less dense matrices to facilitate invasion and promote angiogenesis and it has been predicted to mediate the assembly of protective coating for cancer cells to help evade chemotherapeutic and cytotoxic agents. Further, HA levels are elevated in highly metastatic and poor prognosis tumours [124-126].

1.6.2.1 HA structure and synthesis

HA is a large unbranched negatively charged polysaccharide composed of repeating disaccharide units (2,000-25,000), glucuronic acid and *N*-acetylglucosmaine [-β(1,4)-GlcUA-β(1,3)-GlcNAc-]$_n$. Unlike other GAGs which are synthesized as proteoglycans in the endoplasmic reticulum and Golgi apparatus, HA synthesis is catalyzed by one of three multipass transmembrane proteins, hyaluronan synthases (HAS1, HAS2 and HAS3) located in the plasma membrane [124]. As a result, HA is extruded on the cell surface or into the ECM while its being synthesized. HA chain length is associated with differential functions where shorter chains are primarily synthesized by HAS3, which we show is an eIF4E target whereas HAS1 and HAS2 are not. These shorter forms of HA are associated with malignant phenotypes. Experimental overexpression of HAS enzymes causes increased tumour growth in mouse xenograft of prostate, breast and colon carcinomas and its knockdown with antisense mRNAs reverses this phenotype [127, 128]. Further, HA is cleaved by hyaluronidases (six isoforms exist in humans) which have been suggested to act as tumour suppressors; whereby increased expression inhibits tumour growth in colon and breast xenografts [129-131]. These data strongly support the requirement of elevated levels of short-chain HA for tumour progression.

1.6.2.2 HA-induced signal transduction

HA exerts its effects through binding to specific cell surface receptors, namely CD44, thus triggering downstream signal transduction cascades essential for EMT [124]. Together high levels of HA and its receptors are linked to cancers of circulating cells and those of solid tumours [124].

CD44 is a multistructural and multifunctional cell surface glycoprotein involved in mediating cell-to-cell or cell-to-ECM communication [38, 132, 133]. It is encoded by a single gene locus comprising 20 exons and contains an ectodomain (encoded by exons 1-17), a transmembrane domain (encoded by exon 18) and a cytoplasmic domain (encoded by exons 19 & 20). As a

result of alternative splicing and *N*- or *O*-linked glycosylation, a large array of CD44 isoforms (more than 20) exists ranging in size from 80 to 200 KDa. The smallest isoform, known as standard CD44 (CD44s), 80 KDa in size, is the most widely spread isoform where its expressed on the surface of most vertebrate cells, including hematopoietic stem and progenitor cells. Expression of CD44 variant isoforms is controlled by tissue- and environmental-specific factors as well as oncogenic pathways which can regulate alternative splicing of CD44 [38, 132, 133].

Binding of HA to the amino-terminal HA binding site located in the ectodomain of CD44 triggers three major molecular events that regulate migration and invasion of cancer cells. First, it is reported that in response to HA binding, CD44's cytoplasmic tail interacts with several regulatory and adaptor molecules in a cell context-dependent manner, including SRC, RHO GTPases, GAB1, and the cytoskeletal ERM proteins (ankyrin and ezrin, radixin and moesin); thus activating downstream singling cascades favoring motility [132-134]. For instance, interaction of CD44 with ERM proteins, which are known to regulate cell shape and migration, links the plasma membrane to the actin cytoskeleton which is an essential step for migration. Second, following HA binding, the 'spliced-in' regions of CD44 are shown to form specialized platforms for the recruitment of ligands essential for various signalling events, such as matrix metalloproteinases (MM9 and MMP7), osteopontin and fibroblast growth factors [135-138]. While recruitment of MMP9 is required for degrading the ECM, MMP7 binding suppresses apoptosis through activating ERBB4 (also known as HER4) receptor tyrosine kinase pathway that signals for cell survival [138]. In addition, interaction of CD44 with osteopontin is shown to promote survival [132, 133]. Third, binding of HA to CD44 is linked to CD44 oligomerization and association with lipid rafts known as glycolipid-enriched microdomains (GEMs) [139]. Oligomerization is thought to occur via a short motif composed of 23 hydrophobic residues and 1 cysteine amino acid located within the transmembrane domain of CD44 [132]. The GEM association of CD44 oligomers is required for activation of the aforementioned CD44-mediated downstream signalling and has been also linked to the function of CD44 as a coreceptor. Here, CD44 binds and activates several growth factor receptors essential for invasion, including the epidermal growth factor receptor, EGFR, Grb2, and p185Her2, c-Met, ErbB, TGFβ receptors 1 and 2, and VEGF-2 [38, 132, 133].

1.6.2.3 HA mediates that formation of cell surface protrusions

Consistent with the observed oligomerization of CD44 receptors and the enrichment of proteins and co-receptors essential for the invasion process at the plasma membrane following activation by HA binding, studies have shown that increased expression of endogenous and exogenous HAS3 induces the growth of microvillus-like cell surface protrusions [127, 128]. These protrusions do not require attachment to a given substratum but rather utilize HA coat as an extracellular scaffold mediating cell growth, invasion and metastasis. Evidence show that despite the presence of CD44 in HAS3-induced protrusions, inhibition of CD44 activity with blocking antibodies or siRNA-mediated knockdown of CD44 does not affect the formation of these protrusions; suggesting that this particular activity is CD44 independent. It is noteworthy that neither CD44 nor HA alone can induce cell migration; rather an interaction between the two is necessary to activate this process [140]. Also, loss of CD44 activity or expression has been shown to reduce cancer cell invasion in *in vitro* matrigel assays and animal models [141-143]. These data indicate that CD44-HA dependent and/or independent functions are essential for downstream signalling post-protrusion formation (described in the previous section 1.6.2.2). Thus, identifying factors regulating HA synthesis and CD44 expression could provide a therapeutic means to prevent cancer cell metastasis.

Hypotheses and Aims

- **Project I (Chapter 2-7):**

  -Title: *The Sonic Hedgehog Factor GLI1 Imparts Drug Resistance through Inducible Glucuronidation*

  -Hypothesis: *The sonic hedgehog transcription factor GLI1 drives laboratory and clinical resistance to ribavirin by altering gene expression leading to chemical modification of ribavirin thereby blocking its interaction with eIF4E*

  -Aim 1: *Assess the role of Gli-1 in conferring resistance to ribavirin*
  -Aim 2: *Assess the role of UGT1A family depletion in conferring resistance to ribavirin*
  -Aim 3: *Determine the fate of ribavirin in resistant cells*

- **Project II (Chapter 8):**

  -Title: *The eukaryotic translation initiation factor eIF4E drives production of hyaluronan*

  -Hypothesis: *eIF4E impacts invasion and metastasis by reshaping the surface of migrating cells through regulating the synthesis of hyaluronic acid and the expression of its receptor CD44*

  -Aim 1: *Investigate the role of eIF4E in the synthesis of hyaluronic acid and its receptor CD44 and assess its effects on protrusion formation and tumour invasion*

  -Aim 2: *Examine the effects of eIF4E dependent alterations of HA and CD44 synthesis on AML cell lines with dysregulated eIF4E (THP-1 and MonoMac-6)*

  -Aim 3: *Examine the effects of eIF4E dependent alterations of HA and CD44 synthesis on metastasis of breast cancer cell lines in mouse models*

References

1. Mukherjee, S., *The emperor of all maladies : a biography of cancer*. 1st Scribner hardcover ed. 2010, New York: Scribner. xiv, 571 p., 8 p. of plates.
2. Chen, S.J., et al., *From an old remedy to a magic bullet: molecular mechanisms underlying the therapeutic effects of arsenic in fighting leukemia.* Blood, 2011. **117**(24): p. 6425-37.
3. Leroi, A.M., V. Koufopanou, and A. Burt, *Cancer selection.* Nat Rev Cancer, 2003. **3**(3): p. 226-31.
4. Caulin, A.F. and C.C. Maley, *Peto's Paradox: evolution's prescription for cancer prevention.* Trends Ecol Evol, 2011. **26**(4): p. 175-82.
5. Ducasse, H., et al., *Can Peto's paradox be used as the null hypothesis to identify the role of evolution in natural resistance to cancer? A critical review.* BMC Cancer, 2015. **15**: p. 792.
6. Nagy, J.D., E.M. Victor, and J.H. Cropper, *Why don't all whales have cancer? A novel hypothesis resolving Peto's paradox.* Integr Comp Biol, 2007. **47**(2): p. 317-28.
7. Hsieh, A.C. and D. Ruggero, *Targeting eukaryotic translation initiation factor 4E (eIF4E) in cancer.* Clin Cancer Res, 2010. **16**(20): p. 4914-20.
8. Mamane, Y., et al., *eIF4E--from translation to transformation.* Oncogene, 2004. **23**(18): p. 3172-9.
9. Osborne, M.J. and K.L. Borden, *The eukaryotic translation initiation factor eIF4E in the nucleus: taking the road less traveled.* Immunol Rev, 2015. **263**(1): p. 210-23.
10. Carroll, M. and K.L. Borden, *The oncogene eIF4E: using biochemical insights to target cancer.* J Interferon Cytokine Res, 2013. **33**(5): p. 227-38.
11. Filipowicz, W., et al., *Polypeptide chain initiation in eukaryotes: initiation factor requirements for translation of natural messengers.* Proc Natl Acad Sci U S A, 1976. **73**(1): p. 44-8.
12. Culjkovic, B., I. Topisirovic, and K.L. Borden, *Controlling gene expression through RNA regulons: the role of the eukaryotic translation initiation factor eIF4E.* Cell Cycle, 2007. **6**(1): p. 65-9.

13. Culjkovic-Kraljacic, B. and K.L. Borden, *Aiding and abetting cancer: mRNA export and the nuclear pore.* Trends Cell Biol, 2013. **23**(7): p. 328-35.
14. Sonenberg, N. and A.C. Gingras, *The mRNA 5' cap-binding protein eIF4E and control of cell growth.* Curr Opin Cell Biol, 1998. **10**(2): p. 268-75.
15. Cawley, A. and J. Warwicker, *eIF4E-binding protein regulation of mRNAs with differential 5'-UTR secondary structure: a polyelectrostatic model for a component of protein-mRNA interactions.* Nucleic Acids Res, 2012. **40**(16): p. 7666-75.
16. McClusky, D.R., et al., *A prospective trial on initiation factor 4E (eIF4E) overexpression and cancer recurrence in node-positive breast cancer.* Ann Surg, 2005. **242**(4): p. 584-90; discussion 590-2.
17. Gingras, A.C., B. Raught, and N. Sonenberg, *Regulation of translation initiation by FRAP/mTOR.* Genes Dev, 2001. **15**(7): p. 807-26.
18. Richter, J.D. and N. Sonenberg, *Regulation of cap-dependent translation by eIF4E inhibitory proteins.* Nature, 2005. **433**(7025): p. 477-80.
19. Svitkin, Y.V., et al., *Eukaryotic translation initiation factor 4E availability controls the switch between cap-dependent and internal ribosomal entry site-mediated translation.* Mol Cell Biol, 2005. **25**(23): p. 10556-65.
20. Gingras, A.C., B. Raught, and N. Sonenberg, *eIF4 initiation factors: effectors of mRNA recruitment to ribosomes and regulators of translation.* Annu Rev Biochem, 1999. **68**: p. 913-63.
21. Kozak, M., *The scanning model for translation: an update.* J Cell Biol, 1989. **108**(2): p. 229-41.
22. Raught, B. and A.C. Gingras, *eIF4E activity is regulated at multiple levels.* Int J Biochem Cell Biol, 1999. **31**(1): p. 43-57.
23. Spriggs, K.A., et al., *Re-programming of translation following cell stress allows IRES-mediated translation to predominate.* Biol Cell, 2008. **100**(1): p. 27-38.
24. Lewis, J.D., et al., *A nuclear cap-binding complex facilitates association of U1 snRNP with the cap-proximal 5' splice site.* Genes Dev, 1996. **10**(13): p. 1683-98.
25. Semler, B.L. and M.L. Waterman, *IRES-mediated pathways to polysomes: nuclear versus cytoplasmic routes.* Trends in Microbiology, 2008. **16**(1): p. 1-5.

26. Hershey, J.W.B., *Translational Control in Mammalian-Cells.* Annual Review of Biochemistry, 1991. **60**: p. 717-755.
27. Hershey, J.W.B., N. Sonenberg, and M.B. Mathews, *Principles of Translational Control: An Overview.* Cold Spring Harbor Perspectives in Biology, 2012. **4**(12).
28. Mader, S., et al., *The translation initiation factor eIF-4E binds to a common motif shared by the translation factor eIF-4 gamma and the translational repressors 4E-binding proteins.* Mol Cell Biol, 1995. **15**(9): p. 4990-7.
29. Pause, A., et al., *Insulin-dependent stimulation of protein synthesis by phosphorylation of a regulator of 5'-cap function.* Nature, 1994. **371**(6500): p. 762-7.
30. Rom, E., et al., *Cloning and characterization of 4EHP, a novel mammalian eIF4E-related cap-binding protein.* J Biol Chem, 1998. **273**(21): p. 13104-9.
31. Gingras, A.C., B. Raught, and N. Sonenberg, *mTOR signalling to translation.* Curr Top Microbiol Immunol, 2004. **279**: p. 169-97.
32. Kudchodkar, S.B., et al., *Human cytomegalovirus infection induces rapamycin-insensitive phosphorylation of downstream effectors of mTOR kinase.* J Virol, 2004. **78**(20): p. 11030-9.
33. Iborra, F.J., D.A. Jackson, and P.R. Cook, *Coupled transcription and translation within nuclei of mammalian cells.* Science, 2001. **293**(5532): p. 1139-42.
34. Lejbkowicz, F., et al., *A fraction of the mRNA 5' cap-binding protein, eukaryotic initiation factor 4E, localizes to the nucleus.* Proc Natl Acad Sci U S A, 1992. **89**(20): p. 9612-6.
35. Cohen, N., et al., *PML RING suppresses oncogenic transformation by reducing the affinity of eIF4E for mRNA.* EMBO J, 2001. **20**(16): p. 4547-59.
36. Lang, V., et al., *Initiation factor eIF-4E of Saccharomyces cerevisiae. Distribution within the cell, binding to mRNA, and consequences of its overproduction.* J Biol Chem, 1994. **269**(8): p. 6117-23.
37. Strudwick, S. and K.L. Borden, *The emerging roles of translation factor eIF4E in the nucleus.* Differentiation, 2002. **70**(1): p. 10-22.
38. Rousseau, D., et al., *Translation initiation of ornithine decarboxylase and nucleocytoplasmic transport of cyclin D1 mRNA are increased in cells overexpressing eukaryotic initiation factor 4E.* Proc Natl Acad Sci U S A, 1996. **93**(3): p. 1065-70.

39. Dostie, J., et al., *A novel shuttling protein, 4E-T, mediates the nuclear import of the mRNA 5' cap-binding protein, eIF4E.* EMBO J, 2000. **19**(12): p. 3142-56.
40. Culjkovic, B., et al., *eIF4E promotes nuclear export of cyclin D1 mRNAs via an element in the 3'UTR.* J Cell Biol, 2005. **169**(2): p. 245-56.
41. Culjkovic, B., et al., *eIF4E is a central node of an RNA regulon that governs cellular proliferation.* J Cell Biol, 2006. **175**(3): p. 415-26.
42. Keene, J.D. and P.J. Lager, *Post-transcriptional operons and regulons co-ordinating gene expression.* Chromosome Res, 2005. **13**(3): p. 327-37.
43. Keene, J.D. and S.A. Tenenbaum, *Eukaryotic mRNPs may represent posttranscriptional operons.* Mol Cell, 2002. **9**(6): p. 1161-7.
44. Topisirovic, I., et al., *Molecular dissection of the eukaryotic initiation factor 4E (eIF4E) export-competent RNP.* EMBO J, 2009. **28**(8): p. 1087-98.
45. Delaleau, M. and K.L. Borden, *Multiple Export Mechanisms for mRNAs.* Cells, 2015. **4**(3): p. 452-73.
46. Siddiqui, N. and K.L. Borden, *mRNA export and cancer.* Wiley Interdiscip Rev RNA, 2012. **3**(1): p. 13-25.
47. Culjkovic-Kraljacic, B., et al., *The oncogene eIF4E reprograms the nuclear pore complex to promote mRNA export and oncogenic transformation.* Cell Rep, 2012. **2**(2): p. 207-15.
48. Volpon, L., et al., *Importin 8 mediates m7G cap-sensitive nuclear import of the eukaryotic translation initiation factor eIF4E.* Proc Natl Acad Sci U S A, 2016. **113**(19): p. 5263-8.
49. Jaramillo, M., et al., *Multiple mRNAs encode the murine translation initiation factor eIF-4E.* J Biol Chem, 1991. **266**(16): p. 10446-51.
50. Jones, R.M., et al., *An essential E box in the promoter of the gene encoding the mRNA cap-binding protein (eukaryotic initiation factor 4E) is a target for activation by c-myc.* Mol Cell Biol, 1996. **16**(9): p. 4754-64.
51. Zhu, N., et al., *Transcriptional repression of the eukaryotic initiation factor 4E gene by wild type p53.* Biochem Biophys Res Commun, 2005. **335**(4): p. 1272-9.

52. Hariri, F., et al., *The eukaryotic translation initiation factor eIF4E is a direct transcriptional target of NF-kappaB and is aberrantly regulated in acute myeloid leukemia.* Leukemia, 2013. **27**(10): p. 2047-55.

53. Mainwaring, L.A. and A.M. Kenney, *Divergent functions for eIF4E and S6 kinase by sonic hedgehog mitogenic signalling in the developing cerebellum.* Oncogene, 2011. **30**(15): p. 1784-97.

54. Makhlouf, A.A., A.M. Namboodiri, and P.J. McDermott, *Transcriptional regulation of the rat eIF4E gene in cardiac muscle cells: the role of specific elements in the promoter region.* Gene, 2001. **267**(1): p. 1-12.

55. Tan, N.G., et al., *Human homologue of ariadne promotes the ubiquitylation of translation initiation factor 4E homologous protein, 4EHP.* FEBS Lett, 2003. **554**(3): p. 501-4.

56. Michon, T., et al., *The potyviral virus genome-linked protein VPg forms a ternary complex with the eukaryotic initiation factors eIF4E and eIF4G and reduces eIF4E affinity for a mRNA cap analogue.* FEBS J, 2006. **273**(6): p. 1312-22.

57. Roudet-Tavert, G., et al., *Central domain of a potyvirus VPg is involved in the interaction with the host translation initiation factor eIF4E and the viral protein HcPro.* J Gen Virol, 2007. **88**(Pt 3): p. 1029-33.

58. Landon, A.L., et al., *MNKs act as a regulatory switch for eIF4E1 and eIF4E3 driven mRNA translation in DLBCL.* Nat Commun, 2014. **5**: p. 5413.

59. Osborne, M.J., et al., *eIF4E3 acts as a tumour suppressor by utilizing an atypical mode of methyl-7-guanosine cap recognition.* Proc Natl Acad Sci U S A, 2013. **110**(10): p. 3877-82.

60. Volpon, L., et al., *eIF4E3, a new actor in mRNA metabolism and tumour suppression.* Cell Cycle, 2013. **12**(8): p. 1159-60.

61. Joshi, B., et al., *Phosphorylation of eukaryotic protein synthesis initiation factor 4E at Ser-209.* J Biol Chem, 1995. **270**(24): p. 14597-603.

62. Murata, T. and K. Shimotohno, *Ubiquitination and proteasome-dependent degradation of human eukaryotic translation initiation factor 4E.* J Biol Chem, 2006. **281**(30): p. 20788-800.

63. Topisirovic, I., M. Ruiz-Gutierrez, and K.L. Borden, *Phosphorylation of the eukaryotic translation initiation factor eIF4E contributes to its transformation and mRNA transport activities.* Cancer Res, 2004. **64**(23): p. 8639-42.

64. Xu, X., et al., *Sumoylation of eIF4E activates mRNA translation.* EMBO Rep, 2010. **11**(4): p. 299-304.

65. Waskiewicz, A.J., et al., *Phosphorylation of the cap-binding protein eukaryotic translation initiation factor 4E by protein kinase Mnk1 in vivo.* Mol Cell Biol, 1999. **19**(3): p. 1871-80.

66. Brooks, R.F., *Continuous protein synthesis is required to maintain the probability of entry into S phase.* Cell, 1977. **12**(1): p. 311-7.

67. Polunovsky, V.A., et al., *Translational control of programmed cell death: eukaryotic translation initiation factor 4E blocks apoptosis in growth-factor-restricted fibroblasts with physiologically expressed or deregulated Myc.* Mol Cell Biol, 1996. **16**(11): p. 6573-81.

68. Smith, M.R., et al., *Modulation of the mitogenic activity of eukaryotic translation initiation factor-4E by protein kinase C.* New Biol, 1991. **3**(6): p. 601-7.

69. Borden, K.L. and B. Culjkovic-Kraljacic, *Ribavirin as an anti-cancer therapy: acute myeloid leukemia and beyond?* Leuk Lymphoma, 2010. **51**(10): p. 1805-15.

70. Topisirovic, I., et al., *Aberrant eukaryotic translation initiation factor 4E-dependent mRNA transport impedes hematopoietic differentiation and contributes to leukemogenesis.* Mol Cell Biol, 2003. **23**(24): p. 8992-9002.

71. Assouline, S., et al., *Molecular targeting of the oncogene eIF4E in acute myeloid leukemia (AML): a proof-of-principle clinical trial with ribavirin.* Blood, 2009. **114**(2): p. 257-60.

72. Oran, B. and D.J. Weisdorf, *Survival for older patients with acute myeloid leukemia: a population-based study.* Haematologica, 2012. **97**(12): p. 1916-24.

73. Assouline, S., et al., *A phase I trial of ribavirin and low-dose cytarabine for the treatment of relapsed and refractory acute myeloid leukemia with elevated eIF4E.* Haematologica, 2015. **100**(1): p. e7-9.

74. Bennett, J.M., et al., *Proposals for the classification of the acute leukaemias. French-American-British (FAB) co-operative group.* Br J Haematol, 1976. **33**(4): p. 451-8.

75. Sekeres, M.A., *Treatment of older adults with acute myeloid leukemia: state of the art and current perspectives.* Haematologica, 2008. **93**(12): p. 1769-72.

76. Grimwade, D., et al., *Refinement of cytogenetic classification in acute myeloid leukemia: determination of prognostic significance of rare recurring chromosomal abnormalities among 5876 younger adult patients treated in the United Kingdom Medical Research Council trials.* Blood, 2010. **116**(3): p. 354-65.

77. Vardiman, J.W., N.L. Harris, and R.D. Brunning, *The World Health Organization (WHO) classification of the myeloid neoplasms.* Blood, 2002. **100**(7): p. 2292-302.

78. Topisirovic, I., et al., *The proline-rich homeodomain protein, PRH, is a tissue-specific inhibitor of eIF4E-dependent cyclin D1 mRNA transport and growth.* EMBO J, 2003. **22**(3): p. 689-703.

79. Kentsis, A., et al., *Ribavirin suppresses eIF4E-mediated oncogenic transformation by physical mimicry of the 7-methyl guanosine mRNA cap.* Proc Natl Acad Sci U S A, 2004. **101**(52): p. 18105-10.

80. Dong, K., et al., *Tumour-specific RNAi targeting eIF4E suppresses tumour growth, induces apoptosis and enhances cisplatin cytotoxicity in human breast carcinoma cells.* Breast Cancer Res Treat, 2009. **113**(3): p. 443-56.

81. Graff, J.R., et al., *Therapeutic suppression of translation initiation factor eIF4E expression reduces tumour growth without toxicity.* J Clin Invest, 2007. **117**(9): p. 2638-48.

82. Oridate, N., et al., *Growth inhibition of head and neck squamous carcinoma cells by small interfering RNAs targeting eIF4E or cyclin D1 alone or combined with cisplatin.* Cancer Biol Ther, 2005. **4**(3): p. 318-23.

83. Moerke, N.J., et al., *Small-molecule inhibition of the interaction between the translation initiation factors eIF4E and eIF4G.* Cell, 2007. **128**(2): p. 257-67.

84. Siegele, B., et al., *eIF4E-targeted suicide gene therapy in a minimal residual mouse model for metastatic soft-tissue head and neck squamous cell carcinoma improves disease-free survival.* J Surg Res, 2008. **148**(1): p. 83-9.

85. Pettersson, F., et al., *Ribavirin treatment effects on breast cancers overexpressing eIF4E, a biomarker with prognostic specificity for luminal B-type breast cancer.* Clin Cancer Res, 2011. **17**(9): p. 2874-84.

86. Volpon, L., et al., *Conformational changes induced in the eukaryotic translation initiation factor eIF4E by a clinically relevant inhibitor, ribavirin triphosphate.* Biochem Biophys Res Commun, 2013. **434**(3): p. 614-9.
87. Zahreddine, H.A., et al., *The sonic hedgehog factor GLI1 imparts drug resistance through inducible glucuronidation.* Nature, 2014. **511**(7507): p. 90-3.
88. Tan, K., et al., *Ribavirin targets eIF4E dependent Akt survival signalling.* Biochem Biophys Res Commun, 2008. **375**(3): p. 341-5.
89. Varjosalo, M. and J. Taipale, *Hedgehog: functions and mechanisms.* Genes Dev, 2008. **22**(18): p. 2454-72.
90. Heretsch, P., L. Tzagkaroulaki, and A. Giannis, *Modulators of the hedgehog signalling pathway.* Bioorg Med Chem, 2010. **18**(18): p. 6613-24.
91. Hui, C.C. and S. Angers, *Gli proteins in development and disease.* Annu Rev Cell Dev Biol, 2011. **27**: p. 513-37.
92. Ruiz i Altaba, A., *Gli proteins and Hedgehog signalling: development and cancer.* Trends Genet, 1999. **15**(10): p. 418-25.
93. Goodrich, L.V., et al., *Conservation of the hedgehog/patched signalling pathway from flies to mice: induction of a mouse patched gene by Hedgehog.* Genes Dev, 1996. **10**(3): p. 301-12.
94. Oliver, T.G., et al., *Transcriptional profiling of the Sonic hedgehog response: a critical role for N-myc in proliferation of neuronal precursors.* Proc Natl Acad Sci U S A, 2003. **100**(12): p. 7331-6.
95. Stone, D.M., et al., *The tumour-suppressor gene patched encodes a candidate receptor for Sonic hedgehog.* Nature, 1996. **384**(6605): p. 129-34.
96. Regl, G., et al., *Human GLI2 and GLI1 are part of a positive feedback mechanism in Basal Cell Carcinoma.* Oncogene, 2002. **21**(36): p. 5529-39.
97. Hsia, E.Y., Y. Gui, and X. Zheng, *Regulation of Hedgehog signalling by ubiquitination.* Front Biol (Beijing), 2015. **10**(3): p. 203-220.
98. Brennan, D., et al., *Noncanonical Hedgehog signalling.* Vitam Horm, 2012. **88**: p. 55-72.

99. Chen, Y.J., et al., *Sonic hedgehog signalling protects human hepatocellular carcinoma cells against ionizing radiation in an autocrine manner.* Int J Radiat Oncol Biol Phys, 2011. **80**(3): p. 851-9.
100. Queiroz, K.C., et al., *Hedgehog signalling maintains chemoresistance in myeloid leukemic cells.* Oncogene, 2010. **29**(48): p. 6314-22.
101. Palle, K., et al., *Aberrant GLI1 Activation in DNA Damage Response, Carcinogenesis and Chemoresistance.* Cancers (Basel), 2015. **7**(4): p. 2330-51.
102. Athar, M., et al., *Sonic hedgehog signalling in Basal cell nevus syndrome.* Cancer Res, 2014. **74**(18): p. 4967-75.
103. Ruiz i Altaba, A., C. Mas, and B. Stecca, *The Gli code: an information nexus regulating cell fate, stemness and cancer.* Trends Cell Biol, 2007. **17**(9): p. 438-47.
104. Stecca, B. and I.A.A. Ruiz, *Context-dependent regulation of the GLI code in cancer by HEDGEHOG and non-HEDGEHOG signals.* J Mol Cell Biol, 2010. **2**(2): p. 84-95.
105. Cummings, J., et al., *Glucuronidation as a mechanism of intrinsic drug resistance in human colon cancer: reversal of resistance by food additives.* Cancer Res, 2003. **63**(23): p. 8443-50.
106. Tukey, R.H. and C.P. Strassburg, *Human UDP-glucuronosyltransferases: metabolism, expression, and disease.* Annu Rev Pharmacol Toxicol, 2000. **40**: p. 581-616.
107. Mazur, A., et al., *Characterization of human hepatic and extrahepatic UDP-glucuronosyltransferase enzymes involved in the metabolism of classic cannabinoids.* Drug Metab Dispos, 2009. **37**(7): p. 1496-504.
108. Yokota, H., et al., *Effects on extrahepatic UDP-glucuronosyltransferases in hypophysectomized rat.* J Biochem, 2002. **132**(2): p. 265-70.
109. Nagar, S. and R.P. Remmel, *Uridine diphosphoglucuronosyltransferase pharmacogenetics and cancer.* Oncogene, 2006. **25**(11): p. 1659-72.
110. Collier, A.C., et al., *UDP-glucuronosyltransferase 1a enzymes are present and active in the mouse blastocyst.* Drug Metab Dispos, 2014. **42**(11): p. 1921-5.
111. Guillemette, C., *Pharmacogenomics of human UDP-glucuronosyltransferase enzymes.* Pharmacogenomics J, 2003. **3**(3): p. 136-58.

112. Bellemare, J., et al., *Modulation of the human glucuronosyltransferase UGT1A pathway by splice isoform polypeptides is mediated through protein-protein interactions.* J Biol Chem, 2010. **285**(6): p. 3600-7.
113. Guillemette, C., et al., *UGT genomic diversity: beyond gene duplication.* Drug Metab Rev, 2010. **42**(1): p. 24-44.
114. Bigo, C., et al., *Nuclear receptors and endobiotics glucuronidation: the good, the bad, and the UGT.* Drug Metab Rev, 2013. **45**(1): p. 34-47.
115. Fujiwara, R., T. Yokoi, and M. Nakajima, *Structure and Protein-Protein Interactions of Human UDP-Glucuronosyltransferases.* Front Pharmacol, 2016. **7**: p. 388.
116. Operana, T.N. and R.H. Tukey, *Oligomerization of the UDP-glucuronosyltransferase 1A proteins: homo- and heterodimerization analysis by fluorescence resonance energy transfer and co-immunoprecipitation.* J Biol Chem, 2007. **282**(7): p. 4821-9.
117. Coleman, L.J., et al., *Combined analysis of eIF4E and 4E-binding protein expression predicts breast cancer survival and estimates eIF4E activity.* Br J Cancer, 2009. **100**(9): p. 1393-9.
118. Pettersson, F., et al., *Genetic and pharmacologic inhibition of eIF4E reduces breast cancer cell migration, invasion, and metastasis.* Cancer Res, 2015. **75**(6): p. 1102-12.
119. Byrnes, K., et al., *High eIF4E, VEGF, and microvessel density in stage I to III breast cancer.* Ann Surg, 2006. **243**(5): p. 684-90; discussion 691-2.
120. Nasr, Z., et al., *eIF4F suppression in breast cancer affects maintenance and progression.* Oncogene, 2013. **32**(7): p. 861-71.
121. Klein, C.A., *Cancer. The metastasis cascade.* Science, 2008. **321**(5897): p. 1785-7.
122. Pantel, K. and R.H. Brakenhoff, *Dissecting the metastatic cascade.* Nat Rev Cancer, 2004. **4**(6): p. 448-56.
123. Goncharova, V., et al., *Hyaluronan expressed by the hematopoietic microenvironment is required for bone marrow hematopoiesis.* J Biol Chem, 2012. **287**(30): p. 25419-33.
124. Toole, B.P., *Hyaluronan: from extracellular glue to pericellular cue.* Nat Rev Cancer, 2004. **4**(7): p. 528-39.
125. Cyphert, J.M., C.S. Trempus, and S. Garantziotis, *Size Matters: Molecular Weight Specificity of Hyaluronan Effects in Cell Biology.* Int J Cell Biol, 2015. **2015**: p. 563818.

126. Fuchs, K., et al., *Opposing effects of high- and low-molecular weight hyaluronan on CXCL12-induced CXCR4 signalling depend on CD44.* Cell Death Dis, 2013. **4**: p. e819.
127. Koistinen, V., et al., *Cell protrusions induced by hyaluronan synthase 3 (HAS3) resemble mesothelial microvilli and share cytoskeletal features of filopodia.* Exp Cell Res, 2015. **337**(2): p. 179-91.
128. Kultti, A., et al., *Hyaluronan synthesis induces microvillus-like cell surface protrusions.* J Biol Chem, 2006. **281**(23): p. 15821-8.
129. Bertrand, P., et al., *Expression of HYAL2 mRNA, hyaluronan and hyaluronidase in B-cell non-Hodgkin lymphoma: relationship with tumour aggressiveness.* Int J Cancer, 2005. **113**(2): p. 207-12.
130. Junker, N., et al., *Expression and regulation patterns of hyaluronidases in small cell lung cancer and glioma lines.* Oncol Rep, 2003. **10**(3): p. 609-16.
131. Sa, V.K., et al., *Hyaluronidases and hyaluronan synthases expression is inversely correlated with malignancy in lung/bronchial pre-neoplastic and neoplastic lesions, affecting prognosis.* Braz J Med Biol Res, 2015. **48**(11): p. 1039-47.
132. Ponta, H., L. Sherman, and P.A. Herrlich, *CD44: from adhesion molecules to signalling regulators.* Nat Rev Mol Cell Biol, 2003. **4**(1): p. 33-45.
133. Zoller, M., *CD44: can a cancer-initiating cell profit from an abundantly expressed molecule?* Nat Rev Cancer, 2011. **11**(4): p. 254-67.
134. Mori, T., et al., *Structural basis for CD44 recognition by ERM proteins.* J Biol Chem, 2008. **283**(43): p. 29602-12.
135. Avigdor, A., et al., *CD44 and hyaluronic acid cooperate with SDF-1 in the trafficking of human CD34+ stem/progenitor cells to bone marrow.* Blood, 2004. **103**(8): p. 2981-9.
136. Chetty, C., et al., *MMP-9 induces CD44 cleavage and CD44 mediated cell migration in glioblastoma xenograft cells.* Cell Signal, 2012. **24**(2): p. 549-59.
137. Ohno-Nakahara, M., et al., *Induction of CD44 and MMP expression by hyaluronidase treatment of articular chondrocytes.* J Biochem, 2004. **135**(5): p. 567-75.
138. Yu, W.H., et al., *CD44 anchors the assembly of matrilysin/MMP-7 with heparin-binding epidermal growth factor precursor and ErbB4 and regulates female reproductive organ remodeling.* Genes Dev, 2002. **16**(3): p. 307-23.

139. Murai, T., *Lipid Raft-Mediated Regulation of Hyaluronan-CD44 Interactions in Inflammation and Cancer.* Front Immunol, 2015. **6**: p. 420.
140. Svee, K., et al., *Acute lung injury fibroblast migration and invasion of a fibrin matrix is mediated by CD44.* J Clin Invest, 1996. **98**(8): p. 1713-27.
141. Kim, H.R., et al., *Hyaluronan facilitates invasion of colon carcinoma cells in vitro via interaction with CD44.* Cancer Res, 2004. **64**(13): p. 4569-76.
142. Montgomery, N., et al., *CD44 enhances invasion of basal-like breast cancer cells by upregulating serine protease and collagen-degrading enzymatic expression and activity.* Breast Cancer Res, 2012. **14**(3): p. R84.
143. Jin, L., et al., *Targeting of CD44 eradicates human acute myeloid leukemic stem cells.* Nat Med, 2006. **12**(10): p. 1167-74.

CHAPTER 2

Mechanisms and insights into drug resistance in cancer

(REVIEW)

Published Review in *Front Pharmacol. 2013Mar14;4:28.doi: 10.3389/fphar.2013.00028. eCollection 2013.*

Contribution:

H.A.Z. and K.L.B.B. wrote the manuscript.

frontiers in
PHARMACOLOGY

MINI REVIEW ARTICLE
published: 14 March 2013
doi: 10.3389/fphar.2013.00028

Mechanisms and insights into drug resistance in cancer

Hiba Zahreddine and Katherine L. B. Borden*

Department of Pathology and Cell Biology, Institute of Research in Immunology and Cancer, Université de Montréal, Montreal, QC, Canada

Edited by:
Gerald Batist, McGill University, Canada

Reviewed by:
Jian Hui Wu, McGill University, Canada
Michael Witcher, McGill University, Canada

***Correspondence:**
Katherine L. B. Borden, Department of Pathology and Cell Biology, Institute of Research in Immunology and Cancer, Université de Montréal, Montreal, QC, Canada H3T 1J4.
e-mail: katherine.borden@umontreal.ca

Cancer drug resistance continues to be a major impediment in medical oncology. Clinically, resistance can arise prior to or as a result of cancer therapy. In this review, we discuss different mechanisms adapted by cancerous cells to resist treatment, including alteration in drug transport and metabolism, mutation and amplification of drug targets, as well as genetic rewiring which can lead to impaired apoptosis. Tumor heterogeneity may also contribute to resistance, where small subpopulations of cells may acquire or stochastically already possess some of the features enabling them to emerge under selective drug pressure. Making the problem even more challenging, some of these resistance pathways lead to multidrug resistance, generating an even more difficult clinical problem to overcome. We provide examples of these mechanisms and some insights into how understanding these processes can influence the next generation of cancer therapies.

Keywords: origin of cancer, multidrug resistance, drug metabolism, drug transporters, oncogene addiction, microenvironment, collateral sensitivity, synthetic lethality

CANCER TALE: ITS TREATMENT AND RELAPSE

In 1961, Frei and Freireich initiated the high-dose four-drug combination clinical trial for the treatment of pediatric leukemia (Frei et al., 1965). Despite the threat imposed by administering four drugs at once, few weeks following treatment onset, children began to respond, "*the bone marrow biopsies came back one after another—all without leukemia cells. Red blood cells and white blood cells and platelets sprouted up in an otherwise scorched field of bone marrow. But the leukemia did not return*" (Mukherjee, 2010). Out of the 16 enrolled patients, 11 showed complete remission. This outstanding success, however, was short-lived. With the exception of a handful of children, all patients eventually relapsed, developing a more vigorous form of cancer that was no longer responsive to the treatment: leukemic cells had invaded the blood–brain barrier and colonized the brain "*the only place unreachable by chemotherapy….the children died one after the other-felled by virtue of the adaptation designed to protect them…it was a consequence of the body's defense system subverting cancer treatment*" (Mukherjee, 2010). To date, this story still reflects the same tale of cancer treatment where its resistance and relapse remains a major challenge (Wilson et al., 2009). In this review we provide an overview of advances made in our understanding of the mechanisms that enable cancerous cells to adapt to and eventually overcome therapy, and how identifying these mechanisms can help circumvent resistance and improve treatment.

Despite its complex biological nature, many recent successes have been made in the treatment of cancer, including most strikingly chronic myeloid leukemia (CML) and acute promyelocytic leukemia (APL) which have met with great success as well as many cases of pediatric leukemias, Hodgkin's lymphomas, and testicular cancers (Siegel et al., 2012). These success stories mainly relied on an increased understanding of the diverse molecular mechanisms governing tumor development. Owing to this, various anti-cancer therapies were designed to target disease-specific mechanisms that are absent in normal cells. Such strategies include (i) inhibition of a specific oncoprotein, such as targeting the oncogenic fusion proteins Bcr–Abl and PML–RARA with Gleevec and all *trans* retinoic acid (ATRA) with arsenic trioxide respectively or (ii) activation of a specific immune response against cancerous cells demonstrated by the use of interferon alpha alone or in combination with other anti-cancer drugs including 5-fluorouracil and cytarabine (Raderer and Scheithauer, 1995; Guilhot et al., 1997; Druker et al., 2001; Kreitman et al., 2001; Tallman et al., 2002; Goldman and Melo, 2003; O'Brien et al., 2003; Sawyers, 2004; Kreitman, 2006; Ferrantini et al., 2007; Chin and Gray, 2008; Sellers, 2011). Many of these drugs are currently being used in the clinic and have established positive impact on patient survival. However, a major impediment to their success is the development of therapeutic resistance which in some cases predates clinical intervention (Wilson et al., 2009). Based on tumor response to the initial therapy, cancer resistance can be broadly classified into two categories, primary and acquired (Meads et al., 2009; Lippert et al., 2011). While primary drug resistance exists prior to any given treatment, acquired resistance occurs after initial therapy. Unfortunately, the majority of patients will likely develop resistance at a certain point of treatment. For example, 50–70% of patients with adenocarcinoma relapse following surgery with a chemoresistant phenotype (Castells et al., 2012), and approximately 20% of adults with acute lymphoblastic leukemia suffer from primary resistance to treatment (Testi et al., 1992; Giona et al., 1994; Thomas et al., 1999; O'Connor et al., 2011). In addition, primary resistance has been recognized in nearly 50% of all cancer patients in the 1990s (Pinedo and Giaccone, 1998). Therefore, the design of anti-cancer drugs that are fully effective necessitates a better understanding of the mechanisms by which cancer cells elude treatment. Here we will discuss several features of drug resistant cells including modification of drug transport, mutation of extracellular receptors, amplification and mutation of drug targets as well as related topics. Additionally, we will briefly

address the important question of how resistant cell populations emerge.

MECHANISMS OF DRUG RESISTANCE

Both primary and acquired resistance can be caused by alterations to drug metabolism (sequestrations or enhanced detoxification) or modifications to the drug targets (Gottesman, 2002; Gatti and Zunino, 2005; Teicher, 2006; Wilson et al., 2006; Ullah, 2008). A brief overview of these mechanisms supported with examples of clinical relevance are presented below (**Figure 1**).

Perhaps the most studied mode of resistance involves drug metabolism, including its uptake, efflux, and detoxification. The means by which drugs enter cells depend on their chemical nature, and it mainly necessitates the use of receptors, which they bind to and transmit their effects without cellular entry, or transporters, which allow their cellular entry (Gottesman, 2002). At this level, resistance can result from mutations that modify activity or reduce the expression of surface receptors and transporters. For instance, mutations or reduced expression of the extracellular receptor smoothened (Yauch et al., 2009; Atwood et al., 2012; Kasper and Toftgard, 2013), nucleoside transporters (Galmarini et al., 2001; Damaraju et al., 2003) or one or both folate transporters (Longo-Sorbello and Bertino, 2001) result in defective uptake of cyclopamine, nucleoside drugs, such as cytarabine, and toxic folate analogs, such as methotrexate, respectively. On the other hand, enhanced drug efflux is frequently caused by increased expression of ATP binding cassette (ABC) membrane transporters (Gottesman et al., 2002). Among the 48 known ABC transporters in humans, elevation of three members, P-gp (*MDR1* gene product), Multidrug resistance-associated protein 1 (MRP1) and mitoxantrone resistance protein [MXR; also known as breast cancer resistance protein (BCRP) or placenta ABC protein (ABC-P)], have been correlated with cancer chemoresistance to various drugs (Gottesman, 2002; Gottesman et al., 2002). For instance, P-gp transports a wide variety of hydrophobic anti-cancer drugs such as vinblastine, doxorubicin, vincristine, and taxol, and therefore its increased expression has been correlated with resistance to these (Gottesman et al., 2002). MRP1 on the other hand, transports negatively charged natural-product drugs in addition to drugs that have been modified by the conjugation of glutathione (GSH), glucuronic acid or sulfate (Jedlitschky et al., 1996; Hipfner et al., 1999; Konig et al., 1999; Borst et al., 2000); while, MXR overexpression has been correlated with resistance to topoisomerase I inhibitors, anthracyclines, and mitoxantrone (Gottesman, 2002). As can be seen, these factors comprise a major site for the development of drug resistance.

To exert their cytotoxic effects, many anti-cancer drugs must undergo metabolic activation. For instance, cytarabine (also known as AraC), a nucleoside drug widely used for the treatment of acute myelogenous leukemia (Sampath et al., 2006), necessitates initial phosphorylation by deoxycytidine kinase to cytarabine-monophosphate which is subsequently phosphorylated to the active form cytarabine triphosphate. To circumvent the effects of these drugs, cancer cells develop resistance through decreased drug activation (Kufe and Spriggs, 1985; Bardenheuer et al., 2005). This occurs via the downregulation or mutation of enzymes involved in this metabolic pathway, such as deoxycytidine kinase in the case of cytarabine (Sampath et al., 2006). Drug inactivation can also play a major role in the development of resistance. These mechanisms include, for example, conjugation of the drug to GSH, a powerful anti-oxidant that protects the cells against the damaging effects of reactive oxygen species (Wilson et al., 2006). GSH conjugation to platinum drugs, such as oxaliplatin and cisplatin used in the treatment of various types of cancers, renders them substrates for ABC transporters which enhances drug efflux (Meijer et al., 1992; Ishikawa and Ali-Osman, 1993). Furthermore, the topoisomerase I inhibitor, irinotecan, used for treating colon cancer, have been shown to become inactivated via phase I drug metabolizing enzymes, CYP450 (Xu and Villalona-Calero, 2002). Finally, binding of platinum drugs, particularly cisplatin, to metallothionein (MT), a small cysteine-rich protein, is another means of drug inactivation (Kelley et al., 1988; Kasahara et al., 1991).

Many cancer cells develop an overreliance or dependency on an oncogene. This is referred to as oncogene addiction (Arber et al., 1997; Weinstein, 2002; Weinstein and Joe, 2006; Sharma and Settleman, 2007). Targeting such oncogenes, provided a basis for the development of targeted therapies. Examples of such targeted therapies include: (i) imatinib targeting BCR/ABL tyrosine kinase in CML (Hughes et al., 2003), (ii) gefitinib and erlotinib targeting the epidermal growth factor receptor (EGFR) tyrosine kinase domain in non-small cell lung carcinoma (Lynch et al., 2004; Shepherd et al., 2005; Taron et al., 2005), and (iii) trastuzumab targeting human epidermal growth factor receptor-2 (HER-2) receptor in breast carcinomas (Slamon et al., 2001; Piccart-Gebhart et al., 2005). Unfortunately, the long term effectiveness of these drugs is hindered by the development of drug resistance due to mutation of the targeted protein (Gioeli, 2011; Wong and Lee, 2012). In the case of BCR/ABL and EGFR inhibitors, resistance emerges as a result of mutations occurring at the gatekeeper residues of the kinase domain which disables drug binding (Gorre et al., 2001; Blencke et al., 2003; Kobayashi et al., 2005; Pao et al., 2005; Soverini et al., 2005; Balak et al., 2006; Jabbour et al., 2006, 2008; Nicolini et al., 2006; Apperley, 2007; Costa et al., 2007; Bean et al., 2008; Gioeli, 2011). Furthermore, it has been demonstrated that resistance mutations can be detected prior to treatment in small subpopulations of tumor cells suggesting that these mutant forms were selected via the targeted therapy used (Hofmann et al., 2003; Toyooka et al., 2005; Inukai et al., 2006). In essence, understanding how mutations in the target proteins confer resistance enables the development of new therapeutic approaches to surmount resistance. For instance, second generation CML inhibitors have been developed based on mutational studies of patients who have become Gleevec resistant.

Other mechanisms by which cancerous cells circumvent the effects of targeted inhibitors have also been described, including amplification of alternative oncogenes or inactivation of alternative survival pathways (le Coutre et al., 2000; Engelman et al., 2007). In some cases, targeting of one protein alone (that cells are showing dependency on) can become ineffective because another parallel pathway supports tumor survival. In this case, the two pathways develop a synthetic lethal relationship (Hartman et al., 2001; Tucker and Fields, 2003). This way, the loss/inactivation of one of these genes would be supported by the other pathway and

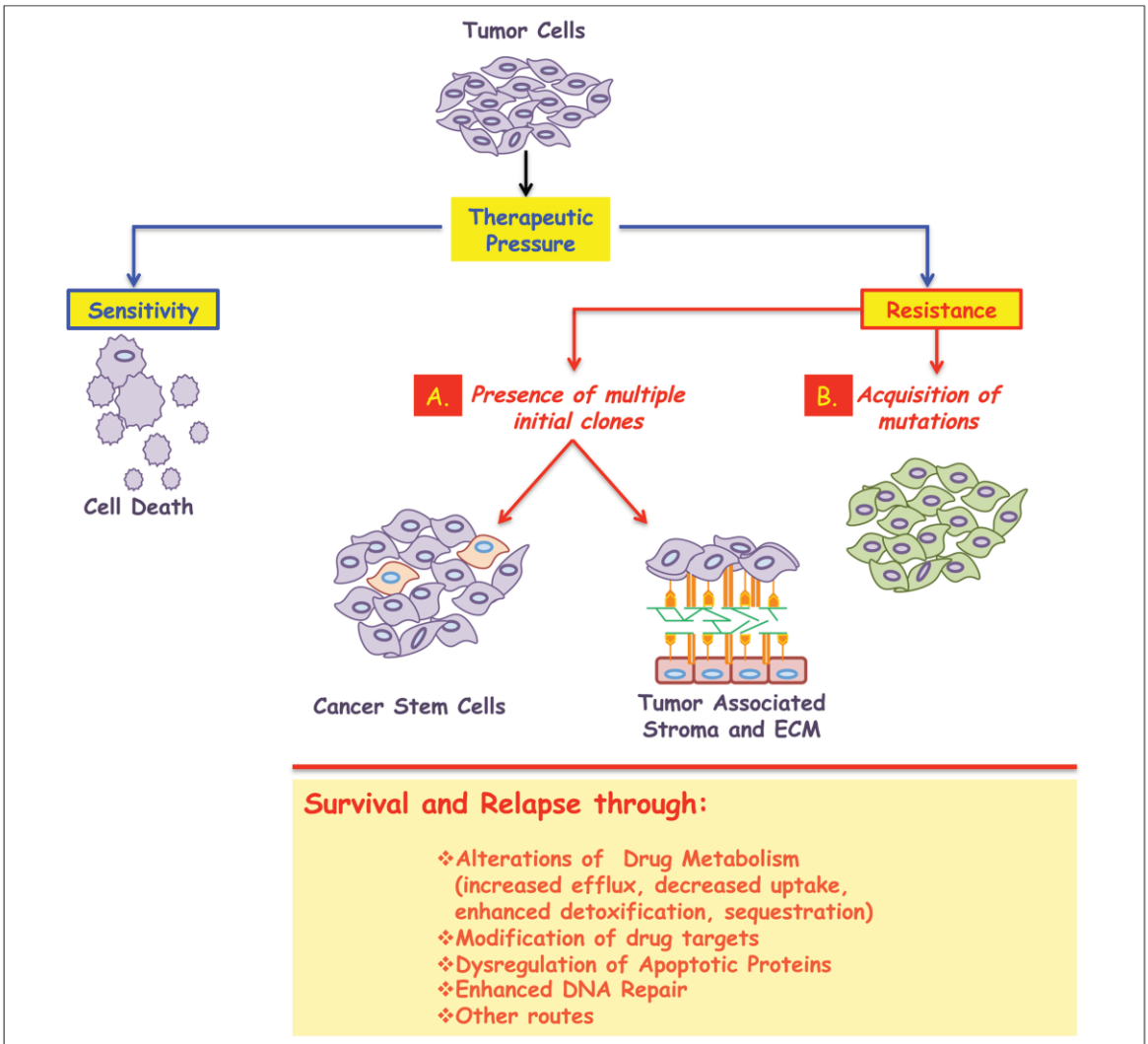

FIGURE 1 | A major impediment in the treatment of cancer is the development of resistance. While most tumors initially respond to the given therapy, the majority will relapse following treatment, and in some cases resistance even predates clinical intervention. Therefore cancer resistance can be classified in to two broad classes: primary or acquired. In both cases, the emergence of resistant cells could be due to, at least, two mechanisms: **(A)** presence of multiple initial clones some of which emerge as dominant after treatment. These subpopulations could possess stem-like characteristics and/or use their interactions with the surrounding microenvironment to enter into a dormant state, thus surviving the insult of therapy. **(B)** Acquisition of stochastic alterations within the cancer cells *per se*. In all cases, the surviving population is less likely to respond to any further therapy and will be responsible for the minimal residual disease and cancer relapse. The biochemical underpinnings of resistance include: alterations to drug metabolism, increased drug efflux, decreased drug uptake, modification of the drug targets, amplification of targeted protein, genetic rewiring, enhanced DNA repair, inactivation of apoptotic proteins, or activation of anti-apoptotic ones, among others.

for the most effective treatment, one would need to target both pathways (Luo et al., 2009; Nijman, 2011).

An example of new pathways emerging once another pathway is targeted comes from the work of Isoyama et al. (2012), showed that acquired resistance to phosphatidylinositol 3-kinase (PI3K) inhibitors (such as ZSTK474) was due to the upregulation of insulin-like growth factor 1 receptor (IGF1R) pathway and that inhibition of this pathway with selective IGF1R inhibitors reverses the acquired PI3Ki resistance phenotype (Isoyama et al., 2012). Additionally, resistance could result from evasion of apoptotic pathways triggered by the acquisition of either inactivating mutations in genes coding for apoptotic proteins, such as p53, or activating mutations in genes coding for anti-apoptotic proteins, such as B cell lymphoma 2 (Bcl-2; Teicher, 2006). Indeed p53

mutations have been correlated with *de novo* resistance to doxorubicin treatment in patients with advanced breast cancer, as well as resistance to anthracyclines in a mouse sarcoma tumor model (Aas et al., 1996; Levine, 1997).

Another excellent example of this phenomenon (i.e., synthetic lethality) is seen in breast and ovarian cancers carrying mutations in the *BRCA1* and *BRCA2* genes, important mediators of DNA double-strand break (DSB) repair. When the poly (ADP-ribose) polymerase (PARP) protein, which is involved in different cellular processes including DNA repair, was targeted in these tumors, selective cancer cell toxicity was achieved (Bryant et al., 2005; Farmer et al., 2005). Several PARP inhibitors (PARPi) are currently being tested in clinical trials, such as iniparib (phase III ongoing; Guha, 2011) and veliparib cancer (Trudeau et al., 2006; Palma et al., 2008, 2009; Kummar et al., 2011), among others. However, despite the promising results these inhibitors showed, whether used as a mono- or combinatorial therapy (Juvekar et al., 2012; Kummar et al., 2012; Riffell et al., 2012), cancer cells once again were capable of evolving resistance to PARPi in preclinical and clinical settings (Chiarugi, 2012; Montoni et al., 2013). The mechanisms of resistance to these inhibitors have been grouped in to at least four categories, as summarized recently (Montoni et al., 2013). But perhaps the most distinct of these, was the ability of cancer cells to revert sensitivity to PARPi by acquiring deletion of the mutation in BRCA gene, thus restoring its function and the subsequent repair of DSBs.

DEVELOPMENT OF CROSS RESISTANCE

An important feature of drug resistance, is that development of resistance to one drug can lead to resistance to other drugs (Ullah, 2008). For instance, loss of a drug transporter can lead to resistance to structurally diverse compounds that utilize it or elevation of ABC transporters resulting from one therapy will influence the efficacy of many other compounds. Since this multidrug resistance phenotype correlates with poor chemotherapy response, drug development strategies to overcome this problem are being designed. These include drugs that are not recognized by transporters and therefore evade efflux, efflux inhibitors, drugs that are selectively lethal to P-gp expressing cells, etc. (Hall et al., 2009; Kelly et al., 2011; Nobili et al., 2012). But, perhaps resistance is not useless after all, as Hall et al. (2009) proposed. The alternative strategy to treat the progeny of the drug imposed Darwinian selection process is to identify their new "Achilles' heel," where resistance to the first given drug conferred a hypersensitivity to an alternate cytotoxic agent to which parental cells were not sensitive to. A phenomenon referred to as "collateral sensitivity", which could be considered as a type of synthetic lethality as well since the same genetic alteration that rendered the cells resistant to one drug now sensitizes them to another (Hall et al., 2009; Pluchino et al., 2012).

WHERE DO RESISTANT CELLS COME FROM?

The development of human cancers is a complex multistage process involving accumulation of both genetic and epigenetic alterations over time (Caulin and Maley, 2011). As a consequence, a single tumor is comprised of heterogeneous populations of cells with distinct genetic fingerprints (Heppner et al., 1978; Marusyk and Polyak, 2010; Michor and Polyak, 2010). As the tumor progresses, some cells undergo genetic alterations, with selection of those having a superior growth advantage in a given context. An excellent example of tumor heterogeneity is provided by breast cancer studies (Schvimer et al., 1995; Shen et al., 2000; Wild et al., 2000). Wild et al. (2000) demonstrated that about 97% of epithelial breast carcinomas possess high levels of intra-tumor diverseness. The relevance of this innate heterogeneity is seen in cancer resistance. Since cancer cell selection obeys the Darwinian law of evolution, hence, under therapeutic pressure, those populations that are most adaptive or resistant to treatment will be selected for. These clones will then dominate and populate the tumor rendering it highly resistant to the given therapy (Williams and Nesse, 1991; Nesse, 2001; Breivik, 2005; Crespi and Summers, 2005; Lichtenstein, 2005; Monceviciute-Eringiene, 2005; Greaves, 2007). The selection process can be rationalized by, at least, two mechanisms. First, the emergence of a dominant cellular population after drug selection since it possesses some favorable characteristics such as a mutated drug binding site (Zhang et al., 2006; O'Brien et al., 2007; Ricci-Vitiani et al., 2007). The second mechanism involves the acquisition of stochastic alterations within the cancer cells which provide a survival advantage (Campbell et al., 2008; Stratton et al., 2009; Negrini et al., 2010; The International Cancer Genome Consortium, 2010; Shen, 2011). The advantage itself, e.g., a mutation in a drug binding site or alteration in drug transporters (as just two examples) could be the same for either of these mechanisms. What is different is the underlying process to generate these biochemical differences.

Two known models, the cancer stem cell (CSC) model, and the environment-mediated drug resistance (EMDR) model, which are not mutually exclusive, could explain the origin of resistant cells. In the CSC model, rare populations of cancer stem cells possess tumor-initiating properties (Teicher, 2006; Nguyen et al., 2012). It is thought that CSCs diverge from normal tissue stem cells or from more-differentiated progenitor cells through dysregulation of self-renewal pathways. Beside modulation of molecular mechanisms, such as increased efficiency of DNA repair (Potten et al., 2002; Cai et al., 2004; Park and Gerson, 2005), changes in cell cycle parameters (Venezia et al., 2004), overexpression of anti-apoptotic proteins (Wang et al., 2003) or drug transporters (Gottesman et al., 2002; Krishnamurthy et al., 2004), etc., resistance of CSCs could be due to their quiescent nature (Teicher, 2006). Thus, in this case, the cell population is present and is difficult to target using traditional chemotherapy strategies many of which depend on active cell cycling.

In the EMDR model, resistance emerges as the cancer cells use their interactions with the surrounding microenvironment to enter into a quiescent or dormant state as a means of circumventing the effects of the given therapy. Under the drug imposed selection pressure, these cells remain in their protective shelter, undergoing genetic changes until they ultimately reach a more permanent acquired resistance phenotype and in turn, alter their surrounding microenvironment (Braun et al., 2000; Meads et al., 2009). These surviving populations, which may or may not be CSCs, can contribute to minimal residual disease (MRD) and cancer relapse (Matsunaga et al., 2003; Bidard et al., 2008; Meads et al., 2009). The EMDR model is relevant

to both hematopoietic and metastatic epithelial malignancies. EMDR could be mediated by either soluble or cell adhesion-related microenvironmental factors. Soluble factor-mediated drug resistance occurs through induction of gene transcription within the tumor cells by cytokines, chemokines, or growth factors secreted by neighboring stroma-like fibroblasts (Meads et al., 2009). One of the known mediators of this resistance mechanism is interleukin-6 (IL-6), whose increased secretion has been correlated with resistance to various cytotoxins both in *in vitro* and *in vivo* models. This includes, for instance, resistance to bortezomib in multiple myeloma and to etoposide and cisplatin in hormone-independent prostate carcinomas (Borsellino et al., 1995, 1999; Frassanito et al., 2001; Voorhees et al., 2007). Further, cell adhesion-mediated drug resistance is triggered by the adhesion of integrins from tumor cells to stromal fibroblasts or to components of the surrounding extracellular matrix. Molecularly, this process could be due to many scenarios including (i) degradation of apoptotic proteins or (ii) enhanced stability or altered subcellular distribution of anti-apoptotic proteins and cell cycle regulators (Hazlehurst et al., 2001, 2007; Shain et al., 2002, 2009; Lwin et al., 2007). One example is provided by studies into melphalan resistance. In this case, the cancerous cells tend to use their adhesion to fibronectin in the surrounding microenvironment to reduce the endogenous levels of the proapoptotic BH3-only Bcl-2 family member, Bim1, thus conferring resistance by disabling apoptosis (Hazlehurst et al., 2003; Hanahan and Weinberg, 2011). From a clinical point of view, it is thought that combining current therapies with inhibitors of EMDR pathways could enhance the effectiveness of the treatment (Croix et al., 1996; Weaver et al., 1997; Hazlehurst et al., 2000; White et al., 2004; Lwin et al., 2007). A proof-of-principle example was demonstrated by the combination of melphalan, a DNA alkylating agent used in the treatment of multiple myeloma and ovarian carcinomas, with an anti-integrin α-4 antibody (natalizumab) which significantly inhibited myeloma growth and reduced tumor burden in patients (Mori et al., 2004; Engelhardt and Kappos, 2008).

CONCLUSION

Resistance to drugs continues to be a major problem in oncology affecting the majority of cancer patients. Here we provide many examples of how cells become resistant to various drugs including alteration in drug metabolism, modification of drug targets, and genetic rewiring of cells to bypass targeted pathways. A better understanding of oncogene networks and oncogene cooperativity will likely improve therapeutic strategies by identifying optimal combinations based on the genetic lesions in the tumors. Importantly, tumors are highly heterogenous and this heterogeneity may well substantially contribute to primary or acquired resistance. Armed with a greater understanding of the mechanisms of drug resistance will undoubtedly lead to more long term remissions and hopefully cures.

ACKNOWLEDGMENTS

This work was supported by National Institutes for Health (NIH) and The Leukemia and Lymphoma Society (USA). Hiba Zahreddine holds a scholarship from the National Council for Scientific Research (CNRS)-Lebanon. Katherine L. B. Borden holds a Canada Research Chair.

REFERENCES

Aas, T., Borresen, A. L., Geisler, S., Smith-Sorensen, B., Johnsen, H., Varhaug, J. E., et al. (1996). Specific P53 mutations are associated with de novo resistance to doxorubicin in breast cancer patients. *Nat. Med.* 2, 811–814.

Apperley, J. F. (2007). Part I: mechanisms of resistance to imatinib in chronic myeloid leukaemia. *Lancet Oncol.* 8, 1018–1029.

Arber, N., Doki, Y., Han, E. K., Sgambato, A., Zhou, P., Kim, N. H., et al. (1997). Antisense to cyclin D1 inhibits the growth and tumorigenicity of human colon cancer cells. *Cancer Res.* 57, 1569–1574.

Atwood, S. X., Chang, A. L., and Oro, A. E. (2012). Hedgehog pathway inhibition and the race against tumor evolution. *J. Cell Biol.* 199, 193–197.

Balak, M. N., Gong, Y., Riely, G. J., Somwar, R., Li, A. R., Zakowski, M. F., et al. (2006). Novel D761Y and common secondary T790M mutations in epidermal growth factor receptor-mutant lung adenocarcinomas with acquired resistance to kinase inhibitors. *Clin. Cancer Res.* 12, 6494–6501.

Bardenheuer, W., Lehmberg, K., Rattmann, I., Brueckner, A., Schneider, A., Sorg, U. R., et al. (2005). Resistance to cytarabine and gemcitabine and in vitro selection of transduced cells after retroviral expression of cytidine deaminase in human hematopoietic progenitor cells. *Leukemia* 19, 2281–2288.

Bean, J., Riely, G. J., Balak, M., Marks, J. L., Ladanyi, M., Miller, V. A., et al. (2008). Acquired resistance to epidermal growth factor receptor kinase inhibitors associated with a novel T854A mutation in a patient with EGFR-mutant lung adenocarcinoma. *Clin. Cancer Res.* 14, 7519–7525.

Bidard, F. C., Vincent-Salomon, A., Gomme, S., Nos, C., De Rycke, Y., Thiery, J. P., et al. (2008). Disseminated tumor cells of breast cancer patients: a strong prognostic factor for distant and local relapse. *Clin. Cancer Res.* 14, 3306–3311.

Blencke, S., Ullrich, A., and Daub, H. (2003). Mutation of threonine 766 in the epidermal growth factor receptor reveals a hotspot for resistance formation against selective tyrosine kinase inhibitors. *J. Biol. Chem.* 278, 15435–15440.

Borsellino, N., Belldegrun, A., and Bonavida, B. (1995). Endogenous interleukin 6 is a resistance factor for *cis*-diamminedichloroplatinum and etoposide-mediated cytotoxicity of human prostate carcinoma cell lines. *Cancer Res.* 55, 4633–4639.

Borsellino, N., Bonavida, B., Ciliberto, G., Toniatti, C., Travali, S., and D'Alessandro, N. (1999). Blocking signaling through the Gp130 receptor chain by interleukin-6 and oncostatin M inhibits PC-3 cell growth and sensitizes the tumor cells to etoposide and cisplatin-mediated cytotoxicity. *Cancer* 85, 134–144.

Borst, P., Evers, R., Kool, M., and Wijnholds, J. (2000). A family of drug transporters: the multidrug resistance-associated proteins. *J. Natl. Cancer Inst.* 92, 1295–1302.

Braun, S., Kentenich, C., Janni, W., Hepp, F., De Waal, J., Willgeroth, F., et al. (2000). Lack of effect of adjuvant chemotherapy on the elimination of single dormant tumor cells in bone marrow of high-risk breast cancer patients. *J. Clin. Oncol.* 18, 80–86.

Breivik, J. (2005). The evolutionary origin of genetic instability in cancer development. *Semin. Cancer Biol.* 15, 51–60.

Bryant, H. E., Schultz, N., Thomas, H. D., Parker, K. M., Flower, D., Lopez, E., et al. (2005). Specific killing of BRCA2-deficient tumours with inhibitors of poly(ADP-ribose) polymerase. *Nature* 434, 913–917.

Cai, J., Weiss, M. L., and Rao, M. S. (2004). In search of "stemness". *Exp. Hematol.* 32, 585–598.

Campbell, P. J., Stephens, P. J., Pleasance, E. D., O'Meara, S., Li, H., Santarius, T., et al. (2008). Identification of somatically acquired rearrangements in cancer using genome-wide massively parallel paired-end sequencing. *Nat. Genet.* 40, 722–729.

Castells, M., Thibault, B., Delord, J. P., and Couderc, B. (2012). Implication of tumor microenvironment in chemoresistance: tumor-associated stromal cells protect tumor cells from cell death. *Int. J. Mol. Sci.* 13, 9545–9571.

Caulin, A. F., and Maley, C. C. (2011). Peto's Paradox: evolution's prescription for cancer prevention. *Trends Ecol. Evol.* 26, 175–182.

Chiarugi, A. (2012). A snapshot of chemoresistance to PARP inhibitors. *Trends Pharmacol. Sci.* 33, 42–48.

Chin, L., and Gray, J. W. (2008). Translating insights from the cancer genome into clinical practice. *Nature* 452, 553–563.

Costa, D. B., Halmos, B., Kumar, A., Schumer, S. T., Huberman, M. S., Boggon, T. J., et al. (2007). BIM mediates EGFR tyrosine kinase inhibitor-induced apoptosis in lung cancers with oncogenic EGFR mutations. *PLoS Med.* 4:e315. doi: 10.1371/journal.pmed.0040315

Crespi, B., and Summers, K. (2005). Evolutionary biology of cancer. *Trends Ecol. Evol.* 20, 545–552.

Croix, B. S., Rak, J. W., Kapitain, S., Sheehan, C., Graham, C. H., and Kerbel, R. S. (1996). Reversal by hyaluronidase of adhesion-dependent multicellular drug resistance in mammary carcinoma cells. *J. Natl. Cancer Inst.* 88, 1285–1296.

Damaraju, V. L., Damaraju, S., Young, J. D., Baldwin, S. A., Mackey, J., Sawyer, M. B., et al. (2003). Nucleoside anticancer drugs: the role of nucleoside transporters in resistance to cancer chemotherapy. *Oncogene* 22, 7524–7536.

Druker, B. J., Talpaz, M., Resta, D. J., Peng, B., Buchdunger, E., Ford, J. M., et al. (2001). Efficacy and safety of a specific inhibitor of the BCR–ABL tyrosine kinase in chronic myeloid leukemia. *N. Engl. J. Med.* 344, 1031–1037.

Engelhardt, B., and Kappos, L. (2008). Natalizumab: targeting alpha4-integrins in multiple sclerosis. *Neurodegener. Dis.* 5, 16–22.

Engelman, J. A., Zejnullahu, K., Mitsudomi, T., Song, Y., Hyland, C., Park, J. O., et al. (2007). MET amplification leads to gefitinib resistance in lung cancer by activating ERBB3 signaling. *Science* 316, 1039–1043.

Farmer, H., Mccabe, N., Lord, C. J., Tutt, A. N., Johnson, D. A., Richardson, T. B., et al. (2005). Targeting the DNA repair defect in BRCA mutant cells as a therapeutic strategy. *Nature* 434, 917–921.

Ferrantini, M., Capone, I., and Belardelli, F. (2007). Interferon-alpha and cancer: mechanisms of action and new perspectives of clinical use. *Biochimie* 89, 884–893.

Frassanito, M. A., Cusmai, A., Iodice, G., and Dammacco, F. (2001). Autocrine interleukin-6 production and highly malignant multiple myeloma: relation with resistance to drug-induced apoptosis. *Blood* 97, 483–489.

Frei, E. III, Karon, M., Levin, R. H., Freireich, E. J., Taylor, R. J., Hananian, J., et al. (1965). The effectiveness of combinations of antileukemic agents in inducing and maintaining remission in children with acute leukemia. *Blood* 26, 642–656.

Galmarini, C. M., Mackey, J. R., and Dumontet, C. (2001). Nucleoside analogues: mechanisms of drug resistance and reversal strategies. *Leukemia* 15, 875–890.

Gatti, L., and Zunino, F. (2005). Overview of tumor cell chemoresistance mechanisms. *Methods Mol. Med.* 111, 127–148.

Gioeli, D. (2011). *Targeted Therapies Mechanisms of Resistance.* New York: Humana Press.

Giona, F., Testi, A. M., Annino, L., Amadori, S., Arcese, W., Camera, A., et al. (1994). Treatment of primary refractory and relapsed acute lymphoblastic leukaemia in children and adults: the GIMEMA/AIEOP experience. Gruppo Italiano Malattie Ematologiche Maligne dell'Adulto. Associazione Italiana Ematologia ed Ocologia Pediatrica. *Br. J. Haematol.* 86, 55–61.

Goldman, J. M., and Melo, J. V. (2003). Chronic myeloid leukemia – advances in biology and new approaches to treatment. *N. Engl. J. Med.* 349, 1451–1464.

Gorre, M. E., Mohammed, M., Ellwood, K., Hsu, N., Paquette, R., Rao, P. N., et al. (2001). Clinical resistance to STI-571 cancer therapy caused by BCR–ABL gene mutation or amplification. *Science* 293, 876–880.

Gottesman, M. M. (2002). Mechanisms of cancer drug resistance. *Annu. Rev. Med.* 53, 615–627.

Gottesman, M. M., Fojo, T., and Bates, S. E. (2002). Multidrug resistance in cancer: role of ATP-dependent transporters. *Nat. Rev. Cancer* 2, 48–58.

Greaves, M. (2007). Darwinian medicine: a case for cancer. *Nat. Rev. Cancer* 7, 213–221.

Guha, M. (2011). PARP inhibitors stumble in breast cancer. *Nat. Biotechnol.* 29, 373–374.

Guilhot, F., Chastang, C., Michallet, M., Guerci, A., Harousseau, J. L., Maloisel, F., et al. (1997). Interferon alfa-2b combined with cytarabine versus interferon alone in chronic myelogenous leukemia. French Chronic Myeloid Leukemia Study Group. *N. Engl. J. Med.* 337, 223–229.

Hall, M. D., Handley, M. D., and Gottesman, M. M. (2009). Is resistance useless? Multidrug resistance and collateral sensitivity. *Trends Pharmacol. Sci.* 30, 546–556.

Hanahan, D., and Weinberg, R. A. (2011). Hallmarks of cancer: the next generation. *Cell* 144, 646–674.

Hartman, J. L. T., Garvik, B., and Hartwell, L. (2001). Principles for the buffering of genetic variation. *Science* 291, 1001–1004.

Hazlehurst, L. A., Argilagos, R. F., and Dalton, W. S. (2007). Beta1 integrin mediated adhesion increases Bim protein degradation and contributes to drug resistance in leukaemia cells. *Br. J. Haematol.* 136, 269–275.

Hazlehurst, L. A., Damiano, J. S., Buyuksal, I., Pledger, W. J., and Dalton, W. S. (2000). Adhesion to fibronectin via beta1 integrins regulates p27kip1 levels and contributes to cell adhesion mediated drug resistance (CAM-DR). *Oncogene* 19, 4319–4327.

Hazlehurst, L. A., Enkemann, S. A., Beam, C. A., Argilagos, R. F., Painter, J., Shain, K. H., et al. (2003). Genotypic and phenotypic comparisons of de novo and acquired melphalan resistance in an isogenic multiple myeloma cell line model. *Cancer Res.* 63, 7900–7906.

Hazlehurst, L. A., Valkov, N., Wisner, L., Storey, J. A., Boulware, D., Sullivan, D. M., et al. (2001). Reduction in drug-induced DNA double-strand breaks associated with beta1 integrin-mediated adhesion correlates with drug resistance in U937 cells. *Blood* 98, 1897–1903.

Heppner, G. H., Dexter, D. L., Denucci, T., Miller, F. R., and Calabresi, P. (1978). Heterogeneity in drug sensitivity among tumor cell subpopulations of a single mammary tumor. *Cancer Res.* 38, 3758–3763.

Hipfner, D. R., Deeley, R. G., and Cole, S. P. (1999). Structural, mechanistic and clinical aspects of MRP1. *Biochim. Biophys. Acta* 1461, 359–376.

Hofmann, W. K., Komor, M., Wassmann, B., Jones, L. C., Gschaidmeier, H., Hoelzer, D., et al. (2003). Presence of the BCR–ABL mutation Glu255Lys prior to STI571 (imatinib) treatment in patients with Ph+ acute lymphoblastic leukemia. *Blood* 102, 659–661.

Hughes, T. P., Kaeda, J., Branford, S., Rudzki, Z., Hochhaus, A., Hensley, M. L., et al. (2003). Frequency of major molecular responses to imatinib or interferon alfa plus cytarabine in newly diagnosed chronic myeloid leukemia. *N. Engl. J. Med.* 349, 1423–1432.

Inukai, M., Toyooka, S., Ito, S., Asano, H., Ichihara, S., Soh, J., et al. (2006). Presence of epidermal growth factor receptor gene T790M mutation as a minor clone in non-small cell lung cancer. *Cancer Res.* 66, 7854–7858.

Ishikawa, T., and Ali-Osman, F. (1993). Glutathione-associated *cis*-diamminedichloroplatinum(II) metabolism and ATP-dependent efflux from leukemia cells. Molecular characterization of glutathione-platinum complex and its biological significance. *J. Biol. Chem.* 268, 20116–20125.

Isoyama, S., Dan, S., Nishimura, Y., Nakamura, N., Kajiwara, G., Seki, M., et al. (2012). Establishment of phosphatidylinositol 3-kinase inhibitor-resistant cancer cell lines and therapeutic strategies for overcoming the resistance. *Cancer Sci.* 103, 1955–1960.

Jabbour, E., Kantarjian, H., Jones, D., Breeden, M., Garcia-Manero, G., O'Brien, S., et al. (2008). Characteristics and outcomes of patients with chronic myeloid leukemia and T315I mutation following failure of imatinib mesylate therapy. *Blood* 112, 53–55.

Jabbour, E., Kantarjian, H., Jones, D., Talpaz, M., Bekele, N., O'Brien, S., et al. (2006). Frequency and clinical significance of BCR–ABL mutations in patients with chronic myeloid leukemia treated with imatinib mesylate. *Leukemia* 20, 1767–1773.

Jedlitschky, G., Leier, I., Buchholz, U., Barnouin, K., Kurz, G., and Keppler, D. (1996). Transport of glutathione, glucuronate, and sulfate conjugates by the MRP gene-encoded conjugate export pump. *Cancer Res.* 56, 988–994.

Juvekar, A., Burga, L. N., Hu, H., Lunsford, E. P., Ibrahim, Y. H., Balmana, J., et al. (2012). Combining a PI3K inhibitor with a PARP inhibitor provides an effective therapy for BRCA1-related breast cancer. *Cancer Discov.* 2, 1048–1063.

Kasahara, K., Fujiwara, Y., Nishio, K., Ohmori, T., Sugimoto, Y., Komiya, K., et al. (1991). Metallothionein content correlates with the sensitivity of human small cell lung cancer cell lines to cisplatin. *Cancer Res.* 51, 3237–3242.

Kasper, M., and Toftgard, R. (2013). Smoothing out drug resistance. *Cancer Cell* 23, 3–5.

Kelley, S. L., Basu, A., Teicher, B. A., Hacker, M. P., Hamer, D. H., and Lazo, J. S. (1988). Overexpression of metallothionein confers resistance to anticancer drugs. *Science* 241, 1813–1815.

Kelly, R. J., Draper, D., Chen, C. C., Robey, R. W., Figg, W. D., Piekarz, R. L., et al. (2011). A pharmacodynamic study of docetaxel in combination with the P-glycoprotein antagonist tariquidar (XR9576) in patients with lung, ovarian, and cervical cancer. *Clin. Cancer Res.* 17, 569–580.

Kobayashi, S., Boggon, T. J., Dayaram, T., Janne, P. A., Kocher, O., Meyerson, M., et al. (2005). EGFR mutation and

resistance of non-small-cell lung cancer to gefitinib. *N. Engl. J. Med.* 352, 786–792.

Konig, J., Nies, A. T., Cui, Y., Leier, I., and Keppler, D. (1999). Conjugate export pumps of the multidrug resistance protein (MRP) family: localization, substrate specificity, and MRP2-mediated drug resistance. *Biochim. Biophys. Acta* 1461, 377–394.

Kreitman, R. J. (2006). Immunotoxins for targeted cancer therapy. *AAPS J.* 8, E532–E551.

Kreitman, R. J., Wilson, W. H., Bergeron, K., Raggio, M., Stetler-Stevenson, M., Fitzgerald, D. J., et al. (2001). Efficacy of the anti-CD22 recombinant immunotoxin BL22 in chemotherapy-resistant hairy-cell leukemia. *N. Engl. J. Med.* 345, 241–247.

Krishnamurthy, P., Ross, D. D., Nakanishi, T., Bailey-Dell, K., Zhou, S., Mercer, K. E., et al. (2004). The stem cell marker Bcrp/ABCG2 enhances hypoxic cell survival through interactions with heme. *J. Biol. Chem.* 279, 24218–24225.

Kufe, D. W., and Spriggs, D. R. (1985). Biochemical and cellular pharmacology of cytosine arabinoside. *Semin. Oncol.* 12, 34–48.

Kummar, S., Chen, A., Ji, J., Zhang, Y., Reid, J. M., Ames, M., et al. (2011). Phase I study of PARP inhibitor ABT-888 in combination with topotecan in adults with refractory solid tumors and lymphomas. *Cancer Res.* 71, 5626–5634.

Kummar, S., Chen, A., Parchment, R. E., Kinders, R. J., Ji, J., Tomaszewski, J. E., et al. (2012). Advances in using PARP inhibitors to treat cancer. *BMC Med.* 10:25. doi: 10.1186/1741-7015-10-25

le Coutre, P., Tassi, E., Varella-Garcia, M., Barni, R., Mologni, L., Cabrita, G., et al. (2000). Induction of resistance to the Abelson inhibitor STI571 in human leukemic cells through gene amplification. *Blood* 95, 1758–1766.

Levine, A. J. (1997). p53, the cellular gatekeeper for growth and division. *Cell* 88, 323–331.

Lichtenstein, A. V. (2005). On evolutionary origin of cancer. *Cancer Cell Int.* 5, 5.

Lippert, T. H., Ruoff, H. J., and Volm, M. (2011). Current status of methods to assess cancer drug resistance. *Int. J. Med. Sci.* 8, 245–253.

Longo-Sorbello, G. S., and Bertino, J. R. (2001). Current understanding of methotrexate pharmacology and efficacy in acute leukemias. Use of newer antifolates in clinical trials. *Haematologica* 86, 121–127.

Luo, J., Solimini, N. L., and Elledge, S. J. (2009). Principles of cancer therapy: oncogene and non-oncogene addiction. *Cell* 136, 823–837.

Lwin, T., Hazlehurst, L. A., Dessureault, S., Lai, R., Bai, W., Sotomayor, E., et al. (2007). Cell adhesion induces p27Kip1-associated cell-cycle arrest through down-regulation of the SCF-Skp2 ubiquitin ligase pathway in mantle-cell and other non-Hodgkin B-cell lymphomas. *Blood* 110, 1631–1638.

Lynch, T. J., Bell, D. W., Sordella, R., Gurubhagavatula, S., Okimoto, R. A., Brannigan, B. W., et al. (2004). Activating mutations in the epidermal growth factor receptor underlying responsiveness of non-small-cell lung cancer to gefitinib. *N. Engl. J. Med.* 350, 2129–2139.

Marusyk, A., and Polyak, K. (2010). Tumor heterogeneity: causes and consequences. *Biochim. Biophys. Acta* 1805, 105–117.

Matsunaga, T., Takemoto, N., Sato, T., Takimoto, R., Tanaka, I., Fujimi, A., et al. (2003). Interaction between leukemic-cell VLA-4 and stromal fibronectin is a decisive factor for minimal residual disease of acute myelogenous leukemia. *Nat. Med.* 9, 1158–1165.

Meads, M. B., Gatenby, R. A., and Dalton, W. S. (2009). Environment-mediated drug resistance: a major contributor to minimal residual disease. *Nat. Rev. Cancer* 9, 665–674.

Meijer, C., Mulder, N. H., Timmer-Bosscha, H., Sluiter, W. J., Meersma, G. J., and De Vries, E. G. (1992). Relationship of cellular glutathione to the cytotoxicity and resistance of seven platinum compounds. *Cancer Res.* 52, 6885–6889.

Michor, F., and Polyak, K. (2010). The origins and implications of intratumor heterogeneity. *Cancer Prev. Res. (Phila)* 3, 1361–1364.

Monceviciute-Eringiene, E. (2005). Neoplastic growth: the consequence of evolutionary malignant resistance to chronic damage for survival of cells (review of a new theory of the origin of cancer). *Med. Hypotheses* 65, 595–604.

Montoni, A., Robu, M., Pouliot, E., and Shah, G. M. (2013). Resistance to PARP-inhibitors in Cancer Therapy. *Front. Pharmacol.* 4:18. doi: 10.3389/fphar.2013.00018

Mori, Y., Shimizu, N., Dallas, M., Niewolna, M., Story, B., Williams, P. J., et al. (2004). Anti-alpha4 integrin antibody suppresses the development of multiple myeloma and associated osteoclastic osteolysis. *Blood* 104, 2149–2154.

Mukherjee, S. (2010). *The Emperor of All Maladies: a Biography of Cancer*. New York: Scribner.

Negrini, S., Gorgoulis, V. G., and Halazonetis, T. D. (2010). Genomic instability – an evolving hallmark of cancer. *Nat. Rev. Mol. Cell Biol.* 11, 220–228.

Nesse, R. M. (2001). How is Darwinian medicine useful? *West. J. Med.* 174, 358–360.

Nguyen, L. V., Vanner, R., Dirks, P., and Eaves, C. J. (2012). Cancer stem cells: an evolving concept. *Nat. Rev. Cancer* 12, 133–143.

Nicolini, F. E., Corm, S., Le, Q. H., Sorel, N., Hayette, S., Bories, D., et al. (2006). Mutation status and clinical outcome of 89 imatinib mesylate-resistant chronic myelogenous leukemia patients: a retrospective analysis from the French intergroup of CML (Fi(phi)-LMC GROUP). *Leukemia* 20, 1061–1066.

Nijman, S. M. (2011). Synthetic lethality: general principles, utility and detection using genetic screens in human cells. *FEBS Lett.* 585, 1–6.

Nobili, S., Landini, I., Mazzei, T., and Mini, E. (2012). Overcoming tumor multidrug resistance using drugs able to evade P-glycoprotein or to exploit its expression. *Med. Res. Rev.* 32, 1220–1262.

O'Brien, C. A., Pollett, A., Gallinger, S., and Dick, J. E. (2007). A human colon cancer cell capable of initiating tumour growth in immunodeficient mice. *Nature* 445, 106–110.

O'Brien, S. G., Guilhot, F., Larson, R. A., Gathmann, I., Baccarani, M., Cervantes, F., et al. (2003). Imatinib compared with interferon and low-dose cytarabine for newly diagnosed chronic-phase chronic myeloid leukemia. *N. Engl. J. Med.* 348, 994–1004.

O'Connor, D., Sibson, K., Caswell, M., Connor, P., Cummins, M., Mitchell, C., et al. (2011). Early UK experience in the use of clofarabine in the treatment of relapsed and refractory paediatric acute lymphoblastic leukaemia. *Br. J. Haematol.* 154, 482–485.

Palma, J. P., Rodriguez, L. E., Bontcheva-Diaz, V. D., Bouska, J. J., Bukofzer, G., Colon-Lopez, M., et al. (2008). The PARP inhibitor, ABT-888 potentiates temozolomide: correlation with drug levels and reduction in PARP activity in vivo. *Anticancer. Res.* 28, 2625–2635.

Palma, J. P., Wang, Y. C., Rodriguez, L. E., Montgomery, D., Ellis, P. A., Bukofzer, G., et al. (2009). ABT-888 confers broad in vivo activity in combination with temozolomide in diverse tumors. *Clin. Cancer Res.* 15, 7277–7290.

Pao, W., Miller, V. A., Politi, K. A., Riely, G. J., Somwar, R., Zakowski, M. F., et al. (2005). Acquired resistance of lung adenocarcinomas to gefitinib or erlotinib is associated with a second mutation in the EGFR kinase domain. *PLoS Med.* 2:e73. doi: 10.1371/journal.pmed.0020073

Park, Y., and Gerson, S. L. (2005). DNA repair defects in stem cell function and aging. *Annu. Rev. Med.* 56, 495–508.

Piccart-Gebhart, M. J., Procter, M., Leyland-Jones, B., Goldhirsch, A., Untch, M., Smith, I., et al. (2005). Trastuzumab after adjuvant chemotherapy in HER2-positive breast cancer. *N. Engl. J. Med.* 353, 1659–1672.

Pinedo, H. M., and Giaccone, G. (1998). *Drug Resistance in the Treatment of Cancer*. Cambridge: Cambridge University Press.

Pluchino, K. M., Hall, M. D., Goldsborough, A. S., Callaghan, R., and Gottesman, M. M. (2012). Collateral sensitivity as a strategy against cancer multidrug resistance. *Drug Resist. Updat.* 15, 98–105.

Potten, C. S., Owen, G., and Booth, D. (2002). Intestinal stem cells protect their genome by selective segregation of template DNA strands. *J. Cell Sci.* 115, 2381–2388.

Raderer, M., and Scheithauer, W. (1995). Treatment of advanced colorectal cancer with 5-fluorouracil and interferon-alpha: an overview of clinical trials. *Eur. J. Cancer* 31A, 1002–1008.

Ricci-Vitiani, L., Lombardi, D. G., Pilozzi, E., Biffoni, M., Todaro, M., Peschle, C., et al. (2007). Identification and expansion of human colon-cancer-initiating cells. *Nature* 445, 111–115.

Riffell, J. L., Lord, C. J., and Ashworth, A. (2012). Tankyrase-targeted therapeutics: expanding opportunities in the PARP family. *Nat. Rev. Drug Discov.* 11, 923–936.

Sampath, D., Cortes, J., Estrov, Z., Du, M., Shi, Z., Andreeff, M., et al. (2006). Pharmacodynamics of cytarabine alone and in combination with 7-hydroxystaurosporine (UCN-01) in AML blasts in vitro and during a clinical trial. *Blood* 107, 2517–2524.

Sawyers, C. (2004). Targeted cancer therapy. *Nature* 432, 294–297.

Schvimer, M., Lash, R. H., and Katzin, W. E. (1995). Intratumoral heterogeneity of DNA ploidy in breast carcinomas: a flow cytometric assessment of sampling techniques. *Cytometry* 22, 292–296.

Sellers, W. R. (2011). A blueprint for advancing genetics-based cancer therapy. *Cell* 147, 26–31.

Shain, K. H., Landowski, T. H., and Dalton, W. S. (2002). Adhesion-mediated intracellular redistribution of c-Fas-associated death domain-like IL-1-converting enzyme-like inhibitory protein-long confers resistance to CD95-induced apoptosis in hematopoietic cancer cell lines. *J. Immunol.* 168, 2544–2553.

Shain, K. H., Yarde, D. N., Meads, M. B., Huang, M., Jove, R., Hazlehurst, L. A., et al. (2009). Beta1 integrin adhesion enhances IL-6-mediated STAT3 signaling in myeloma cells: implications for microenvironment influence on tumor survival and proliferation. *Cancer Res.* 69, 1009–1015.

Sharma, S. V., and Settleman, J. (2007). Oncogene addiction: setting the stage for molecularly targeted cancer therapy. *Genes Dev.* 21, 3214–3231.

Shen, C. Y., Yu, J. C., Lo, Y. L., Kuo, C. H., Yue, C. T., Jou, Y. S., et al. (2000). Genome-wide search for loss of heterozygosity using laser capture microdissected tissue of breast carcinoma: an implication for mutator phenotype and breast cancer pathogenesis. *Cancer Res.* 60, 3884–3892.

Shen, Z. (2011). Genomic instability and cancer: an introduction. *J. Mol. Cell Biol.* 3, 1–3.

Shepherd, F. A., Rodrigues Pereira, J., Ciuleanu, T., Tan, E. H., Hirsh, V., Thongprasert, S., et al. (2005). Erlotinib in previously treated non-small-cell lung cancer. *N. Engl. J. Med.* 353, 123–132.

Siegel, R., Desantis, C., Virgo, K., Stein, K., Mariotto, A., Smith, T., et al. (2012). Cancer treatment and survivorship statistics, 2012. *CA Cancer J. Clin.* 62, 220–241.

Slamon, D. J., Leyland-Jones, B., Shak, S., Fuchs, H., Paton, V., Bajamonde, A., et al. (2001). Use of chemotherapy plus a monoclonal antibody against HER2 for metastatic breast cancer that overexpresses HER2. *N. Engl. J. Med.* 344, 783–792.

Soverini, S., Martinelli, G., Rosti, G., Bassi, S., Amabile, M., Poerio, A., et al. (2005). ABL mutations in late chronic phase chronic myeloid leukemia patients with up-front cytogenetic resistance to imatinib are associated with a greater likelihood of progression to blast crisis and shorter survival: a study by the GIMEMA Working Party on Chronic Myeloid Leukemia. *J. Clin. Oncol.* 23, 4100–4109.

Stratton, M. R., Campbell, P. J., and Futreal, P. A. (2009). The cancer genome. *Nature* 458, 719–724.

Tallman, M. S., Nabhan, C., Feusner, J. H., and Rowe, J. M. (2002). Acute promyelocytic leukemia: evolving therapeutic strategies. *Blood* 99, 759–767.

Taron, M., Ichinose, Y., Rosell, R., Mok, T., Massuti, B., Zamora, L., et al. (2005). Activating mutations in the tyrosine kinase domain of the epidermal growth factor receptor are associated with improved survival in gefitinib-treated chemorefractory lung adenocarcinomas. *Clin. Cancer Res.* 11, 5878–5885.

Teicher, B. A. (2006). *Cancer Drug Resistance*. Totowa: Humana Press.

Testi, A. M., Moleti, M. L., Giona, F., Iori, A. P., Meloni, G., Miniero, R., et al. (1992). Treatment of primary refractory or relapsed acute lymphoblastic leukemia (ALL) in children. *Ann. Oncol.* 3, 765–767.

The International Cancer Genome Consortium. (2010). International network of cancer genome projects. *Nature* 464, 993–998.

Thomas, D. A., Kantarjian, H., Smith, T. L., Koller, C., Cortes, J., O'Brien, S., et al. (1999). Primary refractory and relapsed adult acute lymphoblastic leukemia: characteristics, treatment results, and prognosis with salvage therapy. *Cancer* 86, 1216–1230.

Toyooka, S., Kiura, K., and Mitsudomi, T. (2005). EGFR mutation and response of lung cancer to gefitinib. *N. Engl. J. Med.* 352, 2136; author reply 2136.

Trudeau, M. E., Crump, M., Charpentier, D., Yelle, L., Bordeleau, L., Matthews, S., et al. (2006). Temozolomide in metastatic breast cancer (MBC): a phase II trial of the National Cancer Institute of Canada – Clinical Trials Group (NCIC-CTG). *Ann. Oncol.* 17, 952–956.

Tucker, C. L., and Fields, S. (2003). Lethal combinations. *Nat. Genet.* 35, 204–205.

Ullah, M. F. (2008). Cancer multidrug resistance (MDR): a major impediment to effective chemotherapy. *Asian Pac. J. Cancer Prev.* 9, 1–6.

Venezia, T. A., Merchant, A. A., Ramos, C. A., Whitehouse, N. L., Young, A. S., Shaw, C. A., et al. (2004). Molecular signatures of proliferation and quiescence in hematopoietic stem cells. *PLoS Biol.* 2:e301. doi: 10.1371/journal.pbio.0020301

Voorhees, P. M., Chen, Q., Kuhn, D. J., Small, G. W., Hunsucker, S. A., Strader, J. S., et al. (2007). Inhibition of interleukin-6 signaling with CNTO 328 enhances the activity of bortezomib in preclinical models of multiple myeloma. *Clin. Cancer Res.* 13, 6469–6478.

Wang, S., Yang, D., and Lippman, M. E. (2003). Targeting Bcl-2 and Bcl-XL with nonpeptidic small-molecule antagonists. *Semin. Oncol.* 30, 133–142.

Weaver, V. M., Petersen, O. W., Wang, F., Larabell, C. A., Briand, P., Damsky, C., et al. (1997). Reversion of the malignant phenotype of human breast cells in three-dimensional culture and in vivo by integrin blocking antibodies. *J. Cell Biol.* 137, 231–245.

Weinstein, I. B. (2002). Cancer. Addiction to oncogenes – the Achilles heal of cancer. *Science* 297, 63–64.

Weinstein, I. B., and Joe, A. K. (2006). Mechanisms of disease: oncogene addiction – a rationale for molecular targeting in cancer therapy. *Nat. Clin. Pract. Oncol.* 3, 448–457.

White, D. E., Kurpios, N. A., Zuo, D., Hassell, J. A., Blaess, S., Mueller, U., et al. (2004). Targeted disruption of beta1-integrin in a transgenic mouse model of human breast cancer reveals an essential role in mammary tumor induction. *Cancer Cell* 6, 159–170.

Wild, P., Knuechel, R., Dietmaier, W., Hofstaedter, F., and Hartmann, A. (2000). Laser microdissection and microsatellite analyses of breast cancer reveal a high degree of tumor heterogeneity. *Pathobiology* 68, 180–190.

Williams, G. C., and Nesse, R. M. (1991). The dawn of Darwinian medicine. *Q. Rev. Biol.* 66, 1–22.

Wilson, T. R., Johnston, P. G., and Longley, D. B. (2009). Anti-apoptotic mechanisms of drug resistance in cancer. *Curr. Cancer Drug Targets* 9, 307–319.

Wilson, T. R., Longley, D. B., and Johnston, P. G. (2006). Chemoresistance in solid tumours. *Ann. Oncol.* 17(Suppl. 10), x315–x324.

Wong, A. L., and Lee, S. C. (2012). Mechanisms of resistance to trastuzumab and novel therapeutic strategies in HER2-positive breast cancer. *Int. J. Breast Cancer* 2012, 415170.

Xu, Y., and Villalona-Calero, M. A. (2002). Irinotecan: mechanisms of tumor resistance and novel strategies for modulating its activity. *Ann. Oncol.* 13, 1841–1851.

Yauch, R. L., Dijkgraaf, G. J., Alicke, B., Januario, T., Ahn, C. P., Holcomb, T., et al. (2009). Smoothened mutation confers resistance to a Hedgehog pathway inhibitor in medulloblastoma. *Science* 326, 572–574.

Zhang, P., Zuo, H., Ozaki, T., Nakagomi, N., and Kakudo, K. (2006). Cancer stem cell hypothesis in thyroid cancer. *Pathol. Int.* 56, 485–489.

Conflict of Interest Statement: The authors declare that the research was conducted in the absence of any commercial or financial relationships that could be construed as a potential conflict of interest.

Received: 31 December 2012; paper pending published: 17 January 2013; accepted: 25 February 2013; published online: 14 March 2013.

Citation: Zahreddine H and Borden KLB (2013) Mechanisms and insights into drug resistance in cancer. Front. Pharmacol. ***4****:28. doi: 10.3389/fphar.2013.00028*

This article was submitted to Frontiers in Pharmacology of Anti-Cancer Drugs, a specialty of Frontiers in Pharmacology.

CHAPTER 3

The Sonic Hedgehog Factor GLI1 Imparts drug resistance through inducible glucuronidation

(RESEARCH ARTICLE)

Published Manuscript in *Nature. 2014 Jul 3;511(7507):90-3. doi: 10.1038/nature13283.*

Permissions from Nature Publishing Group (NPG): "Since 2003, ownership of copyright in original research articles remains with the Authors, provided that, when reproducing the Contribution or extracts from it, the Authors acknowledge first and reference publication in the Journal."

Synopsis: Despite many recent successes in the treatment of cancer, development of chemoresistance in many of the initially responding patients, and primary resistance in others, remains a major impediment in therapy development. In this chapter, I present data supporting the discovery of a novel multidrug resistance mechanism: Gli1 dependent drug glucuronidation; and a means of overcoming this impediment using inhibitors of the Sonic Hedgehog pathway.

Contribution:

All data in **Figures 1, 3 and 4** were generated by **Hiba Zahreddine (100%)**

All data in **Extended Data Figures 2, 3, 7 and Extended Table 1** were generated by **Hiba Zahreddine (100%)**

Data in **Figures 2, 6** were generated by **Hiba Zahreddine (50%)** and **Biljana Culjkovic-Kraljacic (50%)**

Data in **Extended Data Figures** 6 were generated by **Hiba Zahreddine (50%)** and **Biljana Culjkovic- Kraljacic (50%)**

Data in **Extended Data Figure 4** was generated by **Biljana Culjkovic- Kraljacic (100%)**

Data in **Extended Data Figure 1** was generated by **Julie Hinsinger (100%)**

Data in **Extended Data Figure 5** were generated by **Pei Shanshan (100%)**

Hiba Zahreddine and Biljana Culjkovic-Kraljacic designed and performed experiments, analysed data and wrote the manuscript; L.C., A.A. and G.C. performed experiments; P.G., S.P. and C.T.J. analysed data; A.A.R. performed experiments and analysed data; J.B.J. and S.J.M. designed experiments; S.A. was medical monitor for the trial, treated patients and analysed clinical data; E.C. coordinated clinical trials and analysed clinical data; B.L., J.B. and M.W.B.

treated patients, provided specimens and analysed clinical data; W.H.M. designed experiments, analysed data and edited the manuscript; K.L.B.B. designed experiments, analysed data and wrote the manuscript.

LETTER

doi:10.1038/nature13283

The sonic hedgehog factor GLI1 imparts drug resistance through inducible glucuronidation

Hiba Ahmad Zahreddine[1], Biljana Culjkovic-Kraljacic[1], Sarit Assouline[2], Patrick Gendron[1], Andrea A. Romeo[3], Stephen J. Morris[3], Gregory Cormack[1], James B. Jaquith[3]†, Leandro Cerchietti[4], Eftihia Cocolakis[2], Abdellatif Amri[1], Julie Bergeron[5], Brian Leber[6], Michael W. Becker[7], Shanshan Pei[8], Craig T. Jordan[8], Wilson H. Miller Jr[2] & Katherine L. B. Borden[1]

Drug resistance is a major hurdle in oncology. Responses of acute myeloid leukaemia (AML) patients to cytarabine (Ara-C)-based therapies are often short lived with a median overall survival of months[1–4]. Therapies are under development to improve outcomes and include targeting the eukaryotic translation initiation factor (eIF4E) with its inhibitor ribavirin[5–7]. In a Phase II clinical trial in poor prognosis AML[5], ribavirin monotherapy yielded promising responses including remissions; however, all patients relapsed. Here we identify a novel form of drug resistance to ribavirin and Ara-C. We observe that the sonic hedgehog transcription factor glioma-associated protein 1 (GLI1) and the UDP glucuronosyltransferase (UGT1A) family of enzymes are elevated in resistant cells. UGT1As add glucuronic acid to many drugs, modifying their activity in diverse tissues[8]. GLI1 alone is sufficient to drive UGT1A-dependent glucuronidation of ribavirin and Ara-C, and thus drug resistance. Resistance is overcome by genetic or pharmacological inhibition of GLI1, revealing a potential strategy to overcome drug resistance in some patients.

To better understand the molecular basis for relapse in our clinical trial (Fig. 1a and Extended Data Fig. 1), we generated resistant cells using head and neck carcinoma FaDu and AML-M5 THP-1 cells, both of which have highly elevated eIF4E and concomitant ribavirin sensitivity[6,7]. Two forms of drug resistance emerged, characterized by unimpaired growth in clinically achievable ribavirin concentrations and a loss of eIF4E targeting (Fig. 1b, c and Extended Data Fig. 2a–c). Type I resistant cells (FRI, THPA, THPB) had severely impaired drug uptake, whereas type II resistant cells (FRII) did not (Fig. 1d and Extended Data Fig. 2d). Type I resistance was characterized by substantial reduction of adenosine kinase (ADK) (Extended Data Fig. 3a, b). ADK acts in cellular retention of ribavirin, as unphosphorylated ribavirin is readily exported by the nucleoside transporter ENT1 (also known as SLC29A1; refs 9, 10). Indeed, ADK reduction alone imparts ribavirin resistance (Extended Data Fig. 3c, d). Analysis of our patient pool indicated that only two patients had features consistent with type I resistance (Extended Data Fig. 3e, f).

Therefore, we investigated type II resistance. Given that eIF4E was not mutated and was functional in FRII cells (Extended Data Fig. 2e–g), we examined whether the ribavirin–eIF4E interaction was disrupted, by assessing the ability of eIF4E to immunoprecipitate ^{3}H-ribavirin (Fig. 1e). Although ^{3}H-ribavirin is enriched ~sixfold in the eIF4E-immunoprecipitated fraction in parental cells, this interaction is lost in FRII cells, despite normal uptake and functional eIF4E.

RNA sequencing (RNA-seq) analysis revealed that 30 transcripts were differentially expressed in FRII cells, including *GLI1* messenger RNA, by 21-fold (Extended Data Table 1). Consistently, GLI1 protein levels were highly elevated, as was GLI1's target SNAIL (Fig. 1f). We investigated the clinical relevance of this elevation in our patients treated with ribavirin monotherapy. At relapse, leukaemic blasts had elevated *GLI1* mRNA levels for 9 out of 9 patients examined (up to tenfold baseline) (Fig. 2a). For instance, *GLI1* mRNA and protein levels were elevated at relapse (for example, patients 8 (complete remission (CR)), 11 (partial remission (PR)) and 17 (blast response (BR); Fig. 2a and Extended Data Fig. 4; confocal microscopy was used owing to limited material at response). Interestingly, GLI1 levels in patient 17 decreased during response and re-emerged at relapse. Patients 9, 13 and 19, who did not respond clinically or molecularly, had highly elevated GLI1 levels before treatment,

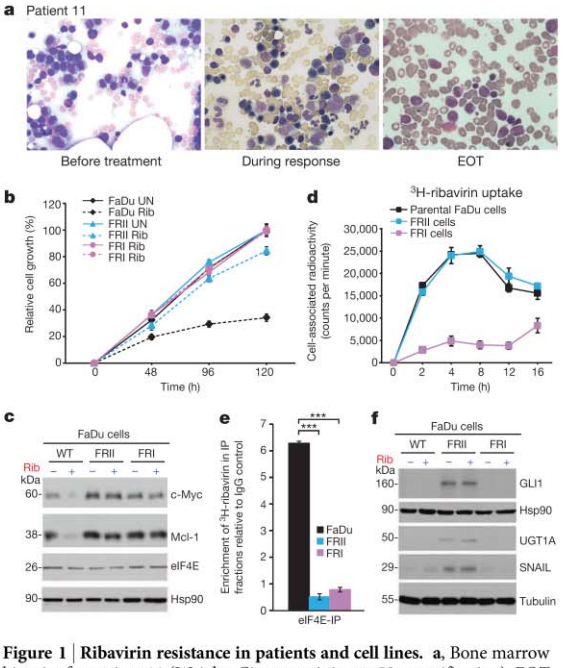

Figure 1 | Ribavirin resistance in patients and cell lines. **a**, Bone marrow biopsies for patient 11 (Wright–Giemsa staining, ×50 magnification). EOT, end of treatment. **b**, Cell growth in untreated (UN) or treated with 20 μM ribavirin (Rib), which is clinically achievable[5]. **c**, Western blots of eIF4E targets Mcl-1 and c-Myc (also known as MCL1 and MYC, respectively). **d**, ^{3}H-ribavirin uptake. **e**, eIF4E co-immunoprecipitation (IP) with ^{3}H-ribavirin relative to IgG. Loading is in Extended Data Fig. 6. **f**, Western blots of GLI1 and UGT1A. For **b**, **d** and **e**, error bars are means ± standard deviations (s.d.). ***$P < 0.001$ (Student's *t*-test). For all panels experiments were completed in triplicate, at least three independent times. Hsp90 and tubulin provide loading controls.

[1]Institute for Research in Immunology and Cancer and Department of Pathology and Cell Biology, Université de Montréal, P.O. Box 6128, Downtown Station, Montréal, Québec H3C 3J7, Canada. [2]Segal Cancer Centre, Lady Davis Institute, Jewish General Hospital, McGill University, 3755 Côte-Ste-Catherine Road, Montréal, Québec H3T 1E2, Canada. [3]Pharmascience Inc., 6111 Royalmount Avenue, Montreal, Quebec H4P 2T4, Canada. [4]Division of Hematology and Oncology, Department of Medicine, Weill Cornell Medical College, Cornell University, 1305 York Avenue, New York, New York 10021, USA. [5]Hôpital Maisonneuve-Rosemont, 5415 Boulevard de l'Assomption, Montréal, Québec H1T 2M4, Canada. [6]McMaster University/Hamilton Health Sciences, 237 Barton Street East, Hamilton, Ontario L8L 2X2, Canada. [7]Department of Medicine, Division of Hematology/Oncology, 601 Elmwood Avenue, University of Rochester, Rochester, New York 14627, USA. [8]Division of Hematology, Department of Medicine, University of Colorado Denver, 13123 East 16th Avenue, Aurora, Colorado 80045, USA. †Present address: JAQJAM Consulting, Montreal J7V 9B6, Canada.

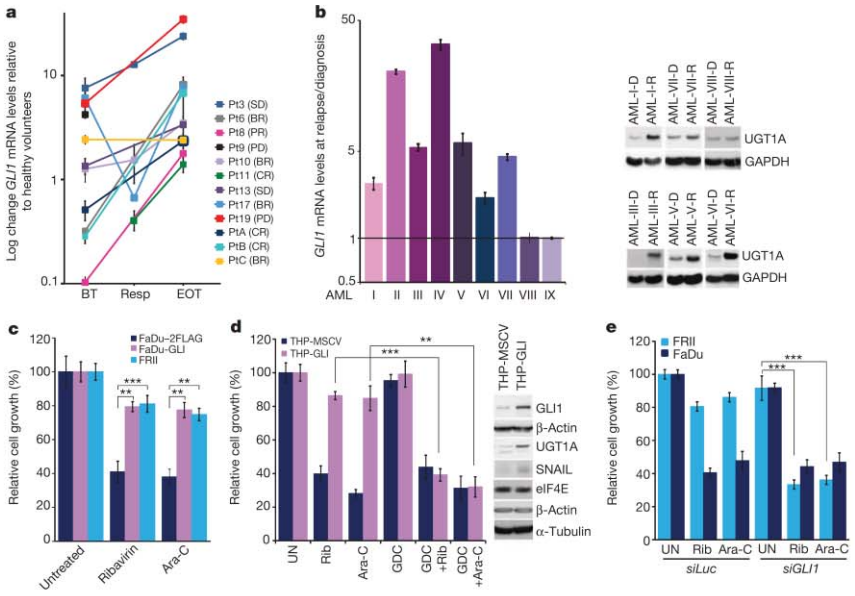

Figure 2 | GLI1 status underpins resistance. **a**, *GLI1* mRNA levels before treatment (BT), at best response (Resp) and EOT for ribavirin-treated patients/healthy volunteers. Pt, patient. **b**, *GLI1* mRNA (right) and UGT1A protein (left) for patients treated with Ara-C therapies at relapse (R)/diagnosis (D). Roman numerals denote patients treated with standard chemotherapy as opposed to ribavirin monotherapy (numbers) or ribavirin plus Ara-C (letters). **c**, **d**, Effects of GLI1 overexpression on drug sensitivity: ribavirin (20 μM), Ara-C (200 nM, clinically achievable[7]). **e**, siRNA to *GLI1* restores drug sensitivity. *siLuc*, nonspecific control RNA. **a**, **b**, RNA results were normalized to ubiquitin. In all panels, error bars denote mean ± s.d. Experiments were completed in triplicate at least three independent times. $^{**}P < 0.01$, $^{***}P < 0.001$ (Student's *t*-test). Figure 4a–c shows corresponding western blots. Actin, tubulin and GADPH provide loading controls.

relative to healthy individuals or responding patients. Moreover, in our ribavirin and low-dose Ara-C Phase I combination trial, patients A (CR, relapsed at 2 years) and B (CR, relapsed at 9 months) had increased GLI1 levels at relapse (Fig. 2a and Extended Data Fig. 4; these patients are denoted by letters so as not to be confused with ribavirin monotherapy patients, denoted by numbers). For patient C (PR, off treatment owing to a dose-limiting toxicity), *GLI1* mRNA levels were unchanged at end of treatment (EOT), consistent with continued remission at that time. Thus, elevated GLI1 is associated with primary and acquired resistance in both ribavirin clinical trials. We observed that type I and type II resistance coexisted in two patients (Fig. 2 and Extended Data Fig. 3e, f). Whether this occurs in the same cells or whether multiple resistant populations emerge is unknown.

We extended these studies to investigate whether GLI1 levels were elevated in patients who failed more commonly used Ara-C therapies (Fig. 2b). *GLI1* mRNA levels were substantially elevated at relapse relative to diagnosis in 7 out of 9 patients examined. Consistently, analysis of The Cancer Genome Atlas AML data set[11] showed that GLI1 elevation was associated with poor prognosis (Extended Data Fig. 5). These data suggest that GLI1 overexpression contributed to drug resistance and clinical relapse in some AML patients.

Next, we investigated whether GLI1 alone imparted drug resistance by generating FaDu and THP1 cells stably overexpressing GLI1 (FaDu-GLI, THP1-GLI; Fig. 2c, d). Growth of GLI1-overexpressing cells was not substantially affected by levels of ribavirin or Ara-C that impaired growth of controls. Further, *GLI1* knockdown re-sensitized FRII cells to ribavirin and Ara-C without affecting growth in the absence of either drug (Fig. 2e).

To identify strategies to restore drug sensitivity, we used a clinically approved inhibitor of sonic hedgehog signalling upstream of GLI1, GDC-0449 (ref. 12) (Figs 2d and 3a). FRII cells were pre-treated with 200 nM GDC-0449 (which is clinically achievable[13]) and subsequently, 20 μM ribavirin. Notably, GDC-0449 treatment followed by ribavirin led to ~60% reduction in growth relative to untreated FRII cells. GDC-0449 treatment alone did not substantially affect growth in either cell line. Importantly, GDC-0449 treatment also restored sensitivity to clinically relevant Ara-C levels (200 nM). Furthermore, GDC-0449 treatment of FaDu-GLI and THP-GLI cells re-sensitized these to ribavirin and Ara-C (Figs 2d and 3a). Finally, a direct inhibitor of GLI1, GANT61 (ref. 14), paralleled the effects of GDC-0449 (Extended Data Fig. 6a). Thus, type II resistance is reversed by pharmacological inhibition of the sonic hedgehog pathway.

To better understand the molecular basis for resistance, we monitored the ability of eIF4E to immunoprecipitate ^{3}H-ribavirin as a function of GLI1 status (Fig. 3b and Extended Data Fig. 6b–d). Although eIF4E–ribavirin complexes were readily detected in controls, they were absent in GLI1-overexpressing cells (Fig. 3b). Conversely, GDC-0449 treatment or *GLI1* knockdown in FRII cells restored ribavirin–eIF4E complexes to control levels (Fig. 3b). Thus, there is a clear correlation between GLI1 elevation, reduction in eIF4E–ribavirin complexes, and resistance.

Given that resistant cells did not form ribavirin–eIF4E complexes but retained active eIF4E (Figs 1e, 3b and Extended Data Fig. 2e–g), we proposed that ribavirin, and possibly Ara-C, underwent some form of GLI1-dependent modification. The drug-metabolizing UGT1A enzymes had elevated protein levels in FRII cells, thereby suggesting a resistance mechanism (Figs 1f and 4a–c). This was also the case for FaDu-GLI and THP-GLI cells, relative to vector controls (Figs 2d and 4b). Significantly, *GLI1* knockdown or GDC-0449 treatment reduced UGT1A protein levels (Fig. 4a, c), confirming the correlation between GLI1 and UGT1A protein expression. Note that GLI1 does not increase mRNA levels but rather the protein stability of UGT1As (Extended Data Fig. 6e–h).

To determine the clinical relevance of these observations, we examined UGT1A protein levels during response and relapse using confocal microscopy (Extended Data Fig. 4). We observed UGT1A elevation upon

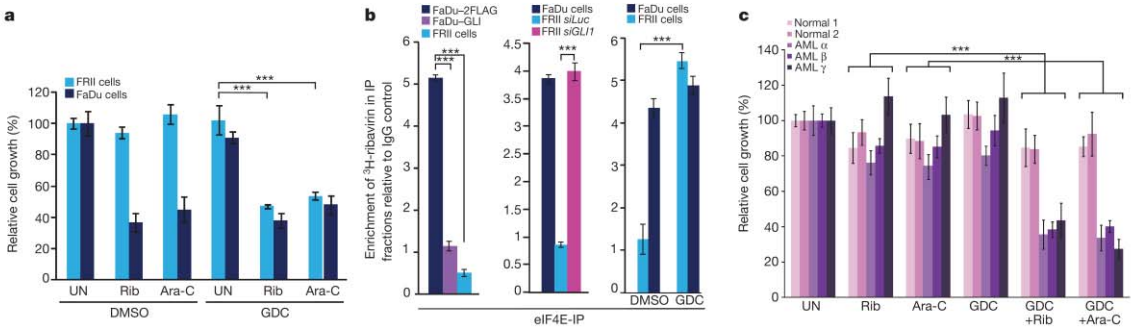

Figure 3 | Targeting GLI1 activity. **a**, FRII cell growth ± GDC-0449 (GDC) and ribavirin or Ara-C. DMSO, dimethylsulphoxide. **b**, The presence of the ribavirin–eIF4E complex is measured as a function of GLI1 status. Ribavirin–eIF4E complexes are detected using ^{3}H-ribavirin and eIF4E immunoprecipitation relative to IgG controls: FaDu–GLI cells, *siGLI1*, GDC-0449 treatment. See Extended Data Fig. 6 for immunoprecipitation controls. **c**, Methylcellulose colony growth assays in specimens from M4/M5 AML patients or healthy volunteers (bone marrow). For all panels error bars are mean ± s.d. Results are representative of at least three independent experiments in triplicate (**a**, **b**) or at least two (**c**) in replicates of 5. $^{**}P < 0.01$, $^{***}P < 0.001$ (Student's *t*-test).

relapse; that is, patients 11 (CR), 8 (PR) and 17 (BR) in the ribavirin monotherapy trial and in patients A (CR) and B (CR) in the combination trial. Patient C (PR) had no change in UGT1A levels at EOT, consistent with still being in remission. In patients treated with standard Ara-C therapies, UGT1A protein levels were elevated in 6 out of 7 specimens at relapse relative to diagnosis, and this occurred in the patients with concomitant elevated GLI1 (Fig. 2b). There was insufficient material for protein analysis of the remaining two specimens.

Next, we used mass spectrometry (MS) to determine whether ribavirin and Ara-C were glucuronidated in resistant cells (Fig. 4d–i and Extended Data Fig. 7). Metabolites were isolated, subjected to hydrophilic chromatography and detected by electrospray ionization-MS. In parental cells, ribavirin diphosphate (RDP) is the major peak (Fig. 4e, l). In FRII cells, a new peak emerged with a mass consistent with the ribavirin-glucuronide (Fig. 4d). Using collision-induced ion fragmentation, we observed the triazole moiety of ribavirin as a major fragment supporting this as a site of glucuronidation (Fig. 4j red arrow, and Extended Data Fig. 7a). Relative peak intensities suggest that there is more ribavirin-glucuronide than RDP (Fig. 4d). Notably, GDC-0449 treatments eliminated ribavirin glucuronidation in FRII cells (Fig. 4f). GLI1 overexpression in parental cells led to formation of ribavirin-glucuronides (Fig. 4h). *In vitro* glucuronidation studies indicated that specific UGT1As are likely to be important to this process, as is ribavirin phosphorylation (Extended Data Fig. 7). Moreover, we observe AraC-glucuronides in FRII but not parental cells, and this modification was lost upon GDC-0449 treatment (Extended Data Fig. 7e, f). Thus, Ara-C and ribavirin

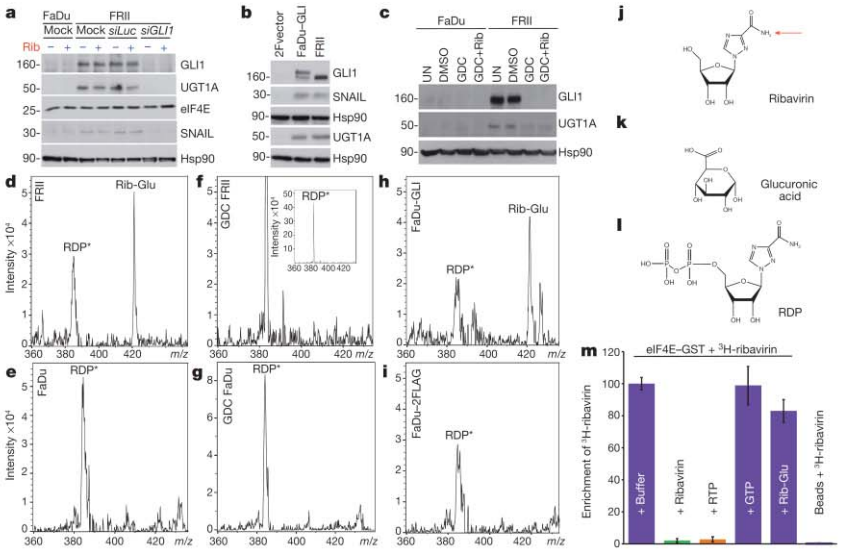

Figure 4 | Link between GLI1, UGT1A and drug glucuronidation. **a**–**c**, Western blots as a function of GLI1. Hsp90 provides a loading control. 2F, 2FLAG. **d**–**i**, MS/MS extracted ion chromatographs are shown. Rib-Glu, ribavirin glucuronide; RDP*, ribavirin diphosphate minus H_2O. Fragmentation of Rib-Glu peak confirms its identity (Extended Data Fig. 7a). **j**, Ribavirin, the best-supported glucuronidation site indicated by red arrow. **k**, Glucuronic acid. **l**, RDP. **m**, ^{3}H-ribavirin–eIF4E–GST complexes competed by equimolar amounts of compounds. ^{3}H-ribavirin did not bind beads alone. See Extended Data Fig. 7d for loading. Error bars are averages ± s.d. Experiments were carried out in triplicate, at least three independent times.

glucuronidation were GLI1-dependent, and elimination of the glucuronides by GLI1 inhibition correlated with restored drug sensitivity.

We examined the capacity of ribavirin-glucuronides to bind eIF4E. Ribavirin-glucuronide was isolated by hydrophilic chromatography and confirmed by MS/MS (Extended Data Fig. 7c). Using eIF4E–glutathione *S*-transferase (GST) immobilized on glutathione agarose, we observed that non-radioactive ribavirin or ribavirin triphosphate (RTP) compete for ^{3}H-ribavirin–eIF4E complexes, whereas neither the negative control GTP nor the ribavirin-glucuronide did so (Fig. 4m). Thus, ribavirin glucuronidation impairs its interaction with eIF4E, underpinning resistance.

To further explore the effects of GLI1 inhibition on drug sensitivity, we monitored colony growth of primary AML specimens as a function of GDC-0449 treatment (Fig. 3c). Specimens were selected from patients that had previously failed induction chemotherapy. We observed that although GDC-0449 has little effect on colony growth alone, it strongly potentiated the effects of Ara-C and ribavirin, presumably by elimination of the respective glucuronides. By contrast, we observed little effect in specimens from healthy volunteers, consistent with our results in control cells.

Several factors probably contribute to GLI1 elevation in FRII cells, including reduced patched 1 levels, but not altered promoter methylation or modified hedgehog ligand levels (Extended Data Fig. 8). Glucuronidation is typically perceived as a detoxification pathway but does not always enhance drug excretion[15]. Similar to our findings with ribavirin and eIF4E, testosterone glucuronidation modifies its targets rather than its efflux[15]. Our findings reveal a role for GLI1 in drug metabolism and resistance. Here, GLI1 inhibition could restore drug sensitivity and thereby provide therapeutic benefit.

METHODS SUMMARY

Ribavirin-resistant cell lines were selected on the basis of prolonged ribavirin exposure, routinely tested for resistance, which was retained even after 6 months in the absence of ribavirin. In the absence of ribavirin, cells grew with indistinguishable doubling times (Extended Data Fig. 2). Drug treatments and cell viability assays were carried out as described[16] using Trypan Blue or in parallel, Cell Counting Kit-8. For ^{3}H-ribavirin immunoprecipitation, cells were incubated with 0.66 μM ^{3}H-ribavirin for 8 h at 37 °C, dounce homogenized, lysates pre-cleared and immunoprecipitated with 8 μg mouse IgG or monoclonal mouse anti-eIF4E antibodies coupled to Protein A/G PLUS-Agarose overnight at 4 °C. Beads were washed, subjected to scintillation counting or western analysis.

Quantitative PCR analysis used the relative standard curve method[5]. Western analysis was described[6] with a modified lysis buffer (40 mM HEPES, pH 7.5, 120 mM NaCl, 1 mM EDTA, 10 mM β-glycerophosphate, 50 mM NaF, 0.5 μM NaVO3, and 1% (v/v) Triton X-100 with protease inhibitors). For mass spectroscopy, cells were treated with ribavirin or Ara-C, mixed with an equal volume of methanol, flash frozen in liquid nitrogen, stored at −80 °C overnight, thawed, centrifuged at 10,000 r.p.m. for 10 min and subjected to hydrophilic chromatography (Inertsil HILIC) using an Agilent 1100 HPLC coupled to an Agilent MSD Trap SL, with an ESI source in positive ion mode. Chromatography used 2 mM ammonium formate, pH 3.2 (solvent A) and 100% acetonitrile (solvent B). For ^{3}H-ribavirin pulldown, eIF4E–GST immobilized on glutathione beads was incubated with 250 nM ^{3}H-ribavirin and the same concentration of purified Rib-Glu, ^{1}H-ribavirin, RTP, GTP or buffer for 30 min in 100 mM sodium phosphate, pH 7.5, 300 mM NaCl, 0.015% NP40, 10 μM BSA with protease inhibitors. Samples were eluted in Laemmli; radioactivity measured by scintillation counting. Colony formation assays in AML specimens were as described[7].

Clinical Trials were approved by each institution ethics board and by Health Canada. Written informed consent was obtained according to the Helsinki protocol. Clinical trials were registered with ClinicalTrials.gov NCT00559091 and NCT01056523.

Online Content Any additional Methods, Extended Data display items and Source Data are available in the online version of the paper; references unique to these sections appear only in the online paper.

Received 15 May 2013; accepted 26 March 2014.
Published online 28 May 2014.

1. Deschler, B., de Witte, T., Mertelsmann, R. & Lubbert, M. Treatment decision-making for older patients with high-risk myelodysplastic syndrome or acute myeloid leukemia: problems and approaches. *Haematologica* **91,** 1513–1522 (2006).
2. Deschler, B. & Lubbert, M. Acute myeloid leukemia: epidemiology and etiology. *Cancer* **107,** 2099–2107 (2006).
3. Pulsoni, A. *et al.* Survival of elderly patients with acute myeloid leukemia. *Haematologica* **89,** 296–302 (2004).
4. Hiddemann, W. *et al.* Management of acute myeloid leukemia in elderly patients. *J. Clin. Oncol.* **17,** 3569–3576 (1999).
5. Assouline, S. *et al.* Molecular targeting of the oncogene eIF4E in acute myeloid leukemia (AML): a proof-of-principle clinical trial with ribavirin. *Blood* **114,** 257–260 (2009).
6. Kentsis, A., Topisirovic, I., Culjkovic, B., Shao, L. & Borden, K. L. Ribavirin suppresses eIF4E-mediated oncogenic transformation by physical mimicry of the 7-methyl guanosine mRNA cap. *Proc. Natl Acad. Sci. USA* **101,** 18105–18110 (2004).
7. Kraljacic, B. C., Arguello, M., Amri, A., Cormack, G. & Borden, K. Inhibition of eIF4E with ribavirin cooperates with common chemotherapies in primary acute myeloid leukemia specimens. *Leukemia* **25,** 1197–1200 (2011).
8. Tukey, R. H. & Strassburg, C. P. Human UDP-glucuronosyltransferases: metabolism, expression, and disease. *Annu. Rev. Pharmacol. Toxicol.* **40,** 581–616 (2000).
9. Jarvis, S. M., Thorn, J. A. & Glue, P. Ribavirin uptake by human erythrocytes and the involvement of nitrobenzylthioinosine-sensitive (es)-nucleoside transporters. *Br. J. Pharmacol.* **123,** 1587–1592 (1998).
10. Willis, R. C., Carson, D. A. & Seegmiller, J. E. Adenosine kinase initiates the major route of ribavirin activation in a cultured human cell line. *Proc. Natl Acad. Sci. USA* **75,** 3042–3044 (1978).
11. Cancer Genome Atlas Research. Genomic and epigenomic landscapes of adult *de novo* acute myeloid leukemia. *N. Engl. J. Med.* **368,** 2059–2074 (2013).
12. Mas, C. & Ruiz i Altaba, A. Small molecule modulation of HH-GLI signaling: current leads, trials and tribulations. *Biochem. Pharmacol.* **80,** 712–723 (2010).
13. LoRusso, P. M. *et al.* Pharmacokinetic dose-scheduling study of hedgehog pathway inhibitor vismodegib (GDC-0449) in patients with locally advanced or metastatic solid tumors. *Clin. Cancer Res.* **17,** 5774–5782 (2011).
14. Lauth, M., Bergstrom, A., Shimokawa, T. & Toftgard, R. Inhibition of GLI-mediated transcription and tumor cell growth by small-molecule antagonists. *Proc. Natl Acad. Sci. USA* **104,** 8455–8460 (2007).
15. Dutton, G. *Glucuronidation of Drugs and Other Compounds* Ch. 1 (CRC, 1980).
16. Olah, E. *et al.* Molecular mechanisms in the antiproliferative action of taxol and tiazofurin. *Anticancer Res.* **16,** 2469–2477 (1996).

Acknowledgements We are grateful for reading of the manuscript by A. Kentsis, M. Osborne, F. Pettersson, S. del Rincon and C. Perreault. We are grateful for the use of Pharmascience facilities thanks to M. Goodman and D. Goodman, for specimens from the Banques de Cellules Leucémiques Du Québec (BCLQ), and for technical discussions with M. Ouellet. We thank nursing and support staff at all the clinical sites, and A. Ramteke for technical support. K.L.B.B. is supported by funds from the National Institutes of Health (RO1 80728 and 98571), IRICoR and Translational Research Program grants from the Leukemia and Lymphoma Society USA. K.L.B.B. holds a Canada Research Chair and H.A.Z. holds a Cole Foundation Fellowship and a CNRS Lebanon Fellowship.

Author Contributions H.A.Z. and B.C.-K. designed and performed experiments, analysed data and wrote the manuscript; L.C., A.A. and G.C. performed experiments; P.G., S.P. and C.T.J. analysed data; A.A.R. performed experiments and analysed data; J.B.J. and S.J.M. designed experiments; S.A. was medical monitor for the trial, treated patients and analysed clinical data; E.C. coordinated clinical trials and analysed clinical data; B.L., J.B. and M.W.B. treated patients, provided specimens and analysed clinical data; W.H.M. designed experiments, analysed data and edited the manuscript; K.L.B.B. designed experiments, analysed data and wrote the manuscript.

Author Information Reprints and permissions information is available at www.nature.com/reprints. Readers are welcome to comment on the online version of the paper. The authors declare competing financial interests: details are available in the online version of the paper. Correspondence and requests for materials should be addressed to K.L.B.B. (katherine.borden@umontreal.ca).

METHODS

Reagents and constructs. Full-length human *GLI1* was obtained from Addgene (K12 Plasmid 16419), subcloned into 2-FLAG-pcDNA3.1 or pMSCV-GFP (bicistronic vector) and the subsequent clones validated by sequencing. Ribavirin was obtained from Kemprotec (CAS 36791-04-5), cytosine β-D-arabinofuranoside (C17680) and GANT61 (G9048) from Sigma Aldrich, vismodegib (GDC-0449, S1082) from Selleckchem, ribavirin-^{13}C2 (^{13}C on the triazole ring and carboxy amide, TLC-ID # R-041, CAS number 36791-04-5) from TLC PharmaChem, ribavirin [triazole-5-^{3}H] (MT540) from Moravek Biochemicals and Radiochemicals, ribavirin 5′-triphosphate trisodium salt (R414505) from Toronto Research Chemicals.

Antibodies for immunoblotting were as follows: monoclonal antibody (mAb) mouse anti-eIF4E (BD PharMingen, 610270), polyclonal antibody (pAb) rabbit anti-eIF4E (Sigma Aldrich, E5906), mAb mouse anti-β-actin (Sigma Aldrich, A5441), mAb mouse anti-α-tubulin (Sigma Aldrich, T5168), pAb goat anti-ADK (D-21) (Santa Cruz, sc-23360), pAb goat anti-ENT1 (N-12) (Santa Cruz, sc-45489), pAb rabbit anti-Mcl-I (S-19) (Santa Cruz, sc-819), mAb mouse anti-c-Myc (9E10) (Santa Cruz, sc-40), mAb mouse anti-HSP90α/β (F-8) (Santa Cruz, sc-13119), mAb mouse anti-eIF4G (A-10) (Santa Cruz, sc-133155), mAb rabbit anti-GLI1 (C68H3) (Cell Signaling, 3538), pAb rabbit anti-UGT1A (Cell Signaling, 4371S), mAb rabbit anti-SNAIL (C15D3) (Cell Signaling, 2522S), mAb rabbit anti-4E-BP1 (53H11) (Cell Signaling, 9644), mAb rabbit anti-IHH (Indian hedgehog; EP1192Y) (Abcam, ab52919), mAb rabbit anti-SHH (sonic hedgehog; C9C5) (Cell Signaling, 2207S), pAb anti-PTCH1 (H-267) (Santa Cruz, sc-9016), mAb mouse anti-SMO (Smoothened; E-5) (Santa Cruz, sc-166685), UGT2B pan antibody (Santa Cruz, sc-50386). Antibody specificity for UGT1A and GLI1 is shown in Extended Data Fig. 8. Results with UGT1A pan antibody above were confirmed with another pan-UGT1A antibody from Santa Cruz sc-25847. The pan-UGT1A antibodies recognize the common carboxy terminus of UGT1As; with UGT1As having approximately the same molecular weight[8]. Importantly, the effects were specific to UGT1A as UGT2B levels were not changed (Extended Data Fig. 6i).

Cell culture and transfection. FaDu cells (ATCC HTB-43) were maintained in MEM supplemented with 1% MEM non-essential amino acids, 10% heat-inactivated FBS and 1% penicillin-streptomycin (Invitrogen). 2FLAG–GLI1 or 2FLAG vector control FaDu cell lines were generated using TransIT-LT1 transfection reagent (Mirus), according to manufacturer guidelines and were selected using geneticin selective antibiotic (G418 Sulphate) (MultiCell). THP1 cells (ATCC TIB202) were maintained in RPMI 1640 (Invitrogen) supplemented with 10% heat-inactivated FBS and 1% penicillin-streptomycin. THP1-GLI cells were generated using pMSCV-GFP as described in ref. 17. HepG2 cells (ATCC HB-8065) were maintained in DMEM supplemented with 10% heat-inactivated FBS and 1% pencillin-streptomycin (Invitrogen). For RNAi experiments, FaDu and HepG2 cells were transfected with Lipofectamine 2000 (Invitrogen) and 40 nM siRNA duplexes, and were analysed 96 h post-transfection. The following siRNA duplexes were used: *siGLI1* (designed by Integrated DNA technology, catalogue number: HSC.RNAI.N005269.12.3_10NM), *si_eIF4E* sense (CCCAAAUCUCGAUUGCUUGACGCAGUC), *si_eIF4E* antisense (CUGCGUCAAGCAAUCGAGAUUUGGG), *siADK* (designed by Integrated DNA technologies, catalogue number HSC.RNAI.N001123.12.5); *siUGT1A* three sequences were used such that the total amount of the siRNA mix is equal to 40 nM (designed by Integrated DNA technologies, catalogue number HSC.RNAI.N001072.12.2_10NM; HSC.RNAI.N001072.12.10_NM; HSC.RNAI.N007120.12.9_NM), Control duplex: *siLuc* sense (CACGUACGCGGAAUACUUCGA), *siLuc* antisense (CAUUUCGAA GUAUUCCGCGUACGUGUU).

Generation of ribavirin-resistant cell lines. FaDu or THP-1 cells were exposed to either a single concentration of ribavirin for a prolonged period (for example, 10 μM for FRII cells) or increased concentrations starting at 1 μM and doubling the concentration every 2 weeks until cells became resistant to 100 μM ribavirin (FRI) or starting with 10 and 20 μM ribavirin and doubling the concentration after 2 months (THP-based cells: TR-A and TR-B). Cells were routinely tested for ribavirin resistance. All cell lines (resistant and parental) were routinely checked to ensure there was no mycoplasma contamination using MycoAlert Mycoplasma Detection kit (Lonza, LT07-418).

Drug treatments and cell viability assay. These assays were carried out as described previously[16]. In brief, 25×10^4 cells per ml were seeded in triplicates/condition in 12-well cell culture plates (BD Biosciences 353043) (except for experiments involving pre-treatments with GDC-0449, where 15×10^4 cells per ml were used). To measure the effect of ribavirin on cell growth, cells were treated on the next day with 0, 10, 20, 50 or 100 μM ribavirin. Treatments were repeated every 48 h and cell viability was assessed by Trypan Blue dye exclusion test at each concentration every 24 or 48 h for up to 5 days. The percentage growth inhibition of treated cultures relative to untreated cultures was determined. Further, the ability of GDC-0449 or GANT61 to restore sensitivity to ribavirin or Ara-C was determined by pre-treating cells with 200 nM GDC-0449 or 20–40 μM GANT61 for 6 and 3 days, respectively, followed by treatments with 20 μM ribavirin or 200 nM Ara-C for 4 days. Cell viability was measured as mentioned above. Note that the IC_{50} for each of the above mentioned drugs was determined a priori and that all of our cell viability experiments were validated by colorimetric assays using the Cell Counting Kit-8 (Dojindo Molecular Technologies, CK04-11) according to the manufacturer's guidelines.

Drug uptake. Cells were plated in triplicates at a density of 0.5×10^6 cells per ml in 12-well plates. 24 h later, cells were incubated with 0.66 μM ^{3}H-ribavirin for 2, 4, 6, 8, 12 and 16 h. After treatment, cells were washed twice with ice-cold PBS and lysed with 2 volumes of NaOH (1N) and then neutralized with equal volume of HCl (1N). Samples were mixed with 5 ml Optiphase 'Hisafe 2' Scintillation cocktail (Perkin Elmer, 1200-436) and radioactivity was measured using a liquid scintillation counter (Tri-Carb 2800 TR, PerkinElmer).

eIF4E–^{3}H-ribavirin immunoprecipitation. Cells were seeded at a density of 1.2×10^6 cells per 900 μl of a 6-well plate (BD Biosciences, 353046) (three wells were used per each cell line tested) and incubated with 0.66 μM ^{3}H-ribavirin for 8 h at 37 °C, 5% CO_2. Following incubation, cells were washed three times with PBS and scraped in IP buffer (50 mM Tris, pH 5.5, 5 mM EDTA, 150 mM NaCl, 0.5% NP40 and 1% Triton X-100). Cells were then homogenized using a glass Dounce homogenizer and left to rotate at 4 °C for 30 min. After centrifugation at 10,000 r.p.m. for 10 min at 4 °C, supernatants were split into two tubes and pre-cleared with normal mouse-IgG beads (Santa Cruz, sc-2343) for 30 min at 4 °C. After spinning at 500*g* for 5 min, protein concentrations were quantified using Pierce BCA Protein assay (Thermo Scientific, 23223). 100–200 μg of protein lysates were used for immunoprecipitation with 8 μg of normal mouse IgG (Millipore, 12-371) or mAb mouse anti-eIF4E (P-2) (Santa Cruz, sc-9976) antibodies coupled to Protein A/G PLUS-Agarose (Santa Cruz, sc-2003). Immunoprecipitations were carried out overnight at 4 °C. Beads were washed six times with IP buffer and eluted with 80 μl 2× Laemmli sample buffer (BioRad) for 15 min at 99 °C. After spinning bead supernatants were used for scintillation counting and western analysis (probed with rabbit anti-eIF4E antibody).

Deep sequencing. Total RNAs were isolated from different cell lines using Trizol (Invitrogen). Samples were prepared into 50-bp fragment libraries and sequenced on the ABI SOLiD v.3 to obtain an average of 3.2 Gbp of transcript sequences. Data were mapped to the reference genome using the RNaseq pipeline found in the Bioscope software (https://products.appliedbiosystems.com/ab/en/US/adirect/ab?cmd=catNavigate2&catID=60680, #2). Keeping only uniquely matching reads, we used fragment count per transcript as an estimate of gene expression. We then used the statistical method based on a negative binomial distribution and implemented in the DESeq package[18] for R to compare samples and obtain a robust measure of differential expression between samples. The resulting *P* values were adjusted for multiple testing with the Benjamin–Hochberg procedure to yield P_{adj} values.

Reverse transcription and quantitative PCR. DNase-treated RNA samples (Turbo DNase, Ambion) were reverse transcribed using MMLV reverse transcriptase (Invitrogen) or Supervilo kit (Invitrogen) for primary specimens. qPCR analyses were performed using EXPRESS SYBR GreenER QPCR SuperMix (Invitrogen) in AB StepOne thermal cycler using the relative standard curve method (Applied Biosystems User Bulletin #2). All conditions were described previously[5,19]. Primers list: GLI1 forward (GGCTGCAGTAAAGCCTTCAGCAAT), GLI1 reverse (TGCAGCCAGGGAGCTTACATACAT), UGT1A forward (ACTGGAACCCGACCATCGAATCTT), UGT1A reverse (CACCAAACAAGGGCATCATCACCA), UGT1A1 forward (AACAAGGAGCTCATGGCCTCC), UGT1A4 forward (GAAGGAATTTGATCGCGTTAC), UGT1A6 forward (TCCTGGCTGAGTATTTGGGCC), UGT1A9 forward (GGAGGAACATTTATTATGCCACCG), common UGT1A reverse2 (CCAATGAAGACCATGTTGGGC), UBC forward (ATTTGGGTCGCGGTTCTTG), UBC reverse (TGCCTTGACATTCTCGATGGT), RPIIa forward (TGACTGCCAACACAGCCATCTACT), RPIIa reverse (GGGCCACATCAAAGTCAGGCATTT), G6PDH forward (TGGCAAAGTCGGTTTCTCTCTGGA), G6PDH reverse (TTGGGAACATGTCTCAGACTGGCA), ADK forward (AGAGGCAGCGAATCGTGATCTTCA), ADK reverse (ACCTCCAACAAATGCATCTCCAGC), ENT1 forward (CTCTCAGTGCCATCTTCAAC), ENT1 reverse (CAGAAACACCAGCAGGATGG).

Western blot analysis. Western analysis was performed as described previously with a modified lysis buffer (phospholysis buffer: 40 mM HEPES, pH 7.5, 120 mM NaCl, 1 mM EDTA, 10 mM β-glycerophosphate, 50 mM NaF, 0.5 μM $NaVO_3$, and 1% (v/v) Triton X-100 supplemented with complete protease inhibitors (all from Sigma-Aldrich)). In addition, blots were blocked in BSA blocking solution (3% (wt/v) BSA (Sigma-Aldrich) or 5% milk in TBS–Tween 20), and primary antibodies were diluted in BSA blocking solution or 5% milk.

Immunofluorescence and laser-scanning confocal microscopy. Immunostaining was carried out as described[5]. In brief, upon methanol fixation (10 min at −20 °C), cells were blocked for 1 h, and incubated with 1° antibodies (1:500 dilution) overnight at 4 °C, followed by three washes in blocking solution. Cells were then incubated with 2° donkey anti-rabbit IgG-Texas Red antibody (Jackson Immunolaboratories, diluted 1:100 in blocking solution), washed four times with 1 × PBS (pH 7.4) and mounted in Vectashield with DAPI (Vector Laboratories). Analysis was

carried out using a laser-scanning confocal microscope (LSM510 META; Carl Zeiss), exciting 405 and 543 nm or 488 nm with a ×100 objective, ×2 digital zoom (where indicated), and numerical aperture of 1.4. Channels were detected separately, with no crosstalk observed. Confocal micrographs represent single sections through the plane of the cell. Images were obtained from LSM510 software version 3.2 (Carl Zeiss) and displayed using Adobe Photoshop CS2 (Adobe).

Mass spectroscopy. FaDu, FRII, 2FLAG, 2FLAG–GLI1 or GDC-0449-treated cells grown in culture were trypsinized and put in to suspension at a density of 10×10^6 cells per ml media[20]. Concentrations of 1 mM ribavirin mix (^{12}C-ribavirin + ^{13}C2-ribavirin in a 50:50 ratio) were added in duplicate per condition and samples were incubated in a 37 °C shaker. A 100-µl aliquot was taken at different time points (0, 10, 30, 60, 120, 180, 240, 300 and 360 min) mixed with equal volume of 100% methanol (Fisher Scientific, HPLC grade, A412P-4) and flash frozen in liquid nitrogen. Samples were stored overnight at −80 °C. At the time of analysis, samples were thawed, centrifuged at 10,000 r.p.m. for 10 min and subjected to hydrophilic chromatography in line with mass spectrometer. The system used was an Agilent 1100 HPLC coupled to an Agilent MSD Trap SL, with an ESI source. The autosampler system was kept at 4 °C. The HPLC column was an Inertsil HILIC, 150 × 4.6 mm, 5 µm and the chromatography was obtained using solvent A (2 mM ammonium formate in water, pH 3.2) and solvent B (100% acetonitrile). The injection volume was 50 µl and the flow rate 1 ml per min. The column compartment was heated at 30 °C. The initial gradient was 95% B and 5% A, which changed during a 30-min course to 5% B and 95% A followed by 6 min equilibration at 95% B and 5% A. The total run time of the gradient was 36 min. The ESI source of the coupled MS ion-trap was set in positive ion mode, the nitrogen drying gas flow at 12 ml per min, the nebulizer pressure at 55 PSI and the temperature of the capillary at 350 °C with a voltage of 4,500 V. The mass analyser was set to scan from 50 to 1,500 *m/z*. For Ara-C glucuronidation assay, the same protocol was applied; however, the initial gradient was ran over a 20 min time course rather than 30 min.

Glucuronidation assay. Glucuronidation of ribavirin by human liver microsomes expressing UGT1A1, UGT1A4, UGT1A6 and UGT1A9 was performed as described previously[21]. In brief, 50 µg of pooled human liver microsomes (BD Biosciences, 452116) were incubated with 25 µg alamethicin (Sigma-Aldrich, A4665) and 50 mM Tris-HCl, pH 7.4, containing 10 mM $MgCl_2$, for 15 min on ice to allow formation of channels in the microsome membrane thus enabling access to the UGT active sites[17]. Following incubation, 8.5 mM saccharic acid 1,4-lactone (β-glucuronidase inhibitor, Sigma-Aldrich, S0375) and 1 mM ribavirin 5′-triphosphate were added and the mixture was incubated at 37 °C for 5 min. Finally, to activate the reaction, 100 µM uridine 5′-diphosphoglucuronic acid (UDPGA, Sigma Aldrich, U6751) was combined and incubations were performed at 37 °C for 6 h. Note that no glucuronides were observed in the absence of UDPGA addition (data not shown). All reactions were made in 100 µl final volume and were terminated by the addition of 100 µl cold methanol (100%). The mixtures were kept at −80 °C for at least 3 h, then thawed and centrifuged for 10 min at 10,000 r.p.m. and the resulting supernatants were analysed by hydrophilic chromatography in line with the mass spectrometer, as described above. We note that RTP was clearly glucuronidated in these microsomes whereas ribavirin was not, suggesting that ribavirin needs to be phosphorylated in order to be efficiently or stably glucuronidated. However, this step would be before glucuronidation as we never observed RTP-glucuronide or other phosphorylated form of the ribavirin-glucuronide. Furthermore, we did not observe glucuronidation of RTP in supersomes that express only UGT1A1, suggesting that other UGT1As must be present. Finally, although we observed glucuronidation of Ara-C efficiently in FRII and FaDu-GLI cells, we did not observe it in the microsomes, suggesting that some other UGT1A (than UGT1A1, UGT1A4, UGT1A6 and UGT1A9) needs to be present for efficient glucuronidation. Clearly this family member is well expressed in the FRII and FaDu-GLI cells.

Purification of ribavirin-glucuronides. Ribavirin-glucuronide was isolated from our microsomal preparation using the same liquid chromatography method described above with the time course for initial gradient being expanded to 40 min in order to obtain a better separation of the different metabolites. In brief, given that the Rib-Glu peak elutes around 8.9 min, three 500-µl fractions were collected bracketing this time and lyophilized by centrifugation using Sarvant SpeedVacc High Capacity Concentrator (Thermo Scientific, SC210A-115). The materials obtained from lyophilisation were re-suspended in a small volume of water: methanol (50:50 v/v) and an aliquot was reanalysed by HPLC-MS to verify the isolation and purity of the metabolite. To estimate the concentration of the purified Rib-Glu, a standard curve with the metabolite versus ribavirin-^{13}C2 (used as an internal standard) was generated. The concentration range for the standard curve was from 10 nM to 1 mM. The curves were constructed by plotting the concentration of the internal standard against the area of the analyte.

^{3}H-ribavirin pulldown. To determine whether Rib-Glu binds eIF4E, we performed an *in vitro* binding assay. In brief, 10 nM purified recombinant eIF4E–GST protein was coupled to 40 µl glutathione sepharose beads (GE Healthcare Life Sciences, 17-5132-01) for 30 min at room temperature in buffer containing 50 mM Tris-HCl, pH 7.4, 300 mM NaCl, 2.5 mM MgCl2, 0.5 mM DTT, 0.015% NP40, 0.5% protease-free BSA, and protease inhibitors. Washed beads were then incubated with 250 nM ^{3}H-ribavirin and an equivalent concentration of either purified Rib-Glu, ^{1}H-ribavirin, RTP, GTP or blank for 30 min at room temperature in a buffer containing 100 mM sodium phosphate, pH 7.5, 300 mM NaCl, 0.015% NP40, 10 µM BSA and protease inhibitors. Washed beads were then eluted in 1× Laemmli sample buffer (containing β-mercaptoethanol) and radioactivity in supernatants was measured by scintillation counting (note that for washing the beads, 100 µM of GTP was added).

m^{7}G-sepharose affinity chromatography. Cells were harvested from 10-cm plate per condition at 80% confluency and lysed in 2 volumes of buffer B (50 mM MOPS/KOH, pH 7.4, 100 mM NaCl, 50 mM NaF, 2 mM EDTA, 2 mM EGTA, 1% NP40, 1% Na-DOC, 7 mM β-mercaptoethanol, protease inhibitors and 1 mM Na_3VO_4) on ice for 15 min with occasional vortexing. Lysates were spun at 16,000*g* for 10 min at 4 °C. m^{7}GDP-agarose beads (GE Healthcare UK, 275025) were washed in buffer C (50 mM MOPS/KOH, pH 7.4, 100 mM NaCl, 50 mM NaF, 0.5 mM EDTA, 0.5 mM EGTA, 7 mM BME, 2 mM benzamidine or 0.5 mM PMSF, 1 mM Na_3VO_4 and 0.1mM GTP). Lysates (~500 µg) were diluted to 1 ml with buffer C and added to washed beads (~50 µl of 50% slurry). After incubation of the reactions for 20 min at 4 °C on the rotating wheel, beads were washed at least three times with buffer C and eluted with 2× Laemmli buffer (BioRad). Note that all centrifugation steps are 500*g* for 1 min at 4 °C.

Protein stability. To determine whether GLI1 regulates UGT1A protein's half-life, we investigated the effect of MG132 proteasome inhibitor (Sigma Aldrich) on UGT1A's half-life. Both FRII and wild-type cells were seeded at 70% confluency in 10-cm plates 24 h before treatment. Cells were then treated with 10 µM MG132 or an equivalent volume of methanol as a control. Ten hours post-treatment, cells were harvested and lysed in phospholysis buffer and UGT1A protein stability was assessed by western analysis using a pan-UGT1A antibody.

Primary AML specimens and healthy volunteers. A total of 19 patients were enrolled in the study in three participating centres; Jewish General Hospital, Hamilton Health Sciences, and Hôpital Maisonneuve Rosemont. In total, 15 patients were eligible for evaluation. Written informed consent was obtained as per the Helsinki Protocol. This study received IRB (all sites) and Health Canada approval. ClinicalTrials.gov registry is NCT00559091. Clinical response was assessed using the Cheson criteria[22]. Patients had to receive a diagnosis of primary or secondary AML, French–American–British (FAB) subtypes M4 or M5 only, relapsed or refractory after at least one cycle of conventional chemotherapy; or newly diagnosed but not be candidates for induction chemotherapy. Patients must also have been at least 18 years of age and must have had an Eastern Cooperative Oncology Group (ECOG) performance status lower than 3 and a life expectancy of at least 12 weeks. Other requirements were as outlined in ref. 5. The ribavirin Ara-C combination Phase I trial (Clinicaltrials.gov NCT01056523) is recently completed, and patients with remissions were analysed for GLI1 and UGT1A levels. Criteria were the same as for the monotherapy trial described above. Written informed consent according to the Declaration of Helsinki was obtained from all patients as for the monotherapy trial. For analysis of primary specimens in colony growth assays, specimens were obtained from the Leukaemia Cell Bank of Quebec (BCLQ), with no identifying information. Leukaemic blasts were isolated by flow cytometry as described in ref. 5. For tissue-matched controls at diagnosis and relapse, patient specimens were collected with written informed consent from either University of Rochester Medical Center RSRB approval and ClinicalTrials.gov NCT01311258 or from the BCLQ. For controls, normal bone marrow, peripheral blood mononuclear cells or normal CD34$^+$ cells were used as indicated, and were obtained from StemCell Technologies. Protein and RNA were isolated as described (see below).

Bone marrow staining. Squash preparations of bone marrow aspirates and touch prints of bone marrow biopsies were air-dried and stained with Wright–Giemsa. To examine the specimens Leica DMLS microscope with the ×50 objective oil immersion lens was used. The Infinity 1-2C-184976 camera was used to capture images and images were analysed on the Infinity Analyze image acquisition software (release 5.0.2, 2002-2009 Infinity corporation). Lysozyme staining was as described previously[23]. Images for lysozyme staining were captured Leica DM LB2 microscope, and Leica DFC 350X camera and displayed with Adobe Photoshop 7.0 software.

Single-locus DNA methylation assays. Total genomic DNA was extracted from 2×10^6 FaDu and FRII cells using the Gentra Puregene cell kit (Qiagen) and eluted in RNase-free water. EpiTYPER assays (Sequenom) were performed on bisulphite-converted DNA. Bisulphite conversion was performed using EZ DNA Methylation kit from Zymo Research. EpiTYPER primers were designed to cover 29 *GLI1* CpGs (25 of them in CpG islands) using Sequenom EpiDesigner beta software (http://www.epidesigner.com/). Primer sequences are below.

EpiTYPER primers. GLI1 forward 1 GGGTTTTGGGGGTGTAATAAGT, GLI1 reverse 1 CCCTAAAAAACTAAACATCCCCTC, GLI1 forward 2 TTTGGGAT GAGTTTTTAAGAAGTTG, GLI1 reverse 2 CCTAAAAATCCTAAAAATACA ATAAACCC.

17. Fisher, M. B., Campanale, K., Ackermann, B. L., VandenBranden, M. & Wrighton, S. A. *In vitro* glucuronidation using human liver microsomes and the pore-forming peptide alamethicin. *Drug Metab. Dispos.* **28,** 560–566 (2000).
18. Anders, S. & Huber, W. Differential expression analysis for sequence count data. *Genome Biol.* **11,** R106 (2010).
19. Culjkovic-Kraljacic, B., Baguet, A., Volpon, L., Amri, A. & Borden, K. L. B. The oncogene eIF4E reprograms the nuclear pore complext to promote mRNA export and oncogenic transformation. *Cell Reports* **2,** 207–215 (2012).
20. Engtrakul, J. J., Foti, R. S., Strelevitz, T. J. & Fisher, M. B. Altered AZT (3′-azido-3′-deoxythymidine) glucuronidation kinetics in liver microsomes as an explanation for underprediction of *in vivo* clearance: comparison to hepatocytes and effect of incubation environment. *Drug Metab. Dispos.* **33,** 1621–1627 (2005).
21. Barbier, O. *et al.* 3′-azido-3′-deoxythimidine (AZT) is glucuronidated by human UDP-glucuronosyltransferase 2B7 (UGT2B7). *Drug Metab. Dispos.* **28,** 497–502 (2000).
22. Cheson, B. D. *et al.* Revised recommendations of the International Working Group for Diagnosis, Standardization of Response Criteria, Treatment Outcomes, and Reporting Standards for Therapeutic Trials in Acute Myeloid Leukemia. *J. Clin. Oncol.* **21,** 4642–4649 (2003).
23. Horny, H. P., Wehrmann, M., Steinke, B. & Kaiserling, E. Assessment of the value of immunohistochemistry in the subtyping of acute leukemia on routinely processed bone marrow biopsy specimens with particular reference to macrophage-associated antibodies. *Hum. Pathol.* **25,** 810–814 (1994).

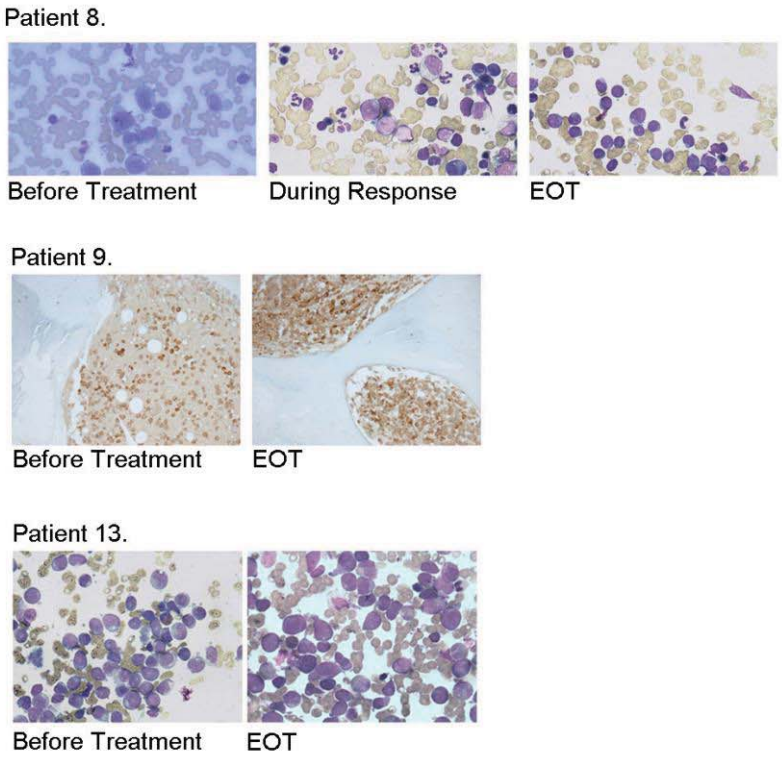

Extended Data Figure 1 | Ribavirin resistance in some ribavirin monotherapy clinical trial patients. Bone marrow biopsies for responding (patient 8 achieved a PR; patient 11, a CR, is shown in Fig. 1a) and non-responding patients (patient 9 was a PD and patient 13 a SD). Note abundance of blasts before treatment and at EOT and reduction in blasts and restoration of haematopoiesis during response. For Wright–Giemsa-stained samples magnification was ×50 with oil (patients 8 and 13), and for lysozyme staining ×20 (patient 9).

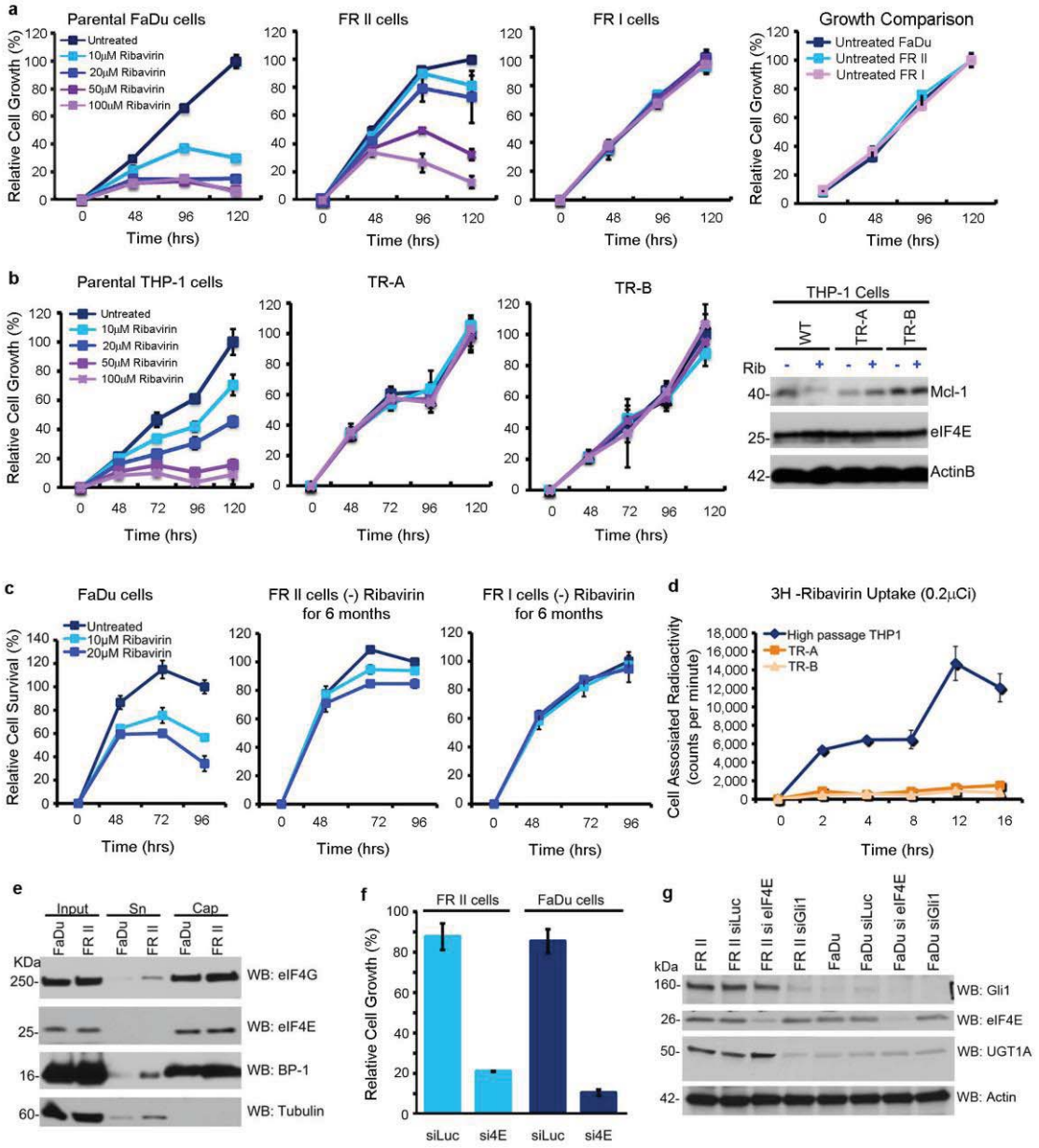

Extended Data Figure 2 | Characterization of FaDu- and THP-1-derived resistant cell lines. **a**, Detailed growth curves for FRI and FRII resistant cells. All cell lines have indistinguishable doubling times in the absence of ribavirin (far right panel). **b**, THP-1 resistant (TR) cell lines are not sensitive to treatment with ribavirin at the doses and times used. Ribavirin no longer targets eIF4E activity (that is, Mcl-1) in resistant cells (far right panel). There were no changes in eIF4E levels between resistant and parental cell lines (and Fig. 1c). Actin provides a loading control. **c**, Resistance is retained after 6 months of growth in the absence of ribavirin. **d**, Incubation of live cells with ^{3}H-ribavirin indicates that THP-1 resistant cells have impaired uptake of ribavirin similar to FRI cells. **e**, eIF4E cap binding and eIF4G binding activity are retained in FRII cells. **f**, FRII cells are sensitive to *eIF4E* knockdown measured by cell growth. **g**, Effects of RNAi-mediated knockdown of *GLI1* or *eIF4E* on UGT1A levels. Western blots were probed as indicated. RNAi-mediated knockdown of *GLI1* led to reduced levels of UGT1A whereas knockdown of *eIF4E* did not. For UGT1A, a pan-UGT1A antibody was used. Antibody controls for UGT1A and GLI1 are shown in Extended Data Fig. 8c. Results are representative of at least three independent experiments. Average values are reported and error bars indicate ±standard deviations. Experiments were carried out in triplicate, three independent times. Western blots are representative of at least three independent experiments.

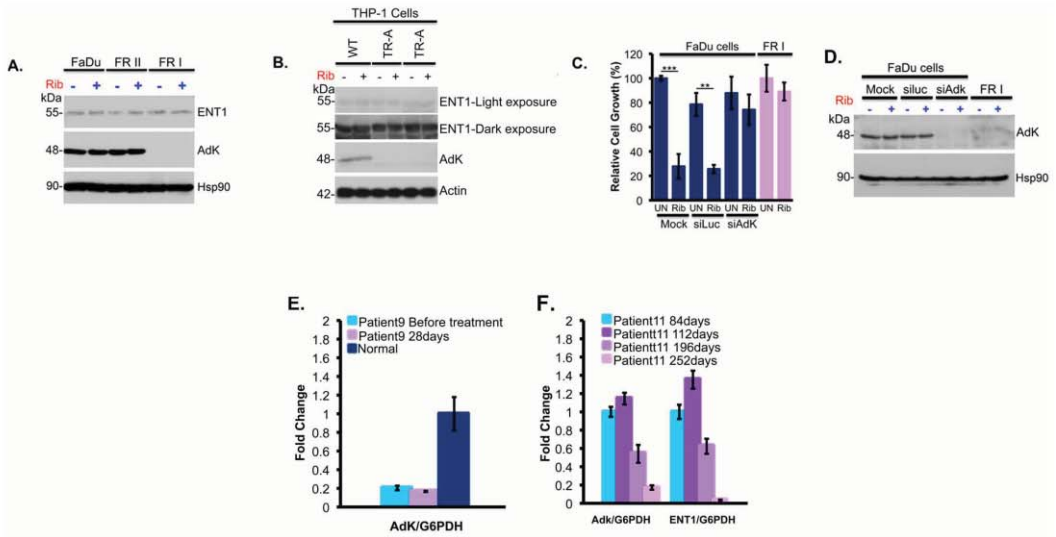

Extended Data Figure 3 | Pro-drug metabolism is impaired in type I resistance. **a**, **b**, Western analysis reveals that ADK levels were reduced in FRI cells (**a**) and THP1 resistant cells (**b**). Treatments were 48 h at 20 μM ribavirin. **c**, **d**, Knockdown of *ADK* leads to ribavirin resistance as shown by cell growth. Western blot confirms knockdown of *ADK*. Hsp90 provides a loading control. **e**, **f**, *ENT1* and A*DK* mRNA levels for patients' specimens. Patient 11 (CR) was responding clinically at (and before) 84 and 112 days and relapsed around day 252, when both *ADK* and *ENT1* mRNA levels decreased. Analysis of RNA samples isolated before and at the end of the first 28-day cycle for patient 9 (who did not respond to ribavirin) compared to a healthy volunteer. Averaged values for *ADK* and *ENT1* RNAs were normalized to glucose 6-phosphate dehydrogenase (G6PDH). Error bars indicate ± s.d.; centre values are averages. All experiments were performed in triplicate at least three independent times. $^{**}P < 0.01$, $^{***}P < 0.001$ (two-tailed Student's *t*-test). Results are representative of at least three independent experiments.

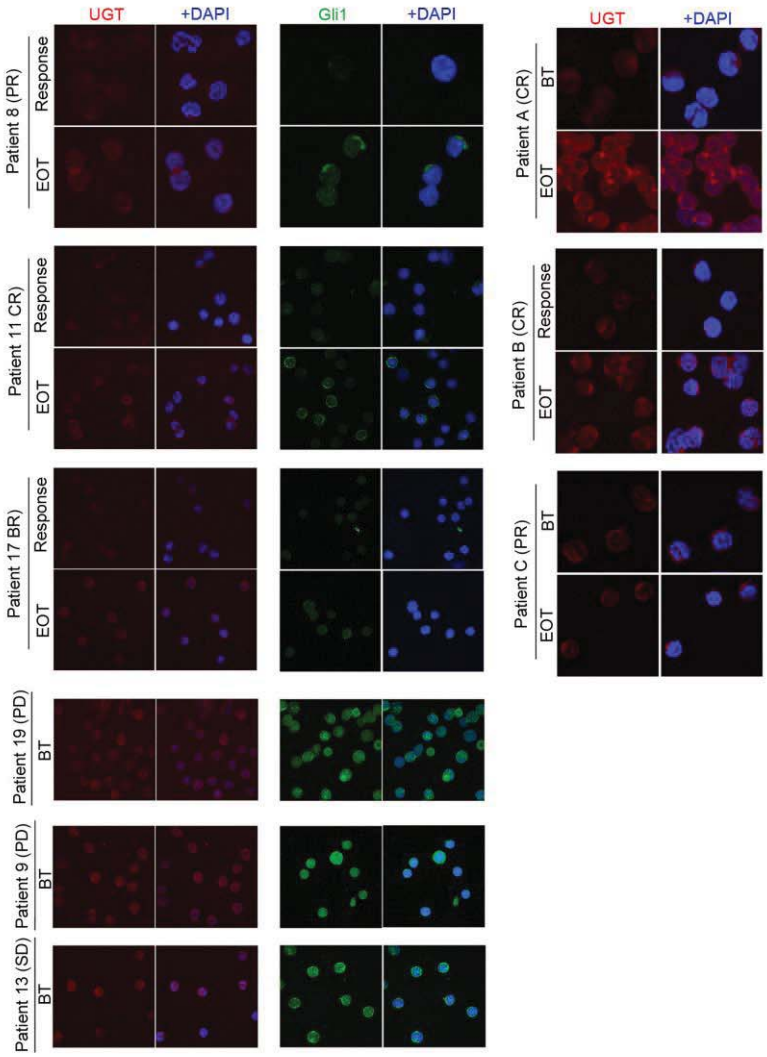

Extended Data Figure 4 | Confocal micrographs of leukaemic blasts isolated from bone marrows of responding and non-responding patients before treatment, at response or at EOT. Immunostaining for GLI1 and UGT1A are shown. DAPI is in blue. Note nuclear accumulation of GLI1 in non-responding patients, indicating elevated GLI1 activity. High levels of GLI1 and UGT1A suggest primary resistance. All confocal settings were identical between specimens and thus lower signal is indicative of less protein. A ×100 objective with no digital zoom was used for patients 9, 11, 13, 17 and 19. The same objective but a digital zoom of ×2 was used for patients 8, A, B and C. Note patient C was still in remission at EOT (see main text). For each patient, staining was carried out three independent experiments. Controls for specificity of GLI1 and UGT1A antibodies are provided in Extended Data Fig. 8c.

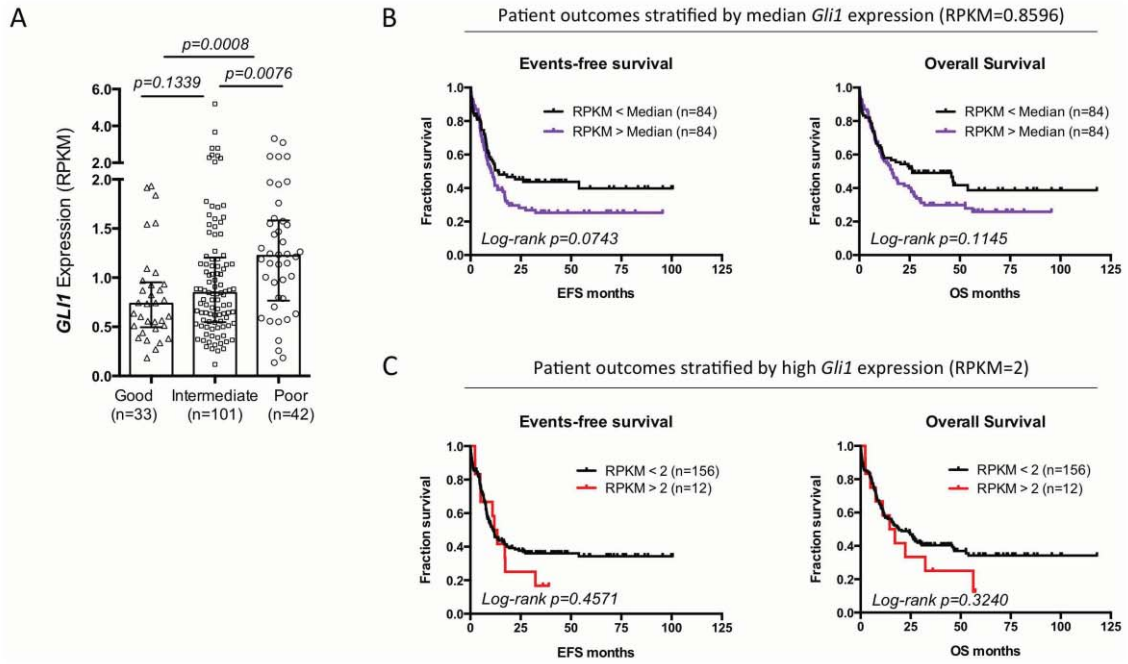

Extended Data Figure 5 | Higher *GLI1* expression is found in poor cytogenetic risk group and predicts a trend of worse survival outcome in AML. To study the prognostic value of *GLI1* gene expression in AML, we mined the publicly available AML data set published by The Cancer Genome Atlas Research Network[11]. **a**, *GLI1* gene expression in 176 *de novo* AML patients grouped by cytogenetic risks. The expression level is represented by RPKM value (reads per kilobase of transcript per million mapped reads in RNA-seq). Each patient is represented by a symbol. Error bars represent median ± IQR (interquartile range) of each group. Nonparametric Mann–Whitney *U*-test was used to analyse the differences between groups. A total of 176 *de novo* AML patients with complete mRNA-seq and cytogenetic risk classification data are included in this analysis. **b**, **c**, Kaplan–Meier plots of events-free survival (EFS) and overall survival (OS) of 168 *de novo* AML patients segregated by median *GLI1* expression (RPKM = 0.8596) (**b**) or high *GLI1* expression (RPKM greater than or equal to 2) (**c**). Each tick on the survival curve represents a censored event because the patient is still alive at the end of the TCGA study. A total of 168 *de novo* AML patients with complete mRNA-seq, and reliable EFS and OS data are included in this analysis (patient information details are described in the Supplementary Table 1 of the NEJM study[11]. Mantel–Cox test was performed to calculate log-rank *P* values. We also observed that abnormally low levels of GLI1 were also correlated with poor outcome (data not shown), suggesting that GLI1 levels must be in a 'Goldilocks' zone.

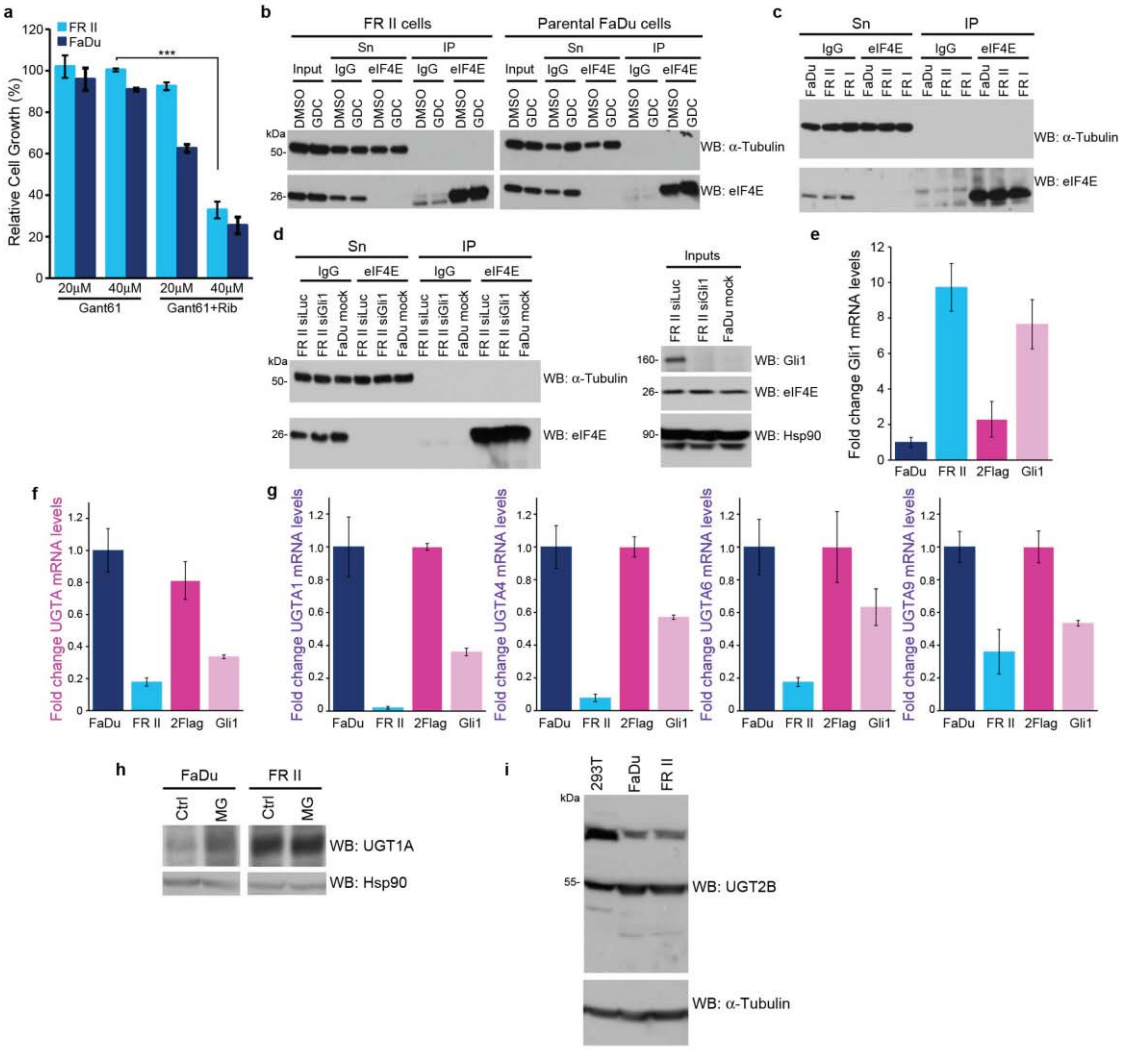

Extended Data Figure 6 | Effects of modulation of GLI1 levels on UGT1A. **a**, Effects of the direct GLI1 inhibitor GANT61 on restoring ribavirin sensitivity (20 μM) in FRII cells. Effects are dependent on GANT61 dose. **b**–**d**, Controls for eIF4E–ribavirin immunoprecipitations (IP) shown in Figs 1e and 3b. Inputs, supernatants (Sn) and IP controls for ^{3}H ribavirin anti-eIF4E IPs are shown for GDC-0449-treated cells (**b**), FRII and FRI cells (**c**), and RNAi-mediated knockdown of *GLI1* (**d**). **e**–**g**, qPCR analysis of *GLI1* (**e**) and *UGT1A* (**f**) using a pan-UGT1A primer or primers for specific UGT1As (**g**). mRNA levels were normalized to RNA polymerase IIa. These findings are consistent with Extended Data Table 1, which indicates lower levels of *UGT1A* mRNA levels. Further, *UGT1A3* and *UGT1A8* decreased similarly (data not shown). Experiments were carried out in triplicate, at least three independent times. Average values are reported and error bars indicate standard deviations. These findings, that GLI1 elevation leads to reduced mRNA levels but increased protein levels, are counterintuitive. We propose that GLI1 elevation increases protein stability of UGT1As (see below) and this leads to some sort of feedback mechanism leading to reduced UGT1As. Other scenarios are possible but the main point that GLI1 elevation leads to increased UGT1A protein production is clear. **h**, GLI1 increases UGT1A protein stability as shown by studies with the proteasomal inhibitor MG132 (MG) and a pan-UGT1A antibody. Here, MG132 addition stabilizes levels of UGT1A in parental cells, but in FRII cells where levels are already increased, there is no further increase with MG132. This indicates that UGT1A proteins are already stabilized in the FRII cells. All results are representative of three independent experiments. **i**, Western blot analysis with a pan-UGT2B antibody indicates that UGT2B levels are unchanged in FRII relative to FaDu cells,suggesting the glucuronidation effects are mediated mostly through the UGT1A family. 293T cells are shown for comparison. Tubulin provides a loading control.

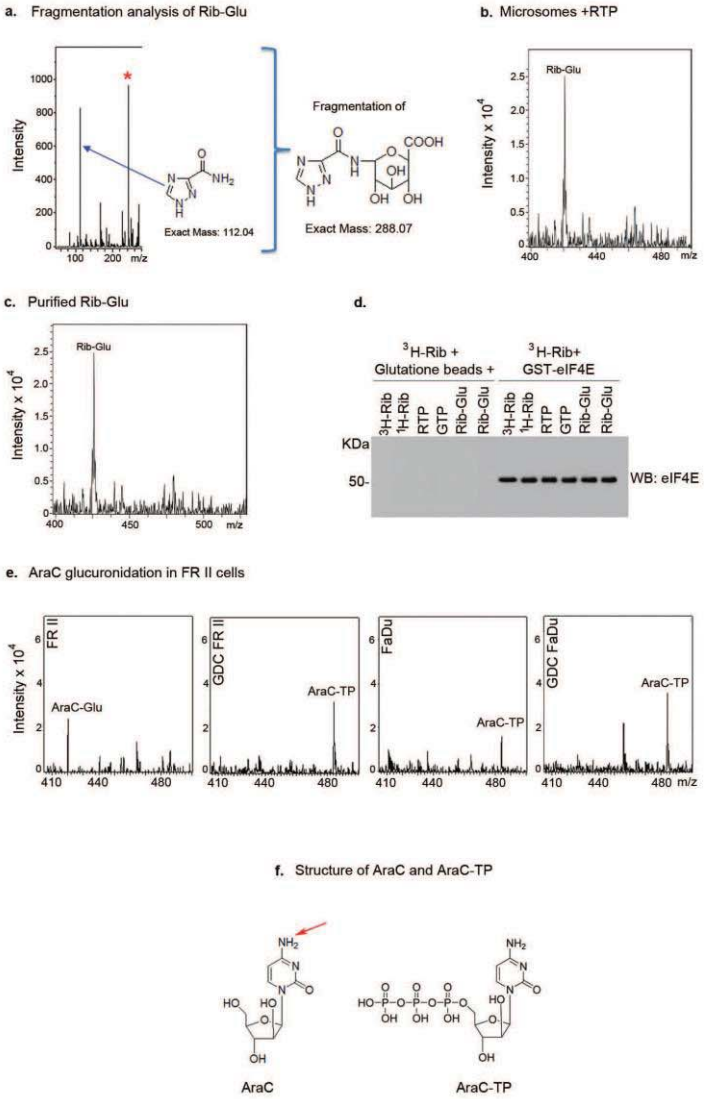

Extended Data Figure 7 | MS analysis of ribavirin and Ara-C glucuronidation. **a**, MS/MS collision-induced fragmentation analysis indicates that a breakdown product of the ribavirin glucuronide missing the ribose ring (exact mass 288.07) was further fragmented into a fragment of this glucuronide (exact mass 244.08, red asterisk) and to the triazole ring, the key moiety of ribavirin (exact mass 112.04). No ribose-glucuronide or ribose fragment was detected in our experiments, suggesting that this is not a major glucuronidation site in these cells. However, we cannot rule out that this exists and could not be detected. **b**, Microsomes expressing UGT1A1, UGT1A4, UGT1A6 and UGT1A9 were treated with RTP, underwent hydrophilic interaction liquid chromatography (HILIC) and the resulting extracted ion chromatogram (EIC) is shown. The Rib-Glu peak is clearly present and fragmentation analysis as in **a** confirms that this is glucuronidated ribavirin. We note that microsomes only expressing UGT1A1 do not glucuronidate RTP; and that RTP, but not ribavirin, is glucuronidated in microsomes. These studies suggest that UGT1A4, UGT1A6 and/or UGT1A9 are required for glucuronidation, as is some phosphorylation event before glucuronidation. **c**, Using HILIC chromatography, we isolated the fraction containing the Rib-Glu peak in **b**. A portion of this was re-assessed by MS/MS to be sure that the correct peak was isolated. This material was used in the ^{3}H-ribavirin competition assay in Fig. 4m. Material was quantified using a standard curve of ribavirin (see Methods). **d**, Western blot demonstrating equal loading of eIF4E–GST in the ^{3}H-ribavirin pulldown assay shown in Fig. 4m. All results are representative of at least three independent experiments. **e**, AraC is glucuronidated (AraC-Glu) in FRII cells but not parental FaDu cells where AraC-TP (triphosphate) is observed. AraC-TP is also observed in FRII cells, but at much lower levels than AraC-Glu. Treatment of FRII cells with GDC-0449 results in the loss of the AraC-Glu peak and causes no alteration to the parental FaDu cells. Fragmentation strongly suggests that the cytosine is the major site of glucuronidation (data not shown). We did not observe masses consistent with an arabinose breakdown product or an arabinose-glucuronide but cannot rule out that they are present at low levels or that our isolation procedure precluded their detection. **f**, Structures of AraC and AraC-TP are shown. The red arrow indicating the most likely glucuronidation site, as per our mass spectrometry data. Note that no glucuronides were observed when reactions were incubated in the absence of UDP-glucuronic acid (data not shown).

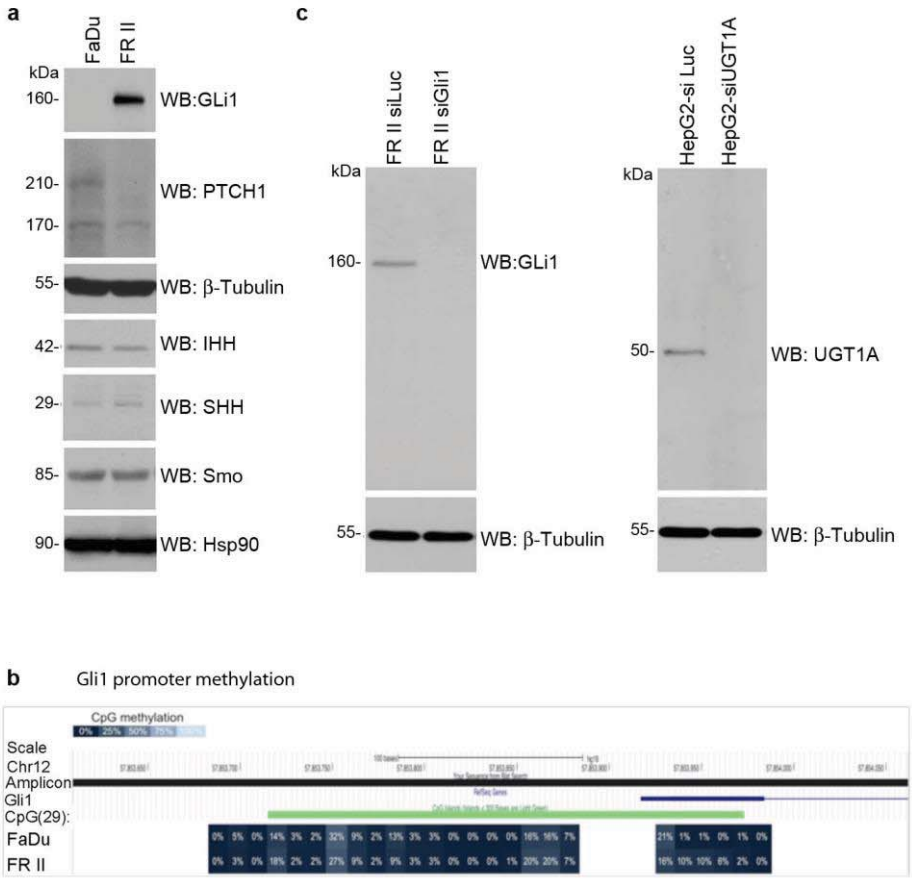

Extended Data Figure 8 | Investigations into why GLI1 levels are elevated in FRII cells. **a**, Analysis of expression of a subset of hedgehog signalling pathway proteins. Western blots are probed as indicated and are representative of three independent experiments. Tubulin and Hsp90 provided loading controls. Patched 1 (PTCH1) was the most significant change. PTCH1 is 210 kDa, with an often observed degradation product at 170 kDa. IHH, Indian hedgehog; SHH, sonic hedgehog, Smo, smoothened. **b**, *GLI1* DNA methylation. CpG methylation was interrogated on bisulphite-converted DNA from *GLI1* promoter region and first exon. The amplicon covered 29 CpGs, 25 of them located within a CpG island. DNA CpG methylation is shown as per cent methylation for FaDu (top) and FRII (bottom) cells. There was no difference observed between the cell lines. **c**, Antibody controls. Analysis of GLI1 and pan-UGT1A antibodies as a function of RNAi-mediated knockdown of these proteins as indicated. Note that UGT1A family members have approximately the same molecular weight. Results are representative of at least three independent experiments.

Extended Data Table 1 | RNA-seq results of genes with different expressions in FRII versus parental and FRI cells

	ID	F old Change	log2FoldChange	padj
NM_005269	GLI1	21.05351195	4.395989005	4.53763E-19
NM_019076	UGT1A8	0.071885361	-3.798158182	5.14486E-10
NM_021027	UGT1A9	0.071885361	-3.798158182	5.14486E-10
NM_019075	UGT1A10	0.071885361	-3.798158182	5.14486E-10
NM_019077	UGT1A7	0.071885361	-3.798158182	5.14486E-10
NM_019093	UGT1A3	0.075269208	-3.731796399	1.09556E-09
NM_205862	UGT1A6	0.071407143	-3.80778779	1.09556E-09
NM_019078	UGT1A5	0.076934805	-3.700219774	1.09556E-09
NM_000463	UGT1A1	0.081523375	-3.616642411	1.75756E-09
NM_001072	UGT1A6	0.079970619	-3.644386132	1.98554E-09
NM_007120	UGT1A4	0.082083144	-3.606770194	1.98554E-09
NM_031479	INHBE	5.823391175	2.541859532	1.36431E-07
NM_003256	TIMP4	12.35630007	3.627174907	2.27095E-07
NM_000728	CALCB	10.86606199	3.441757277	9.14258E-07
NM_006096	NDRG1	4.095561837	2.034061377	1.21428E-05
NM_144717	IL20RB	5.043343881	2.334380599	1.5497E-05
NR_026572	PDE2A	12.80113496	3.678199821	1.79464E-05
NM_005980	S100P	4.549241234	2.185625939	1.94272E-05
NM_002462	MX1	4.548672811	2.185445664	1.99955E-05
NM_016818	ABCG1	7.006493344	2.808692575	2.18839E-05
NM_001144925	MX1	4.464277528	2.158426717	2.78929E-05
NM_001005340	GPNMB	4.317327762	2.110138623	2.78929E-05
NM_138420	AHNAK2	4.477547206	2.162708642	3.45273E-05
NM_002272	KRT4	0.141121624	-2.824989024	3.48607E-05
NM_001795	CDH5	0.13455534	-2.893728445	3.48607E-05
NM_001901	CTGF	0.116697976	-3.099148557	0.000227563
NM_001561	TNFRSF9	10.39142803	3.377322023	0.000410767
NM_019850	NGEF	6.893341444	2.785203477	0.000500665
NM_020318	PAPPA2	6.0439344	2.595488002	0.000763335
NM_018406	MUC4	0.080064648	-3.642690811	0.000783474
NM_006408	AGR2	0.030727143	-5.024342563	0.004759868

The cutoff was set at a P_{adj} value of <0.005.

3.6 Patent: *Canadian informal patent application no. CA 2,752,008 filed September 13th, 2011 (Inventors: Borden K., Culjkovic B., **Zahreddine H.**; Applicant: Université de Montréal). This application entitled Combination Therapy using Ribavirin as elF4E inhibitor relates to the use of a combination therapy for treating patients having a neoplasm or a proliferative disorder. The combination which comprises an inhibitor of the eIF4E gene product, such as ribavirin, and a chemotherapeutic agent, aims at overcoming resistance developed in patients during anti-neoplastic treatment. The invention also relates to the use of a combination therapy for treating patients with cancer or pre-cancerous lesions. This combination comprises an inhibitor of eIF4E gene product, a chemotherapeutic agent, and a therapeutically effective amount of a hedgehog pathway inhibitor, such as GDC-0449.*

UNITED STATES PATENT AND TRADEMARK OFFICE

UNITED STATES DEPARTMENT OF COMMERCE
United States Patent and Trademark Office
Address: COMMISSIONER FOR PATENTS
P.O. Box 1450
Alexandria, Virginia 22313-1450
www.uspto.gov

APPLICATION NO.	ISSUE DATE	PATENT NO.	ATTORNEY DOCKET NO.	CONFIRMATION NO.
14/344,536	01/17/2017	9545416	05727-099USU1	2841

21918 7590 12/28/2016

DOWNS RACHLIN MARTIN PLLC
199 MAIN STREET
P O BOX 190
BURLINGTON, VT 05402-0190

ISSUE NOTIFICATION

The projected patent number and issue date are specified above.

Determination of Patent Term Adjustment under 35 U.S.C. 154 (b)
(application filed on or after May 29, 2000)

The Patent Term Adjustment is 147 day(s). Any patent to issue from the above-identified application will include an indication of the adjustment on the front page.

If a Continued Prosecution Application (CPA) was filed in the above-identified application, the filing date that determines Patent Term Adjustment is the filing date of the most recent CPA.

Applicant will be able to obtain more detailed information by accessing the Patent Application Information Retrieval (PAIR) WEB site (http://pair.uspto.gov).

Any questions regarding the Patent Term Extension or Adjustment determination should be directed to the Office of Patent Legal Administration at (571)-272-7702. Questions relating to issue and publication fee payments should be directed to the Application Assistance Unit (AAU) of the Office of Data Management (ODM) at (571)-272-4200.

APPLICANT(s) (Please see PAIR WEB site http://pair.uspto.gov for additional applicants):

Katherine Borden, Dollard des Ormeaux, QC, CANADA;
Hiba Zahreddine, Montreal, QC, CANADA;
Biljana Culjkovic Kraljacic, Montreal, QC, CANADA;

IR103 (Rev. 10/09)

CHAPTER 4

A Phase I trial of Ribavirin and Low-Dose Cytarabine for the Treatment of Relapsed and Refractory Acute Myeloid Leukemia with Elevated eIF4E

(LETTER TO THE EDITOR)

Published in *Haematologica. 2015 Jan; 100(1): e7–e9. doi: 10.3324/haematol.2014.111245*

Contributions:

S.A. was medical monitor for the trial, treated patients, analysed clinical data and wrote the manuscript; B.C.-K. and H.A.Z. analysed clinical data; E.C., C.L. and C.J. L. coordinated clinical trials and analysed clinical data; J.B. and S.C. treated patients; W.H.M. designed experiments, analysed data and edited the manuscript; K.L.B.B. designed clinical trial, analysed data and wrote the manuscript.

A phase I trial of ribavirin and low-dose cytarabine for the treatment of relapsed and refractory acute myeloid leukemia with elevated eIF4E

The molecular heterogeneity of acute myeloid leukemia (AML) underlies the wide variation in responses to standard therapy. This heterogeneity occurs at multiple regulatory steps affecting cell survival and proliferation.[1] We identified overexpression of the eukaryotic translation initiation factor 4E (eIF4E) as a targetable aberrancy in all examined cases of M4 and M5 FAB (French, American and British classification) AML subtypes, as well as in some M0, M1, and M2 subtypes.[2] eIF4E is both over-expressed and highly enriched in the nucleus of these specimens. eIF4E acts in nuclear mRNA export and translation of specific transcripts necessary for the promotion of proliferation, survival and metastases.[3,4] These eIF4E functions depend on its binding the m^7G cap on the 5' end of mRNAs.[3,4] Use of ribavirin, a competitive inhibitor of the m^7G cap, impairs the biochemical and oncogenic functions of eIF4E.[5,6] The first clinical trial to directly target eIF4E activity used ribavirin in AML patients with elevated eIF4E who were unfit for induction chemotherapy or who had relapsed disease.[7] Complete and partial responses were observed, and responding patients demonstrated a reduction in overall levels of eIF4E, loss of its nuclear localization, and impaired production of eIF4E targets.[7]

In vitro combination studies with ribavirin and cytarabine showed an added impairment in cell growth in primary AML patient samples.[8] Given these findings, we combined ribavirin po BID continuous dosing with low-dose cytarabine (LDAC) sc BID for ten days every 28 days in a phase I trial following a "3+3" design. The primary objective was to determine the recommended phase II dose (RP2D) of the combination based on pharmacokinetics and safety. The secondary objectives revealed predicted cellular changes in eIF4E but also a novel mechanism of resistance to ribavirin and cytarabine.[9] Twenty-nine patients with elevated eIF4E and who were unsuitable for induction chemotherapy or with relapsed/refractory disease were enrolled. Nine of these had not received induction with "7+3" for their AML (median age 70 years) and 3 had received prior therapy for myelodysplastic syndrome (MDS) (Table 1). The combination was generally well tolerated with no unexpected adverse events. Hemolytic anemia, a known ribavirin toxicity, was seen in 4 patients (14%), and was uncontrolled by dose reduction but resolved after ribavirin was discontinued.

In the first dose escalation, four dose levels of ribavirin (1000, 1400, 1800 and 2200 mg BID) were combined with LDAC 20 mg BID. At a ribavirin dose of 2200 mg BID, there were 2 dose-limiting toxicities (DLTs) and no further dose escalation was performed. Importantly, the mean maximum ribavirin plasma levels were below 20 μM for all dose levels (*Online Supplementary Figure S1*). This was in contrast to levels above 20 μM seen with monotherapy, where patients were treated with ribavirin 1000 mg BID. Interestingly, Patient 1 had a doubling of ribavirin serum levels once LDAC was reduced to 10 mg BID for toxicity during cycle 2 (Figure 1). Thereafter, this patient achieved a complete remission (CR) (with incomplete red cell recovery), and molecular targeting of eIF4E, as seen by re-localization to the cytoplasm. This patient remained on ribavirin therapy for two years with LDAC discontinued on day 179.

Given our observations of Patient 1, and the failure to achieve higher plasma levels of ribavirin in the higher dose cohorts, we carried out a second ribavirin dose escalation in the presence of LDAC 10 mg BID. This led to increased ribavirin plasma levels overall (*Online Supplementary Figure S1*). The median maximum level of ribavirin when given with LDAC 10 mg BID was 23 μM (range 6-37 μM, n=9), more than double that observed at LDAC 20 mg BID, which was 11.5 μM (range 2-33 μM, n=10). Increasing doses of ribavirin beyond 1400 mg BID did not result in increased serum steady state levels (*Online Supplementary Figure S1*). No DLTs were observed in this dose escalation. Thus, the recommended phase II dose (RP2D) was determined to be ribavirin 1400 mg BID and LDAC 10 mg BID.

Twenty-one patients treated for 28 or more days were evaluable for response. There were 2 CRs, one partial remission (PR), and 2 blast responses (BR) (Table 2). Responding patients had a median ribavirin plasma level of 33 μM at best response whereas non-responders had a median maximum ribavirin plasma level of 19 μM. In total, 14 patients had a maximum plasma level of ribavirin more than 20 μM, and all 5 responding patients were in this group. The addition of LDAC to ribavirin tended to increase the median time to treatment failure from 104 days for the monotherapy trial (range 93-263 days, n=3) to 225 days (range 96-743 days, n=3), although the number of patients included in

Table 1. Patients' characteristics.

	N (%)
Total n. of patients	29 (100)
Median age, years (range)	65 (22-83)
Sex	
Female	14 (48)
Male	15 (52)
FAB AML subtype	
M4/M5	22 (76)
Other	7 (24)
WHO classification	
AML not otherwise specified	10 (34)
AML with recurrent genetic abnormality	3 (10)
Therapy-related AML	5 (17)
AML with myelodysplasia-related features	11 (38)
Cytogenetics	
Favorable	1 (3)
Intermediate	16 (55)
Adverse	12 (41)
FLT3 and NPM1 status	
FLT3 ITD (n=22)	5 (23)
FLT3 TKD (n=22)	1 (5)
NPM1 mutation (n=17)	4 (24)
ECOG	
0	6 (21)
1	19 (66)
2	3 (10)
3	1 (3)
N. of prior therapies	
0	5 (14)*
1	12 (45)**
2	8 (28)
≥3	4 (14)
Blasts – bone marrow	
Median	74%
Range	(4-100)***

**2 of 5 received therapy for MDS. **4 of 12 did not receive induction with "7+3", 1 of 12 received therapy for MDS. ***Patient 28 with extramedullary disease only. ITD: internal tandem duplication; TKD: tyrosine kinase domain point mutation.*

both trials is small. Patients with adverse cytogenetics were less likely to respond. No difference in FLT3 ITD/mutation or NPM1 mutation among responders and non-responders was observed.

Clinical response correlated with molecular targeting of eIF4E. Targeting was determined by changes in eIF4E mRNA levels and eIF4E protein re-localization to the cytoplasm. Protein levels of eIF4E and its downstream targets were assessed when sufficient material was available. No targeting of eIF4E was observed among patients with progressive disease (PD). Six patients had a full molecular response with both lower eIF4E levels and eIF4E re-localization (*Online Supplementary Table S1*) including the patients who achieved CR, PR, BR (Table 2). All had 20+ μM maximum plasma levels of ribavirin. Patients 3 and 10 had a partial molecular response, whereby they did not have full re-localization of eIF4E. For Patient 3, determination of ribavirin plasma levels was inaccurate because of frequent dose interruptions due to hemolytic anemia. Of the 3 patients (Patients 3, 10 and 22) with partial or full molecular response who did not achieve PR, CR or BR, all showed a decrease in blast count and/or hematologic improvement. Levels above 20 μM ribavirin were also observed in some non-responders, indicating that ribavirin level alone did not predict response. At relapse, all 6 patients with complete eIF4E targeting showed eIF4E re-localization back to the nucleus and elevated eIF4E levels consistent with the loss of clinical activity (*Online Supplementary Table S1*). Similarly, the partial molecular response was lost by Patients 3 and 10 at progression.

In our previous monotherapy trial, we noted upon clinical relapse an increase in the levels of the sonic hedgehog transcription factor Gli1, which led to glucuronidation of ribavirin, loss of the eIF4E-ribavirin interaction, and ultimately drug resistance.[9] Additionally, primary refractory and a few relapsed patients had markers of impaired drug uptake with low levels of the ribavirin transporter (ENT1) and/or an enzyme required for the pro-drug metabolism of ribavirin, adenosine kinase (ADK).[9] We examined these resistance markers here (*Online Supplementary Table S1*). For 5 of 27 patients, we observed lowered ADK and/or ENT1 mRNA and/or protein levels at baseline relative to healthy volunteers, suggesting that ribavirin pro-drug metabolism and drug uptake were impaired. None of these 5 patients responded to treatment. An additional 3 of 18 and 6 of 18 patients had reduced ADK or ENT1 levels at relapse/EOT relative to before treatment, respectively. For 14 of 18 patients, we observed an elevation in Gli1 and/or UDP-glucunosyltransferase 1A (UGT1A) at the end of treatment, relative to before treatment. In our resistance studies, elevated

Table 2. Response and ribavirin plasma levels.

Patient #	Ribavirin dose (mg bid)	LDAC dose (mg bid)	Time to treatment failure	Best response	Time to best response	Ribavirin plasma (μM) at BR	Maximum ribavirin plasma(μM)
1	1000	20	743	**CR***	161	29	47**
2	1000	20	19	PD			8
3	1000	20	71	SD			12
4	1000	20	29	PD			18
5	1400	20	48	SD			19
6	1400	20	78	**BR**	30	33	33
7	1400	20	31	PD			21
8	1800	20	71	SD			12
9	1800	20	21	PD			14
10	1800	20	86	SD			13
11	1800	20	11	n/a			12
12	1800	20	146	SD			11
13	2200	20	2	n/a			n/a
14	2200	20	27	PD			7
15	2200	20	14	n/a			9
16	2200	20	93	**PR**	50	n/a	21
17	2200	20	17	n/a			4
18	2200	20	28	PD			45
19	1000	10	224	**CR**	117	37	37
20	1000	10	69	SD			17
21	1000	10	54	PD			23
22	1400	10	169	SD			69
23	1400	10	113	**BR**	30	33	76
24	1400	10	62	SD			33
25	1800	10	57	SD			43
26	1800	10	18	PD			22
27	1800	10	7	n/a			7
28	1800	10	41	SD			28
29	1800	10	55	SD			20

**At time of best response Patient 1 was on LDAC 10 mg QD. **At time of max PK Patient 1 was on 1400 mg bid ribavirin only. CR: complete remission; PR: partial remission; BR: blast response; SD: stable disease; PD: progressive disease; n/a: not assessable.*

Gli1 correlated with increased UGT1A protein levels, ribavirin and cytarabine glucuronidation and drug resistance.[9] Finally, as in our monotherapy trial, many non-responding patients had elevated Gli1 or low ADK/ENT1 levels underlying their primary resistance. Thus, these patients likely did not respond due to inactive drug. Some patients had markers of both Gli1/UGT1A and ADK/ENT1 mediated resistance.

In summary, we identified the RP2D of ribavirin and LDAC, 1400 mg po BID continuous dosing and 10 mg sc BID for ten days of a 28-day cycle, respectively. This combination is well tolerated, with some patients achieving marked clinical responses. Our results indicate that ribavirin plasma levels are reduced in the presence of LDAC, which impairs the absorption of ribavirin, as was shown with other drugs.[11] In addition, LDAC may interfere with ribavirin activity, as patients in the prior monotherapy trial responded molecularly and clinically to ribavirin at lower serum levels.[7] Nonetheless, once higher levels of ribavirin were achieved the combination with LDAC may have yielded longer time on study compared with ribavirin alone for patients who achieved remission. A phase II study is needed to determine the rate and duration of response for this combination. Importantly, cellular changes in eIF4E required plasma levels of ribavirin above 20 μM in the presence of LDAC, supporting our clinical observation that this level is associated with response.

Tracking eIF4E targeting, ENT1, ADK, Gli1, UGT1A as well as ribavirin and cytarabine uptake likely predict response and relapse, respectively. We will test the efficacy of overcoming Gli1 inducible drug glucuronidation in an AML trial combining a Gli1 inhibitor with ribavirin (*clinicaltrials.gov identifier:02073838*). The development of additional drug combinations is also important. Our previous *ex vivo* AML studies suggest that combinations of eIF4E with azacytidine could be useful.[8] Furthermore, augmenting the inhibitory effects of ribavirin on eIF4E using Mnk kinase inhibitors or rapalogs could be effective. In summary, our second clinical trial targeting eIF4E with ribavirin led to clinical responses and highlighted the importance of monitoring resistance markers in AML.

Sarit Assouline,[1] Biljana Culjkovic-Kraljacic,[2] Julie Bergeron,[3] Stephen Caplan,[1] Eftihia Cocolakis,[1] Caroline Lambert,[1] Cara J. Lau,[1] Hiba Ahmad Zahreddine,[2] Wilson H. Miller Jr,[1] and Katherine L. B. Borden[2*]*

[1]*Segal Cancer Centre, Lady Davis Institute, Jewish General Hospital, McGill University;* [2]*Institute for Research in Immunology and Cancer & Dept. of Pathology and Cell Biology, Université de Montréal; and* [3]*Hôpital Maisonneuve-Rosemont, Montréal, QC, Canada*

Acknowledgments: we are grateful to Morris and David Goodman and Pharmascience Inc. for producing and providing ribavirin. We thank nursing and supporting staff at all the clinical sites and IRIC.

Funding: KLBB is supported by funds from the NIH (RO1 80728 and 98571), IRICoR and Translational Research Program grants from the Leukemia and Lymphoma Society USA. SA holds an FRSQ Clinician Scientist Award. KLBB holds a Canada Research Chair and HAZ holds a Cole Foundation Fellowship and a CNRS Lebanon Fellowship.

The online version of this article has a Supplementary Appendix.

Correspondence: katherine.borden@umontreal.ca
sarit.assouline@mcgill.ca
doi:10.3324/haematol.2014.111245

Key words: AML, eIF4E, ribavirin, phase I, drug resistance.

Information on authorship, contributions, and financial & other disclosures was provided by the authors and is available with the online version of this article at www.haematologica.org.

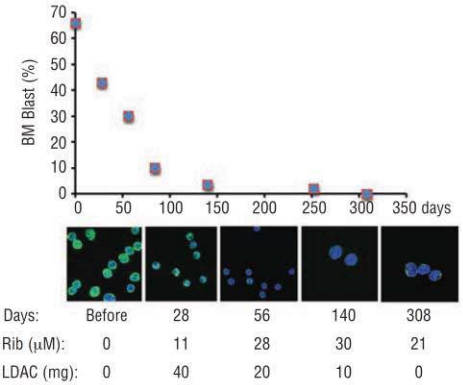

Figure 1. **(Top) Patient 1 percentage bone marrow blast counts *versus* days of treatment. (Middle) Confocal micrographs indicating alterations in eIF4E (green) subcellular distribution as a function of ribavirin treatment indicating molecular response. DAPI, a nuclear marker, is shown in blue. Magnification was 100X with a further 2X zoom for days 140 and 308. Blasts were sorted using flow cytometry gating on CD45 dim and side scatter, as described in the Methods. Note that cells sorted from specimens obtained during CR are likely not leukemic blasts but rather normal primitive progenitors. Note that at lower ribavirin concentrations, 11 μM at 28 days, there was no targeting of eIF4E, but at higher levels of ribavirin, eIF4E re-localization is observed. (Lower) Ribavirin plasma levels (micromolar) were determined by mass spectrometry and total daily dose of LDAC is given below. Patient 1 discontinued LDAC at day 179, as per protocol.**

References

1. Cancer Genome Atlas Research N. Genomic and epigenomic landscapes of adult de novo acute myeloid leukemia. N Engl J Med. 2013; 368(22):2059-74.
2. Carroll M, Borden KL. The oncogene eIF4E: using biochemical insights to target cancer. J Interferon Cytokine Res. 2013;33(5):227-38.
3. Culjkovic B, Tan K, Orolicki S, Amri A, Meloche S, Borden KL. The eIF4E RNA regulon promotes the Akt signaling pathway. J Cell Biol. 2008;181(1):51-63.
4. Culjkovic B, Topisirovic I, Skrabanek L, Ruiz-Gutierrez M, Borden KL. eIF4E promotes nuclear export of cyclin D1 mRNAs via an element in the 3'UTR. J Cell Biol. 2005;169(2):245-56.
5. Kentsis A, Topisirovic I, Culjkovic B, Shao L, Borden KL. Ribavirin suppresses eIF4E-mediated oncogenic transformation by physical mimicry of the 7-methyl guanosine mRNA cap. Proc Natl Acad Sci USA. 2004;101(52):18105-10.
6. Kentsis A, Volpon L, Topisirovic I, Soll CE, Culjkovic B, Shao L, et al. Further evidence that ribavirin interacts with eIF4E. RNA. 2005; 11(12):1762-6.
7. Assouline S, Culjkovic B, Cocolakis E, Rousseau C, Beslu N, Amri A, et al. Molecular targeting of the oncogene eIF4E in acute myeloid leukemia (AML): a proof-of-principle clinical trial with ribavirin. Blood. 2009;114(2):257-60.
8. Kraljacic BC, Arguello M, Amri A, Cormack G, Borden K. Inhibition of eIF4E with ribavirin cooperates with common chemotherapies in primary acute myeloid leukemia specimens. Leukemia. 2011; 25(7):1197-200.
9. Zahreddine HA, Culjkovic-Kraljacic B, Assouline S, Gendron P, Romeo AA, Morris SJ, et al. The sonic hedgehog factor GLI1 imparts drug resistance through inducible glucuronidation. Nature. 2014; 511(7507):90-3.
10. Grimwade D, Hills RK, Moorman AV, Walker H, Chatters S, Goldstone AH, et al. Refinement of cytogenetic classification in acute myeloid leukemia: determination of prognostic significance of rare recurring chromosomal abnormalities among 5876 younger adult patients treated in the United Kingdom Medical Research Council trials. Blood. 2010;116(3):354-65.
11. Kuhlmann J. Inhibition of digoxin absorption but not of digitoxin during cytostatic drug therapy. Arzneimittel-Forschung. 1982; 32(6):698-704.

CHAPTER 5

GLI1-Induced Drug Glucuronidation in Resistant Cancer Cells

(REVIEW)

Published Review in *Clin Cancer Res. 2015 May 15;21(10):2207-10. doi: 10.1158/1078-0432.CCR-14-1370. Epub 2015 Mar 25.*

Contribution:

H.A.Z. and K.L.B.B. wrote the manuscript.

Published OnlineFirst March 25, 2015; DOI: 10.1158/1078-0432.CCR-14-1370

Clinical Cancer Research

Molecular Pathways: GLI1-Induced Drug Glucuronidation in Resistant Cancer Cells

Hiba Ahmad Zahreddine and Katherine L.B. Borden

Abstract

Drug resistance remains a major impediment in the development of durable cancer therapies. Studies in acute myelogenous leukemia (AML) patients revealed a new form of multidrug resistance. Here, increased glioma-associated protein GLI1 leads to elevation of the UDP-glucuronosyl transferase (UGT) enzymes. UGTs add glucuronic acid to xenobiotics and metabolites. Traditionally, the loss of these enzymes is thought to contribute to cancer as a result of impaired clearance of environmental carcinogens. However, we demonstrate that overexpression of UGTs can contribute to oncogenesis by promoting drug resistance. Indeed, UGT levels in AML patients treated with ribavirin and/or cytarabine were elevated at relapse relative to diagnosis. This was reversed by GLI1 inhibition, suggesting a clinically relevant strategy to overcome drug resistance. Further, overexpression of UGTs can also lead to drug resistance in other cancers, such as certain Hsp90 inhibitors and vorinostat in colorectal and chronic lymphoblastic leukemia, respectively. Not all drugs are targets of glucuronidation, suggesting that UGT status could be relevant to treatment choice. Here, we describe several facets of UGT biology and how these could be exploited clinically. These studies demonstrate how drugs in cancer cells can be metabolized differentially than their normal counterparts. In summary, we describe a new form of drug resistance relevant to a variety of cancer contexts. *Clin Cancer Res; 21(10); 2207–10. ©2015 AACR.*

Background

The development of durable cancer therapeutics continues to be impaired by the development of drug resistance. Resistance arises to both traditional chemotherapies and newly developed targeted treatments. Drug resistance can arise for many different reasons, including modulation of drug transporters and/or metabolism, mutation of protein targets of drugs, and rewiring of targeted pathways, to name a few (1, 2). Further complicating matters, the development of resistance to one drug can lead to resistance to drugs that the patient has never received. This is referred to as cross-resistance (1). For instance, increased drug efflux through the MDR transporters affects many drugs. Genetic rewiring can lead to oncogenic bypass, where the drug still hits its cellular target, but no longer has a physiologic effect (2). Below, a new form of multidrug resistance is described, inducible drug glucuronidation (Fig. 1), which was discovered while targeting the eukaryotic translation initiation factor 4E (eIF4E) with a small-molecule inhibitor ribavirin in acute myelogenous leukemia (AML) patients (3). Initially, these results were quite promising, with some refractory and relapsed patients achieving complete and partial remissions with ribavirin monotherapy and also ribavirin in combination with low-dose Ara-C (4, 5). However, all patients eventually relapsed, and investigations into the molecular reasons for this led to the discovery that ribavirin and Ara-C became glucuronidated specifically in resistant cells.

Glucuronidation is an important step in phase II drug metabolism (6). There are several glucuronidation enzymes, UDP-glucuronosyl transferases, which are divided into two major families: UGT1As with nine members and UGT2B with seven members (7). UGT1As catalyze the addition of glucuronic acid to the nucleophilic part of the drug, rendering it more hydrophilic and either enhancing its efflux or modulating its affinity for a given cellular target. Family members differ in their preference to target specific chemical moieties, such as nitrogens, sulphurs, and oxygen (8). This activity, once thought limited to the liver, can occur throughout the body (8). Although glucuronidation is usually considered a steady-state process, it can have somewhat unpredictable effects. For instance, glucuronidation of morphine increases its potency (6), while glucuronidation of testosterone modulates its repertoire of protein partners without altering efflux (6).

Analysis of model systems and material from AML patients who had received either ribavirin or standard-of-care therapies revealed that levels of the sonic hedgehog transcription factor GLI1 became substantially elevated upon drug resistance, and this correlated with an increase in levels of the UGT1As enzymes (3, 5). Here, it was shown that this family of enzymes mediated glucuronidation of ribavirin, resulting in the loss of the ribavirin–eIF4E interaction and ultimately the loss of response to the drug. It was noted that, in this case, glucuronidation did not modulate the efflux of ribavirin. Furthermore, inducible glucuronidation was also observed for cytarabine, the cornerstone in the treatment for AML. Preliminary studies suggest other drugs will also be targets for this mode of inactivation (H.A. Zahreddine and K.L.B. Borden; unpublished results). Excitingly, this mechanism is reversed by the genetic or pharmacologic inhibition of GLI1, including with vismodegib,

Institute of Research in Immunology and Cancer (IRIC), Department of Pathology and Cell Biology, Université de Montréal, Montreal, Quebec, Canada.

Corresponding Author: Katherine L.B. Borden, Institute of Research in Immunology and Cancer (IRIC), Université de Montréal, Pavilion Marcelle-Coutu, 2950, Chemin Polytechnique, Montreal, QC H3T 1J4, Canada. Phone: 514-343-6291; Fax: 514-343-5839; E-mail: katherine.borden@umontreal.ca

doi: 10.1158/1078-0432.CCR-14-1370

Published OnlineFirst March 25, 2015; DOI: 10.1158/1078-0432.CCR-14-1370

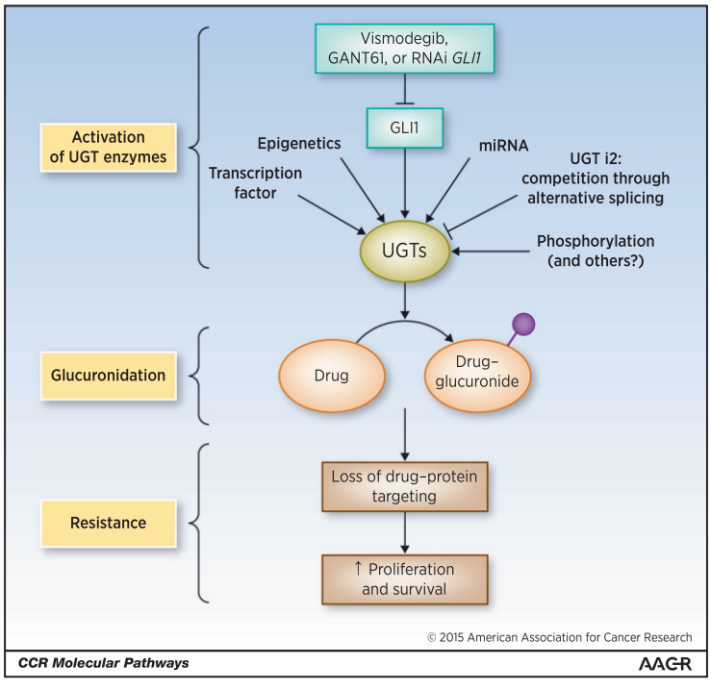

Figure 1.
Summary of means to regulate glucuronidation enzymes. For simplicity, only a subset of pathways are depicted.

a drug approved for metastatic basal cell carcinoma. Thus, our studies reveal a potential strategy to overcome drug resistance, which will be tested in AML patients in the coming months (NCT02073838).

Clinical–Translational Advances

Relevance of UGTs to drug resistance

Most studies on glucuronidation in malignancy have focused on the effects of loss of UGTs. Such losses can lead to reduced clearance of xenobiotics, such as the carcinogens in cigarette smoke (9). In the absence of clearance of these metabolites, increased DNA damage can occur leading to cancer (9). In support of this idea, individuals that lack activity of UGT1A7 have a higher risk of lung cancer (9).

Recent studies demonstrate that glucuronidation can become elevated in malignancy (3, 5, 10, 11). This result suggests that there is some sort of "Goldilocks zone" for UGT expression, where levels should not be too high or too low, but rather "just right." Our studies show that inducible drug glucuronidation can be part of an adaptive response of cancer cells to evade the effects of certain drugs. Furthermore, these new findings demonstrate that cancer cells metabolize drugs differently than normal counterparts. For instance, ribavirin- and cytarabine-glucuronides are not observed in normal tissues. Indeed, this metabolism even differs amongst cancer cell populations (resistant versus responsive). Two other recent studies support this hypothesis and suggest that these findings go beyond AML. First, in chronic lymphocytic leukemia (CLL), elevation of UGT2B17 may also underpin drug resistance (10). In these studies, elevated *UGT2B17* mRNA expression, in conjunction with other prognostic markers for CLL, predicted significantly shorter survival. Indeed, glucuronides are observed for the HDAC inhibitor vorinostat upon UGT2B17 overexpression; suggesting that UGT2B17 may have an impact on drug response at least in some patients. In a separate study, resistance to some Hsp90 inhibitors in a subset of colorectal cancer cell lines directly correlated with increased expression and enzymatic activity of UGT1As (11). Glucuronidation abrogated the Hsp90 interaction of a subset of chemically related inhibitors (11). Chemically unrelated Hsp90 inhibitors were not modified and still targeted Hsp90 in these cells, demonstrating the specificity of targeting in these cells. For the glucuronidation target drugs, knockdown of UGT led to renewed drug sensitivity. Given that not all Hsp90 inhibitors were targets for glucuronidation, specific UGTs likely play a role with these, favoring specific chemical moieties for glucuronidation. In summary, evidence for inducible drug glucuronidation is observed in several contexts, including AML, CLL, and colorectal cancers.

Regulation and targeting of UGTs

In order to develop means to target UGTs, it is critical to understand how these enzymes are regulated (Fig. 1). UGT levels can be regulated both posttranscriptionally and transcriptionally. For the AML case, there is a clear correlation

Published OnlineFirst March 25, 2015; DOI: 10.1158/1078-0432.CCR-14-1370

between elevated GLI1 and UGT protein levels. Further, reduction of GLI1 by knockdown or pharmacologic targeting with vismodegib or GANT61 leads to reduced UGT levels and reverts drug resistance. However, UGT is not a transcriptional target of GLI1, as *UGT1A* mRNA levels are not elevated. However, GLI1 appears to increase UGT1A protein stability. We postulate that GLI1 decreases UGT1A protein turnover through downregulation of specific protein ligases or it induces some posttranslational modifications of these enzymes, rendering them less susceptible to degradation. These possibilities will be examined in the future. Hence, in addition to using GLI1 inhibitors as a means to revert resistance, identifying key factors mediating the link between GLI1 and UGT1A could also serve as potential therapeutic modalities.

It seems likely that there will be many pathways leading to UGT dysregulation upon cancer resistance, in addition to GLI1 dysregulation. Numerous recent studies revealed a variety of molecular mechanisms governing expression and activity of UGT enzymes (11–15). Due to space restraints, only a few of these are described here. Aside from effects on protein stability described above, these include transcriptional regulation, phosphorylation, DNA methylation, histone modification, microRNA regulation, as well as alternative splicing (11–15). For instance, DNA hypermethylation of the *UGT1A1* promoter correlated with reduced transcription and increased sensitivity of colorectal cancer cells to SN-38 (the active metabolite of irinotecan; ref. 12). Also, a recent study identified miRNAs that negatively regulate the expression of UGT2B17 in human liver samples, but the identity of these miRNAs remains to be experimentally validated (14). Another interesting discovery revealed the presence of a novel class of human UGT proteins named UGT isoforms 2 (or i2s; ref. 16). Like isoforms 1, i2s are encoded by the same genetic locus, but instead of incorporating the usual common C-terminus exon 5a, these utilize a shorter exon 5b that causes a premature arrest of translation and subsequent loss of the transmembrane domain. Consequently, UGT i2s are located in the lumen and cytoplasm rather than in the membrane of the endoplasmic reticulum. Functionally, the i2 enzymes lack glucuronidation activity but act in a dominant-negative capacity, possibly by forming inactive heteromeric complexes with i1 enzymes, thus reducing enzymatic activity. Recent reports showed differential i1:i2 expression ratio in normal versus cancer tissues, with increased i2 in liver tumors and decreased levels of i1 and i2 in colon cancer samples, compared with normal specimens (17). Given the close tie between protein levels and activity, it seems likely that these tumors will have different glucuronidation activity relative to normal controls. As such, understanding the mechanisms of regulation of i2s might provide a means for increasing their expression in resistance context, allowing for inhibition of UGT i1s, as one of many possible targeting strategies.

Inducible modifications beyond glucuronidation?

Phase II drug metabolism involves conjugation of drugs via multiple pathways, including sulfation, glutathione addition, acetylation, methylation as well as glucuronidation. Accordingly, similar to glucuronidation, one can speculate that these modifications may also be induced in some forms of drug resistance. As such, a better understanding of the mechanisms that control these enzymes in both normal and cancer contexts could help improve the efficacy of cancer therapy. In addition, our findings suggest that when developing drugs, mechanisms that could drive drug modifications should be considered in patients particularly at relapse and not only in the initial stages of drug development in normal cells.

Conclusions and Future Directions

UGTs could not only serve as a biomarker for drug resistance but also guide choice of treatment. For instance, knowledge of which Hsp90 inhibitors become glucuronidated in cell lines would be important for guiding which inhibitors to administer when UGT levels become elevated in patients. In this way, the most effective Hsp90 inhibitors could be selected based on a patient's UGT status. Once there is a more global understanding of the drugs that become glucuronidated in different cancer contexts, UGT status could be used more globally for guiding the best options for other treatments. In AML, we will examine the efficacy of targeting glucuronidation by combining the GLI1 inhibitor vismodegib to target glucuronidation with ribavirin to target elevated eIF4E (NCT02073838). In this way, we will examine the efficacy of targeting UGT as a means to overcome drug resistance in patients.

One of the great challenges in studying drug metabolism is developing appropriate model systems. Human cell lines have been used for such experiments but are limited in terms of monitoring *in vivo* disease and further recapitulating drug compartmentalization and associated features. However, the substantial differences in drug modifications and even drug transporter distribution, between humans and rodents (18–20), means that this is a difficult solution as well. For instance, rodents have no N-linked glucuronidation, which is a major pathway in humans. Mice with human UGT1As expressed in their liver have more similar, but still not identical, glucuronidation activity as humans (19). Further issues arise as there are glucuronidation enzymes that are mainly in the gastrointestinal track and thus would not be accounted for by the humanized liver model (19). Other species-specific aspects of drug metabolism need to be accounted for as well, such as differences in drug transporter distribution (20). Thus, only with great effort and care can a model system be developed to truly parallel the human system.

In summary, inducible drug glucuronidation as a novel form of multidrug resistance is described. A better understanding of the modalities that cause UGT dysregulation will likely provide therapeutic strategies beyond the GLI1 example used here. Such studies should include monitoring UGTs at the protein level in various types and stages of cancer to assess the scope of this dysregulation. Also, determining which of the UGTs is upregulated in a given type of cancer first will help predict which class(es) of drugs will be subject to glucuronidation and potentially guide treatment choice. Finally, our studies strongly suggest that drug metabolism can differ between cancer and normal cells. These differences need to be better defined and could be a launching point for novel therapeutic strategies.

Disclosure of Potential Conflicts of Interest

No potential conflicts of interest were disclosed.

Authors' Contributions

Conception and design: H.A. Zahreddine, K.L.B. Borden

Published OnlineFirst March 25, 2015; DOI: 10.1158/1078-0432.CCR-14-1370

Development of methodology: H.A. Zahreddine, K.L.B. Borden
Writing, review, and/or revision of the manuscript: H.A. Zahreddine, K.L.B. Borden

Grant Support

H.A. Zahreddine is supported by a Cole Foundation Fellowship. K.L.B. Borden is supported by grants from the NIH (ROI 80728 and 98571), the Leukemia and Lymphoma Society Translation Research Program, and the Canadian Cancer Society Research Institute and holds a Canada Research Chair.

Received November 14, 2014; revised February 10, 2015; accepted February 19, 2015; published OnlineFirst March 25, 2015.

References

1. Zahreddine H, Borden KL. Mechanisms and insights into drug resistance in cancer. Front Pharmacol 2013;4:28.
2. Gottesman MM, Fojo T, Bates SE. Multidrug resistance in cancer: role of ATP-dependent transporters. Nat Rev Cancer 2002;2:48–58.
3. Zahreddine HA, Culjkovic-Kraljacic B, Assouline S, Gendron P, Romeo AA, Morris SJ, et al. The sonic hedgehog factor GLI1 imparts drug resistance through inducible glucuronidation. Nature 2014;511:90–3.
4. Assouline S, Culjkovic B, Cocolakis E, Rousseau C, Beslu N, Amri A, et al. Molecular targeting of the oncogene eIF4E in acute myeloid leukemia (AML): a proof-of-principle clinical trial with ribavirin. Blood 2009;114:257–60.
5. Assouline S, Culjkovic-Kraljacic B, Bergeron J, Caplan S, Cocolakis E, Lambert C, et al. A phase I trial of ribavirin and low-dose cytarabine for the treatment of relapsed and refractory acute myeloid leukemia with elevated eIF4E. Haematologica 2015;100:e7–9.
6. Dutton GJ. Glucuronidation of drugs and other compounds. Boca Raton (FL): CRC Press; 1980.
7. Guillemette C, Levesque E, Rouleau M. Pharmacogenomics of human uridine diphospho-glucuronosyltransferases and clinical implications. Clin Pharmacol Ther 2014;96:324–39.
8. Tukey RH, Strassburg CP. Human UDP-glucuronosyltransferases: metabolism, expression, and disease. Annu Rev Pharmacol Toxicol 2000;40:581–616.
9. Burchell B. Genetic variation of human UDP-glucuronosyltransferase: implications in disease and drug glucuronidation. Am J Pharmacogenomics 2003;3:37–52.
10. Gruber M, Bellemare J, Hoermann G, Gleiss A, Porpaczy E, Bilban M, et al. Overexpression of uridine diphospho glucuronosyltransferase 2B17 in high-risk chronic lymphocytic leukemia. Blood 2013;121:1175–83.
11. Landmann H, Proia DA, He S, Ogawa LS, Kramer F, Beißbarth T, et al. UDP glucuronosyltransferase 1A expression levels determine the response of colorectal cancer cells to the heat shock protein 90 inhibitor ganetespib. Cell Death Dis 2014;5:e1411.
12. Belange AS, Tojcic J, Harvey M, Guillemette C. Regulation of UGT1A1 and HNF1 transcription factor gene expression by DNA methylation in colon cancer cells. BMC Mol Biol 2010;11:9.
13. Oda S, Fukami T, Yokoi T, Nakajima M. Epigenetic regulation of the tissue-specific expression of human UDP-glucuronosyltransferase (UGT) 1A10. Biochem Pharmacol 2014;87:660–7.
14. Rieger JK, Klein K, Winter S, Zanger UM. Expression variability of absorption, distribution, metabolism, excretion-related microRNAs in human liver: influence of nongenetic factors and association with gene expression. Drug Metab Dispos 2013;41:1752–62.
15. Yokoi T, Nakajima M. microRNAs as mediators of drug toxicity. Annu Rev Pharmacol Toxicol 2013;53:377–400.
16. Girard H, Lévesque E, Bellemare J, Journault K, Caillier B, Guillemette C. Genetic diversity at the UGT1 locus is amplified by a novel 3′ alternative splicing mechanism leading to nine additional UGT1A proteins that act as regulators of glucuronidation activity. Pharmacogenet Genomics 2007;17:1077–89.
17. Bellemare J, Rouleau M, Harvey M, Popa I, Pelletier G, Têtu B, et al. Immunohistochemical expression of conjugating UGT1A-derived isoforms in normal and tumoral drug-metabolizing tissues in humans. J Pathol 2011;223:425–35.
18. Rowland A, Miners JO, Mackenzie PI. The UDP-glucuronosyltransferases: their role in drug metabolism and detoxification. Int J Biochem Cell Biol 2013;45:1121–32.
19. Kutsuno Y, Sumida K, Itoh T, Tukey RH, Fujiwara R. Glucuronidation of drugs in humanized UDP-glucuronosyltransferase 1 mice: similarity with glucuronidation in human liver microsomes. Pharmacol Res Perspect 2013;1:e00002.
20. Xu D, Nishimura T, Nishimura S, Zhang H, Zheng M, Guo YY, et al. Fialuridine induces acute liver failure in chimeric TK-NOG mice: a model for detecting hepatic drug toxicity prior to human testing. PLoS Med 2014;11:e1001628.

CHAPTER 6

Inducible Drug Modifications: A New Form of Resistance (REVIEW)

Published Review in *Cell Cycle. 2014 Aug 15; 13(16): 2485–2486. doi: 10.4161/15384101.2014.946372*

Contribution:

B.C.-K., H.A.Z. and K.L.B.B. wrote the manuscript.

Cell Cycle 13:16, 2485–2486; August 15, 2014; © 2014 Taylor & Francis Group, LLC

Inducible drug modification: A new form of resistance

Biljana Culjkovic-Kraljacic, Hiba Ahmad Zahreddine and Katherine LB Borden*

Institute for Research in Immunology and Cancer & Department of Pathology and Cell Biology; Université de Montréal; Montréal, QC Canada

Resistance to chemotherapy is a major problem facing cancer treatment. Understanding the molecular basis for drug resistance has lagged behind our understanding and identification of new pathways to target. Even early on in treatment, patients can become resistant to therapy. For instance, substantial numbers of acute myeloid leukemia (AML) patients will not respond to the first round of standard therapy. While it is important to assess the different molecular events that drive cancer, and target these as part of personalized medicine, it is equally important to further understand why patients do not respond. Ultimately, we must understand these treatment failures in order to make future successes.

We took this approach to better understand why targeting the eukaryotic translation initiation factor eIF4E in AML patients with ribavirin worked dramatically well in many patients, but did not in others, and why all responding patients eventually relapsed. These studies led us to identify a novel form of drug resistance and excitingly, a means to overcome it.[1]

Our study focused on the eukaryotic translation initiation factor eIF4E which is a potent oncogene that is elevated in approximately 30% of human cancers including M4 and M5 subtypes of AML.[1,2] eIF4E regulates the translation and nucleo-cytoplasmic export of a subset of transcripts that are essential for proliferation, survival and malignant transformation. Since association with the 7-methyl guanosine (m^7G) cap structure at the 5′ end of mRNAs is essential for its functions,[2] targeting eIF4E with competitive inhibitors of the m^7G, such as ribavirin, was undertaken.[2] Previous studies by us and others showed that ribavirin potently inhibited eIF4E activity in model systems.[2,3] Our Phase II ribavirin monotherapy clinical trial in poor prognosis AML patients showed that ribavirin led to a significant clinical improvement with a 45% objective response rate (remissions and blast responses).[4] Although striking for this poor prognosis population, all responding patients eventually became resistant to ribavirin and some never responded despite having elevated eIF4E levels.[5]

In order to understand the molecular mechanisms underlying primary and acquired resistance, we generated cell line models and found 2 mechanims of resistance. First, we observed defective ribavirin uptake due to impaired drug influx and metabolism. Specifically, we identified down regulation of the key enzyme involved in ribavirin pro-drug metabolism and/or ribaivirn nucleoside transporter ENT1.[4] Drug metabolism modulation is commonly observed in drug resistance, where drug uptake is abrogated, drug efflux is enhanced (e.g., MDR), or pro-drug metabolism is impaired. Although there have been attempts to target MDR transporters, this has not led to significant clinical benefit as of yet, mainly due to the substantial side effects observed with these therapies.

Since only 2 of our patients (over 15 studied), showed any defects in the transporter or pro-drug metabolism factors, we further explored mechanisms that could allow us to understand what were the factors driving drug resistance in our patients. Strikingly, we identified models where ribavirin uptake was normal, but its interaction with eIF4E was lost. Subsequent analysis indicated that the Glioma associated transcription factor Gli1 was highly elevated in these models and unexpectedly, this correlated with increased protein production of the UGT1A enzymes (**Fig. 1**). UGT1A enzymes are central to phase II drug metabolism where they add glucuronic acid (from the co-factor uridine disphoshate glucuronic acid, UDP-GA) to the drug leading to the loss of target-drug interactions and in some cases increased drug efflux.[6] Here, we observed that ribavirin glucuronidation led to the loss of its interaction with eIF4E thereby underpinning subsequent resistance. Further, Gli1 elevation alone was sufficient to drive UGT1A protein production and drug resistance. Interestingly, Gli1-mediated glucuronidation also drove resistance to another unrelated drug, cytarabine, consistent with previous observations that UGT1As can modify many classes of drugs. Strikingly, addition of the FDA approved pharmacological inhibitors of Gli1 Visomdegib (GDC-0449)[1] or Gli1 knockdown in resistant cells led to a loss of glucuronidation, and drug resensitization. Thus, Gli1, via UGT1A, drives a novel form of multi-drug resistance which is targetable. In our patients, elevation of Gli1 and UGT1A levels were observed in patients who were primarily resistant and in patients at clinical relapse. Indeed, we observed that these factors were elevated in relapsed patients treated with standard AML therapies indicating that it could be a common form of drug resistance in these patients, and perhaps in other cancers as well. This form of drug resistance would be expected to affect a wide variety of drugs.

*Correspondence to: Katherine LB Borden; E-mail: katherine.borden@umontreal.ca
Submitted: 07/07/2014; Accepted: 07/16/2014
http://dx.doi.org/10.4161/15384101.2014.946372

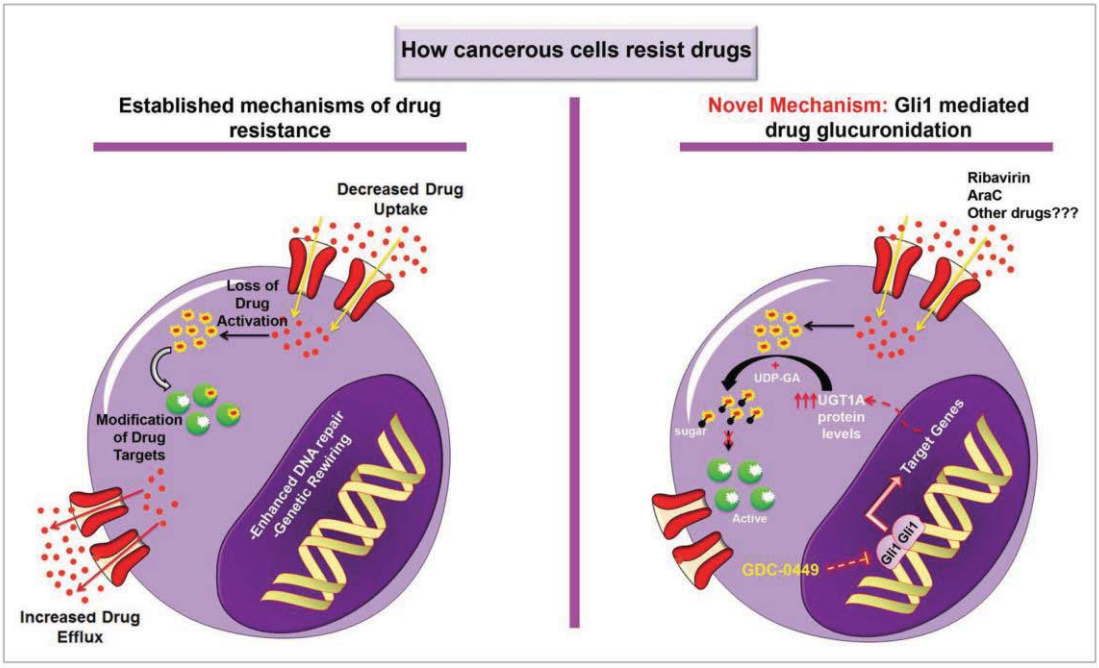

Figure 1. Well established molecular mechanisms underlying drug resistance include altered drug metabolism (increased drug efflux, decreased uptake), modification of drug targets, enhanced DNA repair, and genetic rewiring. In our novel mechanism, upregulation of Gli1 expression indirectly increases UGT1As, which catalyze the addition of glucuronic acid to the drug leading to the loss of drug-to-target interaction. This resistance could be reverted by either indirect or direct Gli1 inhibitors (GDC-0449 and Gant61, respectively). This mechanism might also apply to drugs other than Ribavirin and AraC.

Generally, there are 3 means of drug resistance proposed: impaired drug net uptake (due to either increased efflux or decreased influx), mutation of the drug target or compensatory genetic re-wiring of the relevant pathways (**Fig. 1**).[7] Here we present a fourth model, inducible drug modification. In this case, elevation of UGT1As would explain failure to treat refractory AML patients. We postulate that these modifications will not be limited to glucuronidation, with other aspects of phase II drug metabolism perhaps playing important roles in other forms of drug resistance. In clinical trials, many studies start with promising responses with patients quickly failing therapies. Perhaps this is not due to the fact that the wrong pathway was targeted or that the targeting was ineffectual, but rather to the rapid onset of drug resistance. Future studies focusing on drug resistance in parallel with the development of new therapies will likely lead to the development of the most efficacious therapies.

References

1. Zahreddine H, et al. Nature 2014; 3:511(7507): 90-3; PMID:24870236; http://dx.doi.org/10.1038/nature13283
2. Kentsis A, et al. Proc Natl Acad Sci U S A 2004; 101:18105–10; PMID:15601771; http://dx.doi.org/10.1073/pnas.0406927102
3. Pettersson F, et al. Clin Cancer Res 2011; 17(9):2874–84; PMID:21415224; http://dx.doi.org/10.1158/1078-0432.CCR-10-2334
4. Reyes G, et al. Mol Membr Biol 2011; 6:412–26
5. Assouline S, et al. Blood 2009; 114:257–60; PMID:19433856; http://dx.doi.org/10.1182/blood-2009-02-205153
6. Cummings J, et al. Cancer Res 2003; 1:63(23): 8443–50; PMID:14679008
7. Zahreddine H, et al. Front Pharmacol 2013; 14: 4–28

CHAPTER 7

Sonic Hedgehog Factor GLI1: As good as Resistance

(REVIEW)

Published Review in *Mol Cell Oncol. 2015 Jan-Mar; 2(1): e961827. doi: 10.4161/23723548.2014.961827*

Contribution:

H.A.Z., B.C-K. and K.L.B.B. wrote the manuscript.

Molecular & Cellular Oncology 2:1, e961827; January/February/March 2015; Published with license by Taylor & Francis Group, LLC

Sonic Hedgehog factor Gli1: As good as resistant

Hiba Ahmad Zahreddine, Biljana Culjkovic-Kraljacic, and Katherine LB Borden*

Institute for Research in Immunology and Cancer; University of Montreal; Montreal, QC Canada

Keywords: cancer, drug resistance, Gli1, UGT1A, glucuronidation, Vismodegib, cytarabine, ribavirin, eIF4E

Chemoresistance remains a major impediment in cancer therapy. Although major progress has been made in understanding the mechanisms underlying resistance in cancer, there is still more to learn. Our studies provide evidence that Gli1 drives a novel form of drug resistance involving Phase II drug metabolism enzymes, specifically the UGT1A family.

If you heard the many stories featuring the struggle between cancer treatment, resistance, and relapse throughout the history of cancer research, you might assume that we are very familiar with the topic. Our new data suggest that this is not the case.

While studying the efficacy of ribavirin, a drug that targets eIF4E activity, in acute myeloid leukemia (AML) patients with poor prognosis, we found ourselves dealing with what appears to be the inevitable outcome of targeted monotherapy treatments: clinical relapse and molecular resistance.[1] During our attempt to understand the molecular events underlying drug resistance in our patients, we serendipitously identified a novel form of drug resistance with implications well beyond ribavirin.[2] This new form of resistance involves the well-known Sonic Hedgehog transcription factor Gli1 and the drug modifying enzymes UDP-glucuronysltransferase 1A (UGT1A), and represents a new method by which cancer cells combine the effects of genetic rewiring and metabolic inactivation to evade therapy and allow relapse (**Fig. 1**). Our story depicts Gli1 alone as a sufficient driver of the glucuronidation of several drugs used for the treatment of AML, including cytarabine, the cornerstone of treatment, and ribavirin. Glucuronidation is a process by which drugs are chemically modified by the addition of glucuronic acid, which typically enhances their hydrophilicity and increases efflux.[3] However, in some cases, such as with androgens, glucuronidation alters targeting, rather than drug efflux.[4] In this case, glucuronidation of ribavirin correlates with loss of its interaction with eIF4E and ultimately leads to the loss of growth inhibition with no effect on drug uptake.

Fortunately, this new mechanism is clinically promising for patients with AML, for whom the overall survival is on average 7 months. Using vismodegib, a FDA-approved inhibitor of the Sonic Hedgehog pathway, we showed that targeting Gli1 eliminated ribavirin or cytarabine glucuronidation, allowed the re-emergence of eIF4E-ribavirin complexes, and led to renewed drug sensitivity. Importantly, Gli1 inhibition alone had little effect on cell growth whereas Gli1 inhibition in combination with either ribavirin or cytarabine reverted the drug resistance and restored sensitivity. To date, Gli1 inhibitors have been used for basal cell carcinomas in which the Gli1 pathway is inappropriately activated.[5] Here, we propose a new rationale for targeting the Gli1 pathway to overcome Gli1-inducible drug glucuronidation. A clinical trial combining vismodegib with ribavirin for the treatment of AML is scheduled to open in the near future (ClinicalTrials.gov NCT02073838). Our findings thus far leave us wondering whether this mechanism could also mediate therapeutic resistance in other types of cancer and which drug families might be targets of Gli1-mediated glucuronidation.

Very little is known about the factors regulating the production of UGT1A enzymes.[6] Our studies to date suggest that Gli1 controls the protein stability of UGT1A rather than its transcription. It is also likely that UGT1A expression and activity are regulated by mechanisms other than Gli1-mediated control, a possibility that must be assessed. Furthermore, our studies suggest that ribavirin and cytarabine are glucuronidated by different members of the UGT1A family. Thus, determining the specific member(s) driving resistance is essential to guide the development of selective and specific UGT1A inhibitors in future avenues of research.

To date, the major focus in drug resistance has been on (1) impaired uptake or increased drug efflux as characterized by the multidrug resistant (MDR) drug transporters,[7,8] (2) impaired pro-drug metabolism,[8] (3) mutation of target proteins e.g., BCR-Abl and Gleevec or PML-RARA and retinoic acid,[9] and (4) altered cellular pathways, such as downregulation of target proteins, enhanced DNA repair, activation of alternative survival pathways, inactivation of apoptotic pathways, or activation of antiapoptotic pathways.[10]

*Correspondence to: Katherine LB Borden; Email: katherine.borden@umontreal.ca
Submitted: 07/23/2014; Accepted: 07/30/2014
http://dx.doi.org/10.4161/23723548.2014.961827

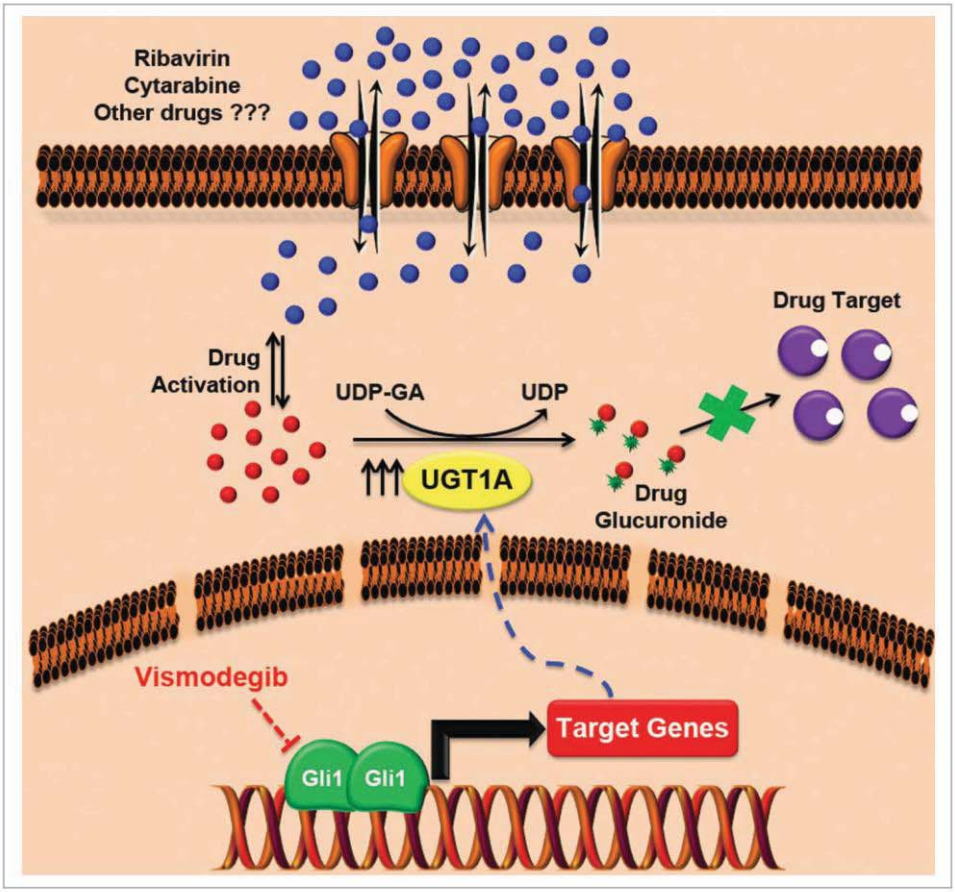

Figure 1. Novel mechanism of multidrug resistance driven by Gli1. Elevated Gli1 levels increase the levels of UGT1As, which in turn catalyze the addition of glucuronic acid to the drug thus leading to the loss of drug–target interaction. This mechanism of resistance applies to ribavirin, cytarabine, and possibly some other drugs and can be reverted by direct or upstream inhibitors of Gli1 such as vismodegib. Note that both ribavirin and cytarabine require an activation step in order to remain in the cell. Our *in vitro* studies suggest that, at least for ribavirin, glucuronidation occurs on the active form. Further studies are required to assess whether the activation step *a priori* is essential for glucuronidation to occur or whether this is specific to the drug and/or the UGT1A protein involved.

This new mechanism of Gli1-mediated resistance and relapse proves that we are still at the very beginning of understanding and overcoming cancer resistance.

In summary, drug resistance is the underlying reason for treatment failure in the majority of cancer patients. Moreover, development of resistance to one therapy often suggests that patients will be resistant to other therapies that they have never been exposed to. Typically, strategies to treat cancer are based on identifying an Achilles' heel in the cancer cell, and when resistance emerges the treatment choices become limited and typically do not account for why the resistance emerged in the first place. Perhaps a better approach to the development of more effective and durable cancer therapies would be to determine the underlying causes of treatment failure and success.

Disclosure of Potential Conflicts of Interest

No potential conflicts of interest were disclosed.

References

1. Assouline S, Culjkovic B, Cocolakis E, Rousseau C, Beslu N, Amri A, Caplan S, Leber B, Roy DC, Miller WH Jr, et al. Molecular targeting of the oncogene eIF4E in acute myeloid leukemia (AML): a proof-of-principle clinical trial with ribavirin. Blood 2009; 114:257-60; PMID:19433856; http://dx.doi.org/10.1182/blood-2009-02-205153
2. Zahreddine HA, Culjkovic-Kraljacic B, Assouline S, Gendron P, Romeo AA, Morris SJ, Cormack G, Jaquith

JB, Cerchietti L, Cocolakis E, et al. The sonic hedgehog factor GLI1 imparts drug resistance through inducible glucuronidation. Nature 2014; 511:90-3; PMID:24870236; http://dx.doi.org/10.1038/nature13283
3. Cummings J, Ethell BT, Jardine L, Boyd G, Macpherson JS, Burchell B, Smyth JF, Jodrell DI. Glucuronidation as a mechanism of intrinsic drug resistance in human colon cancer: reversal of resistance by food additives. Cancer Res 2003; 63:8443-50; PMID:14679008
4. Chouinard S, Yueh MF, Tukey RH, Giton F, Fiet J, Pelletier G, Barbier O, Bélanger A. Inactivation by UDP-glucuronosyltransferase enzymes: the end of androgen signaling. J Steroid Biochem Mol Biol 2008; 109:247-53; PMID:18467088; http://dx.doi.org/10.1016/j.jsbmb.2008.03.016
5. LoRusso PM, Rudin CM, Reddy JC, Tibes R, Weiss GJ, Borad MJ, Hann CL, Brahmer JR, Chang I, Darbonne WC, et al. Phase I trial of hedgehog pathway inhibitor vismodegib (GDC-0449) in patients with refractory, locally advanced or metastatic solid tumors. Clin Cancer Res 2011; 17:2502-11; PMID:21300762; http://dx.doi.org/10.1158/1078-0432.CCR-10-2745
6. Kiang TK, Ensom MH, Chang TK. UDP-glucuronosyltransferases and clinical drug-drug interactions. Pharmacol Ther 2005; 106:97-132; PMID:15781124; http://dx.doi.org/10.1016/j.pharmthera.2004.10.013
7. Szakacs G, Paterson JK, Ludwig JA, Booth-Genthe C, Gottesman MM. Targeting multidrug resistance in cancer. Nat Rev Drug Discov 2006; 5:219-34; PMID:16518375; http://dx.doi.org/10.1038/nrd1984
8. Jordheim LP, Dumontet C. Review of recent studies on resistance to cytotoxic deoxynucleoside analogues. Biochim Biophys Acta 2007; 1776:138-59; PMID:17881132
9. Lovly CM, Shaw AT. Molecular pathways: resistance to kinase inhibitors and implications for therapeutic strategies. Clin Cancer Res 2014; 20:2249-56; PMID:24789032; http://dx.doi.org/10.1158/1078-0432.CCR-13-1610
10. Zahreddine H, Borden KL. Mechanisms and insights into drug resistance in cancer. Front Pharmacol 2013; 4:28; PMID:23504227

CHAPTER 8

The eukaryotic translation initiation factor eIF4E harnesses hyaluronan production to drive its malignant activity

(RESEARCH ARTICLE)

Submitted Manuscript in *Nature. 2016 January.*

Synopsis: The role of eIF4E in cancer invasion and metastasis has been so far correlated with its ability to increase expression and activity of matrix degrading enzymes and factors essential for angiogenesis. In this chapter, I present data supporting the role of eIF4E in cancer cell motility by reshaping the surface of cancer cells, producing microvillus-like protrusions, through coordinately regulating the biosynthesis of Hyaluronic acid and its major receptor CD44. These findings offer a rationale for potentially inhibiting tumour cell metastasis through the combinatorial inhibition of eIF4E and the use of HA degrading enzymes, Hyaluronidases.

Contribution:

All data in **Figures 2, 3, 4, 5, 6 and 7** were generated by **Hiba Zahreddine (100%)**

All data in **Supplementary Figures** were generated by **Hiba Zahreddine (100%)**

Data in **Figures 1** were generated by **Hiba Zahreddine (50%)** and **Biljana Culjkovic-Kraljacic (50%)**

Data in **Supplementary Figures** were generated by **Hiba Zahreddine (50%)** and **Biljana Culjkovic- Kraljacic (50%)**

H.A.Z. designed and performed experiments, analysed data and wrote the manuscript; B.C-K, L.C., L.S., A.D. and S.D.R. performed experiments; M.L., C.V performed experiments, R.M., W.H.M. and V.H.W.H.M. designed experiments, analysed data and edited the manuscript; K.L.B.B. designed experiments, analysed data and wrote the manuscript.

The eukaryotic translation initiation factor eIF4E drives production of hyaluronan

The eukaryotic translation initiation factor eIF4E drives production of hyaluronan

Hiba Ahmad Zahreddine[1], Biljana Culjkovic-Kraljacic[1], Lucy Skrabanek[2], Ronald Midura[3], Mark Lauer[3], Sonia Del Rincon[4], Audrey Emond[4], Valbona Cali[3], Leandro Cerchietti[5], Wilson H Miller[4], Vincent Hascall[3], Katherine LB

1 Institute for Research in Immunology and Cancer & Dept. of Pathology and Cell Biology, Université de Montréal, Montréal, Québec, Canada; 2 Department of Physiology and Biophysics, Institute for Computational Biomedicine Weill Cornell Medical College, Cornell University, New York, USA; 3 Department of Biomedical Engineering and Orthopaedic Research Center, The Cleveland Clinic Foundation, Cleveland, Ohio USA; 4 Segal Cancer Centre, Lady Davis Institute, Jewish General Hospital, McGill University, Montréal, Québec, Canada ;5 Division of Hematology and Oncology, Department of Medicine, Weill Cornell Medical College, Cornell University, New York, USA.

Corresponding author

Contact Katherine L. B. Borden

Nature ***(Submitted _January 2017)***

Abstract

Aggressive cancers invade neighbouring tissues eventually leading to colonization in remote sites of the body. Tumour cells often undergo alterations to facilitate invasion and metastases. Here, we show that the eukaryotic translation initiation factor eIF4E initiates a post-transcriptional programme that fundamentally alters the cell surface architecture. Specifically, eIF4E drives biosynthesis of the glycosaminoglycan hyaluronan (HA) leading to the acquisition of both an HA surface coat and cell surface protrusions. Although HA is a major component of the extracellular matrix, we show that HA on the surface of tumour cells is required for eIF4E-mediated invasion. eIF4E also drives production of HA associated factors e.g. CD44 which arms the HA coat and protrusions subsequently promoting invasion. Targeting eIF4E in mouse models correlates with reduced HA levels, and reduced tumour and metastatic burden. In summary, we demonstrate for the first time that HA biosynthesis can be harnessed by an oncoprotein to drive its malignant phenotype.

Introduction

The tumour microenvironment plays important roles in cancer, providing a niche for the preferential survival and proliferation of tumour cells. A major component of this structure is the glycosaminoglycan hyaluronan (HA). HA is composed of repeating disaccharides units of UDP-Glucuronic Acid and UDP-N-Acetyl Glucosamine. HA is synthesized by hyaluronic acid synthases (HAS), which are single transmembrane proteins localized to the inner-face of the plasma membrane [1, 2]. HA chain length can be associated with differential functions including regulation of various cellular processes such as embryonic development, tissue homeostasis, wound healing and inflammation and when dysregulated can promote EMT, tumour growth, and invasion [3, 4]. Shorter chains are primarily synthesized by HAS3 [5, 6]. These shorter forms of HA are often associated with malignant phenotypes [7-9]. Experimental overexpression of HAS enzymes causes increased tumour growth in mouse xenograft models of prostate, breast and colon carcinomas while its knockdown reverses this phenotype [1, 10]. Further, HA is cleaved by hyaluronidases (six isoforms exist in humans) which have been suggested to act as tumour suppressors; whereby increased expression inhibits tumour growth in colon and breast xenografts [11-13]. Increased HA levels are correlated with formation of less dense matrices to facilitate invasion and promote angiogenesis. Elevated levels of HA in the stroma around tumours is associated with poor outcome [14, 15]. In addition to surrounding tumours in some cases HA can coat the surface of tumour cells with HA-based protrusions radiating from the cell surface [16, 17]. Indeed, overexpression of HAS3 alone is sufficient to induce the formation of an HA coat with microvillus-like protrusions on the cell surface. The major HA receptor CD44 is found to co-localize with these surface HA coats, but is not required for their formation. The number of cancer cell types with cell-surface HA is not yet known, and the extent to which cell-associated HA also plays physiological roles in cancer is an important open question in the field.

Despite the wealth of knowledge relating HA to malignancy, there is virtually no information regarding how HA levels become elevated in cancer and further, there is no understanding of what conditions drive production of cell-surface associated HA. Indeed, the levels of mRNAs encoding the enzymes in the biosynthetic pathways can be poor predictors of HA production

[18]. For instance in endometrial and ovarian carcinomas, RNA levels of HAS enzymes do not predict elevated HA levels in these specimens [18, 19]. These data suggest that this pathway is not always under direct transcriptional control and begs the question how else is HA production regulated. In this study, we demonstrate that the production of HA and its related downstream effectors are coordinately controlled post-transcriptionally by the eukaryotic translation initiation factor eIF4E. eIF4E is highly expressed in many cancers and this correlates with increased invasion, metastases and poor prognosis [20-24]. In early-stage clinical trials, eIF4E targeting with ribavirin led to objective responses including remissions in some acute myeloid leukemia (AML) patients [25-29]. In mouse models, eIF4E overexpression is sufficient to drive tumour formation [30-32]. At the biochemical level, eIF4E modulates expression of selected transcripts through its roles in nuclear mRNA export and translation. Both of these functions contribute to its oncogenic potential [21, 33, 34]. eIF4E-target transcripts are the downstream effectors of its physiological effects. Here we identified the enzymes encoding the HA biosynthetic pathway, HAS3, CD44 and associated factors as eIF4E target transcripts. We demonstrated that this pathway was required for eIF4E to mediate its oncogenic activities.

Results and Discussion

We set out to identify mRNA target transcripts which could encode proteins that were downstream effectors of the oncogenic activities of eIF4E. To identify these mRNAs, we took advantage of a fundamental difference in the RNA-binding properties of eIF4E between cellular compartments. In the cytoplasm eIF4E binds all capped-RNAs regardless of whether it increases their translation efficiency [26, 27, 35, 36]. However, in the nucleus, eIF4E binds transcripts that are functional export targets [26, 27]. Given these considerations, we reasoned that identification of eIF4E-bound transcripts in the nucleus would provide a straightforward strategy for the discovery of downstream factors that execute its biological effects. These included enzymes involved in HA biosynthesis (see below).

We identified eIF4E-bound RNAs using an RNA immunoprecipitation (RIP) strategy. Nuclear lysates from osteosarcoma U2Os cells were immunoprecipitated with anti-eIF4E antibodies,

and results were compared to IgG controls (Fig. 1b and Supp. Fig. 1a, b). To ensure these interactions were functional, we also monitored the mRNA export of candidate transcripts as a function of eIF4E overexpression by monitoring RNA content in nuclear and cytoplasmic compartments. In both experiments, RNAs were detected by quantitative reverse transcription PCR methods (RT-qPCR). Fractionation quality was assessed using U6snRNA and $tRNA^{lys}$ for nuclear and cytoplasmic fractions respectively. Preliminary studies using genome-wide screens of our nuclear eIF4E RIPs provided evidence that factors involved in HA biosynthesis were targets (Fig. 1a). Using RT-qPCR, we determined that the transcripts encoding most of these enzymes bound eIF4E in nuclear RIPs with enrichments ranging from 2.5-15 fold (Fig. 1b). These targets include hyaluronan synthase 3 (HAS3; 2.6 fold), as well as many of the enzymes involved in generating the UDP-Glucuronic acid and UDP-N-Acetyl Glucosamine precursors including hexokinase 1 (HK, ~15 fold), and phosphoglucomutase (PGM5, ~11 fold), amongst others (Fig. 1a). Nuclear mRNA export assays indicated that these mRNA-eIF4E interactions were functional since we observed increased mRNA export 2 to 8-fold upon eIF4E overexpression relative to vector controls depending on the transcript monitored (Fig. 1c). The only transcript which was bound to eIF4E in the nucleus but was not an export target in these cells encoded glucose phosphoisomerase (GPI). In addition to the HA biosynthetic machinery, other eIF4E targets identified in our RIP and fractionation studies included downstream effectors of HA e.g. CD44 as well as its signalling partners e.g. Ezrin and MMP9 (Fig. 1b and c) [37]. Total levels for target RNAs were not affected by eIF4E overexpression confirming that these effects were post-transcriptional (Supp. Fig. 1c). Negative controls RNAs such as GADPH, Hsp90 and β-Tubulin were not in the immunoprecipitations and were not modulated at the export level (Fig. 1b, c). For comparison, we used the S53A eIF4E mutant which is deficient in mRNA export and transformation but active in translation [34, 38]. As expected, the S53A eIF4E mutant did not promote export of any of these mRNAs (Fig. 1c).

Consistent with our above findings, eIF4E overexpression led to increased protein levels of the relevant enzymes, including HAS3, HK, GFPT1, GNPNAT1, UAP1, UGDH, as well as downstream effectors of HA function such as CD44 and Ezrin, relative to vector controls (Fig. 1d and Supp. Fig. 1d). Available antibodies for PGM5, UGP2 and GPI were not of sufficient

quality to assess the respective protein levels. The positive controls Mcl1 and c-Myc were elevated in eIF4E overexpressing cells relative to vector controls, as expected (Fig. 1d and Supp. Fig. 1d). Although the S53A eIF4E mutant did not export the corresponding transcripts, a modest increase relative to vector controls was observed at the protein level for a few of the members of the HA pathway e.g. HAS3, CD44, HK, UAP1 suggesting that these enzymes were also translation targets of eIF4E (Fig. 1d and Supp. Fig. 1d). c-Myc is elevated in S53A eIF4E cells relative to vector controls, consistent with the fact that it is both an mRNA export and translation target [27, 39]. Notably, the changes induced by S53A eIF4E were substantially less than those observed for wildtype eIF4E for all cases, consistent with the role of RNA export in their expression. Thus, eIF4E increases levels of the enzymes in the HA biosynthetic pathway and downstream effectors of HA signalling (e.g. CD44 and Ezrin) through increased mRNA export and for some of these targets, also via elevated translation.

Next, we determined whether eIF4E overexpression drove production of HA. To address this, we monitored HA levels in eIF4E, eIF4E S53A and vector control U2OS cells using biotinylated HA binding protein (HABP) with streptavidin-FITC and confocal microscopy. HA levels were substantially elevated in eIF4E overexpressing cells relative to vector controls or S53A eIF4E cells (Fig. 2a). Strikingly, HA was not extruded into the media, but rather coated the cell surface and formed short, filamentous protrusions radiating from the surface coat in the eIF4E overexpressing cells (Fig. 2a, b). Enzymatic depletion of HA with *Streptomyces* hyaluronidase (HAse) virtually eliminated the HA signal indicating that the staining was specific and suggesting that the structures were HA-dependent (Fig. 2a). Our findings are consistent with studies which used HAS3 overexpression to artificially induce HA production (1) where the protrusions were too narrow (120-130 nm) to be seen by light microscopy but were readily detectable using fluorescent HABP conjugates. We used fluorescence assisted carbohydrate electrophoresis (FACE) to independently validate elevated HA production (Fig. 2c and Supp. Fig. 1e). We observe a ~3-fold increase in HA levels in eIF4E-overexpressing cells relative to vector controls. HA levels in S53A-eIF4E cells were much lower than eIF4E overexpressing cells, and only modestly elevated relative to vector controls consistent with the mutant's modest effects on the HA biosynthetic enzymes. Further, removal of extracellular glucose led to

reduction of HA signalling consistent with the use of glucose as the major metabolic precursor in this pathway (Supp. Fig 1g-h). Thus, eIF4E overexpression induced HA production, and was found associated with cells, coating the surface and forming protrusions. eIF4E required its mRNA export activity for HA production and this was likely augmented by its translation activity.

We hypothesized that HA levels would be repressed by inhibition of eIF4E. eIF4E-overexpressing cells were treated with either RNAi to eIF4E or with a pharmacological inhibitor, ribavirin (Fig. 2c, d). Ribavirin directly binds eIF4E and inhibits its mRNA export and translation functions [23, 25-27]. We observed a reduction in HA to background levels via confocal microscopy using either ribavirin treatment or RNAi knockdown of eIF4E. Using FACE, we similarly observed a ~9-fold reduction in HA levels for both eIF4E knockdown relative to control RNAi and ~2.5-fold for ribavirin treated versus untreated cells (Fig. 2c and Supp. Fig. 1f). Thus, eIF4E is necessary for HA production in these cells.

We extended our studies to assess whether eIF4E drives HA production in cellular contexts characterized by naturally-occurring elevation of eIF4E e.g. acute myeloid leukemia (AML) and breast cancer [20, 23, 40, 41]. First, we examined the MM6 AML cell line which is characterized by elevated nuclear eIF4E levels, and thus with increased mRNA export activity for eIF4E targets (Figure 3a-e and Supp. Fig. 2a-c). Using nuclear RIPs and mRNA export assays, we found that all mRNAs for the HA biosynthesis machinery including HAS3 and CD44 are eIF4E export targets in this cell type (Figure 3a-c). These targets included transcripts encoding GPI, which was not an export target in U2Os cells. This suggests that the ability to promote HA production in these cells might be even more potent. We also note diversity in terms of the enzyme family members associated with eIF4E in MM6 cells versus eIF4E-overexpressing U2Os cells. For instance, transcripts encoding PGM5 which were eIF4E targets in U2Os cells, were not well expressed in MM6 cells. Instead, eIF4E bound to and exported PGM1 mRNAs. Importantly, these conservative substitutions in enzyme content still led to increased HA biosynthesis as observed by FACE and HABP staining (Fig. 3d). Similar to U2Os cells, the surface of MM6

cells was characterized by HA coats. We also found in MM6 cells that eIF4E targeting with ribavirin reduced the mRNA export of the corresponding HA enzymes and CD44 from 2-9 fold depending on the mRNA monitored (Fig 3b). Ribavirin did not alter total mRNA levels consistent with this being a post-transcriptional effect (Supp. Fig. 2b). Consistently, ribavirin treatment dramatically lowered protein levels for the representative members of the HA biosynthetic machinery examined: HAS3, HK, UGDH as well as CD44 (Fig. 3c). HA staining was reduced to background levels by ribavirin or HAse treatment as observed by HABP staining and confocal microscopy (Fig.3d). We paralleled these studies in primary high-eIF4E AML specimens and also in CD34+ bone marrow specimens isolated from healthy volunteers (Fig 3e-f). Consistent with the MM6 cells, 9/9 high-eIF4E AML specimens had HA coats and protrusions with HA staining 4-10 fold higher than the 5 normal human CD34+ specimens which all showed only background HA staining, similar to intensities observed in vector controls U2Os cells (Fig. 2a). These findings suggest that the HA coat is specific to the malignant state and not a general feature of blood cells (Fig 3e-f). These findings point to new functionalities for HA in leukemia cells, where it was previously thought HA only played a role in the bone marrow stroma and not on the leukemia cells themselves. Next we examined another high-eIF4E context, the breast cancer cell line 66cl4. These cells had highly elevated nuclear eIF4E, and also had readily visible HA-surface coats and protrusions as observed by confocal microscopy (Fig. 3g). Ribavirin treatment reduced HAS3 and CD44 levels relative to untreated controls as well as dramatically reduced HA levels (Fig. 3g). Furthermore, we observed by *in situ* translation studies using fluorescence non-canonical amino-acid tagging (FUNCAT), that there could be active translation down the length of the protrusions in eIF4E-overexpressing and 66cl4 cells (Supp. Fig. 3a-b). These translation foci are cyclohexamide dependent validating them as sites of ongoing translation (Supp. Fig 3a-b). We postulate that eIF4E could be involved in localized protein synthesis to spatially couple translation of relevant HA enzymes with HA biosynthesis. In all, our studies demonstrate that eIF4E controls HA biosynthesis at both the mRNA export and translation level thereby coordinately driving HA production.

eIF4E plays well-established roles in invasion, migration and metastasis. We hypothesized that eIF4E co-opted HA synthesis to execute these activities. Starting with invasion, we observed

that eIF4E-overexpressing cells invaded matrigel 4-fold better than vector controls (Fig. 4a, b and Supp. Fig. 4a-b and e-f). By contrast, the S53A eIF4E mutant increased invasion by only 50% relative to vector controls consistent with its more modest effects on HA production by FACE (Supp. Fig. 4e-f and Supp. Fig 1e). In both eIF4E overexpressing and vector control cells, RNAi to eIF4E or ribavirin treatment reduced invasion by ~2.5-fold consistent with the significant reduction in HA levels (Fig. 2c and Supp. Fig. 4e-f). To determine the relevance of HA production specifically to eIF4E mediated invasion, we used RNAi to knockdown HAS3 in eIF4E overexpressing and vector cells (Fig. 4a and Supp. Fig. 4a-b). We focused on HAS3 since this is the last step in the biosynthetic pathway of HA and its inhibition specifically impairs HA synthesis whereas other enzymes in this pathway also participate in unrelated processes. We observed that RNAi to HAS3 reduced the invasion activity of eIF4E by ~5-fold in eIF4E overexpressing cells (to levels of RNAi controls) and 2.5-fold in vector controls where the effects of endogenous eIF4E are likely being targeted. HAS3 knockdown did not affect eIF4E levels as observed by Western blot (Fig. 4d). Furthermore, confocal microscopy experiments revealed that RNAi to HAS3 decreased HA levels to background consistent with its baseline invasion activity (Fig. 4c). FACE studies also revealed that HAS3 knockdown lowered HA levels by ~9-fold relative to RNAi controls (Fig. 2c and Supp. Fig. 1f). Strikingly, eIF4E knockdown and HAS3 knockdown similarly reduced HA to background levels.

We explored the efficacy of HAse treatment for the invasion activity of eIF4E (Fig. 4 e & f). Given the length of time between HAse treatment and re-emergence of HA in eIF4E-overexpressing cells was 12 hours (Supp. Fig. 4h), we treated cells with HAse every 8 hours to ensure HA was depleted during the course of the experiments. We observed that HAse treatment reduced invasion by 40% relative to untreated controls. For comparison, ribavirin decreased invasion by 60% consistent with its reduction of HA to background levels. Strikingly, the combination of ribavirin and HAse reduced invasion by 80% (Fig. 4e-f and Supp. Fig. 4c-d). Importantly, ribavirin affects multiple eIF4E target pathways, not only HA biosynthesis, and thus its effects are expected to be greater than HAse alone. We extended these studies to monitor the role HA production played in the migration activity of eIF4E in wound healing assays. As expected, we observed increased migration in eIF4E-overoxpressing cells relative to vector

control (Fig. 4g, h). Knockdown of HAS3 reduced eIF4E-dependent migration by ~ 4-fold while treatment with HAse reduced it by almost 2-fold indicating this was also an HA dependent phenomenon.

We extended the above studies to examine the role of HA in eIF4E-mediated metastasis *in vivo*. Previously, we demonstrated that ribavirin treatment reduced metastasis by 3-fold in an eIF4E-dependent pulmonary metastatic mouse model using 66cl4 cells [(23)]. Above, we demonstrated that eIF4E drives HA production in these cells and that ribavirin repressed HAS3 and HA production (Fig. 3). Here, we investigated whether inhibition of eIF4E activity correlated not only with reduced lung metastases but also with lower HA levels (Fig. 5). Serial formalin-fixed sections of tumor bearing lungs, from control and ribavirin treated animals, were stained for HA, and hematoxylin (Fig. 5a). Staining intensity and area were quantified using Visiomorph. Tumours from 10 animals for treated and 9 in the untreated groups were analyzed. Strikingly, we observed a 50% decrease in HA levels in the lungs of ribavirin-treated mice relative to controls (Fig. 5a-b). HA surrounded tumour cells indicating that HA was adjacent to and/or on the surface of these cells. As expected, HA was also found in normal tissues, consistent with its major structural role in the microenvironment. HAse treatment of serial sections indicated that the HA staining observed is specific (Fig. 5a). Thus, we demonstrate that eIF4E targeting leads to reduced HA levels and decreased metastasis *in vivo*.

Next, we examined whether CD44, as a representative downstream effector of the HA-network, was also required for eIF4E-mediated invasion (Fig. 1 b-d). eIF4E overexpression led to highly elevated CD44 protein levels (Fig. 1d) and CD44 coated the surface (Supp. Fig. 5a). Indeed, CD44 and HA co-localized on the cell surface (Supp. Fig. 5). These studies are similar to those showing that CD44 bound HA on the surface of HAS3 overexpressing cells [(1)]. Inhibition of CD44 with RNAi or independently with CD44 blocking antibodies (mAb A3D8) reduced eIF4E-mediated invasion by ~4-fold for RNAi and ~3-fold for mAb A3D8 treatment (Supp. Fig. 5 b-c & f-g). The similarity for the reduction induced by CD44 inhibition, knockdown of HAS3 or ribavirin treatment suggests that CD44 plays an important role in this process.

Significantly, modulation of CD44 did not alter HA status, as seen by HABP-staining confocal microscopy (Supp. Fig. 5e). Thus, although HA is essential for eIF4E-mediated invasion, its co-factors CD44 and perhaps others, are likely also required for this activity. This suggests that the HA coat and/or protrusions need to be armed with CD44 to support the invasion potential of eIF4E overexpressing cells. Further in high-eIF4E cells, HA is likely directly binding CD44 to activate this signalling pathways in neighbouring cells and/or in its own cells leading to autocrine stimulation. In either case, these would stimulate cellular signalling cascades that drive the oncogenic phenotype.

Conclusions

Our studies demonstrate that the entire HA-network is subjected to coordinated post-transcriptional control by eIF4E. These findings have several mechanistic and clinical implications. For instance, factors that modulate the levels, localization, or phosphorylation of eIF4E are positioned to profoundly affect HA production and the global activity of the HA network. Indeed, targeting eIF4E with RNAi knockdown or ribavirin treatment reduced HA levels as effectively as direct targeting with HAse. We note that eIF4E drove the production of cell-associated HA which in turn, fundamentally modified the cell-surface architecture facilitating invasion and metastases. Thus eIF4E may specifically drive an oncogenic HA-programme, in contrast to typical situations where this large glycosaminoglycan is extruded into the matrix. It is not yet known if the ability to modulate HA is a property unique to eIF4E, or if other oncoproteins initiate a similar programme.

Materials and Methods

Reagents and Constructs: pcDNA-2Flag-eIF4E wild-type and S53A mutant constructs were previously described [13-14]. Ribavirin was purchased from Kemprotec (CAS 36791-04-5). AMAC (2-aminoacridone) from Molecular probes (A-6289). Sodium Cyanoborohydride from Sigma Aldrich (15,615-9). Chondroitinase ABC from Proteus Vulgaris from Sigma Aldrich (CAT# C3667-10UN). 40% Acrylamide/Bis Solution, 37.5:1 from BioRad technologies (Cat# 1610148).

Antibodies for immunoblotting: Mouse monoclonal anti-eIF4E (BD PharMingen, 610270) or Rabbit monoclonal anti-eIF4E (Millipore, 04-347) for Western Blot analysis. Rabbit anti-eIF4E for RNA immunoprecipitation (MBL international, RN001P). Mouse monoclonal anti-CD44 blocking antibody A3D8 (Novus Biologicals, NB600-1457). Mouse monoclonal anti-CD44 antibody (156-3C11) for Western Blot and Confocal Analysis (Cell Signalling, 3570). Rabbit polyclonal anti-HAS3 antibody (Abcam, ab154104). Rabbit polyclonal anti-phosphoglucomutase 5 (Abgent, AI14638). Rabbit polyclonal anti-Glucose 6 phosphate isomerase antibody [EPR11663(B)] (Abgent, AW5240-U400). Rabbit polyclonal anti-UDP glucose dehydrogenase antibody (Abgent, AP12613b). Mouse monoclonal anti-GFPT1 antibody [EPR4854] (Abgent, AO2212a). Rabbit polyclonal anti-GNPNAT1 antibody (GeneTex, GTX122246). Rabbit monoclonal anti-UAP1 antibody [EPR10259] (Abcam, ab155287). Mouse monoclonal anti-β-actin (Sigma Aldrich, A5441). Mouse monoclonal anti-α-tubulin (Sigma Aldrich, T5168). Rabbit polyclonal anti-Mcl-I (S-19) (Santa Cruz, sc-819). Mouse monoclonal anti-c-Myc (9E10) (Santa Cruz, sc-40). Mouse monoclonal anti-HSP90α/β (F-8) (Santa Cruz, sc-13119). Rabbit polyclonal anti-Lamin A (C-terminal) (Sigma Aldrich, L1293). Rabbit polyclonal anti-Pol II N-20 (Santa Cruz, sc-889). Rabbit polyclonal anti-GAPDH (FL-335) (Santa Cruz, sc-25778).

Cell Culture and Transfection: U2Os cells (ATCC) were maintained in 5% CO2 at 37°C in Dulbecco's modified Eagle's medium (DMEM) (Gibco BRL) supplemented with 10% fetal bovine serum (FBS) and 1% penicillin-streptomycin (Invitrogen). MM6 cells (ATCC TIB202) and 66cl4 (obtained from Dr. Wilson H. Miller, Lady Davis Institute, Montreal, QC, Canada) were maintained in RPMI 1640 (Invitrogen) supplemented with 10% heat-inactivated FBS and 1% penicillin-streptomycin. All cell lines (resistant and parental) were routinely checked to ensure there was no mycoplasma contamination using MycoAlert Mycoplasma Detection kit (Lonza, LT07-418). Transfections for stable cell lines were performed using Trans IT-LT1 Transfection Reagent (Mirus) as specified by the manufacturer, and selected in G418-containing medium (1 mg/mL) for eIF4E stable overexpressing cell lines. For eIF4E, HAS3 or CD44 knockdowns, U2Os cells were transfected with Lipofectamine 2000 and 20-40 nM siRNA duplex according to the manufacturer's instructions. For siHAS3 two sequences were used such

that the total amount of the siRNA mix is equal to 40 nM. Cells were analyzed 96 h after transfection. List of siRNA purchased:

siRNA	Catalog #
siRNA duplex_eIF4E (Mouse)	IDT Technologies
	MMU.RNAI.N0007917.1.1
	MMU.RNAI.N007917.1.2
siRNA duplex _eIF4E (Human)	IDT Technologies
	sense (CUGCGUCAAGCAAUCGAGAUUUGGG)
	antisense (CCCAAAUCUCGAUUGCUUGACGCAGUC)
siRNA duplex _HAS3	IDT Technologies
	HSC.RNAI.N138612.12.5
	HSC.RNAI.N005329.12.3
siRNA duplex _CD44	Qiagen
	FlexiTube siRNA Hs CD44 Cat# S100299705
siRNA duplex _Luciferase	IDT Technologies
	sense (CACGUACGCGGAAUACUUCGAAATG)
	antisense (CAUUUCGAAGUAUUCCGCGUACGUGUU)

Cellular Fractionation and Export Assay: Fractionation protocol was followed as previously described. About 3 x 107 cells were collected and washed twice in ice cold PBS (1,200 rpm/3-5 min) and then re-suspended with slow pipetting in 1 ml of lysis buffer B (10 mM Tris pH 8.4, 140 mM NaCl, 1.5 mM $MgCl_2$, 0.5% (v/v) NP-40, 1 mM DTT and 100 U/ml RNase Inhibitors). The lysate was centrifuged at 1000 g for 3 min at 4°C and supernatant (cytoplasmic fraction) was transferred into a fresh microtube. The pellet (nuclear fraction) was resuspended in 1 ml of lysis buffer B, transferred to round bottom, polypropylene tube and 1/10 volume (100 µL) of detergent stock (3.3% (w/v) Sodium Deoxycholate, 6.6% (v/v) Tween 40 in DEPC H20) was added with slow vortexing (to prevent the nuclei from clumping) and incubated on ice for 5 min. The suspension was transferred to a microtube and centrifuged at 1,000 g for 3 min at 4°C. Supernatant (post-nuclear fraction) was transferred to a fresh tube and the pellet-nuclear fraction

was rinsed in 1 ml of lysis buffer B and centrifuged at 1,000 g for 3 min at 4°C. The nuclei, present in the pellet, were re-suspended in 100 μL of lysis buffer B and sonicated. The postnuclear and cytoplasmic fractions were combined. The RNA was extracted from the different fractions by adding TRIzol reagent (Invitrogen) and processed according to the manufacturer's instructions.

RNA Immunoprecipitation (RIP): RIP from nuclear fractions of cells was performed as previously described [14]. Briefly, 1 mg of nuclear lysate was used for RIP with 7 μg anti-eIF4E antibody (MBL RN001P) or control immunoglobulin G (rabbit, Millipore). After incubation, complexes were eluted by boiling in tris(hydroxymethyl)aminomethane (Tris) EDTA containing 1% (w/v) sodium dodecyl sulfate and 12% (v/v) β-mercaptoethanol. RNA were isolated using TRIzol reagent and isolated using Direct-zol RNA Miniprep Kit (Zymo Research). RNA samples (TurboDNase, Ambion) were reversed transcribed using SuperScript VILO cDNA synthesis kit (for RIP experiments) or M-MLV reverse transcription (Invitrogen).

Reverse transcription and Quantitative PCR: DNAse treated RNA samples (TurboDNase, Ambion) were reverse transcribed using M-MLV reverse transcriptase (Invitrogen). QPCR analyses were performed using SensiFast Sybr Lo-Rox Mix (Bioline) in AB Viia7 thermal cycler using the relative standard curve method (Applied Biosystems User Bulletin #2). All conditions were described previously. Primers list includes:

Name	Sequence
CD44	Sense CGGCTCCTGTTAAATGGTATCT
	Antisense TCTGCTTTGTGGTCTGAGAAG
HAS3	Sense CAGGAGGACCCTGACTACTT
	Antisense GTGGAAGATGTCCAGCATGTA
Hexokinase 1	Sense GAAGATGGTCAGTGGCATGTA
	Antisense GGTGATCCGCCCTTCAAATA
GPI	Sense TCTATGCTCCCTCTGTGTTAGA

	Antisense	CTCCTCCGTGGCATCTTTATT
UGDH	Sense	GTGCCCATGCTGTTGTTATTT
	Antisense	CGCCGTCCATCGAAGATAAA
UAP1	Sense	GCAGTGCTACAAGGGATCAA
	Antisense	CCACCAGCTAGAAGAAGAACTG
PGM5	Sense	TGATCTCCGAATCGACCTATCT
	Antisense	ATATCCACTGGGTCCACTATCT
GNPNAT1	Sense	CCCAACACATCCTGGAGAAG
	Antisense	CTCTGTTAGCTGACCCAATACC
GNPT1/GFAT	Sense	ACTTTGATGGGTCTTCGTTACT
	Antisense	ACAATCTGTCTCCCGTGATATG
Actin B	Sense	GCATGGAGTCCTGTGGCATCCACG
	Antisense	GGTGTAACGCAACTAAGTCATAG
GAPDH	Sense	GAAGGTGAAGGTCGGAGTC
	Antisense	GAAGATGGTGATGGGATTTC
MCL1	Sense	TTTCAGCGACGGCGTAACAAACTG
	Antisense	TGGTTCGATGCAGCTTTCTTGGT
U6	Sense	CGCTTCGGCAGCACATATAC
	Antisense	AAAATATGGAACGCTTCACGA
tRNALys	Sense	GCCCGGATAGCTCAGT
	Antisense	CGCCCAACGTGGGGC T

Western Blot Analysis: Western analysis was performed as described previously [18] with a modified lysis buffer (40 mM Hepes, pH 7.5, 120 mM NaCl, 1 mM EDTA, 10 mM β-glycerophosphate, 50 mM NaF, 0.5 μM NaVO3, and 1% (v/v) Triton X-100 supplemented with complete protease inhibitors [all were purchased from Sigma-Aldrich]). In addition, blots were blocked in 5% (w/v) milk in TBS–Tween 20. Primary antibodies were diluted in 5% milk.

Glucose levels: U2Os cells overexpressing 2Flag-eIF4E or 2Flag-vector control were plated at 1 million cells per well of a 6-well plate. On the next day, cells were starved in DMEM + 0.5% (v/v) FBS + 1% (v/v) Pen/Strep for 16 hours at 37 ºC, 5% CO2. Following starvation, media was replaced with low glucose DMEM (Life technologies, Cat# 11885-084) + 1 g/L D-(+)-Glucose (Sigma Aldrich, Cat# G8644) + 10% (v/v) FBS +1% (v/v) Pen/Strep. Glucose levels were measured at indicated time points using Clarity Plus Blood Glucose Monitoring Kit (Cat# DTG-GL-15PROMO).

HA synthesis growing conditions per cell line: (A) For U2Os or 66cl4 cell lines: Cells were seeded at a density of 80,000 cell per well of 4-well glass Millicell EZ-Slide (Millipore, PEZGS0416) overnight in complete growth media, DMEM or RPMI 1640 respectively. 24 hrs post-seeding, cells were starved in media containing 0.5% (v/v) FBS + 1% (v/v) Pen/Strep. 16 hrs later, media was replaced with either DMEM/RPMI 1640 containing a total of 2 g/L glucose as follows: for U2Os cells low glucose DMEM + 1 g/L D-(+)-Glucose + 10% (v/v) FBS + 1% (v/v) Pen/Strep was used; and for 66cl4 RPMI 1640 + 1 g/L D-(+)-Glucose + 10% (v/v) FBS + (v/v) 1% Pen/Strep. Cells were incubated for 12 hrs at 37 ºC 5% CO2 and then prepared for immunofluorescence staining. (B) For MM6, cells were grown overnight at 1 million cells/ml in RPMI 1640 containing 10% (v/v) FBS and 1% (v/v) Pen/Strep. On the next day, cells were washed two times with 1x PBS (Wisent Biologicals, Cat# 311-010-CL) and resuspended in RPMI 1640 containing a total of 2 g/L glucose + 10% FBS +1% Pen/Strep and incubated at 37ºC 5% CO2 for 4 hours after which prepared for fluorescence staining. CD34+ cells were purchased from ATCC and primary high-eIF4E AML samples were obtained from our phase I clinical trial of ribavirin and low-dose cytarabine [16].

Hyaluronidase treatment: One hour prior to the end of the 12 or 4 hrs incubation of U20s, 66cl4 or MM6 cells, respectively, in media containing 2 g/L glucose, cells where treated with

Hyaluronidase from Streptomyces Hyalurolyticus (Sigma Aldrich, Cat# H1136) at 12 units/ml/1 million cell and incubated at 37ºC 5% CO2 for 1 hour. Hyaluronidase preparation: 1 Ampule (equivalent to 300 units) was resuspended at 1 unit/µl in the following buffer (20 mM sodium phosphate buffer, pH 7.0, with 77 mM sodium chloride and 0.1 mg/ml BSA at 1 mg/ml), incubated at room temperature for 10 minutes and then aliquoted and stored at -80 ºC. After

Immunofluorescence, fluorescence and laser-scanning confocal microscopy: For HA staining biotinylated Hyaluronic acid binding protein (from Bovine Nasal Cartilage, Millipore, Cat# 385911) resuspended in 100 µl water: glycerol (50:50) (v/v) was used. Fluorescence staining was carried out as described (PEG Protocol Cleveland Clinic). Briefly, following incubation with media containing 2 g/L glucose and treatment with Hyaluronidase, cells were washed 3 times with complete growth media followed by 3 washes with 1 x PBS. Slides were then air-dried for 15 minutes and fixed with 4% Paraformaldehyde (32% solution from Electron Microscopy Sciences, Cat# 15714) prepared in 1x PBS for 10 minutes at room temperature. After fixation, slides were air-dried and stained right away. Note that slides can be stored at 4ºC for few days, however longer term storing at 4ºC or -20ºC is not recommended as HA staining is lost due oxidative or mechanical breakdown of HA chains. For staining, slides were blocked for 1 hour at room temperature in blocking solution (10% (v/v) FBS + 0.2% (v/v) Triton-X-100 in 1x PBS) and incubated with HABP (1:100 dilution in blocking solution) overnight at 4ºC; followed by 3 washes in blocking solution (5 minutes each). Slides were then incubated with FITC or Texas Red conjugated Streptavidin (Vector Laboratories, Cat# SA-1200) (1:500 dilution in blocking solution) for 1 hour at room temperature; washed 4 times with 1x PBS (pH 7.4) and mounted in Vectashield with DAPI (Vector laboratories, Cat# H-1200). For CD44 staining: mouse anti-CD44 (A3D8 or 156-3C11) was used at 1:500 dilution in blocking buffer, respectively. Secondary anti-mouse FITC antibody (Jackson Laboratories) was used at 1:500 dilution. Incubations with primary antibodies were carried out overnight at 4ºC and incubations with secondary antibodies were done for 1 hour at room temperature.

Analysis was carried out using a laser-scanning confocal microscope (LSM700 META; Carl Zeiss, Inc.), exciting 405 and 543nm or 488nm with a 63x objective, 2x digital zoom (where indicated), and numerical aperture of 1.4. Channels were detected separately, with no cross talk observed. Confocal micrographs represent single sections through the plane of the cell. Images

were obtained from ZEN software (Carl Zeiss, Inc) and displayed using Adobe Photoshop CS6 (Adobe).

Ribavirin treatment: Treatment of U2Os, MM6 and 66cl4 cells with ribavirin was carried out as follows. For U2Os and 66cl4 cell lines: cells were seeded at 0.7 million (Untreated) or 1.4 million cells (Ribavirin treated) per 10 cm plate. 20 μM ribavirin was used to treat cells for 48 or 96 hrs (for 96 hrs treatments, ribavirin is replenished every 24 or 48 hrs). For MM6 cells were treated with 5μM ribavirin at 0.5 million/ml (Untreated) or 1 million/ml (Ribavirin treated) cell density, and ribavirin was replenished every 24 hrs for 48 or 96 hrs.

In vitro fluoroblok Matrigel invasion assay: Fluoroblok Invasion assays were performed according to manufacturer instructions (Ref1: Automated, Kinetic Imaging of Cell Migration and Invasion Assays using Corning FluoroBlok™ Permeable Supports. Brad Larson et al. BioTek 2014. Ref2: An in vitro FluoroBlok Tumour Invasion Assay. Jeff Partridge et al. BD Biosciences. JOVE 2009 DOI: doi:10.3791/1475). Briefly, fluoroblok 24-well inserts with 8-micron pore size PET membrane (Corning Ct # 351152) were precoated with 1 μg/μl Matrigel matrix basement membrane (BD Biosciences Cat # 356237) diluted in serum free DMEM media for 24 hr at 37 °C. Cells were harvested, centrifuged, rinsed three times with serum free media and suspended at a density of 1 x 10^5 cells/ 300 μl in culture media containing 0.5% (v/v) FBS. Cells were then plated on Matrigel coated and uncoated inserts and 750 μl of culture media containing 10% (v/v) FBS was added to the lower compartment of the chamber. Chambers were incubated at 37°C for 48 hrs. After invasion period, cells were labeled with $DilC_{12}(3)$ perchlorate, ultra-pure (Enzo Life Sciences, Cat # ENZ-52206) diluted at 1:2000 in culture media for 10 minutes at 37°C followed by 15-minute incubation at 4°C. After washing, fluorescence of invaded and migrated cells was measured at wavelengths of 549/565 nm (Ex/Em) on a bottom-reading fluorescent plate reader and images were taken using an inverted fluoresce microscope to verify results. Data is expressed according to the following equation:

$$\% \text{ invasion} = \frac{\text{Mean RFU of cells invaded through matrigel coated inserts towards chemoattractant}}{\text{Mean RFU of cells migrated though uncoated inserts towards chemoattractant}}$$

***In vitro* Scratch Assay:** U2Os cells overexpressing 2Flag-eIF4E or vector control subjected to HAS3 knockdown for 72 hrs were seeded in Millicell EZ slide (4-well glass) at 80,000 cell per well diluted in DMEM containing 10 % (v/v) FBS+1% (v/v) Pen/Step. On the next day, cells were starved in DMEM containing 0.5% (v/v) FBS +1% (v/v) Pen/Strep for 16 hrs. Following incubation, a scratch was made in the cell layer using a 1 ml tip. Cells were then washed with PBS to remove floating cells and fresh DMEM-low glucose media containing 10% (v/v) FBS + 1% (v/v) Pen/Strep + 1 g/l glucose was added (total glucose concentration is 2 g/l). For the HAse treatment conditions, 12 units/ml of *Streptomyces* Hyaluronidase was added per well following media change. Pictures of the scratches were taken at the time of the scratching and after 16 hrs. The area not filled with cells was quantified using TScratch software (available from Computational Science and Engineering lab at ETH University, Zurich, Switzerland).

Fluorophore-Assisted Carbohydrate Electrophoresis (FACE): U2Os cells were seeded at 1 million cells/well of a 6-well plate and incubated at 37ºC 5% CO2 overnight. 24 hrs after, cells were starved in DMEM containing 0.5% (v/v) FBS + 1% (v/v) Pen/Strep for 16 hrs. Media was then replaced with low glucose DMEM + 1 g/L glucose + 10% (v/v) FBS + 1% (v/v) Pen/Strep and incubated for 12 hrs at 37ºC, 5% CO2. Following incubation, samples were prepared for FACE analysis as previously described (PEG protocol Cleveland Clinic). Briefly, media was collected and cells were washed 3 times with 1x PBS. Media and cells were treated with 1x Proteinase K (from Tritirachium album, Sigma Aldrich, Cat# P2308) for 2 hours at 60ºC followed by precipitation and treatment with Hylauronidase and Chondroitinase ABC. Samples were finally lyophilized, resuspended in AMAC solution and separated on acrylamide gels as described. Fluorescence detection of AMAC derivatives was achieved with GelDoc system. DNA was quantified using Quant-iT PicoGreen dsDNA assay kit (ThermoFisher, P11496).

Histochemistry staining: Tumour blocks of mouse mammary tumours and lung metastases of published data [(6)] were analyzed for HA staining as a function of ribavirin treatment from 10 ribavirin and 10 control animals. A total of 3 × 4 μm serial step sections were prepared and stained for each mouse for HABP and H&E. Batch analysis of 10 selected areas of 5.8×10^{-2} mm2 (2.4 × 105 pixels) were run. Percent positive nuclei per section were determined by addition of areas until the average percent positive nuclei for one section did not change. One

tumour section per animal was analyzed, and at least three areas of healthy tissue were taken into consideration for the percent positive nuclei result.

***In situ* Protein Synthesis Assay**: We used Click-iT HPG Alexa Four 488 (Thermo Fisher Scientific, Catalog number C10428) according to the manufacturer's instructions. Briefly, cells pretreated with 20 μM Ribavirin for 48 hours were seeded in Millicell EZ slide (4-well glass) at 80,000 cell per well diluted in DMEM containing 10 % (v/v) FBS+1% (v/v) Pen/Step. On the next day, cells were starved in DMEM containing 0.5% (v/v) FBS +1% (v/v) Pen/Strep for 16 hrs. Following starvation, media was replaced with fresh DMEM-low glucose containing 10% (v/v) FBS + 1% (v/v) Pen/Strep + 1 g/l glucose was added (total glucose concentration is 2 g/l) and cells were incubated for 12 hours to allow synthesis of HA. After incubation, cells were incubated with HPG for 1 hour in methionine free RPMI 1640 + 10% (v/v) FBS +1% (v/v) P/S +1 g/l glucose. Cells were then washed with PBS and fixed with 3.7% formaldehyde for 15 min at room temperature and permeabilized with 0.5% (v/v) Triton X-100. Incorporation of HPG was detected using Click-iT Cell Reaction Buffer Kit according to the manufacturer's instructions. Confocal analysis was used to assess *in situ* protein synthesis.

Acknowledgments

This project was supported by grants to K.L.B.B. from the NIH (80728 & 98571) and the Leukemia and Lymphoma Translational Research Program. K.L.B.B. holds a Canada Research Chair in Molecular Biology of the Nucleus. Special thanks to the PEG funding (the project described was supported by Award Number P01HL107147 from the National Heart, Lung and Blood Institute. The content is solely the responsibility of the authors and does not necessarily represent the official views of the National Heart, Lung and Blood Institute or the National Institutes of Health) as well as the CIHR operating grant MOP-115002.

Contributions: H.A.Z. and B-CK designed and performed experiments, analysed data and wrote the manuscript; A.E., F.P., S.D.R., V.C. and M.L. performed experiments; R.M., W.H.M. and V.H. designed experiments, analysed data and edited the manuscript; K.L.B.B. designed experiments, analysed data and wrote the manuscript.

Conflict of Interest: Authors have no competing financial interests.

References:

1. Kultti A, Rilla K, Tiihonen R, Spicer AP, Tammi RH, Tammi MI. Hyaluronan synthesis induces microvillus-like cell surface protrusions. The Journal of biological chemistry. 2006;281(23):15821-8.
2. Lenart M, Rutkowska-Zapala M, Baj-Krzyworzeka M, Szatanek R, Weglarczyk K, Smallie T, et al. Hyaluronan carried by tumor-derived microvesicles induces IL-10 production in classical (CD14++CD16-) monocytes via PI3K/Akt/mTOR-dependent signalling pathway. Immunobiology. 2017;222(1):1-10.
3. Goncharova V, Serobyan N, Iizuka S, Schraufstatter I, de Ridder A, Povaliy T, et al. Hyaluronan expressed by the hematopoietic microenvironment is required for bone marrow hematopoiesis. The Journal of biological chemistry. 2012;287(30):25419-33.
4. Toole BP. Hyaluronan: from extracellular glue to pericellular cue. Nature reviews Cancer. 2004;4(7):528-39.
5. Itano N, Sawai T, Yoshida M, Lenas P, Yamada Y, Imagawa M, et al. Three isoforms of mammalian hyaluronan synthases have distinct enzymatic properties. The Journal of biological chemistry. 1999;274(35):25085-92.
6. Spicer AP, McDonald JA. Characterization and molecular evolution of a vertebrate hyaluronan synthase gene family. The Journal of biological chemistry. 1998;273(4):1923-32.
7. Slevin M, Krupinski J, Gaffney J, Matou S, West D, Delisser H, et al. Hyaluronan-mediated angiogenesis in vascular disease: uncovering RHAMM and CD44 receptor signaling pathways. Matrix Biol. 2007;26(1):58-68.
8. Slevin M, Kumar S, Gaffney J. Angiogenic oligosaccharides of hyaluronan induce multiple signaling pathways affecting vascular endothelial cell mitogenic and wound healing responses. The Journal of biological chemistry. 2002;277(43):41046-59.
9. West DC, Hampson IN, Arnold F, Kumar S. Angiogenesis induced by degradation products of hyaluronic acid. Science. 1985;228(4705):1324-6.
10. Koistinen V, Karna R, Koistinen A, Arjonen A, Tammi M, Rilla K. Cell protrusions induced by hyaluronan synthase 3 (HAS3) resemble mesothelial microvilli and share cytoskeletal features of filopodia. Experimental cell research. 2015;337(2):179-91.

11. Bertrand P, Courel MN, Maingonnat C, Jardin F, Tilly H, Bastard C. Expression of HYAL2 mRNA, hyaluronan and hyaluronidase in B-cell non-Hodgkin lymphoma: relationship with tumor aggressiveness. International journal of cancer. 2005;113(2):207-12.

12. Junker N, Latini S, Petersen LN, Kristjansen PE. Expression and regulation patterns of hyaluronidases in small cell lung cancer and glioma lines. Oncology reports. 2003;10(3):609-16.

13. Sa VK, Rocha TP, Moreira A, Soares FA, Takagaki T, Carvalho L, et al. Hyaluronidases and hyaluronan synthases expression is inversely correlated with malignancy in lung/bronchial pre-neoplastic and neoplastic lesions, affecting prognosis. Brazilian journal of medical and biological research = Revista brasileira de pesquisas medicas e biologicas. 2015;48(11):1039-47.

14. Anttila MA, Tammi RH, Tammi MI, Syrjanen KJ, Saarikoski SV, Kosma VM. High levels of stromal hyaluronan predict poor disease outcome in epithelial ovarian cancer. Cancer research. 2000;60(1):150-5.

15. Auvinen P, Tammi R, Parkkinen J, Tammi M, Agren U, Johansson R, et al. Hyaluronan in peritumoral stroma and malignant cells associates with breast cancer spreading and predicts survival. Am J Pathol. 2000;156(2):529-36.

16. Ropponen K, Tammi M, Parkkinen J, Eskelinen M, Tammi R, Lipponen P, et al. Tumor cell-associated hyaluronan as an unfavorable prognostic factor in colorectal cancer. Cancer research. 1998;58(2):342-7.

17. Setala LP, Tammi MI, Tammi RH, Eskelinen MJ, Lipponen PK, Agren UM, et al. Hyaluronan expression in gastric cancer cells is associated with local and nodal spread and reduced survival rate. British journal of cancer. 1999;79(7-8):1133-8.

18. Nykopp TK, Rilla K, Tammi MI, Tammi RH, Sironen R, Hamalainen K, et al. Hyaluronan synthases (HAS1-3) and hyaluronidases (HYAL1-2) in the accumulation of hyaluronan in endometrioid endometrial carcinoma. BMC cancer. 2010;10:512.

19. Nykopp TK, Rilla K, Sironen R, Tammi MI, Tammi RH, Hamalainen K, et al. Expression of hyaluronan synthases (HAS1-3) and hyaluronidases (HYAL1-2) in serous ovarian carcinomas: inverse correlation between HYAL1 and hyaluronan content. BMC cancer. 2009;9:143.

20. Assouline S, Culjkovic-Kraljacic B, Bergeron J, Caplan S, Cocolakis E, Lambert C, et al. A phase I trial of ribavirin and low-dose cytarabine for the treatment of relapsed and refractory acute myeloid leukemia with elevated eIF4E. Haematologica. 2015;100(1):e7-9.
21. Culjkovic-Kraljacic B, Borden KL. Aiding and abetting cancer: mRNA export and the nuclear pore. Trends in cell biology. 2013;23(7):328-35.
22. Gao M, Zhang X, Li D, He P, Tian W, Zeng B. Expression analysis and clinical significance of eIF4E, VEGF-C, E-cadherin and MMP-2 in colorectal adenocarcinoma. Oncotarget. 2016;7(51):85502-14.
23. Pettersson F, Del Rincon SV, Emond A, Huor B, Ngan E, Ng J, et al. Genetic and pharmacologic inhibition of eIF4E reduces breast cancer cell migration, invasion, and metastasis. Cancer research. 2015;75(6):1102-12.
24. Xu T, Zong Y, Peng L, Kong S, Zhou M, Zou J, et al. Overexpression of eIF4E in colorectal cancer patients is associated with liver metastasis. Onco Targets Ther. 2016;9:815-22.
25. Culjkovic B, Tan K, Orolicki S, Amri A, Meloche S, Borden KL. The eIF4E RNA regulon promotes the Akt signaling pathway. The Journal of cell biology. 2008;181(1):51-63.
26. Culjkovic B, Topisirovic I, Skrabanek L, Ruiz-Gutierrez M, Borden KL. eIF4E promotes nuclear export of cyclin D1 mRNAs via an element in the 3'UTR. The Journal of cell biology. 2005;169(2):245-56.
27. Culjkovic B, Topisirovic I, Skrabanek L, Ruiz-Gutierrez M, Borden KL. eIF4E is a central node of an RNA regulon that governs cellular proliferation. The Journal of cell biology. 2006;175(3):415-26.
28. Rousseau D, Kaspar R, Rosenwald I, Gehrke L, Sonenberg N. Translation initiation of ornithine decarboxylase and nucleocytoplasmic transport of cyclin D1 mRNA are increased in cells overexpressing eukaryotic initiation factor 4E. Proceedings of the National Academy of Sciences of the United States of America. 1996;93(3):1065-70.
29. Topisirovic I, Guzman ML, McConnell MJ, Licht JD, Culjkovic B, Neering SJ, et al. Aberrant eukaryotic translation initiation factor 4E-dependent mRNA transport impedes hematopoietic differentiation and contributes to leukemogenesis. Molecular and cellular biology. 2003;23(24):8992-9002.

30. Kentsis A, Topisirovic I, Culjkovic B, Shao L, Borden KL. Ribavirin suppresses eIF4E-mediated oncogenic transformation by physical mimicry of the 7-methyl guanosine mRNA cap. Proceedings of the National Academy of Sciences of the United States of America. 2004;101(52):18105-10.

31. Lazaris-Karatzas A, Montine KS, Sonenberg N. Malignant transformation by a eukaryotic initiation factor subunit that binds to mRNA 5' cap. Nature. 1990;345(6275):544-7.

32. Lazaris-Karatzas A, Sonenberg N. The mRNA 5' cap-binding protein, eIF-4E, cooperates with v-myc or E1A in the transformation of primary rodent fibroblasts. Molecular and cellular biology. 1992;12(3):1234-8.

33. Carroll M, Borden KL. The oncogene eIF4E: using biochemical insights to target cancer. Journal of interferon & cytokine research : the official journal of the International Society for Interferon and Cytokine Research. 2013;33(5):227-38.

34. Osborne MJ, Borden KL. The eukaryotic translation initiation factor eIF4E in the nucleus: taking the road less traveled. Immunological reviews. 2015;263(1):210-23.

35. Graff JR, Zimmer SG. Translational control and metastatic progression: enhanced activity of the mRNA cap-binding protein eIF-4E selectively enhances translation of metastasis-related mRNAs. Clin Exp Metastasis. 2003;20(3):265-73.

36. Volpon L, Culjkovic-Kraljacic B, Sohn HS, Blanchet-Cohen A, Osborne MJ, Borden KLB. A biochemical framework for eIF4E-dependent mRNA export and nuclear recycling of the export machinery. RNA. 2017;23(6):927-37.

37. Montgomery N, Hill A, McFarlane S, Neisen J, O'Grady A, Conlon S, et al. CD44 enhances invasion of basal-like breast cancer cells by upregulating serine protease and collagen-degrading enzymatic expression and activity. Breast Cancer Res. 2012;14(3):R84.

38. Culjkovic-Kraljacic B, Baguet A, Volpon L, Amri A, Borden KL. The oncogene eIF4E reprograms the nuclear pore complex to promote mRNA export and oncogenic transformation. Cell reports. 2012;2(2):207-15.

39. Culjkovic B, Topisirovic I, Borden KL. Controlling gene expression through RNA regulons: the role of the eukaryotic translation initiation factor eIF4E. Cell cycle. 2007;6(1):65-9.

40. Assouline S, Culjkovic B, Cocolakis E, Rousseau C, Beslu N, Amri A, et al. Molecular targeting of the oncogene eIF4E in acute myeloid leukemia (AML): a proof-of-principle clinical trial with ribavirin. Blood. 2009;114(2):257-60.

41. Pettersson F, Yau C, Dobocan MC, Culjkovic-Kraljacic B, Retrouvey H, Puckett R, et al. Ribavirin treatment effects on breast cancers overexpressing eIF4E, a biomarker with prognostic specificity for luminal B-type breast cancer. Clinical cancer research : an official journal of the American Association for Cancer Research. 2011;17(9):2874-84.

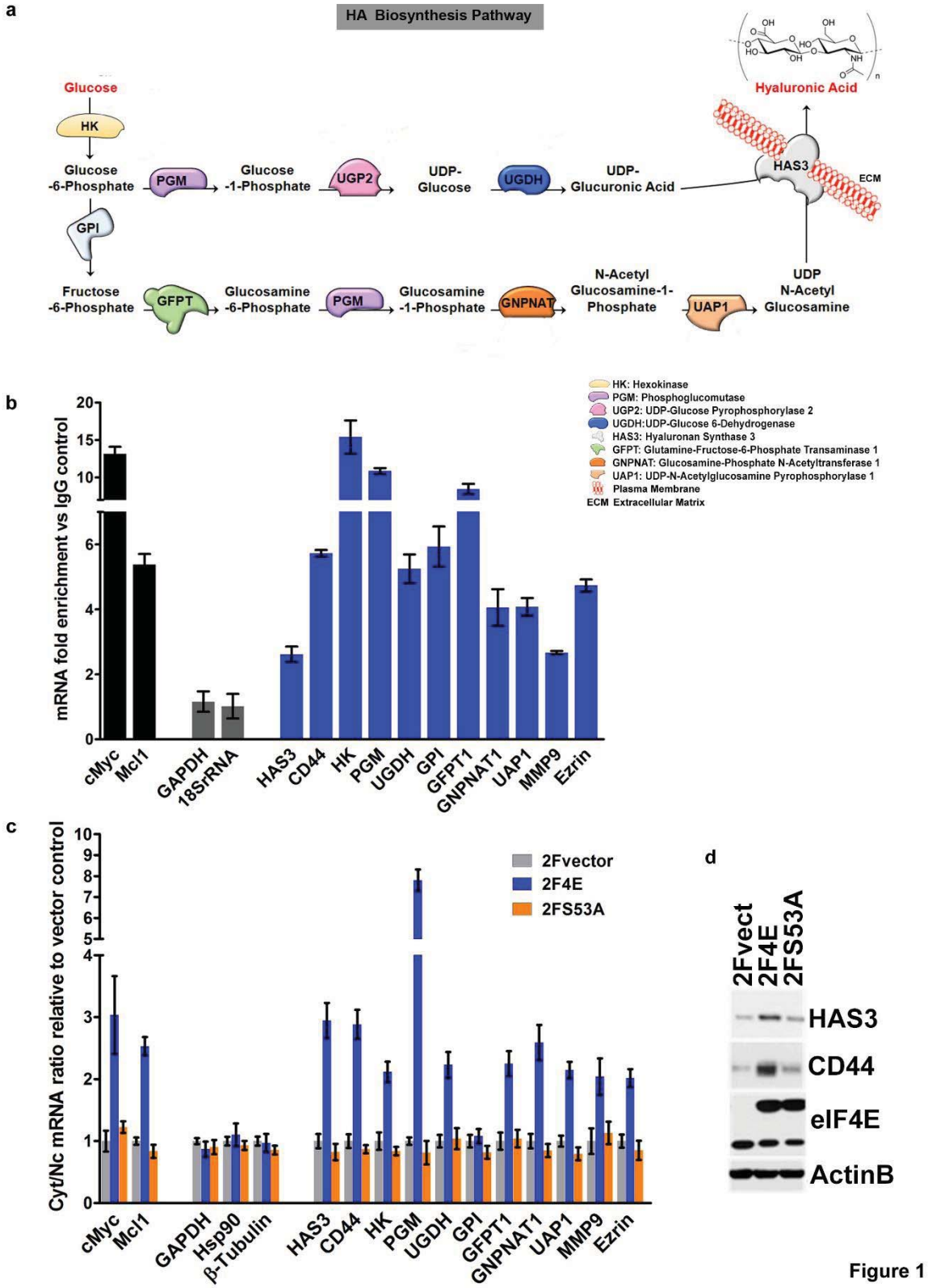
a
HA Biosynthesis Pathway
Hyaluronic Acid
Glucose
HK
Glucose -6-Phosphate
PGM
Glucose -1-Phosphate
UGP2
UDP-Glucose
UGDH
UDP-Glucuronic Acid
HAS3
ECM
GPI
Fructose -6-Phosphate
GFPT
Glucosamine -6-Phosphate
PGM
Glucosamine -1-Phosphate
GNPNAT
N-Acetyl Glucosamine-1-Phosphate
UAP1
UDP N-Acetyl Glucosamine
b
HK: Hexokinase
PGM: Phosphoglucomutase
UGP2: UDP-Glucose Pyrophosphorylase 2
UGDH:UDP-Glucose 6-Dehydrogenase
HAS3: Hyaluronan Synthase 3
GFPT: Glutamine-Fructose-6-Phosphate Transaminase 1
GNPNAT: Glucosamine-Phosphate N-Acetyltransferase 1
UAP1: UDP-N-Acetylglucosamine Pyrophosphorylase 1
Plasma Membrane
ECM Extracellular Matrix
mRNA fold enrichment vs IgG control
cMyc
Mcl1
GAPDH
18SrRNA
HAS3
CD44
HK
PGM
UGDH
GPI
GFPT1
GNPNAT1
UAP1
MMP9
Ezrin
c
2Fvector
2F4E
2FS53A
Cyt/Nc mRNA ratio relative to vector control
cMyc
Mcl1
GAPDH
Hsp90
β-Tubulin
HAS3
CD44
HK
PGM
UGDH
GPI
GFPT1
GNPNAT1
UAP1
MMP9
Ezrin
d
2Fvect
2F4E
2FS53A
HAS3
CD44
eIF4E
ActinB

Figure 1

Figure 1: eIF4E regulates the expression of HA synthesizing enzymes and HA receptor CD44. (A) HA biosynthesis pathway. **(B)** RT-qPCR of HA synthesizing enzymes and its receptor CD44 following RNA immunoprecipitation (RIP) of nuclear eIF4E in U2Os 2Flag-eIF4E cells using rabbit anti-eIF4E antibody. Data are normalized to IgG control and presented as fold change. c-Myc and Mcl-1 are eIF4Es and thus serve as positive controls while GAPDH and 18S rRNA served as negative controls. **(C)** RT-qPCR of HA synthesizing enzymes in cytoplasmic versus nuclear fractions of U2Os cells overexpressing 2Flag-eIF4E (2F4E), S53A mutant (2FS53A) or vector control (2Fvect). Data are normalized to vector control. c-Myc and Mcl-1 served as known eIF4E targets while GAPDH, Hsp90 and β-Tubulin served as negative controls. **(D)** Western blot of HAS3 and CD44 as a function of eIF4E or S53A mutant overexpression. Mcl-1 served as positive eIF4E target control. Actin was used as a loading control. HK: Hexokinase; HAS3: Hyaluronan Synthase 3; PGM5: Phosphoglucomutase 5; UGP2: UDP glucose pyrophosphorylase; UGDH: UDP glucose dehydrogenase; GFPT1: Glutamine fructose 6 phospho transaminase; GNPNAT1: Glucosamine phosphate N-acetyltransferase; UAP1: UDP N-acetyl pyrophosphorylase; GPI: Glucose-6-phosphate isomerase; CD44: HA receptor; MMP9: Matrix Metalloproteinase 9. For bar graphs, the average +/- standard deviation are shown. Experiments were carried out in triplicate, at least three independent times.

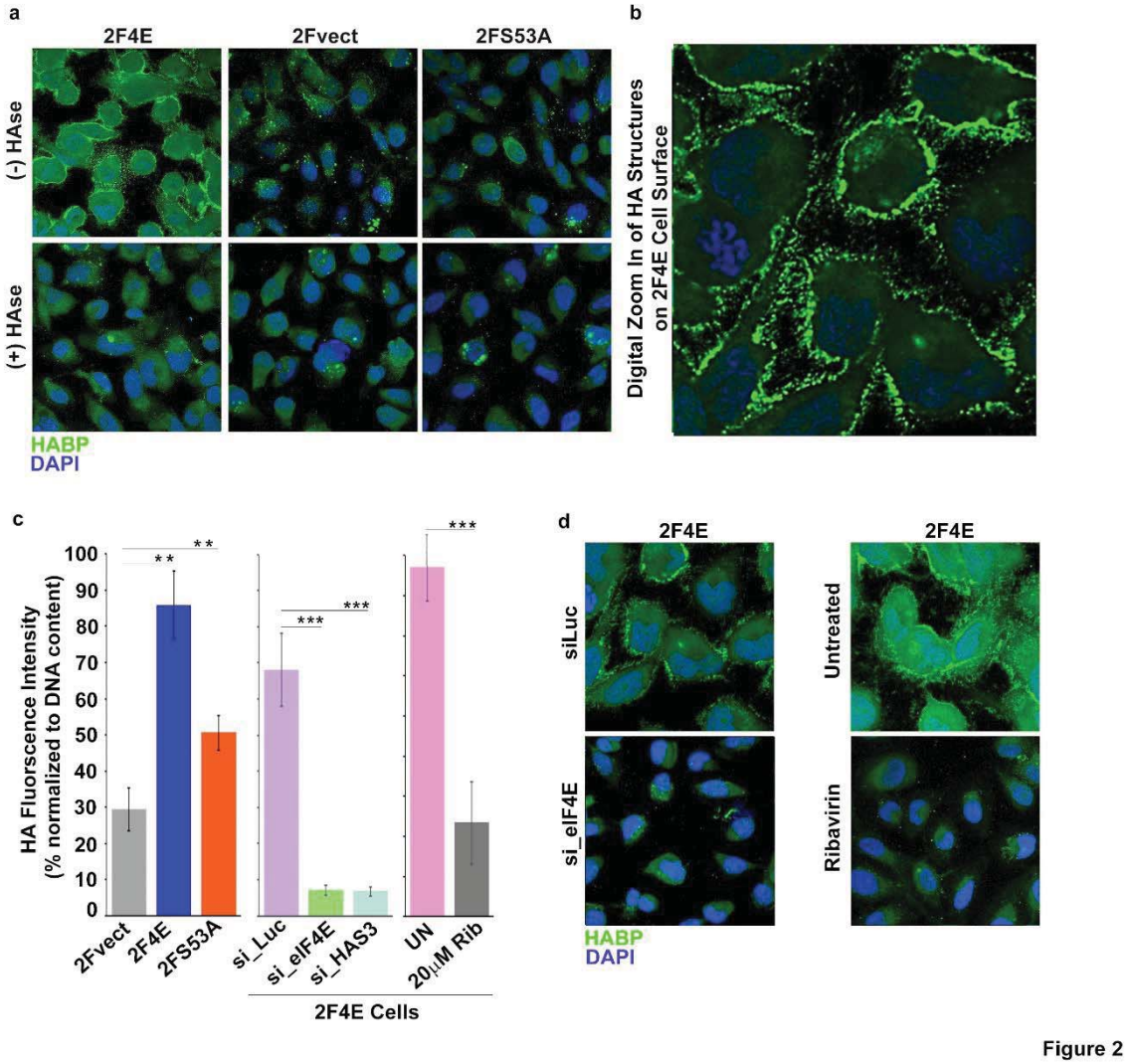

Figure 2

Figure 2: **eIF4E overexpression correlates with increased HA synthesis**. **(A)** Fluorescence staining of HA (in green) using biotinylated HA binding protein with streptavidin-FITC in U2Os cells overexpressing eIF4E, S53A mutant or vector control in the presence or absence of *Streptomyces* Hyaluronidase treatment. DAPI is in blue. Note cell surface expression of HA in response to eIF4E overexpression. All confocal settings are identical between specimens and thus lower signal is indicative of less HA. A ×40 objective with no digital zoom was used. **(B)** 2x digital zoom in confocal images of HA from part (A). **(C)** Quantification of fluorophore-assisted carbohydrate electrophoresis (FACE) gels (Sup Fig 1 e&f) for HA levels in U2Os cells expressing eIF4E, S53A mutant or vector control, and U2Os cells overexpressing eIF4E following HAS3/eIF4E knockdown or pharmacological inhibition with ribavirin. **(D)**

Fluorescence staining of HA (in green) following siRNA to eIF4E or ribavirin treatment in U2Os cells overexpressing eIF4E. DAPI is in blue. A ×63 objective with no digital zoom used. For bar graphs, the mean +/- SD are shown. Experiments were carried out in triplicate, at least three independent times. **P < 0.01, ***P < 0.001 (Student's t-test).

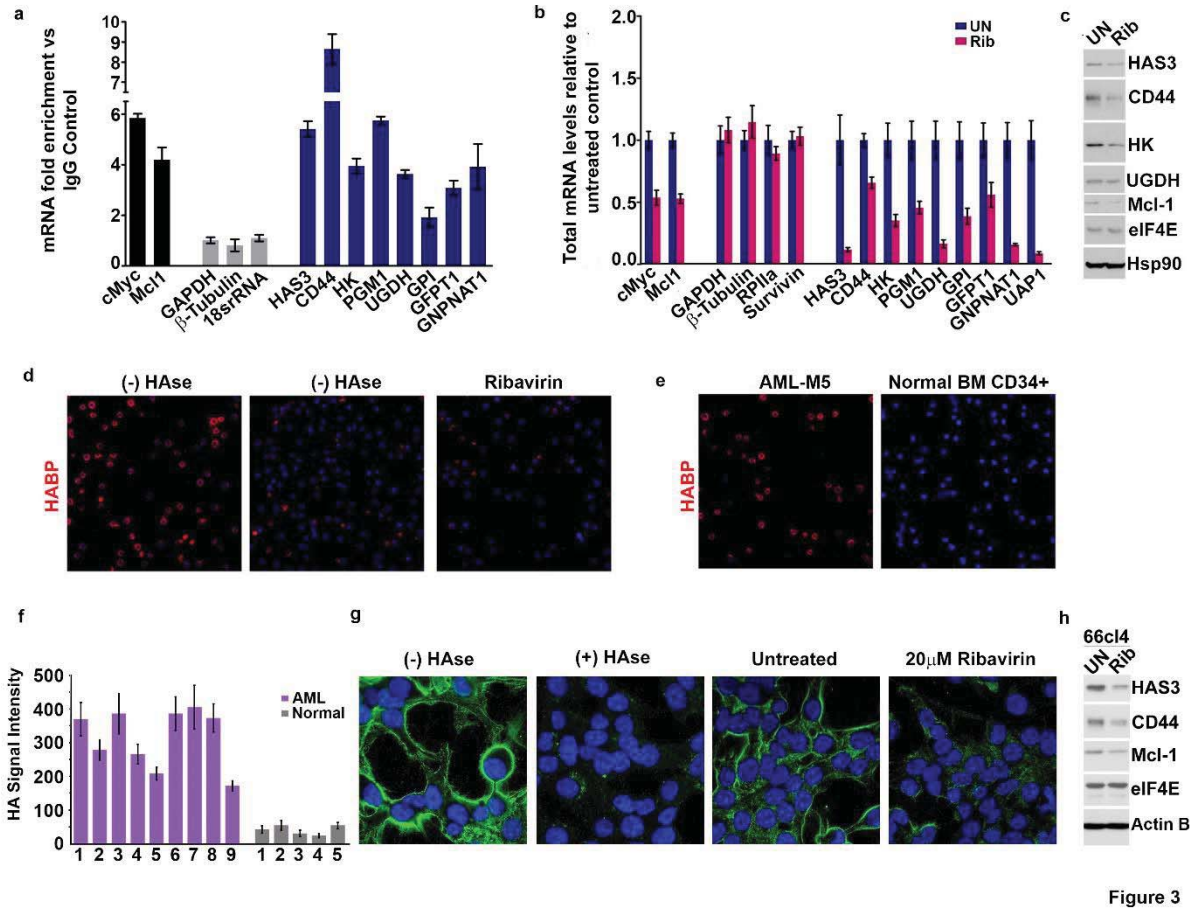

Figure 3: eIF4E elevates HA in cancer cell lines and primary specimens. (A) RT-qPCR of HA synthesizing enzymes and its receptor CD44 following RNA immunoprecipitation of nuclear eIF4E in MM-6 cells using rabbit eIF4E antibody. Data are presented as fold change relative to IgG controls. c-Myc and Mcl-1 served as endogenous eIF4E targets while GAPDH, β-Tubulin and 18SrRNA served as a negative control. **(B)** RT-qPCR of HA synthesizing enzymes in cytoplasmic versus nuclear fractions of MM-6 cells treated with Ribavirin. Data are normalized to untreated control. Error bars are averages ± S.D. c-Myc and Mcl-1 served as known eIF4E targets while GAPDH, β-Tubulin, RPIIa and Survivin served as negative control.

(C) Western blot of HA synthesizing enzymes and CD44 as a function of Ribavirin treatment in MM-6 cell line. Mcl-1 served as endogenous eIF4E target while Hsp90 served as a loading control. **(D)** Fluorescence staining of HA (in red) in MM-6 cell lines treated with Ribavirin (Rib) versus untreated (UN) in the presence or absence of Hyaluronidase treatment. DAPI is in blue. A ×63 objective with no digital zoom is used. **(E)** Fluorescence staining of HA (in red) in Normal human CD34+ specimen compared with leukemic cells from M5 AML Patient. **(F)** Quantification of HA fluorescence staining in M4/M5 AML patients using ZEN software. HA signal intensity is presented as the geometric means of the HA signal in 100 cell normalized to that of Normal human CD34+ specimen. **(G)** Fluorescence staining of HA (in green) in 66cl4 cells in the presence or absence of Hyaluronidase or Ribavirin treatment. DAPI is in blue. A ×63 objective with no digital zoom used. **(H)** Western blot control of HAS3 and CD44 as a function of ribaivirin treatment in 66cl4 cell line. Mcl-1 served as endogenous eIF4E target while ActinB served as loading control. Experiments were carried out in triplicate, at least three independent times. For bar graphs, the mean +/- standard deviation are shown. *$P < 0.05$ (Student's t-test).

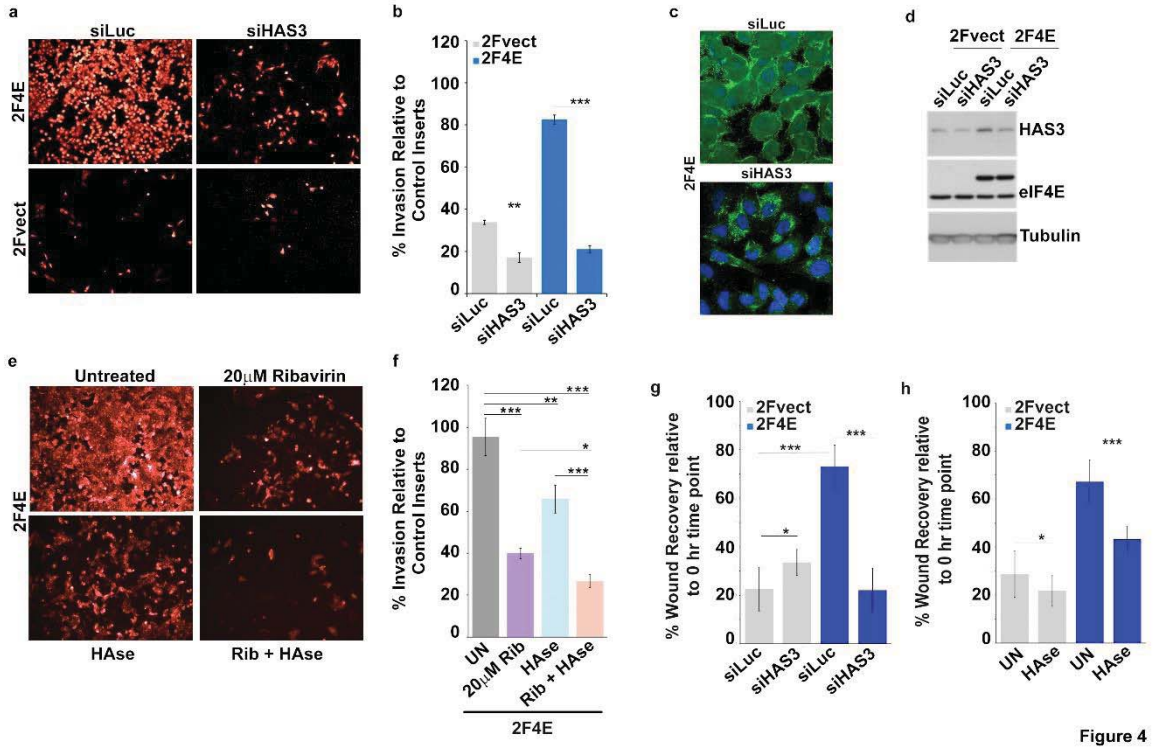

Figure 4: **Surface HA is required for eIF4E-mediated invasion and migration of cancer cells. (A-B)** Cell invasion through matrigel assessed following siRNA-mediated knockdown of HAS3 or scrambled control (Luciferase (siLuc)) in U2Os cells overexpressing eIF4E or vector. Invasion is measured as the percentage of fluorescence staining intensity in matrigel coated inserts versus that of the control inserts. **(C)** Fluorescence staining of HA (in green) following siRNA to HAS3. DAPI is in blue. A ×40 objective with no digital zoom used. **(D)** Western blot to demonstrate knockdown efficiency of HAS3. Tubulin served as loading control. **(E-F)** Cell invasion through matrigel assessed in U2Os cells overexpressing eIF4E following treatment with Ribavirin and/or Hyaluronidase. Invasion is measured as in **0**. **(G-H)** Cell migration across a scratch assessed in U2Os cells overexpression eIF4E or vector control following knockdown of HAS3 or treatment with *Streptomyces* Hyaluronidase. Migration is measured as the percentage of the area not filled with cells at t=16hrs normalized to that of the t=0hr time point. For bar graphs, the mean +/- standard deviation are shown. Experiments were carried out in triplicate, at least three independent times. **P < 0.01, ***P < 0.001 (Student's t-test).

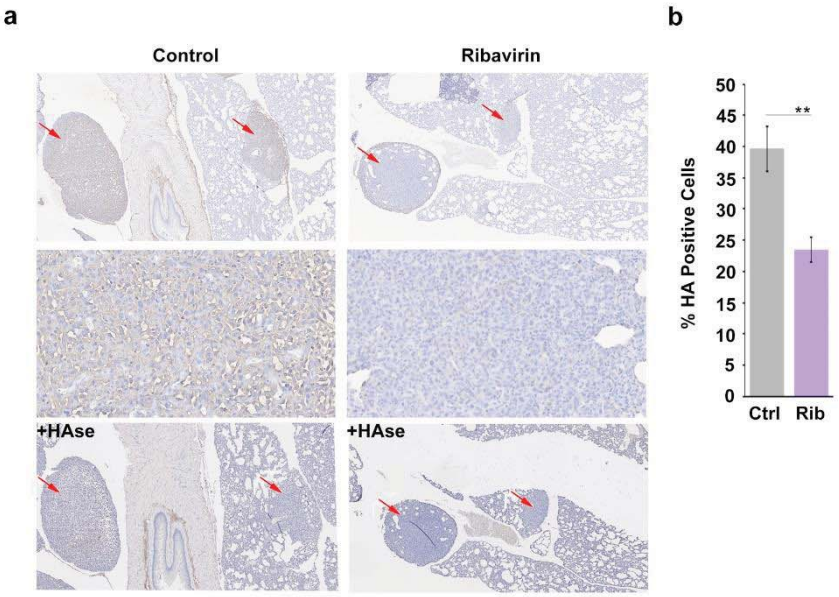

Figure 5

Figure 5: **HA biosynthesis is required for eIF4E-mediated lung metastasis in mice. (A)** Histochemical staining of HA using biotinylated HABP in metastatic mouse tumours. **(B)** Quantification from Visiomorph. For bar graphs, the mean +/- standard deviation are shown. *P < 0.05 (Student's t-test).

Supplementary Figures

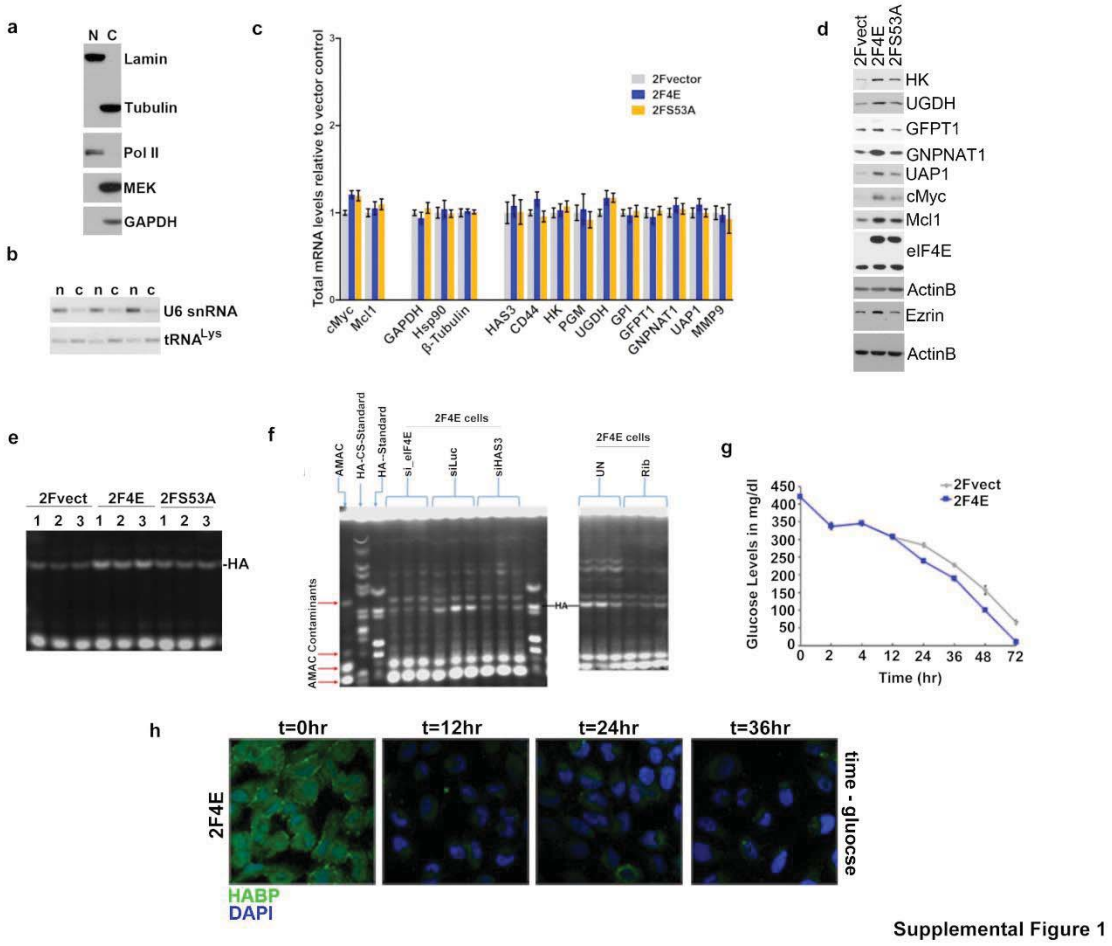

Supplemental Figure 1

Supplementary Figure 1: **eIF4E regulates HA synthesis**. (A) Control Western blot for cellular fractionation corresponding to eIF4E RIP shown in Figure 1B. Lamin and Pol II are used as nuclear markers while GAPDH, β-Tubulin and MEK are used as cytoplasmic markers. (B) Semi-qPCR for tRNAlys and U6 snRNA as control for the cytoplasmic and nuclear fractions, respectively, corresponding to the export assay shown in Figure 1C. (C) RT-qPCR of total mRNA levels corresponding to mRNA export assay shown in Figure 1C. (D) Western blot of HA synthesizing enzymes as a function of eIF4E or S53A mutant overexpression. cMyc served as positive eIF4E target control. Actin was used a loading control. (E-F) Fluorophore-assisted carbohydrate electrophoresis gels corresponding to bar graph presented in Figure 2 c. (G) Glucose levels were measured in mg/dl using Clarity Plus Blood Glucose Monitoring Kit in

Vector or eIF4E U2Os cells as a function of time (in hours). Experiments were carried out in triplicate, at least three independent times. (H) Fluorescence staining of HA (in green) of U2Os cells overexpressing eIF4E collected at different time points following media change (to DMEM containing 2 g/l glucose). DAPI is in blue. A ×40 objective with no digital zoom used. Experiments were carried out in triplicate, at least three independent times. For bar graphs, the mean +/- standard deviation are shown.

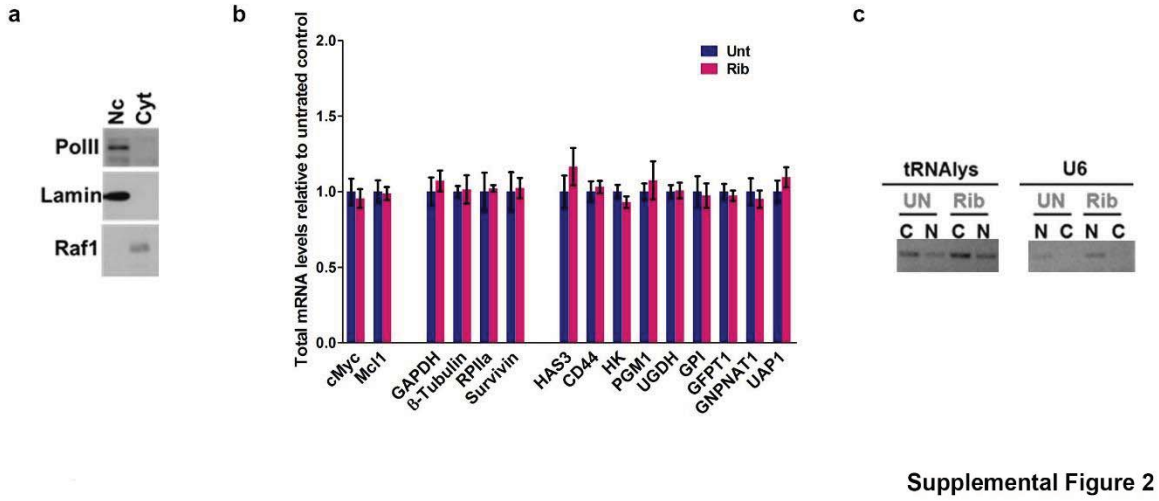

Supplemental Figure 2

Supplemental Figure 2: **eIF4E elevates HA in cancer cell lines and primary specimens.** (A) Control Western blot for cellular fractionation corresponding to eIF4E RIP. Lamin and Pol II are used as nuclear markers while Raf1 is used as cytoplasmic marker. (B) RT-qPCR of total mRNA levels corresponding to mRNA export assay (C) Semi-qPCR for tRNAlys and U6 snRNA served as controls for the cytoplasmic and nuclear fractions, respectively.

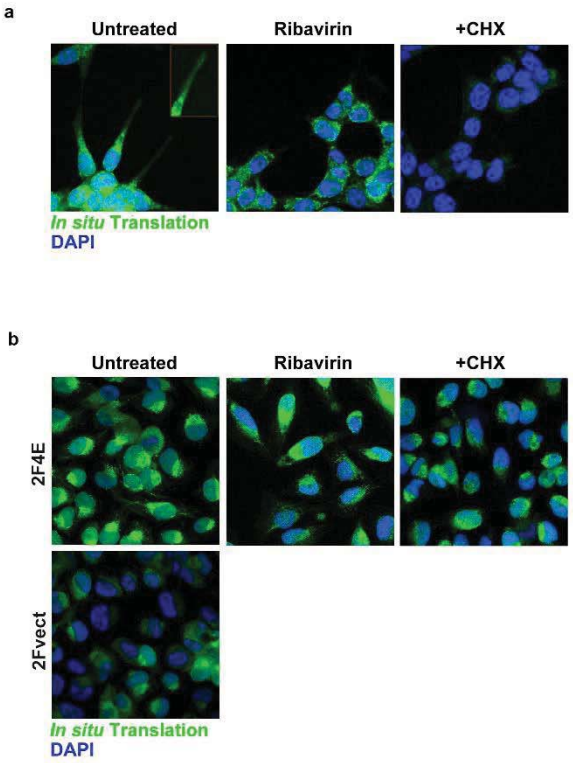

Supplemental Figure 3

Supplementary Figure 3: **eIF4E concentrates in HA rich protrusions and correlates with sites of active translation.** (A-B) Fluorescence staining of Click_iT HPG Alexa Flour 488 in 66cl4 or U2Os cells overexpressing eIF4E cells, respectively, following treatment with 20 µM Ribavirin versus untreated control. Cyclohexamide treatment is used as a negative control. A x40 or 63 objectives is used. Experiments were carried out in triplicate, at least three independent times.

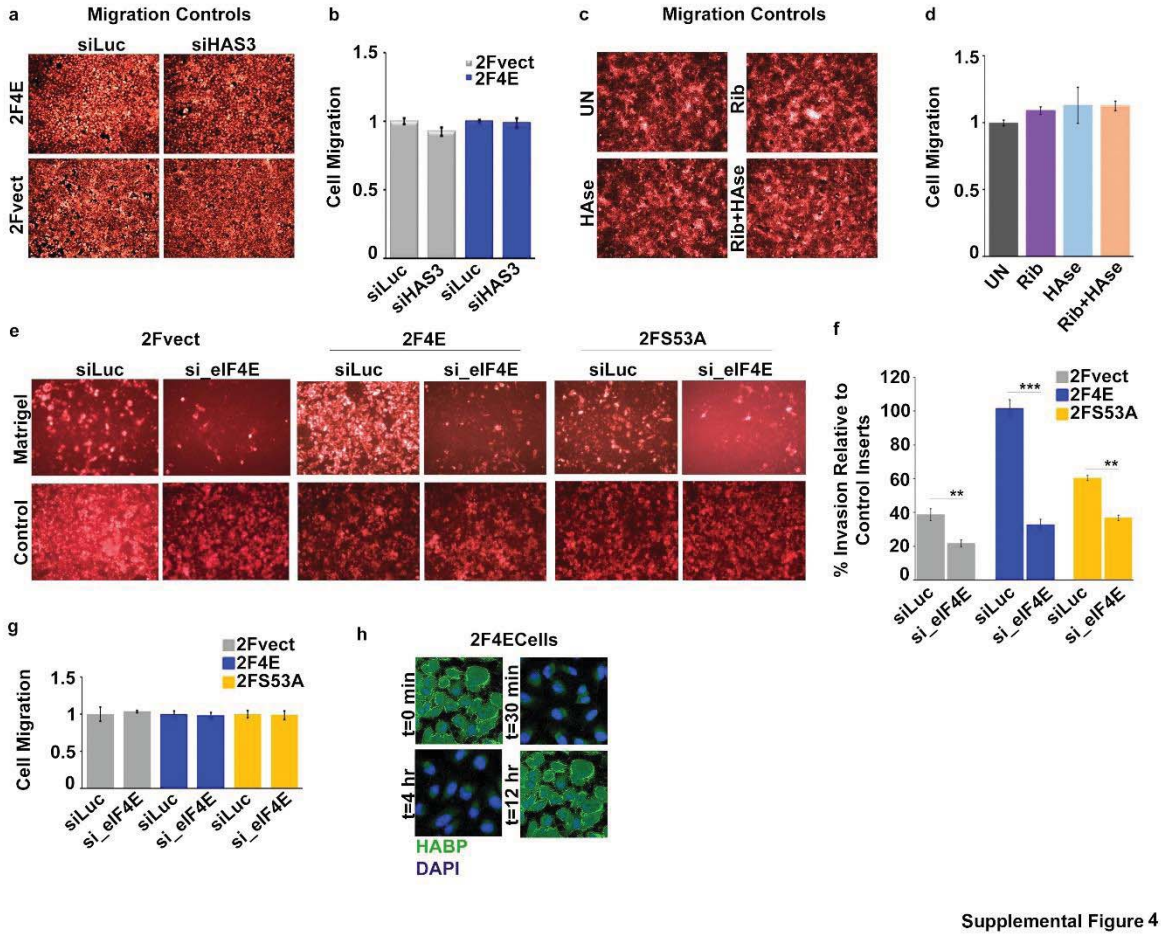

Supplemental Figure 4

Supplementary Figure 4: **Surface HA is required for eIF4E-mediated invasiveness of cancer cells.** (A-D) Control inserts for Matrigel invasion assays shown in Figures 3a and e. (E-F) In vitro Matrigel invasion assay following siRNA mediated knockdown of eIF4E in U2Os cells overexpressing eIF4E, S53A mutant or vector control. (G) Control inserts for invasion assays shown in parts E and F. (H) Fluorescence staining of HA (in green) in U2Os cells overexpressing eIF4E collected at different time points following HAse treatment. DAPI is in blue. A ×40 objective with no digital zoom used. Experiments were carried out in triplicate, at least three independent times. For bar graphs, the mean +/- standard deviation are shown. **P < 0.01, ***P < 0.001 (Student's t-test).

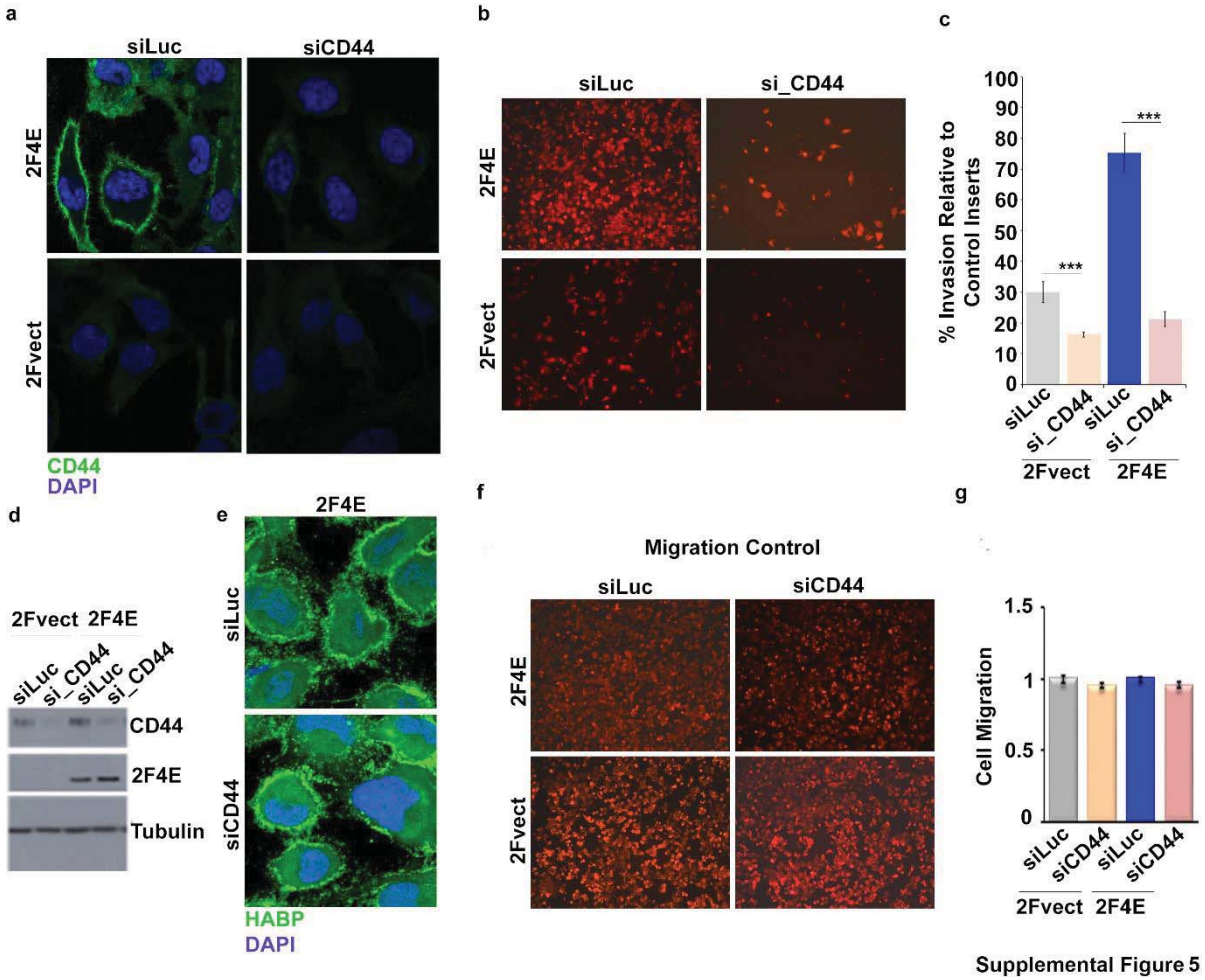

Supplemental Figure 5

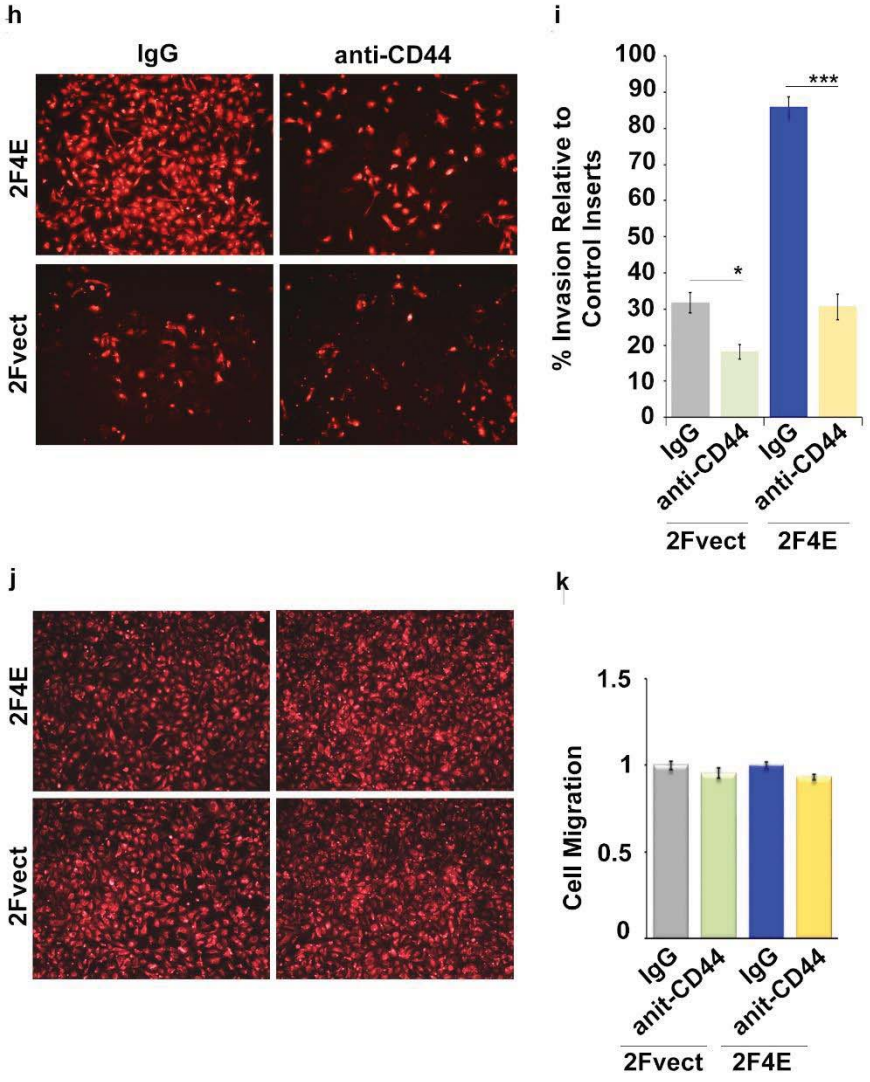

Supplemental Figure 5, cont'd

Supplemental Figure 5: **CD44 is required for the invasion of eIF4E cells.** (A) Immunofluorescence staining of CD44 (in green) following siRNA-mediated knockdown of CD44 in U2Os cells overexpressing eIF4E or vector control. DAPI is in blue. A ×40 objective with no digital zoom used. (B-C) Cell invasion through matrigel assessed following siRNA-mediated knockdown of CD44 in U2Os cells overexpressing eIF4E or vector control. siRNA against Luciferase was used as a control. Invasion was measured as a percentage of fluorescence staining intensity of matrigel coated inserts normalized to control inserts. (D) Western blot

control to assess knockdown efficiency of CD44. (E) Fluorescence staining of HA (in green) following siRNA to CD44 versus scrambled control in U2Os cells overexpressing eIF4E. DAPI is in blue. A ×63 objective with no digital zoom used. (F-G) Control inserts for Matrigel invasion assays shown in part (B). (H-I) Cell invasion through matrigel assessed following treatment with anti-CD44 blocking antibody (A3D8) known to bind the HA-binding domain of CD44. Invasion is measured as percentage of fluorescence staining intensity of matrigel coated inserts normalized to control inserts. (J-K) Control inserts for Matrigel invasion assays shown in part (H-I). For bar graphs, the mean +/- standard deviation are shown. Experiments were carried out in triplicate, at least three independent times. **$P < 0.01$, ***$P < 0.001$ (Student's t-test).

CHAPTER 9

Combinatorial Targeting of Nuclear Export and Translation of RNA Inhibits Aggressive B-cell Lymphomas

(RESEARCH ARTICLE)

Published Manuscript in *Blood 2015 :blood-2015-05-645069; doi:10.1182/blood-2015-05-645069*

Synopsis:

eIF4E is overexpressed in Diffuse Large B Cell Lymphoma (DLBCL), including the most aggressive subtypes. Its activity in driving the mRNA export and translation of known driver oncogenes (BCL6, BCL2, MYC) is maintained through binding to Hsp90. Accordingly, co-inhibition of these two binding partners with known pharmacological inhibitors induces tumor regression in cell line and patient-derived tumorgrafts and sets the stage for a new antilymphoma therapeutic strategy.

Contribution:

Authorship: Conducted cell-based experiments, RIP-seq and analysis: B.C.K., T.F., R.G., R.M., N.C-V., A.V., **H.Z.** and J.P. Conducted animal experiments and established PDX: S.N.Y., F.T., M.G., P.G., M.L., R.M. and G.I. Prepared and provided reagents: T.T. and G.C. Supervised research and designed experiments: A.M, O.E, K.L.B.B. and L.C. Wrote the manuscript: B.C.K., T.F., A.M, K.L.B.B. and L.C

Regular Article

LYMPHOID NEOPLASIA

Combinatorial targeting of nuclear export and translation of RNA inhibits aggressive B-cell lymphomas

Biljana Culjkovic-Kraljacic,[1,*] Tharu M. Fernando,[2,*] Rossella Marullo,[2] Nieves Calvo-Vidal,[2] Akanksha Verma,[3] ShaoNing Yang,[2] Fabrizio Tabbò,[4,5] Marcello Gaudiano,[4] Hiba Zahreddine,[1] Rebecca L. Goldstein,[2] Jayeshkumar Patel,[2] Tony Taldone,[6] Gabriela Chiosis,[6] Marco Ladetto,[5,7] Paola Ghione,[7] Rodolfo Machiorlatti,[5] Olivier Elemento,[3] Giorgio Inghirami,[4] Ari Melnick,[2] Katherine L. B. Borden,[1] and Leandro Cerchietti[2]

[1]Institute for Research in Immunology and Cancer and Department of Pathology and Cell Biology, Université de Montréal, Montréal, QC, Canada; [2]Hematology and Oncology Division, [3]Department of Physiology and Biophysics, Institute for Computational Biomedicine, and [4]Pathology and Laboratory Medicine Department, Weill Cornell Medical College, Cornell University, New York, NY; [5]Department of Molecular Biotechnology and Health Science and Center for Experimental Research and Medical Studies (CeRMS), University of Turin, Turin, Italy; [6]Department of Molecular Pharmacology and Chemistry, Sloan Kettering Institute, Memorial Sloan Kettering Cancer Center, New York, NY; and [7]Division of Hematology, Department of Experimental Medicine and Oncology, University of Turin, Turin, Italy

Key Points

- eIF4E, a protein highly elevated in poor-prognostic lymphomas, simultaneously sustains expression of known driver oncogenes BCL6, BCL2, MYC.
- The tumorigenic form of Hsp90 is a novel partner protein in the process underlying a new therapeutic strategy for these aggressive lymphomas.

Aggressive double- and triple-hit (DH/TH) diffuse large B-cell lymphomas (DLBCLs) feature activation of Hsp90 stress pathways. Herein, we show that Hsp90 controls posttranscriptional dynamics of key messenger RNA (mRNA) species including those encoding BCL6, MYC, and BCL2. Using a proteomics approach, we found that Hsp90 binds to and maintains activity of eIF4E. eIF4E drives nuclear export and translation of BCL6, MYC, and BCL2 mRNA. eIF4E RNA-immunoprecipitation sequencing in DLBCL suggests that nuclear eIF4E controls an extended program that includes B-cell receptor signaling, cellular metabolism, and epigenetic regulation. Accordingly, eIF4E was required for survival of DLBCL including the most aggressive subtypes, DH/TH lymphomas. Indeed, eIF4E inhibition induces tumor regression in cell line and patient-derived tumorgrafts of TH-DLBCL, even in the presence of elevated Hsp90 activity. Targeting Hsp90 is typically limited by counter-regulatory elevation of Hsp70B, which induces resistance to Hsp90 inhibitors. Surprisingly, we identify Hsp70 mRNA as an eIF4E target. In this way, eIF4E inhibition can overcome drug resistance to Hsp90 inhibitors. Accordingly, rational combinatorial inhibition of eIF4E and Hsp90 inhibitors resulted in cooperative antilymphoma activity in DH/TH DLBCL in vitro and in vivo. (*Blood*. 2016;127(7):858-868)

Introduction

Approximately one-third of patients with diffuse large B-cell lymphoma (DLBCL) have disease that is either refractory or relapses after combinatorial chemo-immunotherapy.[1,2] Mutation and constitutive expression of sets of key oncoproteins define DLBCL patients with particularly poor outcome. Among these patients, those with high expression or amplification of MYC (V-Myc avian myelocytomatosis viral oncogene homolog) show the worst outcome with an overall survival below 30% at 2 years.[3-5] Frequently, MYC abnormalities are associated with either BCL2 (B-cell CLL/lymphoma 2) and/or BCL6 (B-cell CLL/lymphoma 6) mutations leading to elevated levels of these proteins.[6] Almost 60% of patients with BCL2 and MYC translocations die within 6 months of diagnosis because of chemorefractory disease, a prognosis that cannot be overcome with intensified chemotherapy.[5] A further hindrance to the development of new treatment regimens is the fact that these double- and triple-hit (DH/TH) lymphomas are frequently found in the elderly[7] who have limited tolerability to chemotherapeutic regimens. However, novel targeted therapies disrupting key DH/TH DLBCL driver mechanisms offer for the first time opportunities to change the devastating natural history of this disease.

Previous reports indicated that the fraction of a stress active form of Hsp90 that is enriched in tumor cells (herein, tumor-enriched Hsp90 [TEHsp90]) plays an important role in lymphomagenesis.[8] TEHsp90 interacts with many proteins and mediates a diverse set of mechanisms beyond its chaperone function.[9,10] For example, TEHsp90 maintains the stability of BCL6 messenger RNA (mRNA) and protein, thus enabling sustained expression of BCL6 in DLBCL.[8] A recently developed small molecule called PU-H71 preferentially inhibits TEHsp90 with relatively less activity against the housekeeping pool of bulk Hsp90 protein.[8,11,12] Hence, PU-H71 is selectively toxic to tumor cells that are TEHsp90 dependent while sparing normal tissue.[8,11,12]

Submitted May 25, 2015; accepted November 20, 2015. Prepublished online as *Blood* First Edition paper, November 24, 2015; DOI 10.1182/blood-2015-05-645069.

*B.C.-K. and T.M.F. contributed equally to this study.

The data reported in this article have been deposited in the Gene Expression Omnibus database (accession number GSE63265).

The online version of this article contains a data supplement.

There is an Inside *Blood* Commentary on this article in this issue.

The publication costs of this article were defrayed in part by page charge payment. Therefore, and solely to indicate this fact, this article is hereby marked "advertisement" in accordance with 18 USC section 1734.

TEHsp90 tends to selectively bind to those proteins that are most critical for maintaining the survival of tumor cells. The small molecule PU-H71 binds tightly to TEHsp90 and locks it into its partner protein-bound configuration.[13] Hence the PU-H71 molecule can serve as the basis for an affinity-capture proteomics strategy to identify TEHsp90 partner proteins that play crucial roles in cancer biology.[13,14] Using this strategy, we recently mapped the TEHsp90 interactome in DLBCLs and found that several proteins regulating RNA metabolism, including eIF4E (eukaryotic translation initiation factor 4E), are part of this TEHsp90-orchestrated network of proteins required to sustain the lymphoma phenotype.[12] eIF4E is a key oncogenic factor in B-cell lymphomagenesis.[15] The oncogenic potential of eIF4E arises from its critical roles in the cytoplasm in the mRNA translation and in the nucleus in the mRNA export of a specific subset of transcripts.[15-18] These transcripts can be regulated at the cytoplasmic (ie, translation), nuclear (ie, export), or at both levels.[18] Nuclear targets are exported in the presence of eIF4E, LRPPRC (leucine-rich pentatricopeptide repeat containing), and XPO1 (exportin 1).[10] eIF4E competitive inhibitors, such as ribavirin, abrogate its prosurvival function and cause antitumoral effect in solid tumors and acute myeloid leukemia (AML).[19,20]

Here, we show that TEHsp90 controls posttranscriptional dynamics of key mRNA species including those encoding BCL6, MYC, and BCL2 in DH/TH DLBCLs. We identify that eIF4E simultaneously modulates the mRNA export and translation of these genes and that TEHsp90 modulates eIF4E activity. We observe that eIF4E inhibition potently suppresses tumor growth through its effects on these transcripts. We also identify Hsp70 mRNA as an eIF4E target, and, in this way, eIF4E inhibition can overcome resistance to Hsp90 inhibitors. Accordingly, rational combination of eIF4E and TEHsp90 inhibitors resulted in cooperative antilymphoma activity in DH/TH DLBCL in vitro and in vivo, offering a potential new strategy for treating poor-outcome lymphomas.

Methods

Cell lines and reagents

DLBCL cell lines OCI-Ly1 and OCI-Ly18 were grown in 90% Iscove's and 10% fetal calf serum medium (supplemented with penicillin G/streptomycin), and DLBCL cell lines SU-DHL6, DoHH2, Toledo, and Karpas422 were grown in 90% RPMI and 10% fetal calf serum medium (supplemented with penicillin G/streptomycin, *N*-2-hydroxyethylpiperazine-*N*'-2-ethanesulfonic acid, and L-glutamine). The cell line U2OS was grown in Dulbecco's modified Eagle medium with 10% fetal bovine serum and 1% penicillin/streptomycin. Cell lines were obtained from American Type Culture Collection, German Collection of Microorganism and Cell Cultures DSMZ, or the Ontario Cancer Institute. We conducted monthly testing for *Mycoplasma* sp. and other contaminants and quarterly cell identification by single-nucleotide polymorphism. Ribavirin was obtained from Kemprotec. PU-H71, PU-H71-beads, and control beads were synthesized and prepared at Memorial Sloan Kettering Cancer Center (T.T. and G.C.). For analysis of mRNA export, protein levels and polysomal profiling cells were treated with PU-H71 0.5 μM for 12 hours (all DLBCL cell lines), ribavirin 10 μM (OCI-Ly1 and DoHH2), or ribavirin 30 μM (SU-DHL6) for 48 hours (or 96 hours for polysomal profiling). eIF4E small-interfering RNA (siRNA) and control sequences are from Culjkovic-Kraljacic et al.[16] U2OS cells were transfected with Lipofectamine (ThermoFisher) and analyzed at 72 hours. DoHH2 cells were transfected by 2 rounds of electroporation 72 hours apart (Amaxa, Lonza AG) and analyzed at 48 hours.

RIP

RNA-immunoprecipitation (RIP) from nuclear fractions of cells was performed as previously described.[16] Briefly, 1 mg of nuclear lysate was used for RIP with 6 μg anti-eIF4E antibody (MBL RN001P) or control immunoglobulin G (rabbit, Millipore). After incubation, complexes were eluted by boiling in tris (hydroxymethyl)aminomethane (Tris) EDTA containing 1% sodium dodecyl sulfate and 12% β-mercaptoethanol. RNA was isolated using Trizol reagent and precipitated in isopropanol with addition of linear acrylamide. DNase-treated RNA samples (TurboDNase, Ambion) were reversed transcribed using SuperScript VILO cDNA synthesis kit (Invitrogen).

Polysomal profiling

Polysomal profiling was done as described.[21] Briefly, cells were treated with cycloheximide (100 mg/mL) 10 minutes before harvesting, and lysates were prepared using polysomelysis buffer (15 mM Tris pH 7.4, 250 mM NaCl, 15 mM $MgCl_2$, 1% Triton X-100, 100 μg/mL cycloheximide, 1 mM dithiothreitol, 400 U/mL RNaseOUT [Invitrogen], and protease inhibitors [Roche]). Equal amounts (4 mg) of protein lysates were layered on a 20% to 50% linear sucrose gradient (20% and 50% sucrose solutions in 15 mM Tris pH 7.4, 15 mM $MgCl_2$, 150 mM NaCl, 1 mM dithiothreitol, 100 mg/μl cycloheximide, and 20 U/mL RNAseOut), mixed on Gradient Station IP Biocomp and centrifuged in a Beckman SW41Ti rotor at 92 000 G for 3 hours at 4°C. Following centrifugation, polysomal fractions were collected by continuously monitoring and recording the A254 on a Gradient Station IP (Biocomp) attached to a UV-MII (GE Healthcare) spectrophotometer. RNAs were isolated from polysomal fractions using Trizol reagent (Invitrogen).

Animal experiments

All animal procedures followed National Institutes of Health protocols and were approved by the Animal Institute Committee of the Weill Cornell Medical College.

Cell line xenografts. SCID mice were subcutaneously injected on the right flank with DLBCL cell lines OCI-Ly1 and SU-DHL6. Tumor volumes were monitored every day using electronic calipers (Fischer Scientific). When tumor reached a palpable size (~75 to 100 mm^3), animals were randomized into 4 groups of 10 mice and treated intraperitoneally with vehicle, ribavirin, PU-H71, or the combination of ribavirin and PU-H71. We used the area-under-the-curve (AUC) as the quantitative metric to represent the evolution of tumor volume over the time frame (10 days) of the experiment. The comparisons between treated and control mice were done using multivariate analysis of variance followed by pairwise comparison using the 2-tailed Student *t* test (Statistix; Analytical Software, Tallahassee, FL).

Patient-derived tumorgrafts. NSG mice were subcutaneously injected in the flank with primary human DLBCL cells. When tumor reached palpable size (as described previously), animals were randomized into 2 groups of mice and received vehicle or ribavirin 80 mg/kg intraperitoneally for 10 days. The measurement of tumor volume and comparisons between treated and control mice were performed as described previously.

Growth inhibition determination, immunohistochemistry and fluorescence in situ hybridization (FISH), RNA nuclear export, immunoblotting, metabolic labeling and capture of newly synthesized protein, RNA-sequencing (RNA-seq) and analysis, and TEHsp90 proteomics and validations are described in the supplemental Data (available on the *Blood* Web site). The Gene Expression Omnibus accession number for the mRNA-seq data sets reported is GSE63265.

Results

TEHsp90 proteomics points to eIF4E as a key driver of DH/TH DLBCL

We first identified DH/TH DLBCL cell lines by FISH for MYC, BCL6, and BCL2. In a panel of 35 DLBCL cell lines, we found 6 with DH or TH mutations (OCI-Ly1, SU-DHL6, DoHH2, Karpas422, OCI-Ly18, and Toledo) (Figure 1A). Hsp90 is universally overexpressed in DLBCL specimens and to a similar extent in DH/TH and non-DH/TH cells.[8] Accordingly, the activity of PU-H71 in DH/TH DLBCL is similar to non-DH/TH DLBCL cell lines (Figure 1B). This suggests

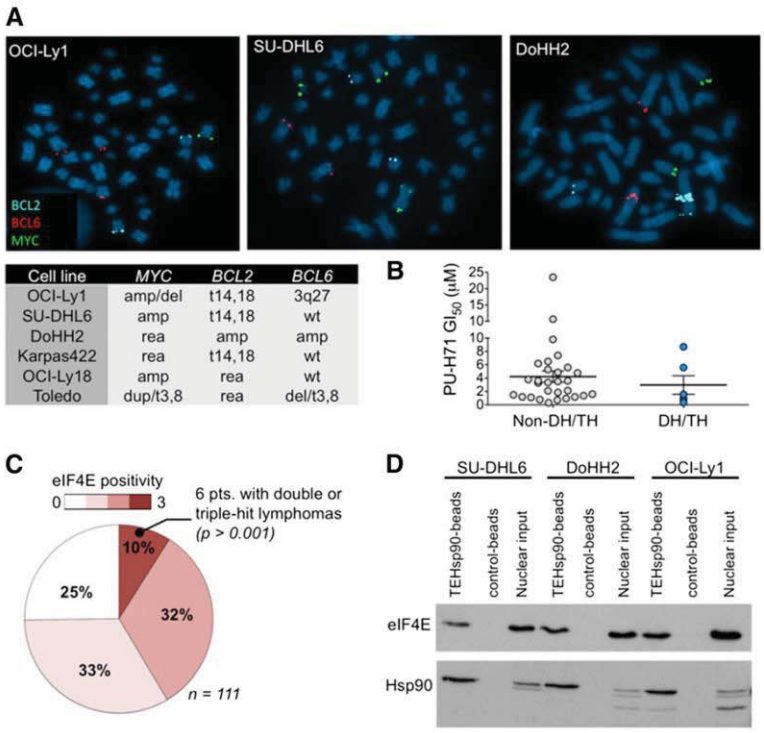

Figure 1. eIF4E is expressed in DH/TH DLBCL. (A) Representative image of BCL2, BCL6, and MYC FISH assay carried out in OCI-Ly1, SU-DHL6, and DoHH2 cell lines. Summary of FISH findings for MYC, BCL2, and/or BCL6 in 6 DLBCL cell lines harboring >1 of such chromosomal abnormalities. (B) Scatter plot for PU-H71 GI_{50} (growth inhibitory concentration 50%) in DH/TH cell lines (n = 6) vs non-DH/TH DLBCL cell lines (n = 29). (C) eIF4E expression by immunohistochemistry from 111 DLBCL cases. Number of positive cells (over total cells) is represented by color scale. All the DH/TH cases in the cohort (n = 6) presented the highest levels of eIF4E staining (n = 10). (D) Affinity purification of eIF4E and TEHsp90 from DH/TH cell lines nuclear lysates using PU-H71-beads vs chemical control beads.

that TEHsp90 may carry out diverse functions required to maintain survival also in these highly aggressive lymphoma cells. To elucidate these functions, we used PU-H71 as a chemical capture reagent to isolate TEHsp90 complexes from cell lysates of the TH lymphoma cell line OCI-Ly1 (MYC amplification, t14,18, and 3q27) by affinity purification followed by mass spectrometry. Proteomic analysis revealed that TEHsp90 was strongly bound to eIF4E (supplemental Figure 1), a critical factor in B-cell lymphomagenesis.[15] Other ribosomal proteins and components of the translational machinery such as eIF4A1 were also enriched (supplemental Figure 1).

The dual nuclear and cytoplasmic localization of eIF4E suggested it might be active in both cellular compartments.[16,18] This is of interest because eIF4E is known to mediate nuclear export of mRNAs in addition to its role in facilitating translation in the cytoplasm.[16,22] Therefore, we next assessed eIF4E expression and cellular localization patterns in primary human DH/TH DLBCL patients. We analyzed eIF4E expression in 111 cases of DLBCLs by immunohistochemistry and found that in 75% of cases (n = 83) the protein was detectable under the conditions used (positive cases) (Figure 1C and supplemental Figure 2). In 72% of positive cases (n = 60 specimens), eIF4E was localized in both nuclei and cytoplasm, whereas in 10% (n = 8) and 18% (n = 15) eIF4E was exclusively detected in either the cytosolic or nuclear compartment, respectively. We then ranked nuclear and cytosolic positive cases according to the number of lymphoma cells expressing eIF4E into high expression (>60% positive lymphoma cells), midexpression (<60 and >30% positive lymphoma cells), and low expression (<30% positive lymphoma cells) (Figure 1C and supplemental Figure 2). We found that from the cohort of patients expressing high levels of eIF4E (n = 11), 6 patients also had DH/TH lymphomas defined as translocations or amplifications in MYC and BCL2 and/or BCL6 by FISH analysis (Figure 1C). There were no DH/TH lymphomas (by FISH) in patients expressing a low level or midlevel of eIF4E ($P > .001$ vs high eIF4E-expressing cases, Fisher's exact test; Figure 1C). These findings suggest potential functional relevance of eIF4E in DH/TH DLBCL. Because the role of nuclear eIF4E has not yet been characterized in DH/TH DLBCL cells,[18] we analyzed the association of TEHsp90 and eIF4E in this compartment. We therefore performed affinity purification of the nuclear TEHSP90 complex using PU-H71 beads and found the presence of eIF4E in the nuclear lysates of OCI-Ly1 (56% of total input), DoHH2 (66% of total input), and SU-DHL6 (54% of total input) DH/TH cell lines (Figure 1D and supplemental Figure 3), suggesting that TEHSp90 and eIF4E form a functional complex in the nuclei of DH/TH cells.

eIF4E activity regulates the nuclear export of BCL6, MYC, and BCL2

The association of high eIF4E expression and its nuclear localization in DH/TH lymphomas led us to wonder whether it could simultaneously regulate the nuclear export of BCL6, MYC, and BCL2 mRNA. MYC and BCL2 were previously described as eIF4E targets.[16,23-25] To mechanistically address whether BCL6 is a nuclear export target, we took advantage of a validated cell-based assay in which U2OS cells are transfected with an eIF4E-expressing plasmid.[23] The overexpression of eIF4E significantly increased the cytoplasmic to nuclear ratios of MYC and BCL2, as expected ($P = .001$ and $P = .007$, respectively; Figure 2A), and also of BCL6 ($P = .0008$; Figure 2A), with no effects on GAPDH. This translates into increased protein expression of MYC, BCL2, and BCL6 (Figure 2B). The effect of eIF4E on MYC, BCL2, and BCL6 nuclear RNA export was validated in reciprocal experiments using siRNA-mediated knockdown of eIF4E in U2OS cells (Figure 2C).

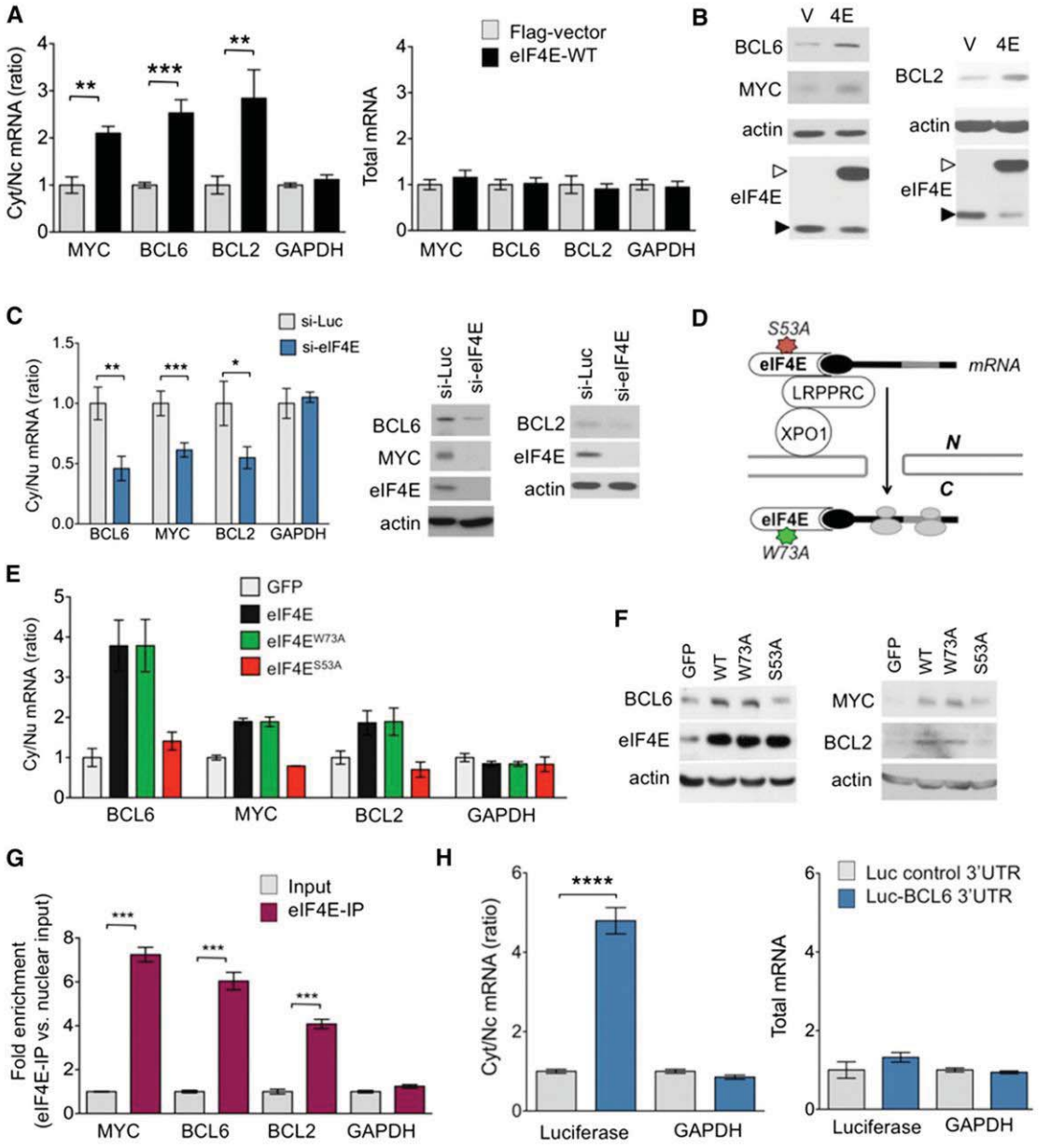

Figure 2. MYC, BCL2, and BCL6 are eIF4E targets. (A) Cytosolic/nuclear ratio (left) and total mRNA (right) of BCL6, BCL2, MYC, and glyceraldehyde-3-phosphate dehydrogenase (GAPDH; as control) transcripts in U2OS cells transfected with eIF4E plasmid (eIF4E-WT) or flag-vector as control. (B) Protein levels of BCL6, BCL2, MYC, actin (as control), and eIF4E in U2OS cells transfected with eIF4E plasmid (4E) or flag-vector (V). Endogenous eIF4E is marked with closed arrowhead and flagged eIF4E is marked with an open arrowhead. (C) Cytosolic/nuclear ratio of BCL6, BCL2, MYC, and GAPDH (as control) transcripts in U2OS cells transfected with siRNA for luciferase (as control) or siRNA for eIF4E. Protein levels of BCL6, BCL2, MYC, and eIF4E from the experiments are shown on the right. (D) Cartoon depicting loss of function caused by each mutant eIF4E construct used in subsequent experiment. (E) Cytosolic/nuclear ratio of BCL6, MYC, and BCL2 transcripts (GAPDH transcripts are shown as a control) and total transcript expression (right) of UOS2 cells transfected with green fluorescent protein (GFP) (as a vector control), wild-type eIF4E, and mutant eIF4E constructs eIF4E^{W73A} and eIF4E^{S53A}. (F) BCL6, MYC, BCL2, and eIF4E protein expression for cells shown in panel E. (G) eIF4E RIP fold enrichment of MYC, BCL2, BCL6, and GAPDH (negative control) mRNAs over input in U2OS cells. (H) Cytosolic/nuclear ratio of luciferase and GAPDH (as negative control) in U2OS cells transfected with luciferase gene with or without BCL6 3′UTR sequence. Total mRNA for the same conditions is shown on the right. ****$P < .0001$.

This procedure resulted in a significantly reduced cytoplasmic to nuclear ratio of BCL6, MYC, and BCL2 mRNAs ($P < .0001$, $P = .004$, and $P = .02$, respectively), without changes in total cell abundance of these transcripts (Figure 2C and supplemental Figure 4A). The negative control transcript (GAPDH) was unaffected (Figure 2C). Accordingly, siRNA-mediated knockdown of eIF4E in U2OS resulted in lower

levels of BCL6, MYC, and BCL2 proteins (Figure 2C). Overall, these results suggest that BCL6, BCL2, and MYC are nuclear export targets of eIF4E.

In order to more rigorously distinguish whether effects of eIF4E on BCL6 are due solely to nuclear export or might also be linked to more efficient translation, we performed similar experiments, but this time using an eIF4E mutant ($eIF4E^{S53A}$) that disrupts its export function leaving translation intact, and an eIF4E mutant ($eIF4E^{W73A}$) that disrupts its effect on translation but not mRNA transport, using U2OS cells as a tractable model for these transfection experiments (Figure 2D).[16,21,23] Similar to wild-type eIF4E overexpression, the nuclear export of BCL6 mRNA was elevated to more than threefold in $eIF4E^{W73A}$ mutant cells relative to vector, whereas GAPDH was unaffected (Figure 2E). This corresponded to increased BCL6 protein levels (Figure 2F). On the contrary, $eIF4E^{S53A}$ did not increase BCL6 (or GAPDH) nuclear mRNA export or protein levels (Figure 2E-F). We observed a similar effect at the transcript and protein levels for BCL2 and MYC expression (Figure 2F). Total levels of BCL6, MYC, BCL2, and GAPDH mRNA were not changed in cells transduced with eIF4E mutants (supplemental Figure 4B).

To directly determine the binding of BCL6 mRNA to nuclear eIF4E, we carried out eIF4E immunoprecipitation from nuclear fractions followed by quantitative polymerase chain reaction (RIP-qPCR). We found that BCL6 transcripts, like BCL2 and MYC, were highly enriched in eIF4E RIPs relative to nuclear input ($P < .0001$ for all genes; Figure 2G), suggesting a direct binding of eIF4E to BCL6 mRNA. RNAs exported by eIF4E contain a 50-nucleotide element in the 3′ untranslated region (UTR) known as a 4E-SE element.[16] We found one of these elements present in the 3′UTR of BCL6. To determine the role of the 3′UTR in the mRNA export of BCL6, we transfected U2OS cells overexpressing wild-type eIF4E with a construct expressing luciferase fused to the 3′UTR of BCL6 (luc-BCL6) or luciferase only control and monitored the export of luciferase transcripts. Consistently, eIF4E overexpression leads to a significantly increased export of luc-BCL6 but not luciferase alone ($P < .0001$; Figure 2H), whereas total mRNA levels of luc-BCL6 were not affected (Figure 2H). Importantly, there was no effect on endogenous GAPDH mRNAs (negative control), which are not eIF4E targets (Figure 2H). BCL6 is thus a direct mRNA export target of eIF4E. Our data suggest eIF4E regulates BCL6 expression through increased mRNA export but not through more efficient translation. To further investigate this, we carried out polysomal fractionation in U2OS cells overexpressing eIF4E or control GFP and analyzed BCL6 mRNA in each fraction by qPCR. Here, BCL6 exhibited only a modest shift to higher-molecular-weight polysomes in the presence of eIF4E. In contrast, vascular endothelial growth factor A, an established translational target of eIF4E,[26] manifested a substantial polysomal shift (supplemental Figure 5A-C). These results further underline that eIF4E facilitates BCL6 protein expression mainly through nuclear export of its mRNA, at least in this cell type.

Nuclear eIF4E controls an extended oncogenic program in lymphoma cells

The nuclear targets of eIF4E are cell-type specific. We therefore determined whether eIF4E regulates BCL6, MYC, and BCL2 transcripts in the context of DH/TH DLBCL cells. Similar to U2OS cells, siRNA-mediated knockdown of eIF4E in the TH DoHH2 cell line resulted in lower levels of BCL6, MYC, and BCL2 proteins (Figure 3A and supplemental Figure 6). We then performed RIP-qPCR in nuclear extracts of DoHH2, OCI-Ly1, and SU-DHL6 DH/TH cell lines. We found that BCL6, BCL2, and MYC transcripts were significantly enriched compared with control mRNA in eIF4E RIPs relative to input in OCI-Ly1 ($P < .0001$ for all genes; Figure 3B), SU-DHL6 cells ($P < .0001$, $P = .005$, and $P < .0001$, respectively; Figure 3B), and DoHH2 cells ($P < .0001$ for all genes; Figure 3B) indicating that nuclear eIF4E binds to these transcripts in this specific cellular context. There were no significant changes in GAPDH transcripts used as negative control (Figure 3B).

To determine the extent of nuclear eIF4E activity in DH/TH DLBCLs and how these programs can support the oncogenic activity of BCL6, MYC, and/or BCL2 transcripts, we conducted eIF4E RIP of nuclear RNA followed by RNA-seq in OCI-Ly1 cells in biological triplicates. Compared with the nuclear input, eIF4E binding was significantly enriched in 3958 transcripts (Figure 3C and supplemental Table 1). BCL6, MYC, and BCL2 were enriched 5.4-, 1.2-, and 2.7-fold, respectively, by this method. Pathways analysis suggested a role of eIF4E preferential nuclear cargos in processes like B-cell receptor signaling (eg, *AKT*, *BTK*, *BCL6*, *CD19*, *CD22*, *CSK*, *NFAT*, *RELA*, *SHC1*), DNA methylation and epigenetic regulation (eg, *DNMT1*, *DNMT3A*, *HDAC1*, *MBD2*, *MBD3*), and transfer RNA charging/metabolism (eg, *AARS*, *CARS*, *HARS*, *LARS*) (Figure 3C and supplemental Figure 7), overall indicating that eIF4E regulates a vast network of lymphoma-sustaining pathways. eIF4E target transcripts include components of BCL6 corepressor complexes like SMRT, NCOR, BCOR, HDAC1, HDAC3, HDAC7, PPARD, and SIN3A (Figure 3D); MYC transcriptional complexes like MAX, EP300, RELA, YY1AP1, E2F1, NCL, TERT, and TRRAP (Figure 3D); and BCL2 interacting proteins like BCL-W (BCL2L2), APAF1, and BNIPL (Figure 3D).

We next examined whether disruption of eIF4E binding to BCL6, MYC, and BCL2 transcripts could impair their export and preferential translation in the DH/TH cell lines OCI-Ly1, SU-DHL6, and DoHH2. For these studies, we used the small molecule ribavirin, which competes for the methyl-cap binding site and so prevents eIF4E from binding to its mRNA targets.[22] We found that ribavirin significantly decreased cytosolic to nuclear ratios of BCL6, MYC, and BCL2 mRNA, but not of GAPDH, in all the cell lines tested (Figure 3E).

TH lymphomagenic transcripts are simultaneously targeted by ribavirin in vitro and in vivo

The data discussed above indicate that ribavirin decreases the nuclear export of BCL6, MYC, and BCL2 in DH/TH lymphoma cells overexpressing these transcripts. To determine the effect of eIF4E inhibition on the cytosolic translation of these genes, we exposed OCI-Ly1, DoHH2, and SU-DHL6 cells to ribavirin followed by polysomal fractionation and qPCR. We found that ribavirin depleted these mRNAs (but not GAPDH) from the higher-molecular-weight polysomal fractions (Figure 4A and supplemental Figure 8A). Importantly, ribavirin did not affect ribosomal assembly (Figure 4B) or change total mRNA levels in these DLBCL cell lines (supplemental Figure 8B). Ribavirin did not impact global protein production as shown in the TH cell line OCI-Ly1 (Figure 4C). Overall, these data suggest that in the context of DH/TH lymphoma cells, eIF4E influences both nuclear export and translation of oncogenic transcripts. Accordingly, ribavirin treatment of 48 hours resulted in reduced protein levels of BCL6, MYC, and BCL2 in the DH/TH DLBCL cell lines SU-DHL6 (Figure 4D, blot), OCI-Ly1, and DoHH2 (Figure 4D, blots shown in Figure 5A and supplemental Figure 10). Is noteworthy that, unlike U2OS cells, we also observed translational control of these transcripts in lymphoma cells highlighting the relevance of context to this type of regulation.

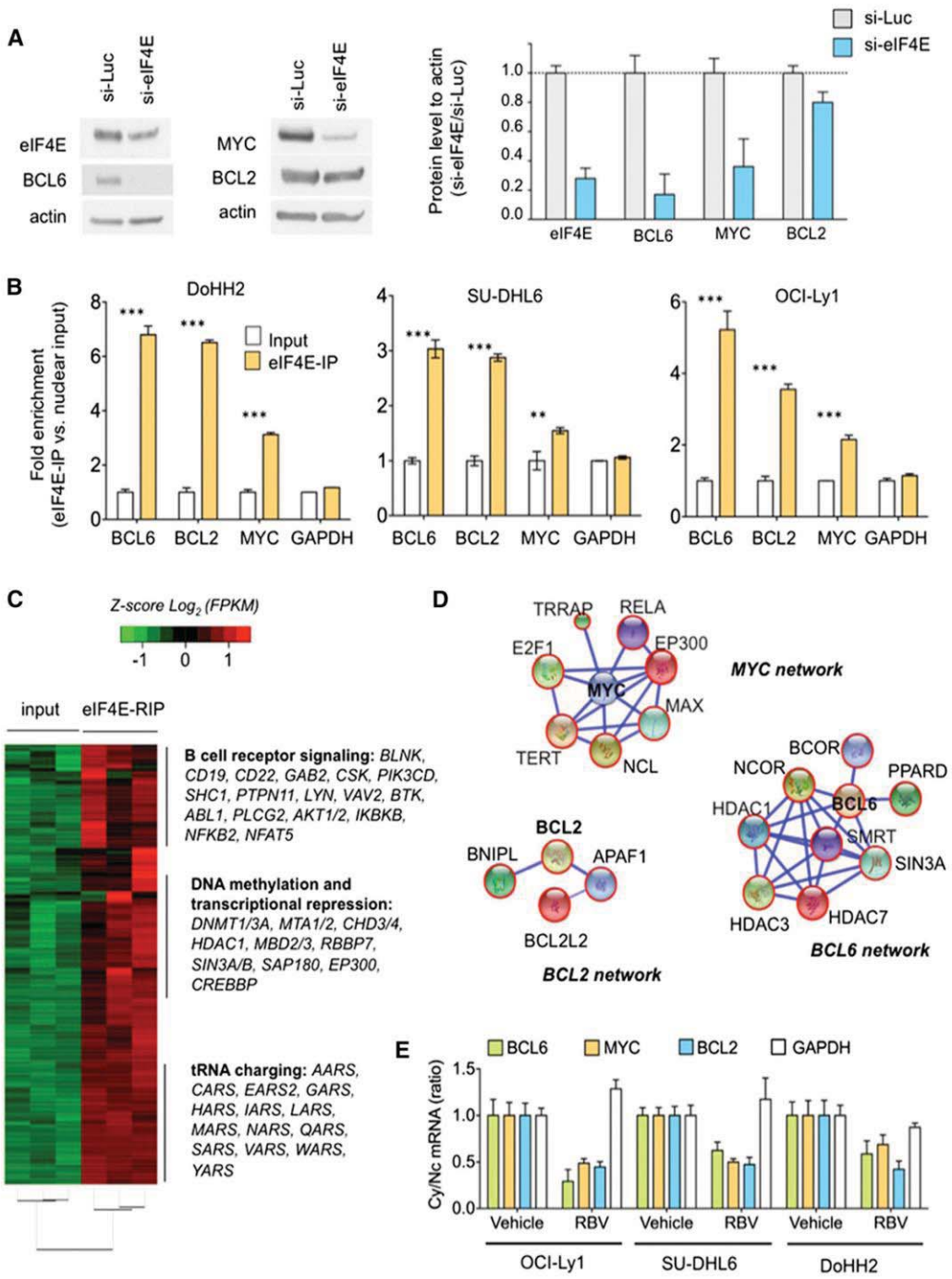

Figure 3. Nuclear eIF4E regulates the export of lymphomagenic transcripts. (A) Protein levels of BCL6, BCL2, MYC, and eIF4E in the DH/TH DoHH2 cells transfected with siRNA for luciferase (as control) or siRNA for eIF4E. Protein quantification is shown on the right for triplicate experiments as mean ± standard error of the mean (SEM). (B) eI4FE mRNA immunoprecipitation for BCL6, MYC, BCL2, and GAPDH (as control) in DoHH2, SU-DHL6, and OCI-Ly1 nuclear fractions. Results expressed as fold enrichment over nuclear input. ***$P < .001$ and **$P < .05$ (Student t test for triplicates). (C) eI4FE RIP sequencing (RIP-seq) in OCI-Ly1 cells (vs nuclear input). Selected transcripts and pathways differentially enriched in eIF4E RIPs are shown on the right. (D) eIF4E nuclear targets that sustain BCL6, MYC, and BCL2 activity in lymphoma cells depicted as "networks" from Search Tool for the Retrieval of Interacting Genes/Proteins analysis. Transcripts identified in this eIF4E RIP-seq are shown in red circles. (E) Effect of ribavirin (RBV) on the mRNA nuclear export (determined by mRNA cytosolic/nuclear ratio) of BCL6, MYC, BCL2, and GAPDH (as control) in SU-DHL6, OCI-Ly1, and DoHH2 cells.

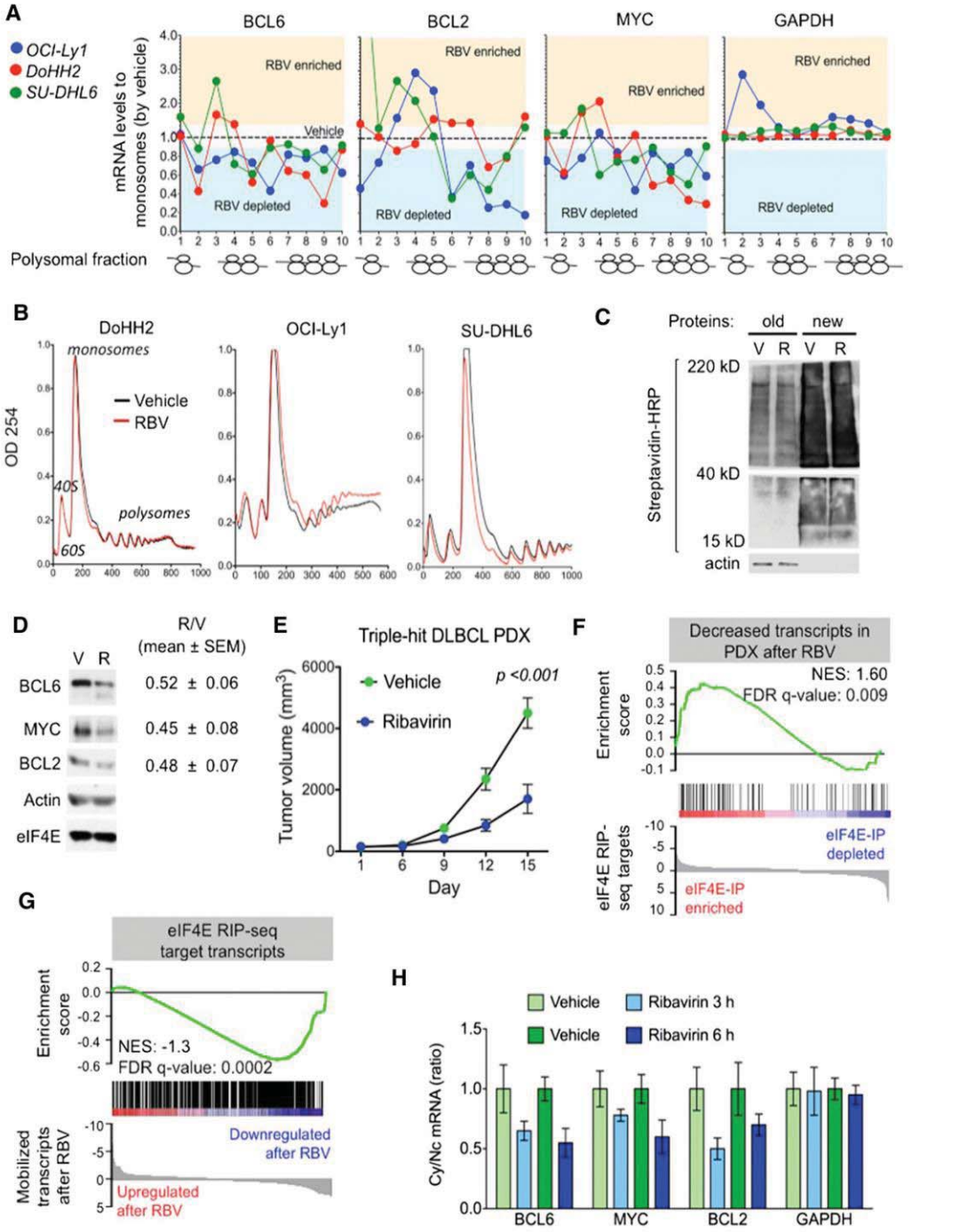

Figure 4. Ribavirin is active a TH DLBCL patient-derived xenograft (PDX) model. (A) Polysomal profiling of BCL6, BCL2, MYC, and GAPDH (as control) transcripts in OCI-Ly1, DoHH2, and SU-DHL6 cells treated with vehicle (black dotted line) vs ribavirin (RBV). Each profiling is normalized to the respective vehicle represented with a dotted central line. Points localized above and below the line represent polysome fractions enriched and depleted in RBV-treated cells. (B) Total polysomal profiling of DoHH2, OCI-Ly1, and SU-DHL6 cells treated with vehicle (black line) vs ribavirin (red line). (C) Total protein levels in OCI-Ly1 cells treated with vehicle (V) and ribavirin (R). Previously synthesized protein is marked as old and newly synthesized protein is marked as new. Actin was used as control. (D) Protein levels of BCL6, BCL2, MYC, eIF4E, and actin (as control) in SU-DHL6 cells treated with vehicle (V) vs ribavirin (R) for 48 hours. Densitometry analysis is shown on the right for replicates experiments as mean ± SEM conducted in SU-DHL6, OCI-Ly1, and DoHH2 cell lines. (E) In vivo effect of ribavirin (blue dots) vs vehicle (green dots) in the PDX-4 mice. (F-G) Gene Set Enrichment Analysis of decreased transcripts upon ribavirin treatment in PDX-4 mice and eIF4E nuclear targets from RIP-seq experiments. (H) Cytosolic vs nuclear distribution of BCL6, BCL2, MYC, and GAPDH (as control) mRNAs from the PDX-4 after ribavirin treatment of 3 hours or 6 hours. FDR, false discovery rate; NES, normalized enrichment score.

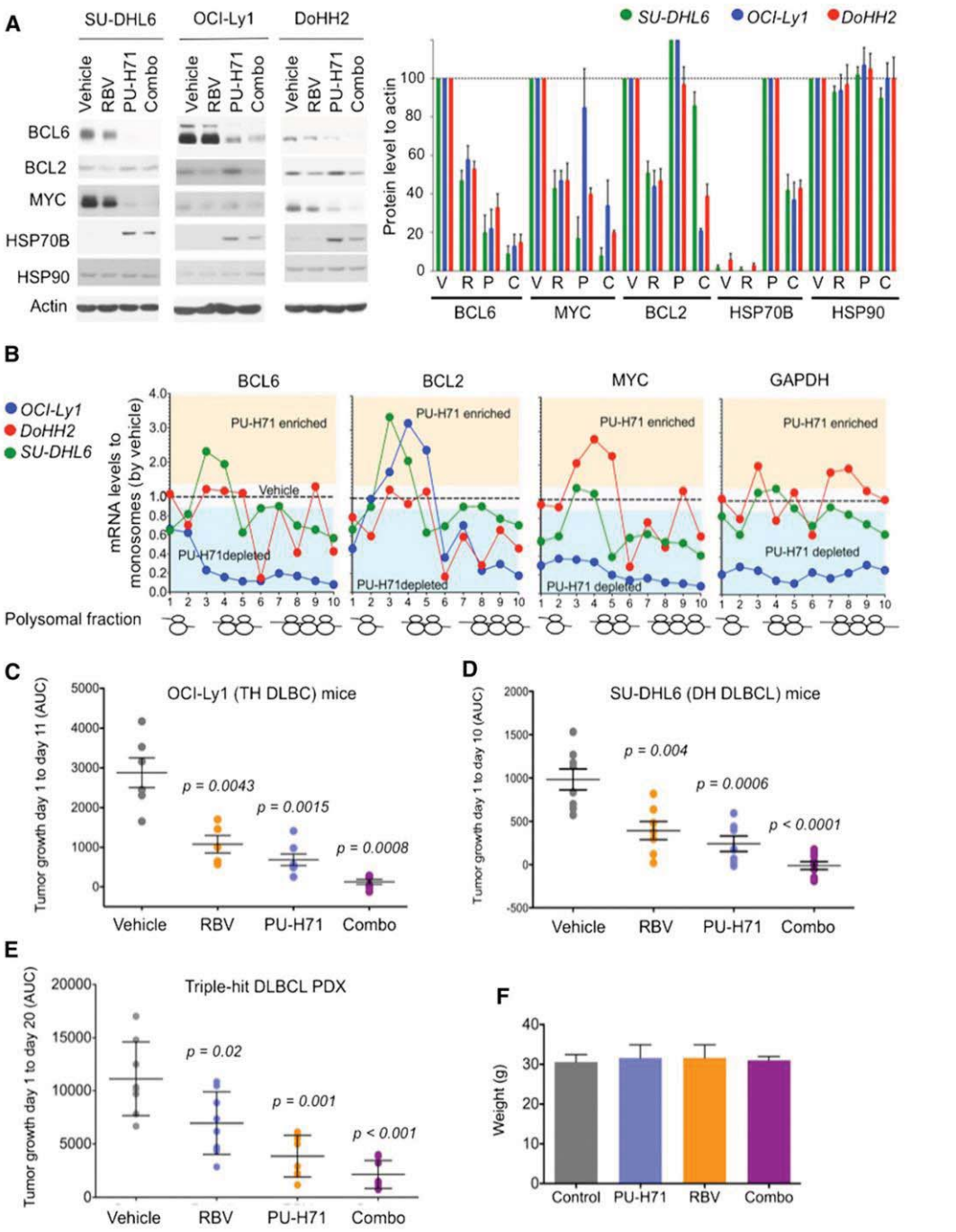

Figure 5. Antilymphoma effect of combined inhibition of eIF4E and TEHsp90. (A) Effect on BCL6, BCL2, MYC, Hsp70, Hsp90, and actin (as control) protein abundance of vehicle, ribavirin (RBV), PU-H71, and their combination (combo) in SU-DHL6 (SU6), DoHH2 (Do2), and OCI-Ly1 (Ly1) cells. Densitometry analysis is shown on the right for triplicate experiments as mean ± SEM. C, combination; P, PU-H71; R, ribavirin; V, vehicle. (B) BCL6, MYC, BCL2, and GAPDH polysomal profiling of OCI-Ly1, DoHH2, and SU-DHL6 cells treated with vehicle (black dotted line) or the TEHsp90 inhibitor PU-H71. Each profiling is normalized to its respective vehicle represented with a dotted central line. Points localized below the line represent polysome fractions depleted in PU-H71-treated cells. (C-D) Tumor growth (in AUC from day 1 to day 10) of OCI-Ly1 and SU-DHL6 xenografted mice. *P* values are shown on top for each group for the comparison with vehicle-treated mice. (E) Tumor growth (in AUC from day 1 to day 20) of TH DLBCL PDX xenografted mice. *P* values are shown on top for each group for the comparison with vehicle-treated mice. (F) Body weight at day 21 of mice from panel E.

To assess the antilymphoma effect of eIF4E inhibition, we established a PDX in NSG mice. The specimen was isolated from a newly diagnosed patient harboring a TH DLBCL. The patient presented a stage IVb, International Prognostic Index 4 disease with bone marrow infiltration and was refractory to multiple therapeutic regimens (supplemental Figure 9A). Once engrafted in NSG mice, the specimen was followed by FISH and immunoblotting for MYC, BCL2, and BCL6 to ensure it remained a TH disease with similar expression levels of these proteins (supplemental Figure 9A). The fourth generation of PDX (PDX-4) was tested ex vivo for doxorubicin and ribavirin response. Once we proved PDX-4 was chemoresistant to doxorubicin and responsive to ribavirin ex vivo (supplemental Figure 9B), we expanded into NSG mice for preclinical therapeutic assessment. To determine whether primary human DLBCL is eIF4E dependent in vivo, we implanted PDX-4 tumors into the flanks of 10 NSG mice, and when tumors were palpable (75-100 mm^3), mice were randomized to receive vehicle or ribavirin 80 mg/kg twice daily intraperitoneally for 10 days. We found a significant reduction in tumor growth in PDX-4 after ribavirin treatment ($P < .001$, Student t test; Figure 4E) with no signs of toxicity by weight or by macroscopic and microscopic examination of organs including liver, kidney, lungs, bone marrow, and heart. We then analyzed the transcriptome in vehicle vs ribavirin-treated PDX-4 (at day 10) by RNA-seq followed by Gene Set Enrichment Analysis. We found that significantly decreased transcripts in PDX-4 after ribavirin were significantly enriched in eIF4E RIP-seq targets obtained from the TH cell line OCI-Ly1 (NES, 1.60; FDR q value, 0.009; Figure 4F). Conversely, eIF4E RIP-seq transcripts were characterized by decreased enrichment of these transcripts upon ribavirin treatment (NES, −1.3; FDR q value, 0.0002; Figure 4G).

To further confirm the pharmacodynamic action of ribavirin on mRNA transport in the primary human PDX setting, we examined the abundance of BCL6, BCL2, and MYC transcripts in the cytoplasm of implanted PDX-4 cells. The patient lymphoma cells were implanted into the flanks of 8 NSG recipients followed by exposure to ribavirin 80 mg/kg intraperitoneally (n = 4) for 3 and 6 hours (n = 2 mice, respectively), a clinically achievable dose in patients. An additional 4 PDX-4-implanted mice were treated in similar fashion with vehicle. We observed a decrease in the cytosolic/nuclear ratio of BCL6, BCL2, and MYC as early as 3 hours after the administration (Figure 4H).

Ribavirin and PU-H71 show cooperative antilymphoma activity in DH/TH DLBCL

Given our initial findings showing eIF4E is a partner of TEHsp90 in the nuclei of DH/TH cells, we reasoned that combining TEHsp90- and eIF4E-targeted therapies would achieve greater target inhibition and hence antilymphoma activity. We therefore compared and contrasted the effect of ribavirin, PU-H71, or the combination on the expression of BCL6, MYC, and BCL2 by immunoblotting in the DH/TH DLBCL cell lines OCI-Ly1, SU-DHL6, and DoHH2. Compared with either drug alone, the combination more potently suppressed the expression of BCL6 and MYC in all 3 cell lines (Figure 5A and supplemental Figure 10) and BCL2 in OCI-Ly1 cells (Figure 5A and supplemental Figure 10). At this time point, PU-H71 stabilizes or increases BCL2 protein expression, a known effect of Hsp90 inhibitors before inducing protein degradation.[12] Next, we explored the effects of PU-H71 on mRNA translation because other components of the translational machinery complex like eIF4A1, eIF2, eIF3, and PABP were also associated with TEHsp90 in the TH DLBCL cell line OCI-Ly1 (supplemental Figure 1).[12] We found that TEHsp90 inhibition rapidly promotes ribosomal disassembly (ie, decreases polysomes) while increasing 40S, 60S, and monosome fractions in OCI-Ly1, DoHH2, and SU-DHL6 cells (supplemental Figure 11). This effect was more pronounced for actively translated mRNAs like BCL6, MYC, and BCL2 in DH/TH cell lines (Figure 5B and supplemental Figure 12) and likely contributes to the decreased MYC and BCL6 protein levels observed with PU-H71 (Figure 5A). The effects on polysomal assembly are unique to TEHsp90 inhibition because ribavirin treatment does not affect polysome integrity[22] (see also Figure 4B). Hence, suppression of TEHsp90 has additional effects on translation than those conferred by its interaction with eIF4E. This is also evident in the disassembling of polysomes on GAPDH in OCI-Ly1 cells (Figure 5B and supplemental Figure 12).

To examine the antilymphoma effect of this combination, we xenografted TH OCI-Ly1 cells (n = 21) and DH SU-DHL6 cells (n = 31) in SCID mice, and TH PDX-4 (n = 32) in NSG mice. Once tumors developed to a palpable size (75-100 mm^3), we treated them with vehicle control (n = 6, 8, and 8 in OCI-Ly1, SU-DHL6, and PDX-4, respectively), ribavirin 40 mg/kg per day (n = 5, 7, and 8 in OCI-Ly1, SU-DHL6, and PDX-4, respectively), PU-H71 25 mg/kg per day (n = 5, 7, and 8 in OCI-Ly1, SU-DHL6, and PDX-4, respectively), or the combination (n = 5, 9, and 8 in OCI-Ly1, SU-DHL6, and PDX-4, respectively) for 10 days. Compared with vehicle-treated mice, ribavirin and PU-H71 significantly decreased lymphoma growth in OCI-Ly1 mice ($P = .0043$ and $P = .0015$, respectively; Figure 5C), SU-DHL6 mice ($P = .004$ and $P = .0006$, respectively; Figure 5D), and PDX-4 mice ($P = .001$ and $P = .02$, respectively; Figure 5E). Compared with vehicle-treated mice, the combination of ribavirin with PU-H71 suppressed lymphoma growth more profoundly in the 3 models ($P = .0008$ in OCI-Ly1, $P < .0001$ in SU-DHL6, and $P < .0001$ in PDX-4; Figure 5C-E). There was no macroscopic or microscopic evidence of toxicity in any mice. There were no changes in body weight by the end of the treatment (Figure 5F) or in blood biochemistry values (supplemental Figure 2).

In the previous studies, we monitored Hsp70 as a control for TEHsp90 inhibition. It is well-known that Hsp70 becomes activated under these conditions.[9,10] This elevation of Hsp70 induces antiapoptotic mechanisms[27] leading to resistance to Hsp90 inhibitors and limiting the activity of these drugs in the clinic. Surprisingly, we noted that eIF4E inhibition reduced the increase in Hsp70 (40%-60%) (Figure 5A). Given these findings, we examined whether Hsp70 was a direct eIF4E target. Indeed, we found that ribavirin decreased the nuclear export of Hsp70 without affecting its total RNA levels in OCI-Ly1, SU-DHL6, and DoHH2 cells (Figure 6A). Accordingly, Hsp70 transcripts specifically bound eIF4E in the nuclear fraction in all these DH/TH cell lines, supporting that Hsp70 (*HSPA6*) mRNA is a direct eIF4E target (Figure 6B). Further, ribavirin decreased the amount of Hsp70 on heavy polysomes as demonstrated in OCI-Ly1 cells (Figure 6C). Overall, this led to a ribavirin-induced decrease in Hsp70 abundance in SU-DHL6, OCI-Ly1, and DoHH2 cells (Figure 6D). This suggests that an additional reason for the potentiation between the 2 drugs is because ribavirin treatment enhances PU-H71 activity by reducing Hsp70. Hence, the combination of ribavirin and PU-H71 enhances each other's activity at multiple levels.

Discussion

Our findings provide a molecular basis for previous data showing that TEHsp90 had effects on mRNA metabolism on BCL6 and other

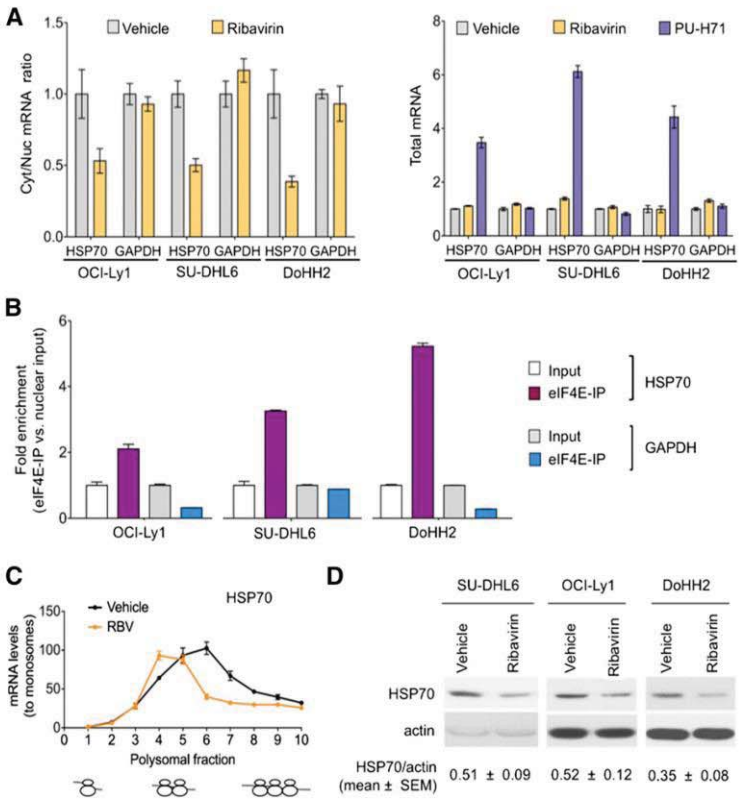

Figure 6. Ribavirin decreases TEHsp90 inhibition–induced Hsp70 upregulation. (A) Effect of ribavirin on the mRNA nuclear export (determined by mRNA cytosolic/nuclear ratio) of HSP70B (*HSPA6*) and GAPDH (as control) in OCI-Ly1, SU-DHL6, and DoHH2 cells. The effect on total mRNA is sown on the right with PU-H71 effect as control. (B) eI4FE mRNA immunoprecipitation for HSP70B and GAPDH (as control) in OCI-Ly1, SU-DHL6, and DoHH2 nuclear fractions. Results expressed as fold enrichment over nuclear input. (C) Polysomal profiling of HSP70B transcript in OCI-Ly1 cells treated with vehicle vs ribavirin (RBV). (D) Effect on Hsp70 and actin (as control) protein abundance in ribavirin- and vehicle-treated SU-DHL6, OCI-Ly1, and DoHH2 cells. Immunoblots from 50 μg of cell lysates were exposed for optimal time to visualize Hsp70 at baseline. Hsp70 protein quantification (to actin) is shown at the bottom for quadruplicate experiments as mean ± SEM.

oncogenic transcripts in DLBCL.[8] We demonstrate that TEHsp90 sustains eIF4E activity in the nucleus and cytoplasm of DH/TH lymphoma cells and that, through this interaction, the oncogenic activities of Hsp90 and eIF4E are mutually reinforced. Further, we demonstrate that eIF4E elevation, through its effects on Hsp70 mRNA export and translation, likely drives Hsp90 drug resistance. Thus, eIF4E inhibition increases the potency of Hsp90 inhibitors, as we observe in our xenograft models. These findings suggest a role for eIF4E in the regulation of the cellular stress response, particularly in the oncogenic milieu. In this context, we described for the first time that nuclear eIF4E controls an extensive network of transcripts with roles in B-cell receptor signaling (BTK, CD19, CD22); folate, glucose and amino acid metabolism (MTHFD1, MTOR, PI3Ks, MAPKs, YARS, CARS); DNA repair and cellular stress (PARPs, XRCC1, RAD50, RAD52, Hsp70, Hsp40); and transcriptional regulation including chromatin remodeling and epigenetic enzymes (DNMTs, HDACs, MBDs, CHDs, EP300). These findings explain the dependence of lymphoma cells on the activity of eIF4E to fully express the transformation capabilities of classic lymphoma oncogenes such as BCL6, BCL2, and MYC that are also eIF4E targets. Therefore, by targeting eIF4E both the oncogenes and their supporting network of genes are simultaneously dismantled.

Our findings provide a strong rationale for translating eIF4E inhibitors and TEHsp90 inhibitors in the treatment of aggressive diseases such as DH/TH lymphomas. Importantly, ribavirin is well tolerated and leads to responses in patients with AML.[19] In this trial, ribavirin showed single-agent activity in patients with poor-prognosis AML, including 6 patients (out of 11 evaluable for response) with remissions or blast responses.[19] Micromolar plasma concentrations used here are achievable in humans with minimal toxicity.[19,28,29] Similar to ribavirin, early stage trials (www.clinicaltrials.gov, #NCT01581541) indicate that the TEHsp90 inhibitor PU-H71 is safe, and thus the combination of these 2 drugs seems feasible, as our studies in mice indicate. Remarkably, by decreasing Hsp70 export and translation, ribavirin could diminish one of the most important mechanisms in the acquired resistance to this class of Hsp90 inhibitors. In summary, our data provide a novel and potentially nontoxic mechanistic-based approach to target aggressive B-cell lymphomas harboring multiple oncogene activation.

Acknowledgments

The authors thank Drs Cristina Montagna and Jidong Shan of the Molecular Cytogenetic Core of the Albert Einstein College of Medicine for their help with FISH assays in cell lines.

This work was supported by grants from the Leukemia and Lymphoma Society (LLS 6078-14 to L.C., LLS 6478 and LLS 6160 to K.L.B.B.), the Raymond and Beverly Sackler Scholar (L.C.), and the National Institutes of Health, National Cancer Institute (grants R01 98571 and R01 80728) (K.L.B.B.). K.L.B.B. holds a Canada Research Chair.

Authorship

Contribution: B.C.-K., T.M.F., R.L.G., R. Marullo, N.C.-V., A.V., H.Z., and J.P. conducted cell-based experiments, RIP-seq, and analysis; S.Y., F.T., M.G., P.G., M.L., R. Machiorlatti, and G.I. conducted animal experiments and established PDX; T.T. and G.C. prepared and provided reagents; A.M., O.E., K.L.B.B., and L.C. supervised research and designed experiments; and B.C.-K., T.M.F., A.M., K.L.B.B., and L.C. wrote the manuscript.

Conflict-of-interest disclosure: Memorial Sloan Kettering Cancer Center holds the intellectual rights to PU-H71. Samus Therapeutics, of which G.C. has partial ownership, has licensed PU-H71. The remaining authors declare no competing financial interests.

Correspondence: Katherine L. B. Borden, Institute for Research in Immunology and Cancer and Department of Pathology and Cell Biology, Université de Montréal, Montréal, QC, Canada; e-mail: katherine.borden@umontreal.ca; and Leandro Cerchietti, Hematology and Oncology Division, Weill Cornell Medical College, 1300 York Ave, C620B, New York, NY 10065; e-mail: lec2010@med.cornell.edu.

References

1. Larouche JF, Berger F, Chassagne-Clément C, et al. Lymphoma recurrence 5 years or later following diffuse large B-cell lymphoma: clinical characteristics and outcome. *J Clin Oncol.* 2010; 28(12):2094-2100.
2. Sehn LH, Connors JM. Treatment of aggressive non-Hodgkin's lymphoma: a North American perspective. *Oncology (Williston Park).* 2005; 19(4, suppl 1):26-34.
3. Barrans S, Crouch S, Smith A, et al. Rearrangement of MYC is associated with poor prognosis in patients with diffuse large B-cell lymphoma treated in the era of rituximab. *J Clin Oncol.* 2010;28(20):3360-3365.
4. Savage KJ, Johnson NA, Ben-Neriah S, et al. MYC gene rearrangements are associated with a poor prognosis in diffuse large B-cell lymphoma patients treated with R-CHOP chemotherapy. *Blood.* 2009;114(17):3533-3537.
5. Johnson NA, Savage KJ, Ludkovski O, et al. Lymphomas with concurrent BCL2 and MYC translocations: the critical factors associated with survival. *Blood.* 2009;114(11):2273-2279.
6. Vegliante MC, Royo C, Palomero J, et al. Epigenetic activation of SOX11 in lymphoid neoplasms by histone modifications. *PLoS One.* 2011;6(6):e21382.
7. Niitsu N, Okamoto M, Miura I, Hirano M. Clinical features and prognosis of de novo diffuse large B-cell lymphoma with t(14;18) and 8q24/c-MYC translocations. *Leukemia.* 2009;23(4):777-783.
8. Cerchietti LC, Lopes EC, Yang SN, et al. A purine scaffold Hsp90 inhibitor destabilizes BCL-6 and has specific antitumor activity in BCL-6-dependent B cell lymphomas. *Nat Med.* 2009;15(12): 1369-1376.
9. Trepel J, Mollapour M, Giaccone G, Neckers L. Targeting the dynamic HSP90 complex in cancer. *Nat Rev Cancer.* 2010;10(8):537-549.
10. Taldone T, Ochiana SO, Patel PD, Chiosis G. Selective targeting of the stress chaperome as a therapeutic strategy. *Trends Pharmacol Sci.* 2014;35(11):592-603.
11. Cerchietti LC, Hatzi K, Caldas-Lopes E, et al. BCL6 repression of EP300 in human diffuse large B cell lymphoma cells provides a basis for rational combinatorial therapy. *J Clin Invest.* 2010; 120(12):4569-4582.
12. Goldstein RL, Yang SN, Taldone T, Chang B, Gerecitano J, Elenitoba-Johnson K, Shaknovich R, Tam W, Leonard JP, Chiosis G, et al. Pharmacoproteomics identifies combinatorial therapy targets for diffuse large B cell lymphoma. *J Clin Invest.* 2015;2015:80714.
13. Moulick K, Ahn JH, Zong H, et al. Affinity-based proteomics reveal cancer-specific networks coordinated by Hsp90. *Nat Chem Biol.* 2011; 7(11):818-826.
14. Taldone T, Patel PD, Patel M, et al. Experimental and structural testing module to analyze paralogue-specificity and affinity in the Hsp90 inhibitors series. *J Med Chem.* 2013;56(17): 6803-6818.
15. Ruggero D, Montanaro L, Ma L, et al. The translation factor eIF-4E promotes tumor formation and cooperates with c-Myc in lymphomagenesis. *Nat Med.* 2004;10(5):484-486.
16. Culjkovic-Kraljacic B, Baguet A, Volpon L, Amri A, Borden KL. The oncogene eIF4E reprograms the nuclear pore complex to promote mRNA export and oncogenic transformation. *Cell Reports.* 2012;2(2):207-215.
17. Truitt ML, Conn CS, Shi Z, et al. Differential requirements for eIF4E dose in normal development and cancer. *Cell.* 2015;162(1): 59-71.
18. Osborne MJ, Borden KL. The eukaryotic translation initiation factor eIF4E in the nucleus: taking the road less traveled. *Immunol Rev.* 2015; 263(1):210-223.
19. Assouline S, Culjkovic B, Cocolakis E, et al. Molecular targeting of the oncogene eIF4E in acute myeloid leukemia (AML): a proof-of-principle clinical trial with ribavirin. *Blood.* 2009; 114(2):257-260.
20. Pettersson F, Del Rincon SV, Emond A, et al. Genetic and pharmacologic inhibition of eIF4E reduces breast cancer cell migration, invasion, and metastasis. *Cancer Res.* 2015;75(6): 1102-1112.
21. Tcherkezian J, Cargnello M, Romeo Y, et al. Proteomic analysis of cap-dependent translation identifies LARP1 as a key regulator of 5'TOP mRNA translation. *Genes Dev.* 2014;28(4): 357-371.
22. Kentsis A, Topisirovic I, Culjkovic B, Shao L, Borden KL. Ribavirin suppresses eIF4E-mediated oncogenic transformation by physical mimicry of the 7-methyl guanosine mRNA cap. *Proc Natl Acad Sci USA.* 2004;101(52):18105-18110.
23. Culjkovic B, Topisirovic I, Skrabanek L, Ruiz-Gutierrez M, Borden KL. eIF4E is a central node of an RNA regulon that governs cellular proliferation. *J Cell Biol.* 2006;175(3):415-426.
24. Graff JR, Konicek BW, Vincent TM, et al. Therapeutic suppression of translation initiation factor eIF4E expression reduces tumor growth without toxicity. *J Clin Invest.* 2007;117(9): 2638-2648.
25. Soni A, Akcakanat A, Singh G, et al. eIF4E knockdown decreases breast cancer cell growth without activating Akt signaling. *Mol Cancer Ther.* 2008;7(7):1782-1788.
26. Mamane Y, Petroulakis E, Rong L, Yoshida K, Ler LW, Sonenberg N. eIF4E–from translation to transformation. *Oncogene.* 2004;23(18): 3172-3179.
27. Lianos GD, Alexiou GA, Mangano A, et al. The role of heat shock proteins in cancer. *Cancer Lett.* 2015;360(2):114-118.
28. Zahreddine HA, Culjkovic-Kraljacic B, Assouline S, et al. The sonic hedgehog factor GLI1 imparts drug resistance through inducible glucuronidation. *Nature.* 2014;511(7507):90-93.
29. Assouline S, Culjkovic-Kraljacic B, Bergeron J, et al. A phase I trial of ribavirin and low-dose cytarabine for the treatment of relapsed and refractory acute myeloid leukemia with elevated eIF4E. *Haematologica.* 2015;100(1):e7-e9.

Supplementary Methods:

Growth inhibition determination. DLBCL cells (OCI-Ly1, OCI-LY3, OCI-LY4, OCI-LY7, OCI-Ly8, OCI-LY10, OCI-LY18, OCI-LY19, SUDHL-4, SUDHL-5, SUDHL-6, SUDHL-7, SUDHL-8, SUDHL-10, Pfeiffer, Farage, Toledo, Karpas-422, Karpas-231, WSU-NHL, VAL, DoHH2, DB, SC-1, RC-K8, HT, WSU-DLCL2, NU-DHL-1, NU-DUL-1, RL, OZ, RI-1 or RIVA, Granta-452, HBL-1 and TMD8) were grown on U-bottom 96-well plates at respective concentrations sufficient to keep untreated cells under exponential growth by the time of read-out 48h after treatment. Cell viability was determined using a fluorometric assay based on the resazurin reduction activity of the cells (Cell Titer Blue, Promega) and trypan blue dye-exclusion (Sigma). Fluorescence was determined for controls and three replicates per treatment condition using the Synergy4 microplate reader (BioTek). Standard curves were obtained for each individual cell line with the cell count and luminescence values. The number of viable cells was obtained using the least-squares regression method of the standard curve and by doing a ratio metric quantification of viable cells normalized to the respective controls. Experiments were conducted in triplicates. A cell killing effect was calculated as the 1 – normalized viability value. Dose necessary for 50% of growth inhibition (GI_{50}) was determined using the CompuSyn software (Biosoft).

Immunohistochemistry and FISH. Immunohistochemistry: Tissues were fixed in 4% formaldehyde and embedded in paraffin. Sections were prepared, cleared in xylene, and hydrated through a descending alcohol series. Slides were boiled with antigen retrieval buffer (10 mM sodium citrate buffer pH 6.4 or 1 mM EDTA buffer pH 8.0) and cooled. Endogenous peroxidase activity was quenched by treatment with 3% hydrogen peroxide in methanol and permeabilized. After blocking, slides were incubated with biotin-conjugated antibodies. Avidin-horseradish peroxidase (HRP) was applied, and peroxidase activity was detected with DAB color substrates (Vector Laboratories) and counterstained with hematoxylin. Images were obtained using an Axioskop imaging microscope (Zeiss Inc). FISH: primary lymphoma tissues were tested for MYC mutations and positive cases were further analyzed for BCL6 and BCL2 mutations with commercial available probes. DLBCL cell lines were tested for all three mutations simultaneously using probes (BAC clones with genomic DNA of interest and labeled green for MYC, aqua for BCL2 and red for BCL6) generated and analyzed at the Molecular Cytogenetic Core of the Albert Einstein College of Medicine.

RNA nuclear export: Cellular fractionation: Briefly, around $3x10^7$cells were collected and washed twice in ice cold PBS and then resuspended in 1ml of lysis buffer B (10 mMTris pH: 8.4, 140 mM NaCl, 1. 5 mM MgCl2, 0.5% NP40, 1 mM DTT and 100U/ml RNaseOUT). Pellet-nuclear fraction was resuspended in 1ml of lysis buffer B and 1/10 volume of detergent stock (3.3% sodium deoxycholate, 6.6% Tween-40 in DEPC water) was added. This suspension was transferred back to 1.5 ml Eppendorf and spun. Pelleted nuclear fraction was rinsed in 1 ml of lysis buffer B and spun. Final pellet were resuspended in 100ml of lysis buffer B and sonicated. For RNA extraction, fractions were added to Trizol reagent (Invitrogen) and processed according to the manufacturer's instructions. RNA samples were DNAse treated (Turbo DNAse, Ambion) and reverse transcribed using MMLV reverse transcriptase (Invitrogen). RT-PCR**:** qRT-PCR analyses were performed using EXPRESS SYBR® GreenER™ qPCRSuperMix (Invitrogen) in AB StepOne thermal cycler using the relative standard curve method. Actin or GAPDH mRNA were used to normalize total and fractionated mRNA samples.

Immunoblotting. Cell pellets containing 5 x 10^6 were washed with ice-cold phosphate buffer saline and lysed with RIPA buffer (Tris-HCl 50 mM, NaCl, 150 mM, NP-40 1%, sodium deoxylcholate 0.25%, SDS 0.1%) containing fresh protease inhibitor cocktail (Roche). Lysate protein concentration was determined by BCA assay (Pierce) and 15 µg (50 µg for Hsp70) of protein sample were loaded on polyacrylamide electrophoresis pre-cast gels (BioRad). Experiments were conducted at least in independent triplicates. We used the following primary antibodies: mouse anti-BCL6 (SC-7388, Santa Cruz), rabbit anti-BCL2 (SC-7382, Santa Cruz), mouse anti-MYC (Santa Cruz SC-40), mouse anti-eIF4A1 (Santa Cruz), mouse anti-actin (SIGMA AC-15), mouse anti eIF4E (BD Biosciences), rabbit anti eIF4E (CT 040347 Millipore) and mouse monoclonal anti-HSP 70/HSC 70 (W27, SC-24, Santa Cruz).

Metabolic labeling and capture of newly synthesized protein. Newly synthesized proteins were labeled using the Click-iT Protein Labeling Kit (Invitrogen). For this, $15x10^6$ OCI-LY1 cells were pre-treated with or without freshly prepared 100 µM ribavirin (Ox-chem) for 14 h. After one wash, cells were resuspended in methionine-free RPMI 1640

medium (Gibco) supplemented with 10% dialyzed FBS (Gibco) and 100 μM ribavirin for 30 min, at which point the methionine analog L-azidohomoalanine (AHA) was added to the cell cultures (50 μM, 6 h) to allow incorporation of AHA into nascent proteins. Cells were harvested and lysed in 50 mM Tris-HCl, pH 8.0, 1% SDS, with protease and phosphatase inhibitor mixes (cOmplete and PhosSTOP, Roche). 155 μg of total protein (up to 50 μL of lysate) were used in the crosslinking of AHA-labeled nascent proteins to an alkyne-derivatized biotin in the Click-iT Protein Reaction Buffer (Invitrogen) according to manufacturer's instructions. The resulting precipitated total protein pellet was resolubilized in 100 μL of 1% SDS DPBS with protease inhibitors, followed by quenching of the SDS with 100 μL of 6% NP-40 in DPBS with inhibitors. Biotin-crosslinked nascent proteins were then captured overnight with streptavidin-coated Dynabeads M-280 (Invitrogen) and then eluted from the beads by boiling the samples for 5 min in 2% SDS loading buffer for Western Blot. The whole volume of AHA-labeled, biotin-crosslinked, streptavidin-pulled down protein was separated by SDS-PAGE together with lysate depleted of nascent protein after streptavidin incubation (10 μg theoretical total protein).

TEHsp90 proteomics. As previously described(1-6), OCI-Ly1 cells were lysed in Felts buffer (20 mM HEPES, 50 mM KCl, 5 mM $MgCl_2$, 0.01% (w/v) NP-40, freshly prepared 20 mM Na_2MoO_4) with added protease inhibitors (Roche) on ice. PU-H71 or control (HSP90 inactive chemical 2-methoxyethlamine) beads were washed three times in Felts buffer. Lysates were pre-cleared with washed control beads for one hour at 4°C. Following pre-clearing, half of each sample was incubated with either control or PU-H71 beads at 4°C overnight, saving 10% as input. Following incubation, bead conjugates were washed 3 times with Felts buffer, boiled in SDS loading buffer and resolved by PAGE followed by standard immunoblotting procedure(7). For proteomic validation experiments nuclei were fractionated from 10^7cells OCI-Ly1, SU-DHL6 and DoHH2 cells according to manufacturer's protocol (Sigma NUC-201) and then lysed in 1 mL Felts buffer. Protein concentration was assayed and 400 μg of either cytoplasmic or nuclear protein was incubated with 50 μL of control or PU-H71 beads overnight at 4C. The next day, beads were washed three times with fresh Felts buffer and complexes were resolved by SDS-PAGE followed by western blot for eIF4E and Hsp90. Twenty μg of each fraction was loaded as input and in a separate gel to determine the purity of the fractionation by blotting with MEK (cytoplasmic) and Histone H3 (nuclear).

RNA-sequencing. RIP-sequencing library preparation and analysis**:** Total nuclear input RNA and RIP samples in triplicates were treated with DNase and concentration and purity was determined by the Nanodrop (Thermo Scientific). RNA integrity was verified using the Agilent 2100 Bioanalyzer (Agilent Technologies). RIP-seq libraries were prepared using the TruSeq Stranded total RNA library prep kit (Illumina). Briefly 200 ng total nuclear RNA was RiboZero-depleted and chemically fragmented. RIP samples were already depleted of rRNAs and taken directly to chemical fragmentation. The remaining steps of the library preparation were followed according to the manufacturers instructions. Libraries were cluster amplified and sequenced for 50 cycles using the Illumina HiSeq2500. Reads were aligned to human hg19 using the STAR aligner. Genes present in the RIP and input samples were evaluated by counting how many reads map uniquely to the union of all gene exons using HTseq-count(8). Pairwise LIMMA analysis was performed on voom normalized counts using the LIMMA package(9). mRNA-sequencing library preparation and analysis: Sequencing libraries were generated with polyA+ RNA using the TruSeq RNA sample prep kit (Illumina) according to the manufacturer's instructions. Libraries were cluster amplified and sequenced for 50 cycles using the Illumina HiSeq2500. Reads were aligned to human hg19 using the STAR aligner. Gene expression values were calculated using HTseq-count, and differentially expressed genes were identified with the EdgeR package. Genes with a FDR value < 0.05 were considered differentially expressed. The Gene Expression Omnibus (GEO) accession number for the RNA-seq data sets reported are GEO: GSE63265

Supplementary Figures:

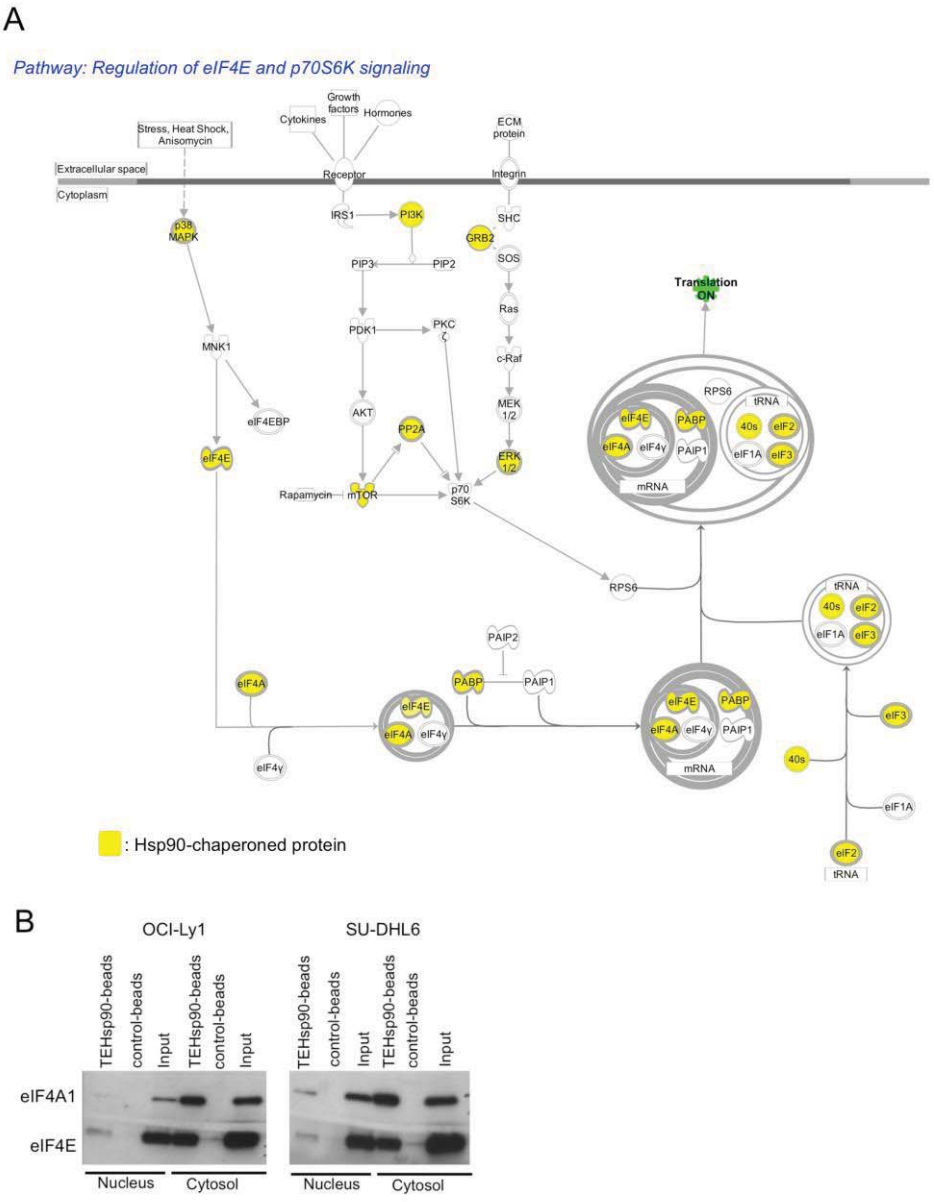

Figure S1: TEHsp90 proteomics pathway visualization. A: Ingenuity Pathway Analysis representation of the "eIF4E and p70S6K signaling" pathway from the Hsp90-chaperoned proteomics conducted in OCI-Ly1 cells. Hsp90 chaperoned proteins are shown in yellow. **B:** Affinity purification (TEHsp90 beads vs. control beads) of eIF4A1 and EIF4E in nuclear and cytosolic lysates of the TH OCI-Ly1 and DH SU-DHL6 cell lines.

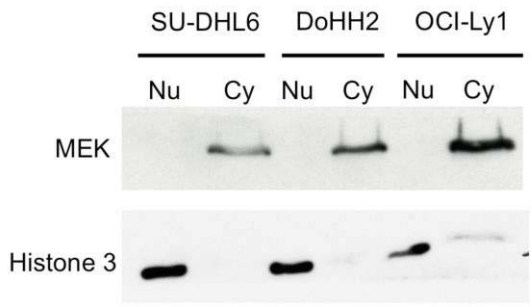

Figure S2: Nuclear and cytosolic fractionation of SU-DHL6, DoHH2 and OCI-Ly1 cells. MEK is a marker for cytosolic fraction and Histone H3 is enriched in nuclear fractions.

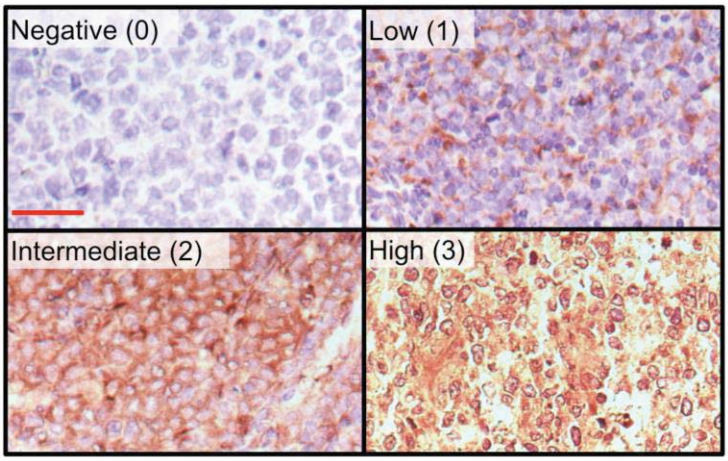

Figure S3: EIF4E is expressed in DLBCL. Representative microphotographs of eIF4E staining from 0 (negative) to 3 (positive) according to the number of eIF4E positive cells compared to total number of cells. Bar represents 50 μm.

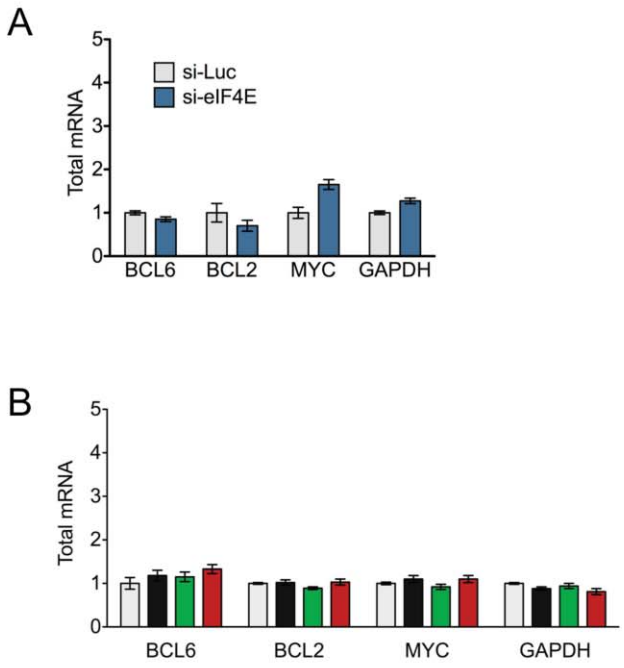

Figure S4. Total mRNA levels in U2OS overexpressing eIF4E plasmids or siRNA. **A:** Total mRNA levels of BCL6, BCL2, MYC and GAPDH in in U2OS cells transfected with siRNA for luciferase (as control) or siRNA for eIF4E. **B:** Total mRNA levels of BCL6, BCL2, MYC and GAPDH in U2OS cells engineered to express GFP (as control), eIF4E-WT, eIF4E-W73A and eIF4E-S53A.

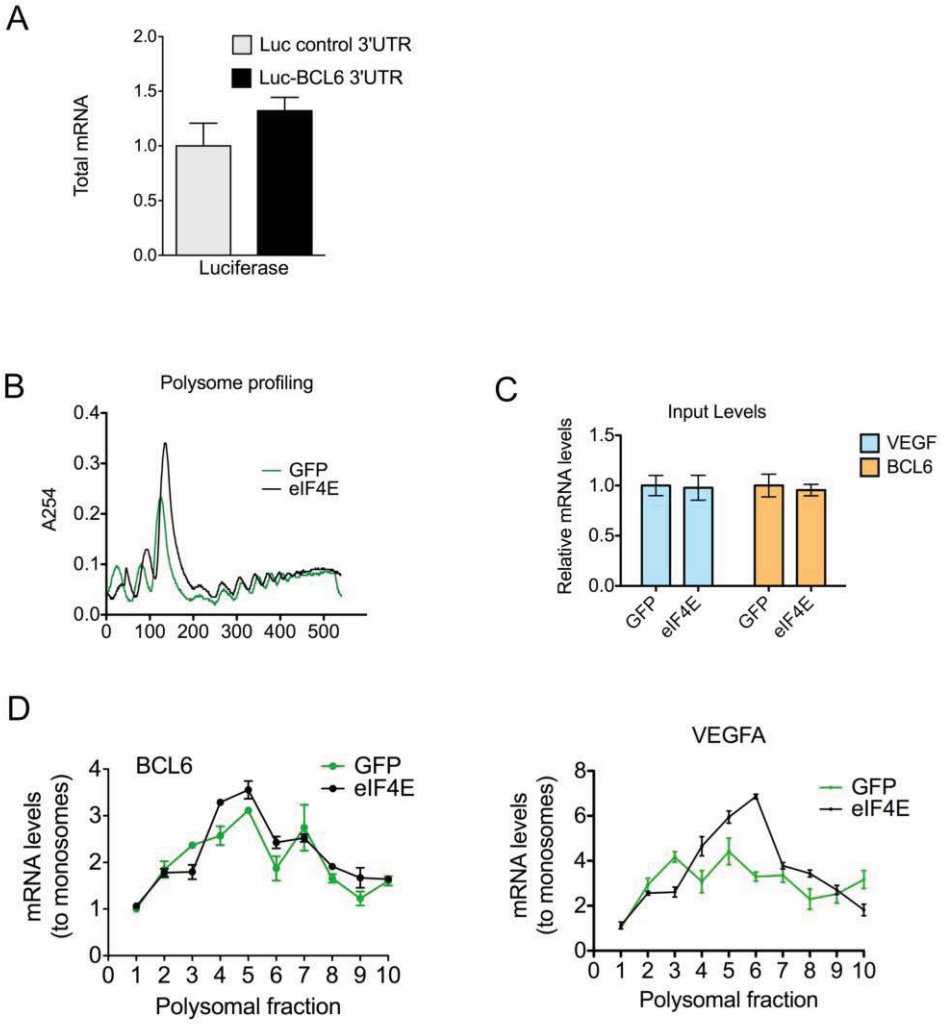

Figure S5. Control mRNA levels in U2OS cells. A: Total mRNA levels of luciferase in U2OS cells transfected with luciferase gene containing either a BCL6 3'UTR sequence or control 3'UTR sequence. **B:** Total polysomal profiling of UOS2 cells expressing eIF4E (black line) or GFP (green line). **C:** Input levels of VEGFA and BCL6 in UOS2 cells expressing eIF4E or GFP. **D:** polysomal profiling of BCL6 and VEGFA (polysomal fractions are indicated in the x-axis) in UOS2 cells expressing eIF4E (black line) or GFP (green line). Data is expressed as fold of mRNA to monosomes.

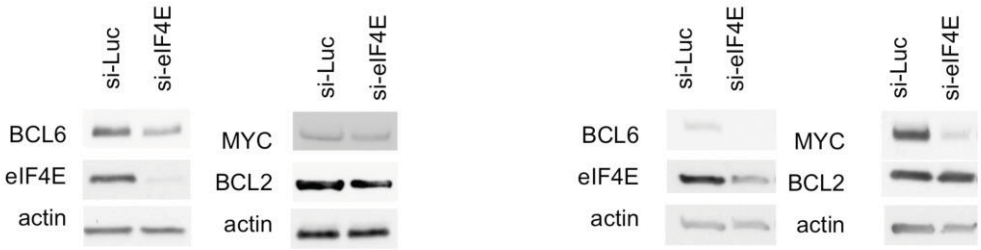

Figure S6. eIF4E regulates protein levels of lymphomagenic transcripts. Immunoblots for BCL6, BCL2, MYC and eIF4E (and actin as control) in DoHH2 cells transfected with siRNA for luciferase (as control) or siRNA for eIF4E in duplicate experiments.

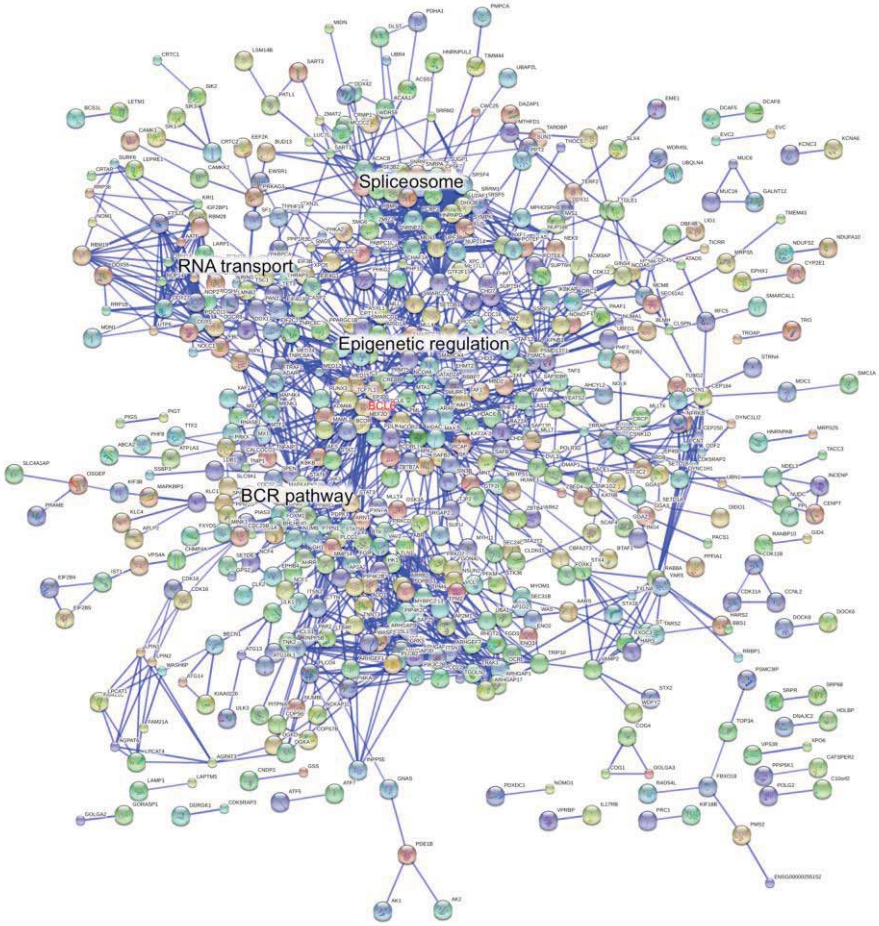

Figure S7. STRING visualization of eIF4E-RIP sequencing top 1000 most significant transcripts with 0.70 confidence.

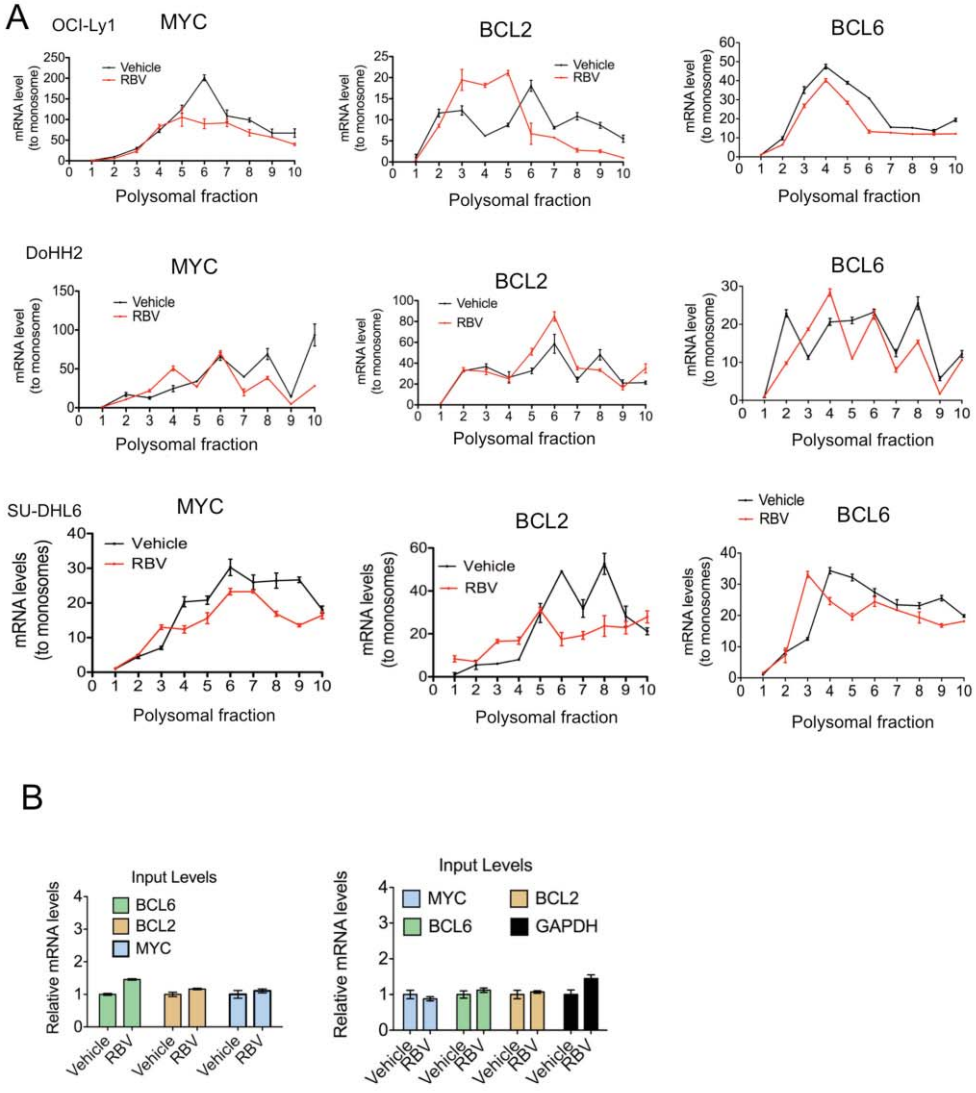

Figure S8. Polysomal profiling and input levels in DLBCL cell lines treated with ribavirin. A: Polysomal profiling of BCL6, BCL2 and MYC transcripts in OCI-Ly1 (top), DoHH2 (middle) and SU-DHL6 (bottom) cells treated with vehicle (black line) vs. ribavirin (red line). **B:** Input levels of BCL6, BCL2, MYC and GAPDH (SU-DHL6) in OCI-Ly1 (left) and SU-DHL6 (right) cells treated with vehicle vs. ribavirin (RBV).

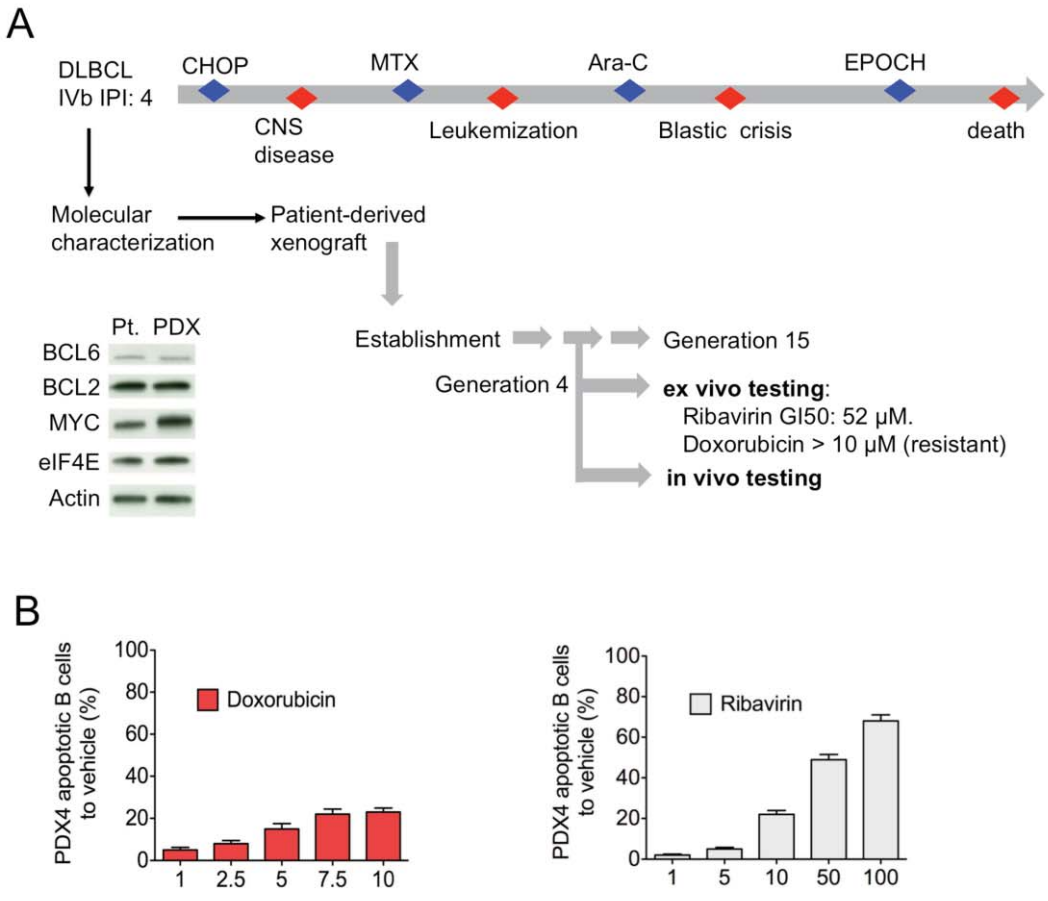

Figure S9. Establishment of a triple-hit DLBCL patient-derived xenograft. A: Time line of patient evolution (treatments are indicated in blue and disease events in red). GI_{50} of ribavirin and doxorubicin in ex vivo treatment of PDX-4 are shown on the right. Insert shows immunoblots for BCL6, BCL2, MYC, eIF4E and actin (as control) for the original sample and the PDX-4. **B:** Effect of doxorubicin and ribavirin in *ex vivo* treatment of PDX-4 as percent of apoptotic cells to vehicle.

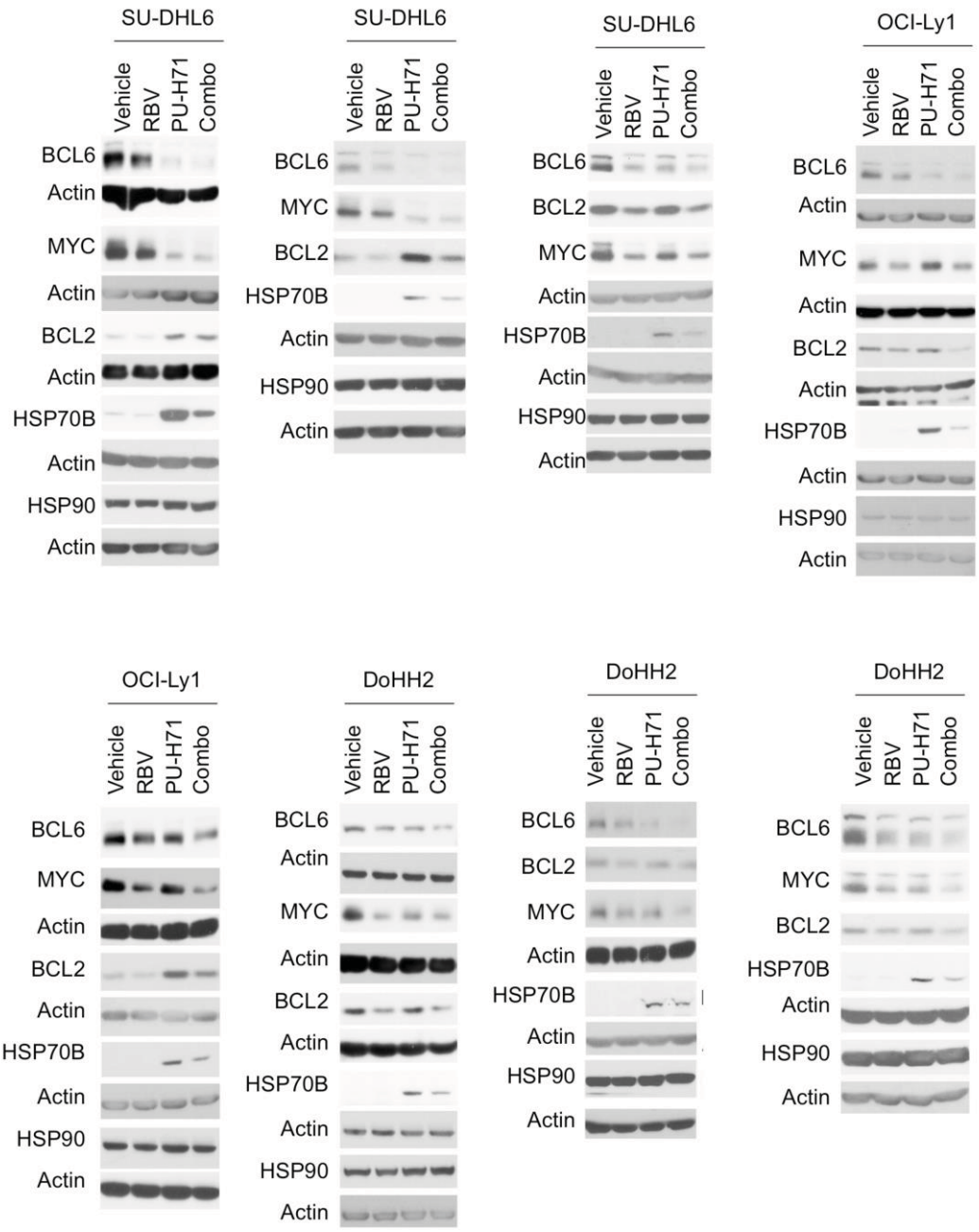

Figure S10. Effect of combined inhibition of eIF4E and TEHp90 in oncoproteins expression. Effect on BCL6, BCL2, MYC, Hsp70, Hsp90 and actin (as control) protein abundance of vehicle, ribavirin (RBV), PU-H71 and their combination (combo) in SU-DHL6, DoHH2 and OCI-Ly1 cells.

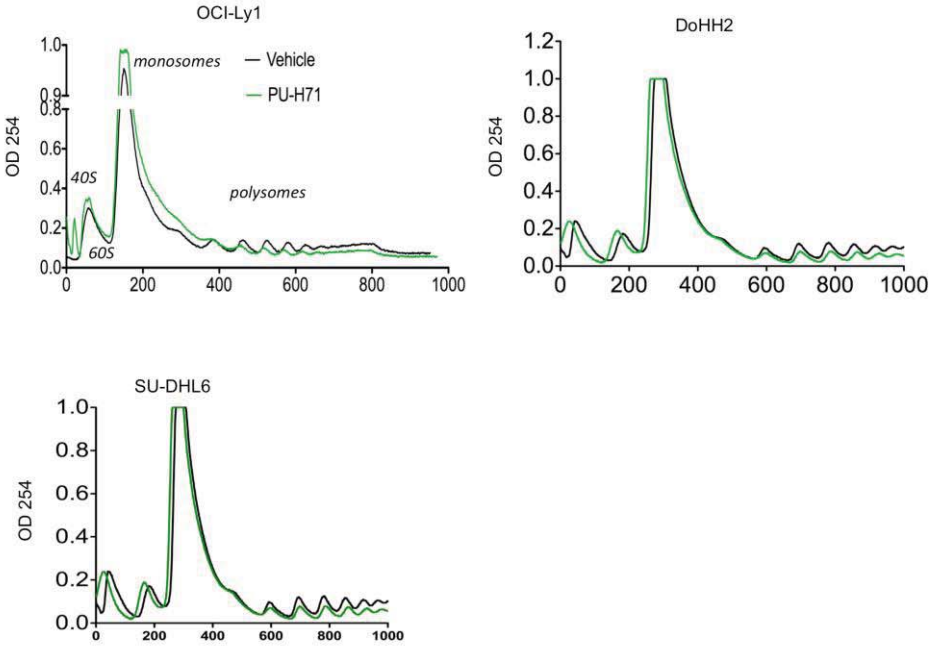

Figure S11. Polysomal profiling of DLBCL cell lines treated with PU-H71. Total polysomal profiling of OCI-Ly1, DoHH2 and SU-DHL6 cells treated with vehicle (black line) vs. PU-H71 (green line).

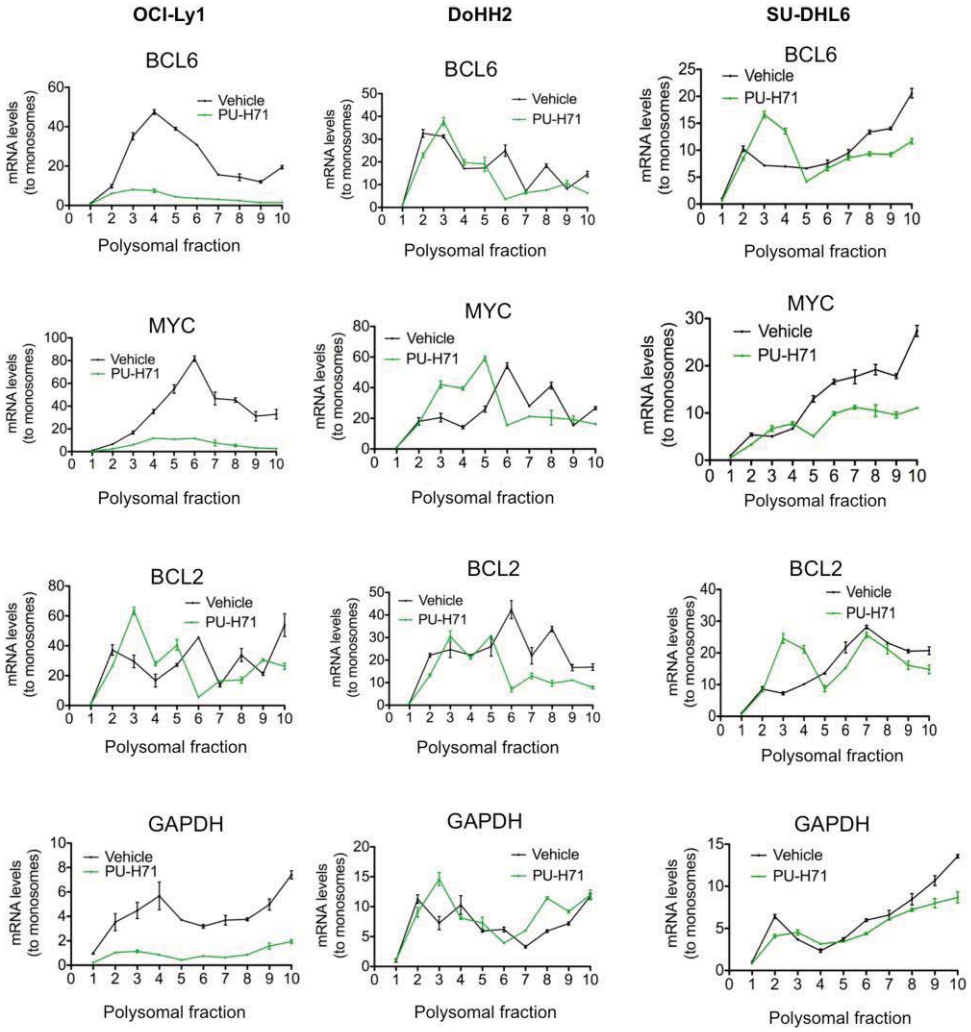

Figure S12: MYC, BCL2, BCL6 and GAPDH polysomal profiling of OCI-Ly1 (left), DoHH2 (middle) and SU-DHL6 (right) cells treated with vehicle (black line) or the Hsp90 inhibitor PU-H71 (green lines).

Supplementary Tables:

Table S1: eIF4E-RIP seq transcripts

Table S2: Blood biochemistry from PDX-4 mice

	Control		PU-H71		Ribavirin		Combination	
	Mean	SEM	Mean	SEM	Mean	SEM	Mean	SEM
BUN (mg/dL)	22.2	1.3	22.6	0.8	21.4	0.9	20.6	0.9
CREA (mg/dL)	0.2	0.0	0.2	0.0	0.2	0.0	0.2	0.0
BUN/CREA ratio	91.4	8.0	105.8	3.9	79.4	11.5	113.0	0.7
ALP (U/L)	29.4	3.9	63.2	30.2	44.4	9.9	29.6	4.1
ALT (U/L)	1315.4	606.2	681.4	497.6	614.8	498.5	1717.2	895.6
AST (U/L)	1634.4	737.4	1524.6	1282.3	713.4	531.4	1797.4	893.6
GGT (U/L)	0.0	0.0	0.0	0.0	0.0	0.0	0.0	0.0
TBIL (mg/dL)	0.6	0.3	0.4	0.1	0.3	0.1	0.4	0.1
DBIL (mg/dL)	0.0	0.0	0.0	0.0	0.0	0.0	0.0	0.0
IBIL (mg/dL)	0.4	0.1	0.3	0.0	0.2	0.0	0.3	0.1
TP (g/dL)	5.1	0.2	5.3	0.3	5.3	0.3	5.6	0.1
ALB (g/dL)	2.7	0.1	2.8	0.2	2.9	0.2	3.0	0.1
GLOB (g/dL)	2.4	0.1	2.5	0.1	2.4	0.1	2.6	0.1
A/G ratio	1.1	0.0	1.1	0.0	1.2	0.0	1.1	0.0
P (mg/dL)	11.4	1.0	8.4	0.5	8.7	0.7	12.5	1.5
Ca (mg/dL)	11.0	0.5	11.3	0.4	10.6	0.2	10.6	0.3
GLU (mg/dL)	183.5	14.7	161.2	22.9	159.6	23.4	234.2	41.0
CHOL (mg/dL)	99.5	6.1	115.6	17.3	90.8	8.3	106.0	4.3
TRIG (mg/dL)	134.8	9.3	147.8	4.9	118.6	9.4	149.0	11.0
CK (U/L)	1484.8	787.8	2065.4	1706.4	968.6	649.5	1949.8	910.5
TCO2 (mEq/L)	12.5	2.9	17.5	1.7	17.3	0.4	13.2	1.4
Na (mEq/L)	150.5	1.7	154.5	1.2	155.8	0.8	151.0	2.9
K (mEq/L)	12.4	0.9	10.4	1.1	8.3	0.2	13.3	2.1
Cl (mEq/L)	111.0	1.0	113.8	0.6	112.5	0.4	111.2	1.6
Na/K ratio	12.3	1.1	15.8	2.2	19.0	0.5	12.8	2.2
Anion Gap	39.5	3.2	36.5	2.4	34.5	0.6	43.0	3.0

Supplementary References

1. Moulick K, Ahn JH, Zong H, Rodina A, Cerchietti L, Gomes DaGama EM, et al. Affinity-based proteomics reveal cancer-specific networks coordinated by Hsp90. Nature chemical biology. 2011;7:818-26.

2. Cerchietti LC, Lopes EC, Yang SN, Hatzi K, Bunting KL, Tsikitas LA, et al. A purine scaffold Hsp90 inhibitor destabilizes BCL-6 and has specific antitumor activity in BCL-6-dependent B cell lymphomas. Nat Med. 2009;15:1369-76.

3. Caldas-Lopes E, Cerchietti L, Ahn JH, Clement CC, Robles AI, Rodina A, et al. Hsp90 inhibitor PU-H71, a multimodal inhibitor of malignancy, induces complete responses in triple-negative breast cancer models. Proc Natl Acad Sci U S A. 2009;106:8368-73.

4. Nayar U, Lu P, Goldstein RL, Vider J, Ballon G, Rodina A, et al. Targeting the Hsp90-associated viral oncoproteome in gammaherpesvirus-associated malignancies. Blood. 2013;122:2837-47.

5. Rodina A, Taldone T, Kang Y, Patel PD, Koren J, 3rd, Yan P, et al. Affinity purification probes of potential use to investigate the endogenous Hsp70 interactome in cancer. ACS chemical biology. 2014;9:1698-705.

6. Taldone T, Patel PD, Patel M, Patel HJ, Evans CE, Rodina A, et al. Experimental and structural testing module to analyze paralogue-specificity and affinity in the Hsp90 inhibitors series. J Med Chem. 2013;56:6803-18.

7. Goldstein RL, Yang SN, Taldone T, Chang B, Gerecitano J, Elenitoba-Johnson K, et al. Pharmacoproteomics identifies combinatorial therapy targets for diffuse large B cell lymphoma. J Clin Invest. 2015;2015.

8. Anders S, Pyl PT, Huber W. HTSeq--a Python framework to work with high-throughput sequencing data. Bioinformatics. 2015;31:166-9.

9. Ritchie ME, Phipson B, Wu D, Hu Y, Law CW, Shi W, et al. limma powers differential expression analyses for RNA-sequencing and microarray studies. Nucleic Acids Res. 2015;43:e47.

CHAPTER 10

Conformational Changes Induced in the Eukaryotic Translation Initiation Factor eIF4E by a Clinically Relevant Inhibitor, Ribavirin Triphosphate

(RESEARCH ARTICLE)

Published Manuscript in *Biochem Biophys Res Commun. 2013 May 10;434(3):614-9. doi: 10.1016/j.bbrc.2013.03.125. Epub 2013 Apr 10.*

Synopsis:

To date, ribavirin is the only direct inhibitor of eIF4E to reach clinical trials. However, the structural changes induced in eIF4E by binding of RTP (the active metabolite of ribavirin, ribavirin triphosphate) are unknown. Our NMR studies indicate RTP binds eIF4E in the m7G cap binding pocket and revealed an unexpected concentration dependence on RTP affinity for eIF4E.

Contribution:

Authorship: Conducted biophysics-based experiments: L.V. and M.O. Conducted mass spectroscopy experiments: A.A. Conducted cell-based experiments: **H.Z.** Supervised research and designed experiments: K.L.B.B. Wrote the manuscript: L.V., M.O. and K.L.L.B

Biochemical and Biophysical Research Communications 434 (2013) 614–619

Contents lists available at SciVerse ScienceDirect

Biochemical and Biophysical Research Communications

journal homepage: www.elsevier.com/locate/ybbrc

Conformational changes induced in the eukaryotic translation initiation factor eIF4E by a clinically relevant inhibitor, ribavirin triphosphate

Laurent Volpon [a,1], Michael J. Osborne [a,1], Hiba Zahreddine [a], Andrea A. Romeo [b], Katherine L.B. Borden [a,*]

[a] Institute of Research in Immunology and Cancer (IRIC), Department of Pathology and Cell Biology, Université de Montréal, Pavilion Marcelle-Coutu, Chemin Polytechnique, Montreal, Qc, Canada H3T 1J4
[b] Aegera Therapeutics (Pharmascience Inc.), 810 Chemin du golf, Verdun, Montreal, Qc, Canada H3E 1A8

ARTICLE INFO

Article history:
Received 21 March 2013
Available online 10 April 2013

Keywords:
NMR
Ribavirin
Methyl 7-guanosine (m^7G) cap
Drug design

ABSTRACT

The eukaryotic translation initiation factor eIF4E is highly elevated in human cancers including acute myeloid leukemia (AML). A potential anticancer agent, ribavirin, targets eIF4E activity in AML patients corresponding to clinical responses. To date, ribavirin is the only direct inhibitor of eIF4E to reach clinical trials. We showed that ribavirin acts as a competitive inhibitor of the methyl 7-guanosine (m^7G) cap, the natural ligand of eIF4E. Here we examine the conformational changes occurring in human eIF4E upon binding the active metabolite of ribavirin, ribavirin triphosphate (RTP). Our NMR data revealed an unexpected concentration dependence on RTP affinity for eIF4E. We observed NMR spectra characteristic of tight binding at low micromolar concentrations (2–5 μM eIF4E) but much weaker affinity at more typical NMR concentrations (50–200 μM). Comparison of chemical shift perturbation and line broadening suggest that the two eIF4E-RTP complexes differ in the precise positioning of RTP within the cap binding pocket, with the high affinity complex showing more extensive changes to the central β-sheet and dorsal surface of eIF4E, similar to m^7G cap. The differences between high and low affinity complexes arise due to concentration dependent aggregation of eIF4E and RTP. Given the intracellular concentrations of eIF4E and RTP and the differential binding toward the W56A eIF4E mutant the high affinity complex is the most physiologically relevant. In summary, these findings demonstrate that RTP binds in the cap-binding site but also suggests new features of this pocket that should be considered in drug design efforts and reveal new insights into ligand eIF4E recognition.

1. Introduction

The eukaryotic translation initiation factor eIF4E is overexpressed in about 30% of human cancers [1,2]. eIF4E modulates the expression of transcripts involved in proliferation and survival by modulating their mRNA export and translation [1,2]. In both cases, eIF4E must associate with the methyl-7 guanosine (m^7G) cap structure on the 5′ end of mRNAs [1–3]. NMR and X-ray crystal structures indicate that the m^7G cap intercalates between two tryptophan residues (W56 and W102) which recognize the m^7G moiety [4–6]. The cap-binding pocket also includes other residues such as W166 which contacts the m^7G as well as positively charged residues (R157 and K162) representing the phosphate binding site. This cap-binding activity of eIF4E is required for its ability to oncogenically transform cells [7]. In cancers with elevated eIF4E, the cells develop an oncogene addiction or dependency on eIF4E [8,9]. This provides a therapeutic window for targeting eIF4E in patients.

The activity of eIF4E has been targeted in poor prognosis acute myeloid leukemia (AML) patients with ribavirin, a competitive inhibitor of m^7G cap [9–11]. Targeting of eIF4E activity in a Phase II clinical trial correlated with clinical responses including 1 complete remission, 2 partial remissions, 2 blast responses (50+% reduction in leukemia blast count) and 6 patients with stable disease reported in the original 11 evaluable patients [10]. For comparison targeting the mTOR pathway via the 4E-BP1 inhibitor, rapamycin led to 0 out of 22 responses in a similar patient population [10].

In cells, ribavirin antagonized the ability of eIF4E to export or translate target transcripts with an indistinguishable profile from

Abbreviations: AML, acute myeloid leukemia; RTP, ribavirin triphosphate; mTOR, mammalian target of rapamycin; CD, circular dichroism; m^7G, 7-methyl-guanosine; m^7GTP, 7-methyl-guanosine-5′-triphosphate; HSQC, heteronuclear single quantum coherence; RING, really interesting new gene; PML, promyelocytic leukemia; ITC, isothermal calorimetry.

* Corresponding author. Address: Institute of Research in Immunology and Cancer (IRIC), Université de Montréal, Pavilion Marcelle-Coutu, 2950, Chemin Polytechnique, Montreal, Qc, Canada H3T 1J4. Fax: +1 (514) 343 7379.
E-mail address: katherine.borden@umontreal.ca (K.L.B. Borden).

[1] These authors contributed equally to this work.

0006-291X/$ - see front matter © 2013 Elsevier Inc. All rights reserved.
http://dx.doi.org/10.1016/j.bbrc.2013.03.125

RNAi-mediated knockdown of eIF4E [9,10,12]. As expected, ribavirin inhibited eIF4E-mediated oncogenic transformation in cell and animal models as well as in AML patients [9,12]. The active metabolite in cells is ribavirin triphosphate (RTP) [13]. Multiple biophysical studies showed that RTP and ribavirin directly bind to eIF4E with a similar affinity as cap [9,11]. Mutation of the cap-binding site (W56A) reduced ribavirin binding by nearly 15-fold similar to effects for the cap [9,10]. The eIF4E-RTP complex was studied in different solution conditions including at 0.2 μM eIF4E protein in 10 mM sodium phosphate, pH 7.5, 150 mM NaCl, or by mass spectrometry at 20 μM eIF4E in 5% aqueous acetonitrile, 20 mM ammonium acetate (pH 6.5) [11]. Complexes were not detected in 20 mM HEPES, 0.2 mM EDTA, 100 mM KCl, pH 8.0 [11] where substantial aggregation is observed relative to phosphate buffers.

The structural changes induced in eIF4E by RTP binding are unknown. A better understanding of how RTP binds is necessary for future drug design efforts. Here, we demonstrate that RTP and m^7GTP induce changes in eIF4E upon binding while GTP does not have these effects, as observed by circular dichroism (CD). Chemical shift mapping of ^1H–^{15}N HSQC NMR experiments were used to monitor eIF4E-RTP complexes as a function of eIF4E concentrations ranging from 2 to 200 μM. These NMR data showed that increasing eIF4E concentrations led to weaker affinities for RTP. This affinity dependence was concomitant with aggregation of eIF4E and RTP. Chemical shift mapping of the amide NMR resonances in the high and low affinity eIF4E–RTP complexes show similar but, importantly, different perturbations at or surrounding the cap-binding site suggesting that the precise molecular contacts underlying the high and low affinity eIF4E–RTP complexes are distinct.

2. Materials and methods

Human eIF4E was purified as described previously [6]. The absence of any cap was verified as described in the Supplementary methods and Supplementary Fig. 1A. ^1H–^{15}N HSQC spectra were collected in 10 mM sodium phosphate, 150 mM NaCl, pH 7.5 and 20 °C on a 600 MHz Varian Inova spectrometer equipped with a HCN coldprobe. Other materials and methods are given in the Supplementary data.

3. Results

3.1. RTP, but not GTP, induces changes in the secondary structure of eIF4E

Far ultraviolet (UV) circular dichroism (CD) has shown that eIF4E undergoes a detectable change in its peptide backbone conformation upon m^7GTP binding [7,14,15]. We therefore monitored the changes in molar ellipticity by far UV CD of eIF4E upon addition of RTP, GTP and m^7GTP. In contrast to RTP or m^7GTP where changes are observed upon addition of ~20:1 molar ratio, GTP induced no changes in molar ellipticity (Fig. 1). The extent of conformational change observed is consistent with previous observations [14,15]. Thus eIF4E binds both m^7GTP and RTP, but not GTP. These data correlate with our previous cap chromatography experiments showing that GTP did not compete for eIF4E bound to a cap column while RTP and m^7GTP did [11].

3.2. NMR studies of the eIF4E–RTP complex

To understand the molecular basis of RTP binding to eIF4E we used NMR chemical shift mapping studies. Spectral changes induced by RTP addition as a function of concentration for human eIF4E (2–200 μM) were monitored using ^1H–^{15}N HSQC experiments. Experiments within 2–5 μM eIF4E, where 2 μM was our lowest limit of detection, were chosen based on our CD and previous biophysical studies. Given the 6–10 days required for acquisition of the HSQC at low eIF4E concentration, the integrity of apo-eIF4E was checked before and after acquisition by SDS–PAGE with no detectable degradation over this time period.

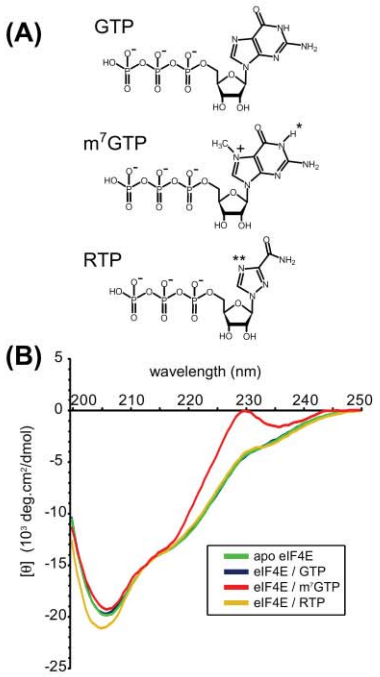

Fig. 1. Analysis of RTP binding and protein samples. (A) The chemical structures of GTP, m^7GTP and RTP. * denotes proton that partially dissociate at pH 7.2 and ** denotes where protonation would cause a positive charge on the free triazole. (B) Circular dichroism spectra in the far ultraviolet upon addition of GTP, m^7GTP or RTP to human eIF4E.

3.3. eIF4E exhibits a concentration dependent affinity for RTP

Example ^1H–^{15}N HSQC spectra recorded for eIF4E in the absence and presence of RTP at low eIF4E concentrations (2–5 μM) and high eIF4E concentrations (50–200 μM) are shown in Figs. 2A and 3A, respectively. These data reveal two complexes in different exchange regimes on the NMR timescale, signifying different affinities for RTP. At high eIF4E concentrations we observed peaks in fast exchange consistent with a weak affinity for RTP. In contrast, the low concentration eIF4E sample (2 μM) exhibited loss of peaks and in some cases, appearance of new peaks upon addition of RTP at ~20-fold excess. These spectra indicate the low concentration eIF4E–RTP complex is in intermediate to slow exchange, consistent with affinities detected for this complex from previous biophysical studies (K_d of 0.13 μM [9]). For the low concentration complex with 40 μM RTP, it is important to note this concentration is readily achievable in patients with no toxicity [10,16]. Importantly, many regions of the protein did not undergo detectable changes in either complex indicating the effects of RTP are specific.

3.4. Chemical shift mapping reveals distinct complexes at high and low eIF4E concentrations

Mapping of the spectral changes onto the eIF4E structure indicates that a similar set of residues are perturbed in both complexes

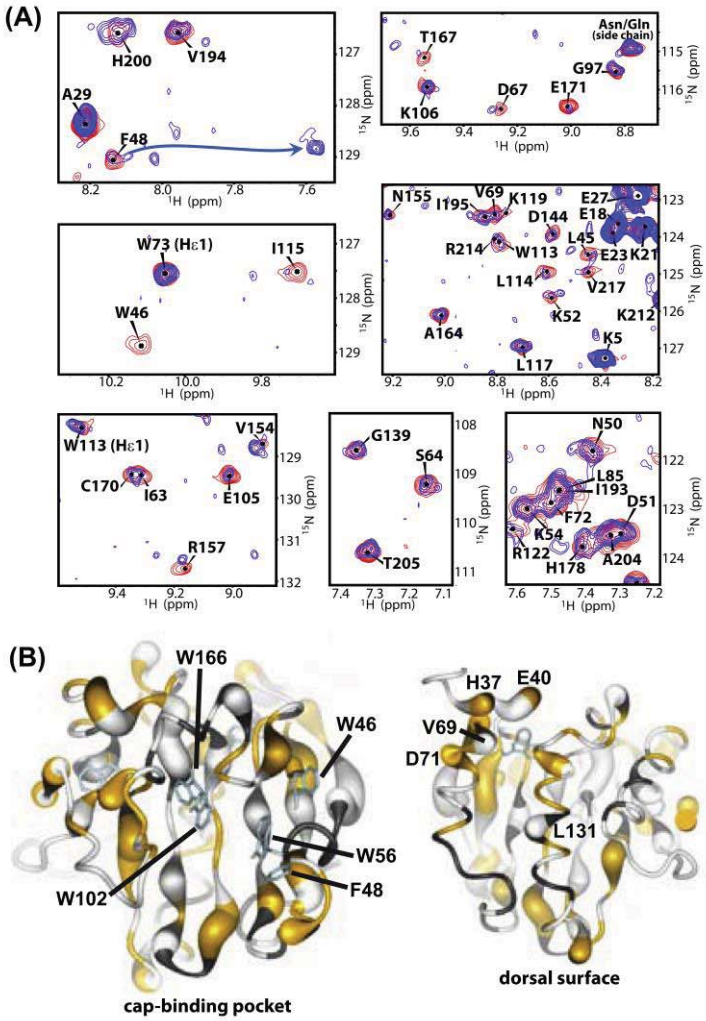

Fig. 2. NMR analysis of the low micromolar eIF4E–RTP complex is characterized by intermediate and slow exchange. (A) Regions highlighting specific residues of ^{1}H–^{15}N HSQC spectra of apo eIF4E (red) with ~20-fold molar excess of RTP (blue). Representative result is shown that was repeated independently three times. Spectra were normalized to W73 indole (middle left panel). (B) Line broadening was mapped as the width of the tube onto the structure of the cap bound eIF4E [28] (pdb code: 3AM7) where gold indicates a RTP induced shift relative to apo, white is no shift and black is unknown due to spectral overlap. Two views are shown, the cap (left panel) binding site and the helical dorsal surface (right panel).

(Figs. 2B, 3B and Supplementary Fig. 2C and D). These residues (colored cyan in Fig. 4A) are centered around the cap binding pocket, including the β-strands at the bottom of the cap-binding pocket (e.g. β-strands 1 and 4–6), the phosphate binding region (R157 and K162) as well as the surface loops important for m^7G cap binding. A substantial number of resonances, however, are perturbed differentially indicating the high and low affinity complexes have distinct binding modes (dark blue and green in Fig. 4A). For instance, while the N50 and T205 (Fig. 3) are among the most affected residues in the low affinity complex, these are not altered in the high affinity complex (Fig. 2). One of the most striking changes in the high affinity complex involves F48 (adjacent to W56 in the eIF4E structure, Fig. 2B), which undergoes broadening with a new peak found at almost the exact position of the F48 cross peak corresponding to the m^7GTP bound form of eIF4E (see the arrow in Fig. 2A). In the low affinity complex the F48 peak is only minimally perturbed relative to apo-eIF4E. Similarly, many peaks that disappear in the high affinity complex are not affected in the low affinity complex, e.g. I115, T167, K52 among others (compare Figs. 2A and 3A).

Mutation of W56 to alanine substantially abrogates eIF4E affinity for both RTP and m^7GTP [7,9]. The ^{1}H-^{15}N HSQC of apo W56A eIF4E induces a large shift to F48, and only a minimal perturbation to N50 compared to wild-type eIF4E. Thus these residues, which may be considered as 'reporters' of high and low affinity complexes respectively, although close in sequence, can be differentially affected by both mutation and ligand binding.

Binding of RTP (at a 60-fold excess) to W56A eIF4E at high (50 μM) and low (2–5 μM) concentrations by NMR revealed different results. No significant changes compared to the wildtype spectra were evident from the high concentration titration (see Supplementary Fig. 2B, e.g. peaks N50 and T205 were similarly al-

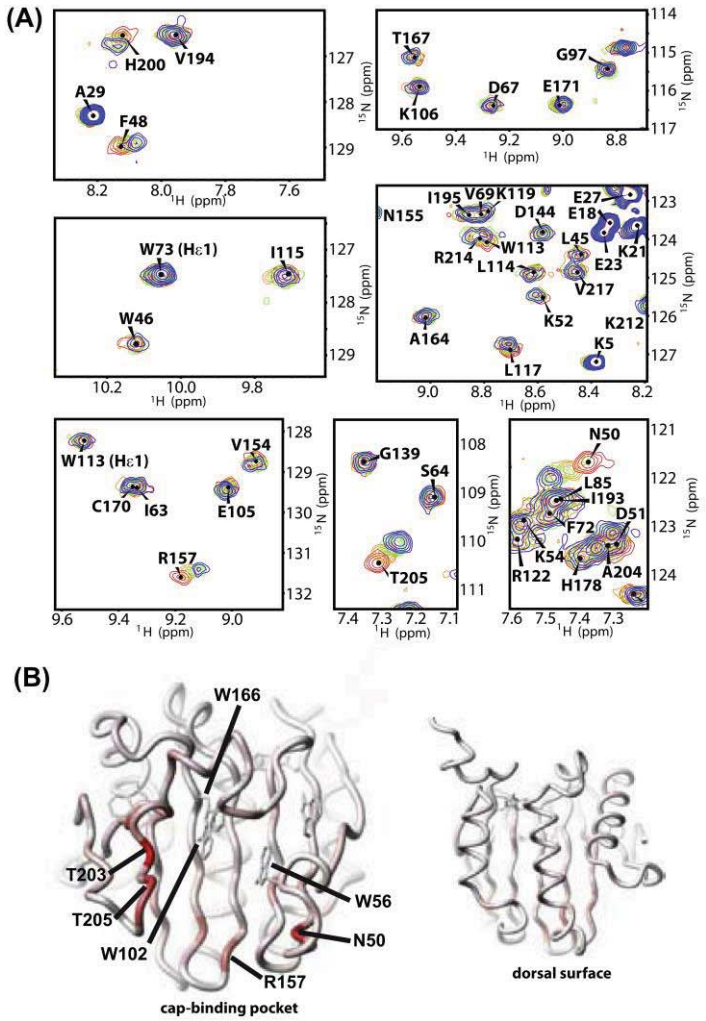

Fig. 3. NMR analysis of the high micromolar eIF4E-RTP complex is characterized by fast exchange. (A) ^{1}H–^{15}N HSQC spectra of 50 μM eIF4E (red) as a function of increasing concentration of RTP (up to 1:50; blue). The same regions as in Fig. 2A are shown. (B) ^{1}H-^{15}N HSQC chemical shift perturbations are mapped onto the eIF4E structure upon addition of RTP. Residues are color-coded according to the extent of chemical shift perturbation from white (no variation) to red (large variation). The same views as in Fig. 2B are shown.

tered in mutant and wildtype spectra). In contrast, at low eIF4E concentrations, RTP no longer bound eIF4E (Supplementary Fig. 2A). Thus W56 is only important for binding in the low concentration complexes, strongly supporting the notion that there are fundamental differences between the high and low concentration complexes. Significantly, the low concentration NMR complex has similar characteristics to the eIF4E–RTP complexes studied previously biophysically and in cells, such as high affinity and sensitivity to W56A, strongly suggesting this is the complex important for cellular function.

3.5. Comparison of conformational changes in the RTP- and m^{7}GTP–eIF4E complexes

Several crystal and NMR studies indicate that the m^{7}G cap intercalates between W56 and W102 with additional contacts made by E103, W166, and for the phosphates, K162 and R157 [4]. Consistent with binding at the cap site, all these residues are perturbed upon addition of RTP to eIF4E. Chemical shift perturbations of eIF4E upon binding of m^{7}GTP and RTP (at 2 μM eIF4E) are highlighted in Fig. 4B. Clearly a number of residues are similarly perturbed (colored in yellow), including F48 which undergoes among the largest shifts in both m^{7}GTP and RTP complexes. However, important differences are observed upon RTP binding. Notably, perturbations to the indole peaks of W56/102 were not as extensive which likely reflects the substantial differences in both size and charge between m^{7}GTP and RTP. Indeed there is substantial structural plasticity in the cap binding pocket as evidenced by high affinity binding of significantly bulkier ligands [17,18] and high *B*-factors for the W56/102 loops even when cap bound [5,19,20]. Thus, the lack of significant movement of the W56 and W102 indoles (note the W102 backbone amide is substantially af-

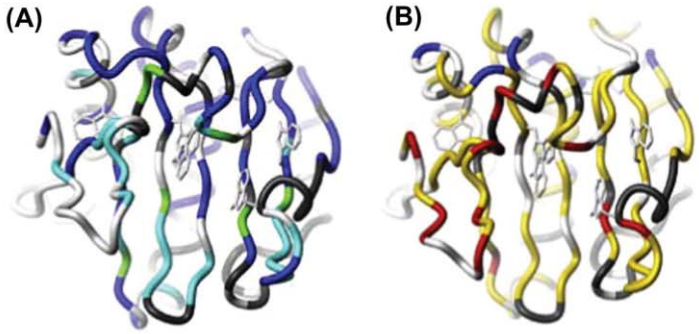

Fig. 4. Comparison of the residues affected in the RTP and m^7GTP eIF4E complexes. (A) Comparison of high and low affinity RTP complexes (low and high micromolar eIF4E samples, respectively). Results of spectral perturbations were mapped onto eIF4E cap bound structure. Color coding is as indicated: dark blue, change in high affinity complex relative to apo exclusively; light blue, change in both complexes relative to apo; green, change only in the low affinity complex relative to apo upon RTP binding; white, no change in either complex relative to apo; dark gray, unknown due to spectra overlap. (B) Comparison of high affinity RTP and m^7GTP complex, color-coding as above except for changes in both complexes relative to apo (yellow) and changes only in the m^7GTP complex relative to apo (red).

fected) upon RTP binding might reflect one or many of these mechanisms. It is possible that RTP binds deeper in the eIF4E pocket (given the effects on F48 and other nearby residues) and its smaller size allows the motions that are present in the apo eIF4E to persist, and of course, RTP could adopt multiple conformations in this pocket. Thus, for both cap binding and likely more so for RTP binding, there is likely substantial motion within the complexes.

Similar to m^7GTP binding to eIF4E, RTP induces substantial changes at the dorsal surface of eIF4E (Supplementary Fig. 3). These changes (which are important for increasing affinity for regulatory proteins [6,21–23]) are not identical to m^7GTP but are likely mediated via a similar allosteric path previously identified for eIF4E, e.g. via β-strands 5–6 to W130 on the internal face of helix 2 and adjacent residues lying on the dorsal surface, and in particular for a cluster comprising the residues H37, E40, V69 and D71. Notably we do not see any movement for W73 suggesting no involvement of the dorsal surface.

3.6. eIF4E concentration considerations

Our observations with RTP binding led us to examine whether the affinity of eIF4E for m^7GTP was similarly dependent on eIF4E concentration. Using ITC, we observe a steep concentration dependence with an affinity reduction of 8-fold in the range of 1.6–12.4 μM with stronger binding at low eIF4E concentrations (Supplementary Fig. 4B).

We hypothesized that reduced binding of eIF4E at higher concentration was due to aggregates. Consistently, we detected a concentration dependent aggregation of eIF4E using a variety of methods, including size exclusion chromatography (SEC), NMR self-diffusion and AUC (see Supplementary materials and Supplementary Fig. 4A and C). The results of the SEC showed only monomer at 0.5 μM eIF4E, with increasing amounts of aggregate (6%, 11% and 25%) at 2, 22 and 60 μM eIF4E, respectively. The aggregate eluted in the void volume, indicating a minimum molecular weight of 200 kDa. AUC data for 20 μM eIF4E estimated a molecular weight centered around 700 kDa with a very broad distribution indicating substantial heterogeneity (data not shown). Using SEC, we also observed time-dependent effect aggregation for the more concentrated eIF4E samples (60 μM) increasing from 25% to 50% aggregates after 3 days. In contrast, the low concentration samples (2–5 μM) showed no additional aggregation during even longer timeframes (data not shown). Thus, the concentration dependence on ligand affinity is not specific to RTP but appears related to the propensity of eIF4E to form very large aggregates.

Adding complexity to the system, guanosine analogs, which include ribavirin, are known to self-stack and in certain conditions can even form gels [24]. Using hydrophilic chromatography and mass spectrometry we detected an equimolar amount of dimer and monomer at 100 μM RTP and predominantly dimer (>98%) at 5 and 9 mM RTP.

Taken together, this strongly suggests that the active concentrations of both ligand and protein are lower than anticipated and account for some of the differences in affinity we observe as a function of eIF4E concentration. At very high concentrations of RTP, which would be typically used in NMR, the majority of RTP is dimer. We cannot rule out the presence of even higher aggregates that likely have poorer ionization efficiency than monomers and so the extent of aggregation for RTP reported here could well be an underestimate.

3.7. Ribavirin binds eIF4E in human cells

Ultimately, it is important to demonstrate that RTP interacts with eIF4E in human cells. RTP is not cell permeable and thus ribavirin, which is converted into RTP intracellularly [1] is used for these studies. From the clinical perspective, 20–40 μM ribavirin levels were routinely observed in AML patient plasma in the ribavirin monotherapy and ongoing ribavirin combination trials, and thus this concentration was used here [10,16] (see Supplementary methods). We observe a 6-fold enrichment of ^{3}H ribavirin in the eIF4E immunoprecipitations relative to controls indicating a strong interaction between eIF4E and RTP in cells consistent with the high affinity complexes we observe (Supplementary Fig. 5).

4. Discussion

Our NMR studies demonstrate that there are at least two modes for eIF4E binding to RTP dependent on concentration and likely driven by concentration dependent aggregation. Physically, both complexes utilize residues at or near to the cap-binding site, but the molecular contacts, relative binding affinity and sensitivity to the W56A mutation are distinct. The low concentration (2–5 μM) eIF4E-RTP complex exhibits similar high affinity binding and sensitivity to the W56A mutant as seen in previous biophysical studies[6,9,11]. Similar to m^7GTP binding, the low affinity RTP complex induced changes in the NMR spectrum at the dorsal sur-

face via an allosteric mechanism. However, we observe no changes to W73 consistent with previous studies showing mutation of W73 to alanine had no effect on RTP affinity for eIF4E [9]. The observation of a concentration dependent aggregation of eIF4E and concentration dependent affinity of eIF4E for RTP suggests these phenomena may be linked. A possible model for the observed binding is that aggregation at higher concentration obscures RTP from entering the cap binding pocket, and RTP-eIF4E association occurs at the surface loops, consistent with the large changes observed for N50, R167, T203 and T205; whereas at lower concentrations eIF4E is predominantly monomeric facilitating deeper access within the binding pocket.

The molecular details driving binding of RTP likely differ from m^7GTP. The cap-binding site is adjustable allowing for binding of cap-analogs with bulky substitutions, such as benzene in place of the methyl group on the guanosine ring where this actually increases affinity to eIF4E [18,25,26]. Similarly, eIF4E from nematodes binds both the mono- and trimethyl cap with similar affinity but mutation of E103 only impairs binding to monomethylated cap [26]. Taken together, these findings suggest that ligands can use different features to interact in eIF4E's cap-binding pocket. This is likely the case for RTP and m^7GTP. Further, given that RTP is much smaller than the cap, its precise position in the cap binding pocket may be more prone to "sliding" suggesting that there could be exchange within bound forms that could also contribute to the line broadening observed.

Our studies suggest that the high affinity/low concentration complex is the most physiologically relevant. For instance eIF4E is estimated to be present in the submicromolar range in cell lines [27], and ribavirin and thus RTP levels in patients are not typically more than 40 μM or so and certainly do not reach the millimolar level. The necessity of capturing the high affinity complex at low protein concentrations coupled with intermediate exchange phenomena, will make its structure determination particularly challenging. Given our biophysical studies at 0.2 μM eIF4E yield K_d's in the 0.17 μM range for RTP, it is likely that lowering concentrations in the NMR would lead to even tighter binding, but the technical limitations of collecting data on such dilute samples preclude such experiments. Notwithstanding, the clear differences in the binding site albeit within the cap-binding pocket, strongly suggest that these sorts of issues need to be considered for eIF4E drug design initiatives and also more generally as these phenomena are unlikely restricted to eIF4E. Further, a deeper understanding of multiple binding modes of eIF4E will be important in future drug design efforts.

Acknowledgments

We are grateful to Dr. Jack A. Kornblatt (CSFG and Department of Biology, Concordia University, Montreal) for carrying out ITC experiments. Studies were supported by NIH (RO1 98571). KLBB holds a Canada Research Chair. The Institute for Research in Immunology and Cancer receives support from the CIHR and FRSQ.

Appendix A. Supplementary data

Supplementary data associated with this article can be found, in the online version, at http://dx.doi.org/10.1016/j.bbrc.2013.03.125.

References

[1] K.L. Borden, B. Culjkovic-Kraljacic, Ribavirin as an anti-cancer therapy: acute myeloid leukemia and beyond?, Leuk Lymphoma 51 (2010) 1805–1815.
[2] B. Culjkovic, K.L. Borden, Understanding and targeting the eukaryotic translation initiation factor eIF4E in head and neck cancer, J. Oncol. 2009 (2009) 981679.
[3] W. Filipowicz, S.N. Bhattacharyya, N. Sonenberg, Mechanisms of post-transcriptional regulation by microRNAs: are the answers in sight?, Nat Rev. Genet. 9 (2008) 102–114.
[4] J. Marcotrigiano, A.C. Gingras, N. Sonenberg, et al., Cocrystal structure of the messenger RNA 5′ cap-binding protein (eIF4E) bound to 7-methyl-GDP, Cell 89 (1997) 951–961.
[5] K. Tomoo, Y. Matsushita, H. Fujisaki, et al., Structural basis for mRNA Cap-Binding regulation of eukaryotic initiation factor 4E by 4E-binding protein, studied by spectroscopic, X-ray crystal structural, and molecular dynamics simulation methods, Biochim. Biophys. Acta 1753 (2005) 191–208.
[6] L. Volpon, M.J. Osborne, I. Topisirovic, et al., Cap-free structure of eIF4E suggests a basis for conformational regulation by its ligands, EMBO J. 25 (2006) 5138–5149.
[7] N. Cohen, M. Sharma, A. Kentsis, et al., PML RING suppresses oncogenic transformation by reducing the affinity of eIF4E for mRNA, Embo J. 20 (2001) 4547–4559.
[8] J.R. Graff, B.W. Konicek, T.M. Vincent, et al., Therapeutic suppression of translation initiation factor eIF4E expression reduces tumor growth without toxicity, J. Clin. Invest. 117 (2007) 2638–2648.
[9] A. Kentsis, I. Topisirovic, B. Culjkovic, et al., Ribavirin suppresses eIF4E-mediated oncogenic transformation by physical mimicry of the 7-methyl guanosine mRNA cap, Proc. Natl. Acad. Sci. USA 101 (2004) 18105–18110.
[10] S. Assouline, B. Culjkovic, E. Cocolakis, et al., Molecular targeting of the oncogene eIF4E in AML: a proof-of-principle clinical trial with ribavirin, Blood 114 (2009) 257–260.
[11] A. Kentsis, L. Volpon, I. Topisirovic, et al., Further evidence that ribavirin interacts with eIF4E, RNA 11 (2005) 1762–1766.
[12] F. Pettersson, C. Yau, M.C. Dobocan, et al., Ribavirin treatment effects on breast cancers overexpressing eIF4E, a biomarker with prognostic specificity for luminal B-type breast cancer, Clin. Cancer. Res. 17 (2011) 2874–2884.
[13] T. Page, J.D. Connor, The metabolism of ribavirin in erythrocytes and nucleated cells, Int. J. Biochem. 22 (1990) 379–383.
[14] W.D. McCubbin, I. Edery, M. Altmann, et al., Circular dichroism and fluorescence studies on protein synthesis initiation factor eIF-4E and two mutant forms from the yeast Saccharomyces cerevisiae, J. Biol. Chem. 263 (1988) 17663–17671.
[15] T. von Der Haar, P.D. Ball, J.E. McCarthy, Stabilization of eukaryotic initiation factor 4E binding to the mRNA 5′-Cap by domains of eIF4G, J. Biol. Chem. 275 (2000) 30551–30555.
[16] S. Assouline, B. Kraljacic-Culjkovic, E. Cocolakis, et al., A Phase I combination study of ribavirin and low dose cytarabine arabinoside (ara-C) in M4/M5 acute myeloid leukemia (AML) and AML with high eIF4E, Blood (ASH Annual Meeting Abstracts) 118 (2011) 3606.
[17] X. Chen, D.J. Kopecky, J. Mihalic, et al., Structure-guided design, synthesis, and evaluation of guanine-derived inhibitors of the eIF4E mRNA-cap interaction, J. Med. Chem. 55 (2012) 3837–3851.
[18] C.J. Brown, I. McNae, P.M. Fischer, et al., Crystallographic and mass spectrometric characterisation of eIF4E with N7-alkylated cap derivatives, J. Mol. Biol. 372 (2007) 7–15.
[19] A. Niedzwiecka, J. Marcotrigiano, J. Stepinski, et al., Biophysical studies of eIF4E cap-binding protein: recognition of mRNA 5′ cap structure and synthetic fragments of eIF4G and 4E-BP1 proteins, J. Mol. Biol. 319 (2002) 615–635.
[20] J. Marcotrigiano, A.C. Gingras, N. Sonenberg, et al., Cap-dependent translation initiation in eukaryotes is regulated by a molecular mimic of eIF4G, Mol. Cell 3 (1999) 707–716.
[21] M. Ptushkina, T. von der Haar, M.M. Karim, et al., Repressor binding to a dorsal regulatory site traps human eIF4E in a high cap-affinity state, Embo J. 18 (1999) 4068–4075.
[22] M. Ptushkina, T. von der Haar, S. Vasilescu, et al., Cooperative modulation by eIF4G of eIF4E-binding to the mRNA 5′ cap in yeast involves a site partially shared by p20, Embo J. 17 (1998) 4798–4808.
[23] L. Volpon, M.J. Osborne, A.A. Capul, et al., Structural characterization of the Z RING-eIF4E complex reveals a distinct mode of control for eIF4E, Proc. Natl. Acad. Sci. USA 107 (2010) 5441–5446.
[24] W. Saenger, Principles of Nucleic Acid Structure, Springer-Verlag, New York, 1984.
[25] S.E. Carberry, E. Darzynkiewicz, J. Stepinski, et al., A spectroscopic study of the binding of N-7-substituted cap analogues to human protein synthesis initiation factor 4E, Biochemistry 29 (1990) 3337–3341.
[26] W. Liu, M. Jankowska-Anyszka, K. Piecyk, et al., Structural basis for nematode eIF4E binding an m(2,2,7)G-Cap and its implications for translation initiation, Nucleic Acids Res. 39 (2011) 8820–8832.
[27] M.J. Osborne, L. Volpon, J.A. Kornblatt, et al., EIF4E3 acts as a tumour suppressor by utilizing an atypical mode of methyl-7 guanosine cap recognition, Proc. Natl. Acad. Sci. USA (2013).
[28] A. Fukuyo, Y. In, T. Ishida, et al., Structural scaffold for eIF4E binding selectivity of 4E-BP isoforms: crystal structure of eIF4E binding region of 4E-BP2 and its comparison with that of 4E-BP1, J. Pept. Sci. 17 (2011) 650–657.

Supplementary Materials

Conformational changes induced in the eukaryotic translation initiation factor eIF4E by a clinically relevant inhibitor, ribavirin triphosphate

Laurent Volpon[a,†], Michael J. Osborne[a,†], **Hiba Zahreddine**[a], Andrea A. Romeo[b] and Katherine L.B. Borden[a,*]

[a]Institute of Research in Immunology and Cancer (IRIC), Department of Pathology and Cell Biology, Université de Montréal, Pavilion Marcelle-Coutu, Chemin Polytechnique, Montreal, Qc, H3T 1J4, Canada.

[b]Aegera Therapeutics (Pharmascience Inc.), 810 Chemin du golf, Verdun (Montreal), Qc, H3E 1A8, Canada.

Materials and Methods

1. Materials

GTP and m^7GTP were purchased from Sigma and RTP was synthesized from Ribavirin (Kemoprotec) as described by Kimoto [1]. ^{31}P NMR and mass spectrometry experiments indicated the RTP was intact and in the triphosphate form.

2. eIF4E purification and characterization

Human eIF4E was purified using the established procedure of elution with m^7G (a cap analogue) from a cap affinity column followed by extensive dialysis and ion exchange chromatography to remove the remaining cap [2]. To ensure our samples were free of m^7G, we compared the ^{1}H-^{15}N HSQC spectra obtained from this method with human apo eIF4E produced using a His tag. Differences were observed only at the N-terminus because of differences in the sequence due to cloning (Supplementary Fig. 1A). This is also supported by our recent crystal structure of apo eIF4E form purified using the cap affinity chromatography protocol [3]. Next, we looked at the aggregation state of eIF4E over our experimental concentration range and no obvious change in the apo-eIF4E ^{1}H-^{15}N HSQC spectra could be detected (Supplementary Fig. 1B).

3. CD spectroscopy

CD studies were carried out on a JASCO 810 spectropolarimeter using a 0.1 cm cuvette at 20°C. Buffer and nucleotide absorbance were subtracted out. Experiments were performed at pH 7.5, 150 mM NaCl, 10 mM sodium phosphate and 20°C with ~2 μM eIF4E conditions based on our previous fluorescence and cap chromatography studies with ribavirin [4,5]. Protein concentration was estimated by UV-Vis absorption spectroscopy (ε = 52940 $M^{-1}cm^{-1}$) to be 2 μM and samples with approximately

20-fold molar excess of the different nucleotide triphosphates were incubated for 30 minutes before data acquisition.

4. NMR spectroscopy

^{1}H-^{15}N HSQC spectra were collected in 10 mM sodium phosphate, 150 mM NaCl, pH 7.5 and 20°C on a 600 MHz Varian Inova spectrometer. Experiments were processed with NMRPipe [6] and analyzed using Sparky [7]. Chemical shift perturbations were weighted by calculating the average chemical shift differences, $\Delta_{av}(NH)$, using the equation $\Delta_{av}(NH) = [(\Delta\delta_H^2 + (\Delta\delta_N/5)^2)/2]^{1/2}$, where $\Delta\delta_H$ and $\Delta\delta_N$ are the differences between free and bound chemical shifts [8]. Translation diffusion experiments were performed using the stimulated echo with bipolar gradient pulses [9] and Watergate for solvent suppression.

5. FPLC experiment

Samples were applied to a Superdex 75pg (Pharmacia) equilibrated with 50mM phosphate pH 7.5, 100mM NaCl, 50 μM TCEP, and were eluted in the same buffer at 1 $ml.min^{-1}$, under a pressure of 0.35 MPa at 4°C. The column was standardized by eluting a series of marker proteins of known molecular mass and calculating the partition coefficient.

6. ITC

ITC was performed with a VP-ITC instrument from Microcal, Inc. at 20°C. The eIF4E sample and the m^7GTP were in 10 mM sodium phosphate, 150 mM NaCl, pH 7.4.

7. AUC experiments

AUC experiments were performed at 20°C using a Beckman Coulter XL-I analytical ultracentrifuge. All experiments were performed in dual-sector, charcoal-filled Epon centerpieces that had been filled with 390 μl of sample in the sample sector and 400 μl of buffer (10 mM sodium phosphate, 150 mM NaCl, pH 7.4, 100 μM TCEP) without proteins in the reference sector. Assembled cells (one per sample) were loaded into a four-hole An60Ti rotor. AUC data were collected at 30,000 rpm in absorbance mode at 280 nm. Three different eIF4E concentrations (2, 10 and 20 μM) were analyzed from the same stock eIF4E sample. Data were analysed using SEDNTERP and SEDFIT [10,11]. Sedimentation profiles were obtained by fitting the absorbance data to the continuous c(s) or c(M) models, affording estimates of the sedimentation coefficient and molecular weight.

8. Mass spectroscopy

Hydrophilic chromatography was used in conjunction with mass spectrometry. The system used was an Agilent 1100 HPLC coupled to an Agilent MSD Trap SL, with an ESI source. The autosampler system

was kept at 4°C. The HPLC column was an Inertsil HILIC, 150 x 4.6 mm, 5 µm and the chromatography was obtained using solvent A (2 mM ammonium formate in water, pH 3.2) and solvent B (100% acetonitrile). The injection volume was 50 µl and the flow rate 1 ml/min. The column compartment was heated at 30°C. The initial gradient was 95% B and 5% A which changed during a 30 min course to 5% B and 95% A followed by 6 min equilibration at 95 % B and 5 % A. The total run time of the gradient was 36 min. The ESI source of the coupled MS ion-trap was set in positive mode, the nitrogen drying gas flow at 12 ml/min, the nebulizer pressure at 55 PSI and the temperature of the capillary at 350°C with a voltage of 4500 V. The mass analyzer was set to scan from 50 to 1500 m/z.

9. Detection of the RTP in human cells

The head and neck carcinoma cell FaDu (obtained from the ATCC) was treated with 0.7 µM ^{3}H ribavirin for 8 hours, the maximal uptake of ribavirin. Cells were lysed and immediately immunoprecipitated with an anti-eIF4E antibody (Sigma Aldrich) or immunoglobulin IgG as a negative control as described [12]. ^{3}H ribavirin content was determined by scintillation counting.

Supplementary Figures

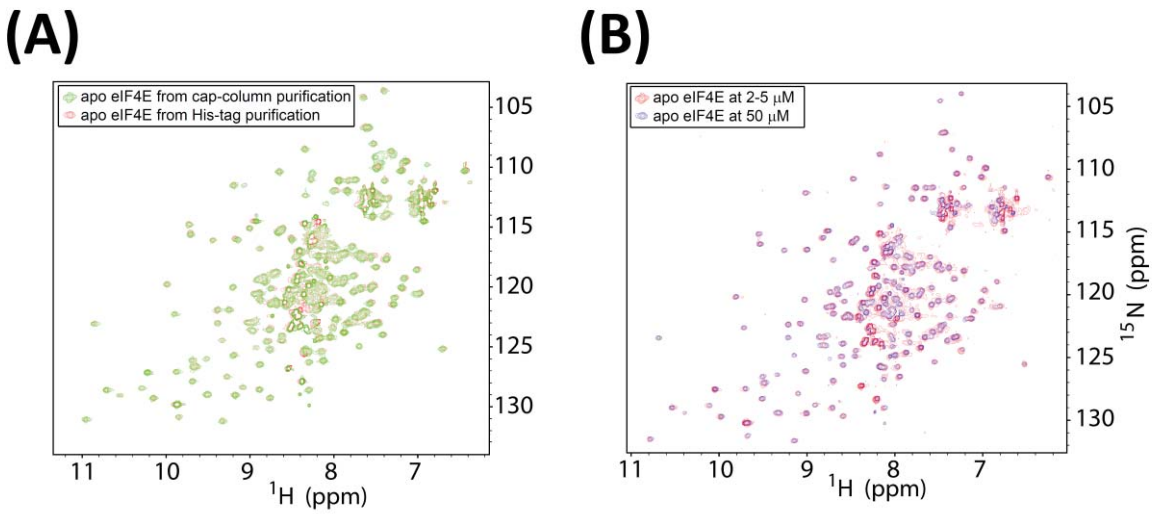

Supplementary Figure 1. (A). ^{1}H-^{15}N HSQC spectra of human eIF4E purified either by nickel agarose chromatography (red) or by cap chromatography (green). (B) ^{1}H-^{15}N HSQC spectra of the apo-eIF4E corresponding to the low (red) and high (blue) concentrated samples.

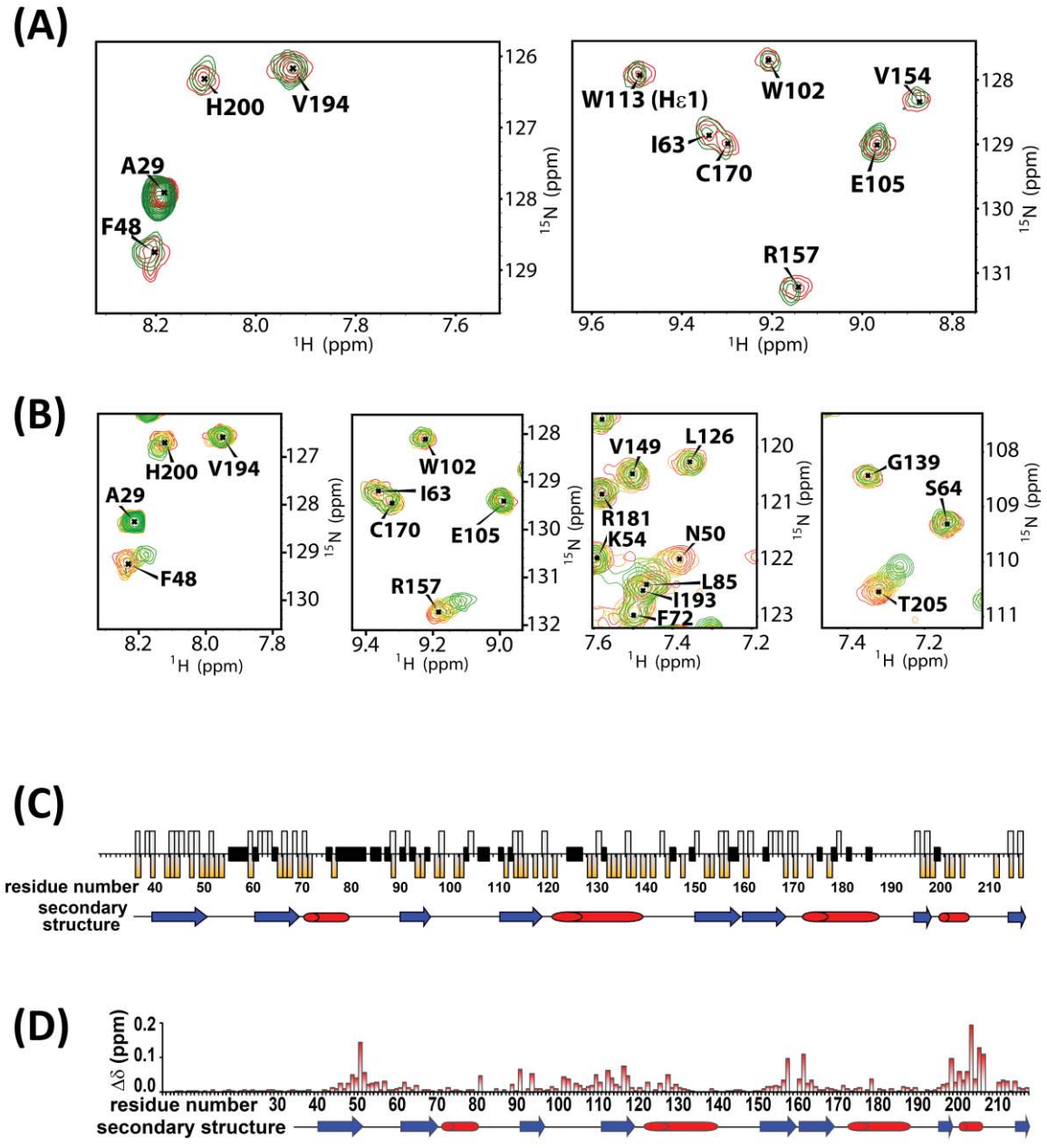

Supplementary Figure 2. NMR analysis of the low and high micromolar eIF4E-RTP complex. (A) Regions highlighting specific residues of ^{1}H-^{15}N HSQC spectra of apo eIF4E W56A (red) with ~20-fold molar excess of RTP (green). (B) ^{1}H-^{15}N HSQC spectra of 50 μM eIF4E W56A (red) as a function of increasing concentration of RTP (up to 1:60; green). (C) Per-residue line broadening upon binding of RTP with eIF4E (2-5 μM) at ratio 1:20. Positive (white) and negative (gold) bars are representative of

residues that broaden, and/or shift relative to apo eIF4E, respectively. Black is unknown due to spectral overlap. (D) Per-residue chemical shift perturbations upon binding of RTP with eIF4E (50 μM) at a ratio of 1:50.

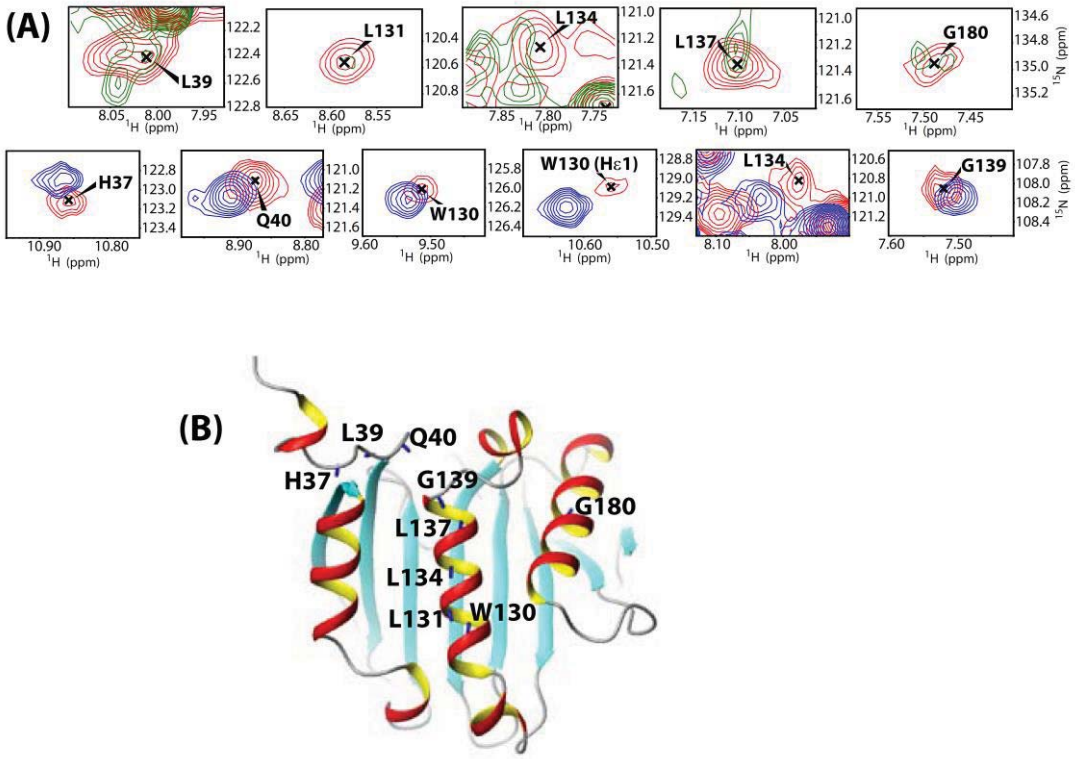

Supplementary Figure 3. Comparison of the residues affected on the dorsal surface in the RTP and m^{7}GTP eIF4E complexes. (A). Selected regions of ^{1}H-^{15}N HSQC spectra centered on specific residues located on the dorsal surface of eIF4E. The apo eIF4E (red) is superposed with either ~20-fold molar excess of RTP (green) or m^{7}GTP (blue). (B) Position of the different residues shown in (A) are represented on the eIF4E structure.

(A)

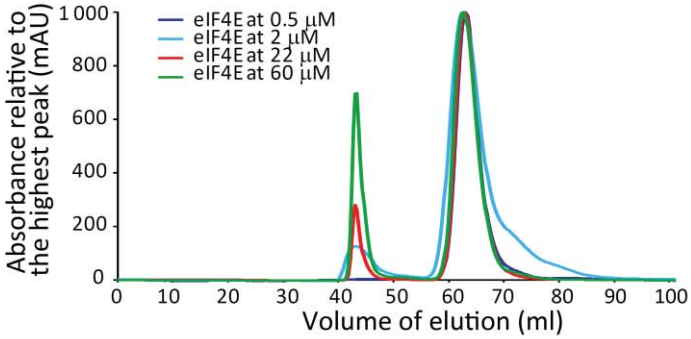
Absorbance relative to the highest peak (mAU)
1 000
800
600
400
200
0
eIF4E at 0.5 µM
eIF4E at 2 µM
eIF4E at 22 µM
eIF4E at 60 µM
0 10 20 30 40 50 60 70 80 90 100
Volume of elution (ml)

(B)

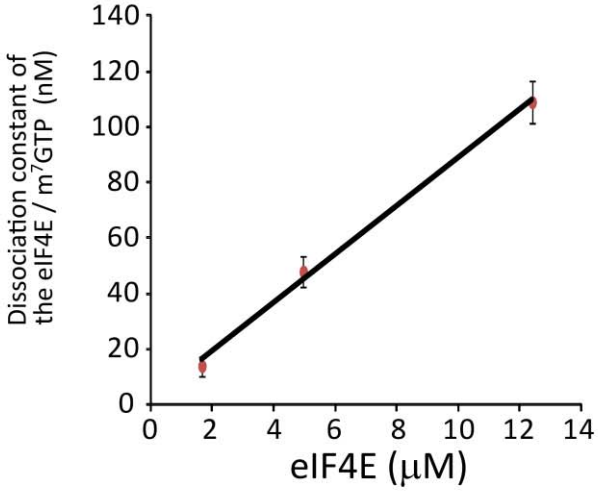
Dissociation constant of the eIF4E / m7GTP (nM)
140
120
100
80
60
40
20
0
0 2 4 6 8 10 12 14
eIF4E (µM)

(C)

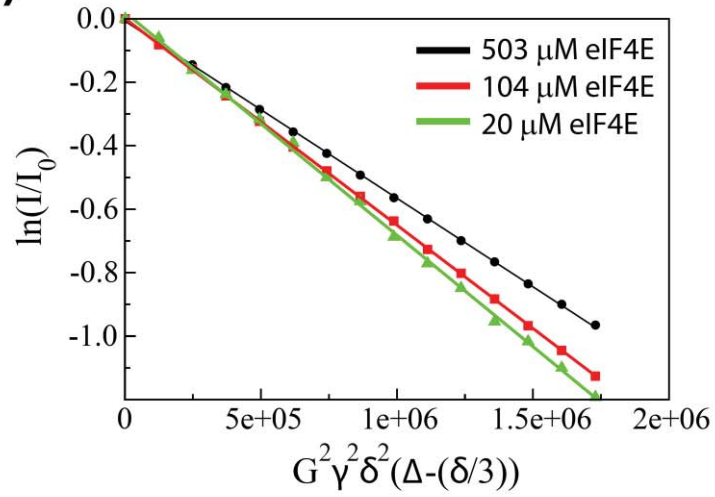
ln(I/I0)
0.0
-0.2
-0.4
-0.6
-0.8
-1.0
503 µM eIF4E
104 µM eIF4E
20 µM eIF4E
0 5e+05 1e+06 1.5e+06 2e+06
G2γ2δ2(Δ-(δ/3))

Supplementary Figure 4. The concentration dependence of eIF4E and its cap ligand. (A) FPLC elution profile of eIF4E at different concentrations. The peaks at 43 and 63 ml correspond to the void volume and the monomeric form of eIF4E (~25kDa), respectively. All four profiles were standardized to the highest peak at 63ml (1000 mAU). (B) Plot of the dissociation constants for the eIF4E / m^7GTP complex obtained by ITC at indicated eIF4E concentrations. (C) Translation diffusion experiments calculated at different apo eIF4E concentrations. The calculated diffusion coefficients D_s are $0.56.10^{-6} \pm 2.6.10^{-11}$, $0.65.10^{-6} \pm 2.7.10^{-11}$ and $0.72.10^{-6} \pm 6.1.10^{-11}$ cm^2/s for eIF4E samples at 503, 104 and 20 μM, respectively.

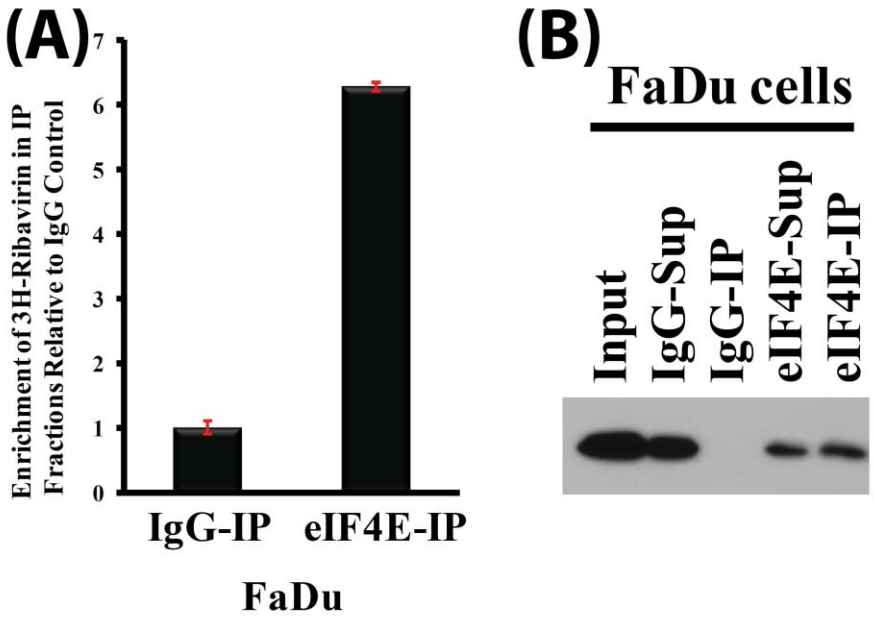

This experiment is representative of three independent experiments each carried out in triplicate. ^3H ribavirin enrichment in IgG controls is arbitrarily set to 1. Error bars represent standard deviations.

References

[1] M. Kimoto, M. Endo, T. Mitsui, et al., Site-specific incorporation of a photo-crosslinking component into RNA by T7 transcription mediated by unnatural base pairs, Chem Biol 11 (2004) 47-55.

[2] L. Volpon, M.J. Osborne, I. Topisirovic, et al., Cap-free structure of eIF4E suggests a basis for conformational regulation by its ligands, EMBO J 25 (2006) 5138-5149.

[3] N. Siddiqui, W. Tempel, L. Nedyalkova, et al., Structural insights into the allosteric effects of 4EBP1 on the eukaryotic translation initiation factor eIF4E, J Mol Biol 415 (2012) 781-792.

[4] A. Kentsis, I. Topisirovic, B. Culjkovic, et al., Ribavirin suppresses eIF4E-mediated oncogenic transformation by physical mimicry of the 7-methyl guanosine mRNA cap, Proc Natl Acad Sci U S A 101 (2004) 18105-18110.

[5] A. Kentsis, L. Volpon, I. Topisirovic, et al., Further evidence that ribavirin interacts with eIF4E, RNA 11 (2005) 1762-1766.

[6] F. Delaglio, S. Grzesiek, G.W. Vuister, et al., NMRPipe: a multidimensional spectral processing system based on UNIX pipes, J Biomol NMR 6 (1995) 277-293.

[7] T.D. Goddard, D.G. Kneller, Sparky 3, University of California, San Francisco, CA., (2003).

[8] S. Grzesiek, A. Bax, G.M. Clore, et al., The solution structure of HIV-1 Nef reveals an unexpected fold and permits delineation of the binding surface for the SH3 domain of Hck tyrosine protein kinase, Nat Struct Biol 3 (1996) 340-345.

[9] D.H. Wu, A.D. Chen, C.S. Johnson, An Improved Diffusion-Ordered Spectroscopy Experiment Incorporating Bipolar-Gradient Pulses, J. Magn. Reson., Ser. A 115 (1995) 260-264.

[10] J. Lebowitz, M.S. Lewis, P. Schuck, Modern analytical ultracentrifugation in protein science: a tutorial review, Protein Sci 11 (2002) 2067-2079.

[11] P. Schuck, Size-distribution analysis of macromolecules by sedimentation velocity ultracentrifugation and lamm equation modeling, Biophys J 78 (2000) 1606-1619.

[12] B. Culjkovic, I. Topisirovic, L. Skrabanek, et al., eIF4E is a central node of an RNA regulon that governs cellular proliferation, J Cell Biol 175 (2006) 415-426.

CHAPTER 11

Discussion and Perspectives

DISCUSSION

The tale of cancer treatment and its relapse remains a major challenge in medical oncology. Since Richard Nixon, the former U.S. president, has declared the "War on Cancer" almost 40 years ago [(1)], moderate progress has been made in improving the survival rates of patients. This impediment is, in part, due to our constant search for novel Achilles heels and finding ways to target them while undermining two important aspects that if were addressed in parallel will most likely lead to the development of most efficacious therapies. Cancer invasion and treatment evasion remain to date the major cause of cancer related mortality among patients.

Cancer Treatment Escape and Evasion

The development of longstanding anti-cancer therapeutics is constantly hindered by the development of primary or acquired multidrug resistance. Mechanisms by which cancer cells circumvent treatment can be generally divided into three categories: impaired drug net uptake (due to either enhanced efflux or decreased uptake), mutation of drug targets or compensatory genetic rewiring of relevant pathways [(2)]. In my thesis, I present a fourth model "inducible drug glucuronidation". Here, cancer cells hijack UGT1A enzymes to chemically modify drugs and block drug-target interactions.

While earlier studies investigating the role of UGTs in malignancy were focused on the effects of loss of UGTs and the accompanying deficiency in xenobiotics clearance, this is the first report to demonstrate that UGTs can be upregulated in an inducible-manner. Supporting our model, two subsequent studies have been published, since, showing a direct correlation between UGT expression and activity with the development of resistance to HDAC and Hsp90 inhibitors in CLL and colorectal cancer cell lines, respectively [(3, 4)]. As such, induced drug glucuronidation could be extended to other types of cancers; an interesting future perspective that can be addressed using tissue microarrays on large databank of patients to detect the commonality of this resistance mechanism in different cancer types and stages.

Understanding the mechanism(s) regulating inducible glucuronidation is essential for developing means to target UGTs and reverse the phenotype. In the AML case presented in my thesis, increased expression of GLI1 leads to elevation of UGTs. The mechanism by which GLI1

controls UGT1A expression does not appear to be at the transcriptional level, given the disconnect between UGT1A protein and mRNA levels. Treatment of resistant cell lines with the proteasome inhibitor MG132, indicates the GLI1 increases UGT1A protein stability. It is therefore plausible that GLI1 proteins indirectly either (i) decrease UGT1A turnover through downregulation of specific protein ligases, (ii) induce some posttranslational modifications or (iii) increase UGT1A ER-retention. Preliminary data from antibody arrays in GLI1 overexpressing cells predict GLI1-mediated increase of ER-retention as a possible mechanism. Hence, identifying factors mediating the link between GLI1 and UGT1A could serve as an alternative therapeutic modality to using GLI1 inhibitors as a means to revert resistance.

In addition to GLI1 dysregulation, it seems likely that other pathways can lead to UGT dysregulation in cancer. These include, DNA methylation, transcriptional regulation, phosphorylation, histone modification, microRNA regulation as well as alternative splicing. An interesting recent discovery revealed the presence of a novel class of human UGTs encoded by the same genetic loci but instead of possessing the common C-terminus exon 5a, utilize a shorter exon 5b which leads to premature translation termination. The resulting truncated UGT proteins, coined UGT_i2s, lack glucuronidation activity but act in a dominant-negative capacity possibly through forming inactive heteromeric complexes with full length UGT isoforms thus reducing enzymatic activity [5, 6]. Accordingly, understanding the mechanisms of regulation of UGT and UGT_i2s might provide a means for many possible therapeutic strategies, beyond the GLI1 model, to decrease or increase the expression of these enzymes, respectively. Such studies should include monitoring UGT protein levels and identifying which of the UGTs are dysregulated in various types of cancers.

Another effective strategy for reversing GLI1-dependent glucuronidation resistance is perhaps identifying inhibitors for UGT1A enzymes that are directly responsible for glucuronidation. This can be achieved by screening UGT1A enzymes against fragment libraries using NMR techniques. Screening of fragment libraries is a relatively new screening technique that has been successful in generating clinical compounds, even for difficult drug targets. In this technique small molecules (typically < 300 Da) are screened against a target protein, multiple hits are typically identified and linked together to form a strong specific inhibitor. Critically fragments are chosen with good drug-like properties, such as solubility, PK and toxicity profiles which are

often exhibited in the final drug. Since initial hits are expected to be weak, NMR has been the technique of choice for screening. After initial hits have been identified, their binding site on the UGT1A protein is assessed via competition experiments with known substrate binders and binders at the cofactor site. Alternatively, expressing the N- and C-terminal domains separately or using well known mutants known to be important for substrate or cofactor binding can be tested. Identified hits are collated based on affinity and/or tested in microsome assays for glucuronidation of ribavirin. An offshoot of this analysis is discovery of unique mechanisms for each glucuronidation target. In the absence of structure for the full-length UGT1A enzyme, interligand NOE's between bound molecules can be assessed to help guide linking strategies for stronger binders. Additionally, the UGT1A enzyme of interest will be modeled based on homologous plant and yeast structures to aid in drug design (there are examples of this in the literature).

An important feature of drug resistance is that development of resistance to one drug can lead to resistance to others. Given the broad range of substrates recognized by UGT enzymes, inducible drug glucuronidation could potentially target a wide variety of chemically distinct drugs. To determine which FDA approved drugs are potential clients for this resistance mechanism, high-throughput screening of cells overexpressing GLI1 can be established. Our preliminary results reveal a list of approximately 130 compounds whose inhibition of cell growth was impaired following GLI1 upregulation. Amongst, were drugs that are used as standards in the treatment of cancer, including Methotrexate, Floxuridine, and Idarubicin. Validation of these hits, followed by mass spectrometry analysis to determine if the drugs get glucuronidated or whether multiple forms of GLI1-dependent drug resistance occurs still needs to be done. As a control, treatment with Vismodegib and other GLI1 inhibitors will be useful to assess if resistance to these drugs can be reversed. Interestingly, preliminary analysis of the drug screen also revealed a list of approximately 23 compounds reverting drug resistance. Most of these drugs belong to a family of ATP synthesis inhibitors, including Gossypol, Aurovertin B, and Quinidine sulfate. Even though validation of this list still needs to be established, and thus could provide an alternative therapeutic venue to overcome GLI1 mediated drug resistance, a study aimed at understanding the sensitivity of GLI1 overexpressing cells to ATP inhibition would be of great value.

Beside glucuronidation, phase II drug metabolism includes other biotransformation reactions that serve to detoxify drugs. These conjugation reactions include, sulfation, acetylation, methylation and glutathione addition, among others. A recent study revealed a correlation between elevated glutathione levels and the inactivation and subsequent resistance to seven platinum drugs; indicating that similar to glucuronidation, other drug modifications could also be exploited by cancer cells to evade treatment. As such, phase II machinery needs to be characterized in cancer patients, particularly at resistance, as this might aid in impeding cancer and improving survival rates for patients.

My work demonstrates that resistance to a given therapeutic agent does not mean the end of our war against cancer, but rather the beginning a new battle where collateral hypersensitivity to alternative drugs can be exploited, only if we stand our grounds and strike back. It further demonstrates a new form of drug resistance "inducible drug modification" that should be taken into account not only during initial drug development but also upon resistance; turning around the one favorited hallmark of cancer cells "survival of the fittest" into our own advantage.

Cancer Invasion and Metastasis: *Spawning Pioneer Cells in the Strive for Survival*

From the cancer principle "survival of the fittest" comes the 6th hallmark defined by local invasion and distant metastasis, "*a growing tumour will eventually spawn pioneer cells; these move out of the original clump of mutant cells to invade…*" *by Buddhini Samarasinghe.*

Over the past two decades, the mechanism(s) regulating invasion and metastasis are becoming increasingly evident. It is now believed that in favor of motility, cancer cells genetically rewire to hijack and activate an important developmental program, the EMT, used in normal embryonic development and in response to inflammation [7, 8]. During EMT, a set of pleiotropically acting transcription factors orchestrates the expression of molecules used to alter the shape of cancer cells, change cell polarity, loosen cell adhesion junctions, and degrade the ECM [7, 8]. One of the known migratory events in EMT is characterized by the production of CD44 on the surface of cancer cells to aid their movement on stromal or endothelial hyaluronic acid chains [9-11]. The findings I present in chapter 8, alter this long-held dogma of CD44-assisted cancer cell migration on HA chains. Instead, I show that cancer cells *per se* express short chains of HA that form

microvillus-like surface protrusions which recruit CD44, among other receptors. These architectural changes are not observable by light microscopy because the HA filaments are too narrow, and thus these alterations have gone undetected for decades. I show the surprising finding that HA on the surface of tumour cells is required for eIF4E-mediated invasion. Specifically, eIF4E engages a post-transcriptional programme that drives the production of HA leading to the acquisition of an HA surface coat and cell surface protrusions. These studies demonstrate for the first time that HA biosynthesis and related structural changes can be harnessed by an oncoprotein to drive its malignant phenotype. Further, these findings alter the usual conception of glucose derivatives changing the metabolism of cancer cells to depict them as building blocks used to construct extracellular structures armed with factors that increase the metastatic phenotype.

Interestingly, the data presented in chapter 8 indicate that eIF4E might be a key regulator of HA-rich microvilli, beyond regulation of HA enzymes and CD44. Our RIP and export assays indicate that in addition to HA synthesizing enzymes and CD44, matrix metalloproteinases (including MMP9 and MMP2), collagenases, as well as ERM proteins (namely Ezrin) are potential targets of eIF4E. These findings support a model whereby HAS3 overexpression on the surface of cancer cells catalyzes the synthesis of HA which in turn coats the surface and mediates the formation of microvillus-like protrusions. Concomitantly, the microvilli-recruited CD44, on one hand, forms a scaffold for the binding of active MMPs that aid motility through proteolysis of the ECM, and on the other hand, interacts with cytoplasmic ERM proteins linking the plasma membrane with the actin cytoskeleton. It is noteworthy that neither CD44 nor HA alone can induce cell migration; rather an interaction between the two is necessary to activate this process. Also, despite the presence of CD44 in HAS3-induced protrusions, inhibition of CD44 activity with blocking antibodies or siRNA-mediated knockdown of CD44 does not affect the formation of these protrusions; suggesting that this particular activity is CD44 independent. These data indicate that CD44-HA dependent and/or independent functions are essential for downstream signalling post-protrusion formation. Subsequent studies focused on determining the composition of eIF4E-induced HA-rich protrusions would be of great interest as this will provide more profound mechanistic insights into the process of invasion and metastasis and ultimately aid the development of therapeutic means to prevent it.

Data shown in chapter 8 demonstrate, for the first time, that leukemic cells can also be sugar-coated (the presence of protrusions still needs to be assessed). If the expression of surface protrusions represents a means by which carcinoma cells locally invade the ECM, then what are the implications of having an HA-coat, and perhaps the associated microvillus-like protrusions, on the surface of AML cells? Throughout their lifespan, leukemic cells can circulate and take up residence in organs such as the liver and spleen, however, the vast majority are found in bone marrow (BM) niches where interactions with various BM cells provide them with factors favouring their survival. Bone homing of AML cells has been shown to rely on leukemic CD44-endothelial HA interaction to mediate the rolling of these cells on the endothelial wall [9, 12-14]. I propose that the HA rich protrusions on the surface of leukemic cells are required for the homing process post-extravasation. It is plausible that once inside the bone marrow, AML cells use their HA coats/protrusions to invade through ECM towards the niche where they can hide and escape treatment. This proposition can support the development of ribavirin resistant eIF4E AML cells discussed in chapter 3. Alternatively, the HA-CD44 interaction in AML can also play a role in cell-cell communication between cancer cells or cancer cells with BM cells in favor of survival or might mediate bone marrow exit of AML cells (a topic that, to date, is still largely uncovered). Accordingly, assessing the role of the HA coat in AML biology needs to be assessed by using mouse xenograft models.

Would HA-rich surface protrusions contribute to the release of microvesicles prior to the spawning of pioneer cells from the primary tumour? Recent evidence has shown that cancer cells can produce nano-sized vesicles termed “microvesicles” that carry cargo necessary for multiple aspects of cancer development including invasion, metastasis and enhancing drug-resistance potential [15, 16]. This cargo consists of DNA, mRNAs, microRNAs, proteins and lipids that can be delivered to local as well as distant cells [15, 16]. One of the interesting features of these microvesicles is depicted during metastasis whereby their migration to pre-metastatic sites creates an ideal milieu in which primary tumour cells can now grow [17-19]. As such, the shedding of such microvesicles from the HA rich protrusions presented on the surface of eIF4E overexpressing cells to aid metastasis might be a logical choice for these cells during late stages of their development. Indeed, preliminary data of HA immunofluorescence staining in eIF4E overexpressing cells shows the secretion of these microvesicles between cells. Further, it is

shown that in various types of cancers, production of interleukin 10 (IL-10) by monocytes is induced by low molecular weight HA located in tumour-derived microvesicles [15]. As such, characterizing the type of microvesicles produced following eIF4E overexpression as well as identifying their composition and their role in determining subsequent organotropic metastasis could be used to predict metastatic propensity as well as organ-specific metastasis.

In conclusion, HA-rich protrusions on the surface of AML and carcinoma cells could serve a dual role mediating cancer invasion and treatment evasion. Accordingly, eIF4E overexpression provides AML cells with a proliferative as well as survival advantage placing eIF4E not only as a central node of an RNA regulon that governs cellular proliferation but also as a central node of a second RNA regulon, a "Sugar Regulon", governing invasion; where eIF4E regulates the expression of HA biosynthesis as well as microvilli-based factors essential for invasion. A better understanding of the mechanisms underlying bone marrow homing of eIF4E high AML cells is required to develop better treatment options. Here, I present the use of a clinically available HA degrading enzyme, Hyaluronidase, to augment the cytotoxic effects of ribavirin on AML and carcinoma models. Indeed, the design of future clinical trials combining ribavirin and Hyaluronidases are currently in progress.

Conclusion

Cancer invasion and treatment evasion remain to date the two leading cause of cancer related mortalities among patients. Studies focused on understanding the molecular mechanisms governing these two processes will aid in the development of targeted therapeutics. The case presented in this thesis, demonstrates an example of how this can be accomplished. The data presented herein, illustrate how cancer cells develop oncogenic dependency on the roles of eIF4E for their invasion and treatment escape and also presents ways to overcome these phenotypes clinically. While cancer treatment escape can be established via inducible drug glucuronidation, and its invasion through presentation of surface sugar coats containing weapons of metastatic destruction, using combinations of clinically available inhibitors to synthetically eradicate tumor cells provides rays of hope for improving the survival rates of these patients.

References:

1. Vanchieri, C., *National Cancer Act: a look back and forward.* J Natl Cancer Inst, 2007. **99**(5): p. 342-5.
2. Zahreddine, H. and K.L. Borden, *Mechanisms and insights into drug resistance in cancer.* Front Pharmacol, 2013. **4**: p. 28.
3. Gruber, M., et al., *Overexpression of uridine diphospho glucuronosyltransferase 2B17 in high-risk chronic lymphocytic leukemia.* Blood, 2013. **121**(7): p. 1175-83.
4. Landmann, H., et al., *UDP glucuronosyltransferase 1A expression levels determine the response of colorectal cancer cells to the heat shock protein 90 inhibitor ganetespib.* Cell Death Dis, 2014. **5**: p. e1411.
5. Bellemare, J., et al., *Modulation of the human glucuronosyltransferase UGT1A pathway by splice isoform polypeptides is mediated through protein-protein interactions.* J Biol Chem, 2010. **285**(6): p. 3600-7.
6. Guillemette, C., et al., *UGT genomic diversity: beyond gene duplication.* Drug Metab Rev, 2010. **42**(1): p. 24-44.
7. Klein, C.A., *Cancer. The metastasis cascade.* Science, 2008. **321**(5897): p. 1785-7.

8. Pantel, K. and R.H. Brakenhoff, *Dissecting the metastatic cascade.* Nat Rev Cancer, 2004. **4**(6): p. 448-56.
9. Avigdor, A., et al., *CD44 and hyaluronic acid cooperate with SDF-1 in the trafficking of human CD34+ stem/progenitor cells to bone marrow.* Blood, 2004. **103**(8): p. 2981-9.
10. Chanmee, T., et al., *Key Roles of Hyaluronan and Its CD44 Receptor in the Stemness and Survival of Cancer Stem Cells.* Front Oncol, 2015. **5**: p. 180.
11. Misra, S., et al., *Interactions between Hyaluronan and Its Receptors (CD44, RHAMM) Regulate the Activities of Inflammation and Cancer.* Front Immunol, 2015. **6**: p. 201.
12. Baaten, B.J., et al., *Regulation of Antigen-Experienced T Cells: Lessons from the Quintessential Memory Marker CD44.* Front Immunol, 2012. **3**: p. 23.
13. McDonald, B. and P. Kubes, *Interactions between CD44 and Hyaluronan in Leukocyte Trafficking.* Front Immunol, 2015. **6**: p. 68.
14. Suarez-Alvarez, B., A. Lopez-Vazquez, and C. Lopez-Larrea, *Mobilization and homing of hematopoietic stem cells.* Adv Exp Med Biol, 2012. **741**: p. 152-70.
15. Lenart, M., et al., *Hyaluronan carried by tumour-derived microvesicles induces IL-10 production in classical (CD14++CD16-) monocytes via PI3K/Akt/mTOR-dependent signalling pathway.* Immunobiology, 2017. **222**(1): p. 1-10.
16. Wang, Z., et al., *Exosomes in tumour microenvironment: novel transporters and biomarkers.* J Transl Med, 2016. **14**(1): p. 297.
17. Balaj, L., et al., *Tumour microvesicles contain retrotransposon elements and amplified oncogene sequences.* Nat Commun, 2011. **2**: p. 180.
18. Hoshino, A., et al., *Tumour exosome integrins determine organotropic metastasis.* Nature, 2015. **527**(7578): p. 329-35.
19. Martins, V.R., M.S. Dias, and P. Hainaut, *Tumour-cell-derived microvesicles as carriers of molecular information in cancer.* Curr Opin Oncol, 2013. **25**(1): p. 66-75.